UNIVERSITY OF LIVERPOOL

Department of Chemistry

Spheres on Sphere Silica Particles – Mechanism and Modification

Thesis submitted in accordance with the requirements of the University of Liverpool for the degree of Doctor in Philosophy

Richard Hayes

April 2016

Supervisors:

Dr. Haifei Zhang

Prof. Peter Myers

Examiners:

Prof. Jeremy Glennon

Dr. Alexander Steiner

Contents

	Abstract		i
	List of Figures		iii
	List of Tables		vii
	Abbreviations		viii
	Acknowledgments		xii
	Objectives		xiii
1	**Introduction**		**1**
	1.1	Overview	1
	1.2	Preparation Methods for Core-Shell Particles	8
	1.3	The Fundamentals of Core-Shell Particles for HPLC	23
	1.4	Core-Shell Silica Microspheres in Liquid Chromatography	34
	1.5	Applications of Core-Shell Particle Columns	42
	1.6	Summary	50
	1.7	Thesis Overview	51
	1.8	References	52
2	**Synthesis of Spheres on Sphere Silica Particles**		**61**
	2.1	Introduction	61
	2.2	Literature Review	61
	2.3	Experimental	72
	2.4	Results and Discussion	79
	2.5	Conclusion	110
	2.6	References	113
3	**Microwave Assisted Bonding**		**116**
	3.1	Introduction	116
	3.2	Literature Review	116
	3.3	Experimental	123
	3.4	Results and Discussion	130
	3.5	Conclusion	144
	3.6	References	147

4 Spheres on Sphere Particles for Chromatography 150

4.1 Introduction 150

4.2 Literature Review 150

4.3 Experimental 160

4.4 Results and Discussion 162

4.5 Conclusion 183

4.6 References 186

5 Alternative Morphologies 190

5.1 Introduction 190

5.2 Experimental 190

5.3 Results and Discussion 192

5.4 Conclusion 205

5.5 References 207

6 Conclusion 208

Abstract

Spheres on Sphere Silica Particles – Mechanism and Modification

Richard Hayes

Supervisors: Dr. Haifei Zhang, Prof. Peter Myers

One of the current challenges in chromatography is the fast separation of large biomolecules. The demand for this is huge in pharmaceutical and biological research. To meet this challenge a new type of porous, large pore support material is required. A new, unique type of silica support, named spheres on sphere (SOS) silica, has recently been discovered which may meet these demands. SOS particles are produced via a one-pot synthesis and are comprised of a nanoparticle shell surrounding a larger core microsphere. High performance liquid chromatography (HPLC) columns packed with such particles have shown remarkably fast separation of proteins. These new particles show high potential as a revolutionary HPLC technology compared to widely used core-shell silica particles, which are prepared by a tedious layer by layer procedure and suffer with the issue of poor mass transfer for large analytes.

This thesis outlines the experimental work undertaken to develop SOS particles which are specifically designed for the separation of proteins and large molecules using HPLC. The synthesis method has been optimised to achieve particles with a complete, densely packed, single-layer shell and a diameter suitable for use in HPLC. Additionally, a narrow particle size distribution is achieved, removing the need for a time-consuming and wasteful classification process.

The suitability of microwave irradiation for the surface functionalisation of silica materials has been investigated. This includes the development of a bonding method for SOS particles which is shown to be highly reproducible and capable of providing comparable bonding density to conventional reflux heating methods. The use of microwave heating also results in significantly shorter reaction times and lower power consumption compared to commonly used equipment such as hot plates or heating mantles.

Following surface functionalisation, the performance of HPLC columns packed with SOS particles have been assessed in both isocratic and gradient elution mode. Parameters such as column permeability, total porosity and impedance have been determined in isocratic mode, which allows direct comparison with other column packing materials. In gradient elution mode the SOS columns have been used for the analysis and separation of a wide range of peptides and proteins. Excellent performance has been obtained using the SOS material where fast gradient analysis is applied, in some cases outperforming a commercial core-shell column specifically designed for protein analysis.

This work is supported by the Engineering and Physical Sciences Research Council and Thermo Fisher Scientific.

List of Figures

1.1	SEM image showing the porous structure of a silica monolith material	2
1.2	SEM image of classified 3 µm porous silica particles	5
1.3	Schematic representation of different types of core-shell particles	9
1.4	Coacervative method for synthesis of superficially porous particles	12
1.5	LbL process for synthesis of core-shell particles	13
1.6	Morphology and pore structure of Halo 2.7 µm particles	14
1.7	Morphology evolution at different reaction times for SOS particles	20
1.8	Preparation of silica-titania core-shell particles by a microfluidic approach	22
1.9	The van Deemter equation and plot	23
1.10	Effects of retention and porosity on longitudinal diffusion	27
1.11	Effects of B and C terms on diffusion	29
1.12	Comparison of efficiency for different packing materials	30
1.13	Comparison of back pressure for different packing materials	32
1.14	Comparison of impedance for different packing materials	33
1.15	Schematic of instrumentation used for 2D-LC	41
1.16	Effect of increasing pore size for protein separation	43
1.17	Effect of pore size on peak width and resolution of peptides and proteins	44
1.18	Peptide test mix separated on three core-shell columns	45
1.19	LC-MS/MS chromatograms for the analysis of BADGEs	47
2.1	Acid catalysed hydrolysis and condensation	62
2.2	Base catalysed hydrolysis and condensation	63
2.3	Formation of the mesoporous silica material MCM-41	68
2.4	SEM image of SOS particles and nitrogen adsorption data	69
2.5	HKUST-1 nanocrystals synthesised onto SOS silica particles	71
2.6	SOS particles produced from the standard reaction	74
2.7	Nitrogen isotherm and mercury intrusion plot for SOS particles	78
2.8	Differential thermogravimetric curve for SOS particles	79
2.9	Resultant particle morphology when varying ammonia concentration	82

2.10 Particles produced when using alternative bases 83

2.11 Particles produced when varying molecular weight and concentration of PVA 84

2.12 Effect of PVP molecular weight on particle morphology 85

2.13 Chemical structure of polymers studied in the SOS reaction 87

2.14 Resultant morphology from changing concentration of CTAB 89

2.15 Resultant morphology from changing concentration of TWEEN 20 90

2.16 Morphology changes when varying the amount of MPTMS added 92

2.17 Effect of the ratio of methanol:water on particle morphology 94

2.18 Particles obtained from the reaction using PVP (10k) in the absence of CTAB 95

2.19 Particles produced when varying the concentration of CTAB in the reaction with 5% PVP (10k). 96

2.20 SOS particles obtained from the optimised reaction 97

2.21 Nitrogen isotherm plot and mercury intrusion plot for SOS particles prepared from the optimised reaction 98

2.22 SOS particles obtained from the scaled up optimised reaction 99

2.23 SOS particles obtained from the standard reaction using 1.4% ammonia concentration 102

2.24 Particles produced when changing the addition rate of MPTMS into the reaction using a syringe pump 104

2.25 Particles produced using syringe pump addition at 0.125 and 0.065 mL/min after addition of 0.5, 1 and 2 mL MPTMS 107

2.26 Fractal SOS particles obtained via initial MPTMS addition volume of 1 mL, followed by syringe pump addition at 0.06, 0.04 and 0.02 mL/min 108

3.1 Bonding methods onto the Si-OH surface 118

3.2 The role of base in the silanisation reaction 118

3.3 Radar plot of Tanaka test results and carbon loading for commercial, microwave and conventional C18 phases 122

3.4 SEM images showing surface morphology of SOS particles 124

3.5 CEM Explorer microwave reactor with autosampler 126

3.6 Column packing equipment 129

3.7 Overlaid chromatogram of protein test mixture separation on microwave and oil bath bonded columns 134

3.8 Overlaid chromatogram of protein test mixture separation on three columns from batch MB-3 138

3.9 Overlaid chromatogram of protein test mixture separation on three columns from batch MB-4 139

3.10 Overlaid chromatogram of protein test mixture separation on three columns from batch MB-5 139

3.11 Overlaid chromatogram of protein test mixture separation on the first column from each batch 141

4.1 van Deemter plot showing the contribution of individual terms to band broadening and the area where optimum efficiency is obtained 155

4.2 An example of a scalable fractal, the Koch curve 158

4.3 SOS particle morphology and dispersity 161

4.4 Plot of reduced plate height versus reduced linear velocity and impedance plot for the analysis of butylparaben on the SOS-C4-1 column 164

4.5 Separation of reversed phase test mixture on the SOS-C4-1 column 166

4.6 Separation of the peptide standard mixture on SOS-C4-1 and SOS-C8 columns 167

4.7 Separation of the peptide standard mixture on Accucore 150-C4 and SOS-C4-1 columns 168

4.8 Overlaid chromatograms of individual protein separation on the SOS-C4-1 and Accucore 150-C4 columns 169

4.9 Overlaid chromatograms of protein test mixture separation on SOS-C4-1, SOS-C4-2 and Accucore 150-C4 columns 171

4.10 Overlaid chromatograms of large protein separation on SOS-C4-1 and Accucore 150-C4 columns 172

4.11 Peak capacity plot for the SOS-C4-1 column 174

4.12 Comparison of peak capacity values obtained on SOS and Accucore columns 175

4.13 Chromatograms from the analysis of intact and reduced rituximab on SOS C4 and three commercial wide-pore test columns 177

4.14 Chromatograms from the analysis of reduced brentuximab vetodin on SOS C4 and three commercial wide-pore test columns 178

4.15 Fractal particle morphology and dispersity 180

4.16 Plot of reduced plate height versus reduced linear velocity and impedance plot for the analysis of butylparaben on the fractal-C4 column 181

4.17 Overlaid chromatograms for separation of individual proteins and large proteins on the fractal-C4 column 182

5.1 SEM images of particles produced from the optimised reaction plus secondary addition of 100 µL TEOS 193

5.2 SEM images showing detail of surface morphology following secondary TEOS addition after 20 minutes 193

5.3 SEM images of particles produced from the optimised reaction plus secondary addition of 100 µL TEOS:MPTMS 194

5.4 SEM images of particles produced from the optimised reaction plus secondary addition of 200 µL TEOS:MPTMS 195

5.5 SEM images of particles produced from the optimised reaction, with varying ratio of TEOS:MPTMS 196

5.6 Detail of surface morphology from addition of TEOS:MPTMS 196

5.7 Reduction in surface area with increasing secondary addition of TEOS 197

5.8 SEM images of particles produced from TEOS:MPTMS when changing molecular weight and concentration of PVP 198

5.9 SEM images of cluster-type particles produced when using PVP (55k) 198

5.10 SEM images showing packing structure of clusters in the HPLC column 199

5.11 Separation of the peptide standard mixture on Cluster-C4 column 200

5.12 Protein separation on the Cluster-C4 column 201

5.13 SEM images, PSD and nitrogen adsorption data for smooth spheres 203

5.14 Nitrogen isotherm and pore size distribution of silica particles following pore expansion treatment 204

List of Tables

1.1	Development of HPLC particles since the 1950s	6
2.1	Effect of calcination temperature on physical properties of SOS particles	75
2.2	Influence of ammonia concentration on physical properties	81
2.3	Ratio of PVA (9-10k):PVP (10k) and particle sizing data	86
2.4	Physical data for particles shown in figure 2.26	108
3.1	Effect of superheating on carbon loading and bonding density	130
3.2	Effect of microwave reaction time on carbon loading and bonding density	131
3.3	Comparison of bonding results obtained from microwave and reflux heating methods	133
3.4	Bonding results from batch to batch reproducibility study	137
3.5	Comparison of retention times for analytes on each column	140
3.6	Comparison of bonding results when using various reaction solvents	143
4.1	Physical properties of bonded core-shell materials	162

Abbreviations

2D-LC	Two dimensional liquid chromatography
α	Bonding density in µmol/m^2
ADC	Antibody-drug conjugate
AMT	Advanced Materials Technology
BADGE	Bisphenol A-diglycidyl ether
BET	Brunauer-Emmett-Teller
BFDGE	Bisphenol F-diglycidyl ether
BJH	Barrett-Joyner-Halenda
BMMS	Bis(dimethylamino)dimethylsilane
BPA	Bisphenol A
BSA	Bovine serum albumin
CEC	Capillary electrochromatography
CMC	Critical micelle concentration
CTAB	Cetyltrimethylammonium bromide
CTAC	Cetyltrimethylammonium chloride
d_{10}	10^{th} percentile of the size distribution
d_{90}	90^{th} percentile of the size distribution
$d^{90}/_{10}$	Ratio of 90^{th} and 10^{th} percentile of the size distribution
DACH-BS	N,N'-bis-[(triethoxysilyl)propyl]-trans-(1R,2R)-bis-(ureido)-cyclohexane
d_c	Column diameter
DCM	Dichloromethane
DiCTAB	Dihexadecyldimethylammonium bromide
DMF	Dimethylformamide
d_p	Particle diameter
DTT	Dithiothreitol
E	Impedance
E_{min}	Minimum impedance
EPA	Environmental Protection Agency

ESI-MS	Electrospray ionisation mass spectrometry
ε_T	Total column porosity
GC	Gas chromatography
GC-MS	Gas chromatography-mass spectrometry
GY	Glycine-tyrosine
h	Reduced plate height
H	Height equivalent to a theoretical plate
HBC	Hydrogen bonding capacity
Hc	Heavy chain
HETP	Height equivalent to a theoretical plate
HILIC	Hydrophilic interaction liquid chromatography
HMDS	Hexamethyldisilazane
h_{min}	Minimum reduced plate height
H_{min}	Minimum plate height
HPLC	High performance liquid chromatography
i.d.	Internal diameter
IEX	Ion exchange
kDa	Kilodalton
K_V	Column permeability
L	Column length
LbL	Layer-by-layer
Lc	Light chain
LC	Liquid chromatography
LC-MS	Liquid chromatography-mass spectrometry
LC-MS/MS	Liquid chromatography-tandem mass spectrometry
Leu-enk	Leucine enkephalin
LLC	Liquid-liquid chromatography
mAb	Monoclonal antibody
MCM	Mobil Composition of Matter
Met-enk	Methionine enkephalin

MLbML	Multilayer-by-multilayer
MPTMS	3-mercaptopropyltrimethoxysilane
MOF	Metal organic framework
MTMS	Methyltrimethoxysilane
M_W	Molecular weight
N	Number of theoretical plates, theoretical plate count
NPC	Normal phase chromatography
ΔP	Backpressure, operating pressure, pressure drop
PAH	Polycyclic aromatic hydrocarbon
P_C	Peak capacity
PDA	Photo diode array
PDADMA	Poly(diallyldimethylammonium chloride)
PEEK	Polyether ether ketone
PEG	Poly(ethylene glycol)
PMVE	Poly(methyl vinyl ether)
PSD	Particle size distribution
PTFE	Polytetrafluoroethylene
PVA	Poly(vinyl alcohol)
PVP	Polyvinylpyrrolidone
QC	Quality control
RPC	Reversed phase chromatography
RSD	Relative standard deviation
SBA	Santa Barbara Amorphous
SDS	Sodium dodecyl sulfate
SEM	Scanning electron microscope
SFC	Supercritical fluid chromatography
SIC	Sequential injection chromatography
$SiCl_4$	Silicon tetrachloride
SOS	Spheres on sphere
SPE	Solid phase extraction

t_0	Unretained peak time
TBT	Tetrabutyl titanate
TEM	Transmission electron microscope
TEOS	Tetraethylorthosilicate
TFA	Trifluoroacetic acid
t_g	Gradient time
TGA	Thermogravimetric analysis
TMOS	Tetramethylorthosilicate
TMSI	Trimethylsilylimidazole
t_R	Retention time
u	Mobile phase linear velocity
UPLC	Ultra-high pressure liquid chromatography
UV	Ultra violet
v	Reduced mobile phase linear velocity
VYV	Valine-tyrosine-valine
$W_{50\%}$	Peak width measured at 50% height
W_B	Peak width measured at the base

Acknowledgments

I would firstly like to thank my supervisors Haifei Zhang and Peter Myers for the opportunity to study at Liverpool. Their guidance and support has been a massive help throughout my PhD. A special mention must also be given to Tony Edge for his advice, enthusiasm and invaluable chromatography knowledge.

Many thanks to everyone within the Zhang and Myers Research Groups for the friendship, thesis advice, tea breaks, jokes and laughter during my studies, especially Ulrike Wais, Alex Ho and Aled Roberts. A massive thank you also to everyone within the Chromatography Group at Thermo Scientific, Runcorn for all the help and advice, sample analysis and technical support.

This thesis is dedicated to my parents, Angela and John, for their continual support throughout my studies.

Objectives

This thesis describes the development of spheres on sphere (SOS) particles for use in HPLC, with the aim of improving the separation of proteins and large biomolecules. Commercial core-shell particles for protein analysis are typically comprised of a thin shell with a large pore diameter to reduce the mass transfer effects observed for large molecules. While particles possessing this morphology have been shown to provide high performance in this type of application, the method of production is a slow and inefficient process. The synthesis methods, development and chromatographic performance of core-shell particles will be discussed in detail in the introduction chapter.

SOS silica particles are a new type of core-shell material with a single layer shell of nanoparticles surrounding a solid core, produced from a one-pot reaction without the need for further modification or classification. Particles have been found to be microporous, meaning they are effectively non-porous for analyte molecules. However the unique morphology provides interstitial macroporosity due to the shallow shell structure composed of relatively large nanoparticles. This combination of large pores and shallow shell depth appears to be ideal for large compounds such as proteins, as the diffusive effects should be greatly reduced.

The experimental objectives in this thesis will focus on three main areas:

1) Optimisation of the SOS synthesis method. By understanding the role of each reagent in the reaction, the aim is to be able to control the particle morphology to produce SOS materials with narrow particle size distribution, complete single layer shell and suitable diameter for use in HPLC.

2) Functionalisation of SOS particles using microwave irradiation. Recent research has shown microwave heating to be extremely effective when producing silica bonded phases, however its use in this capacity is currently very limited. The aim is to assess the suitability and reproducibility of microwave bonding for SOS particles and compare this method with conventional heating.

3) HPLC assessment of bonded SOS particles. The aim is to assess the chromatographic performance of SOS particles under isocratic and gradient modes. The particle morphology suggests that the SOS material should be ideal for large molecule separation and experimentation will be performed to determine this, with comparison to commercial materials.

These three areas of study will describe the development of a new type of particle for use in chromatography. Prior to the introduction of modern core-shell materials in 2007, there had been little development in the basic morphology of silica particles other than continual reduction of the particle diameter. As such, advances in chromatographic performance have been mainly reliant on reducing the particle size. There is clearly a limit on how small particles can be made and therefore the future of chromatography will depend on the development of completely new materials. The experimental work in this thesis describes efforts to achieve this, starting with the basic synthesis of particles and optimisation of the process, through to the creation of packed bonded phases.

1 Introduction

1.1 Overview

Among different types of chromatography, high performance liquid chromatography (HPLC) has been most widely used as an essential analysis tool for research, manufacturing, clinical tests, and diagnostics. This is due to its universal applicability and remarkable assay precision.[1] Two main types of column, packed particles and monoliths, are used for routine HPLC. Silica microspheres are the most frequently used packing materials for particle packed columns, while for monolithic columns both porous silica and crosslinked polymers are commonly used. The challenges in HPLC are to obtain efficient and fast separation with high resolution preferably with low back pressure for various types of samples, for example pharmaceuticals, food, life science, environmental and routine analysis in research labs.[2]

This introduction aims to describe the types of stationary phase currently used in HPLC. The main emphasis will be on core-shell type particles, a concept first introduced in 1969 by Horváth *et al.*,[3] which have recently seen reintroduction and investigation for use as the packing material for HPLC columns. The preparation methods for producing core-shell particles will be described, followed by discussion on the performance advantages over totally porous silica particles and monoliths. There will also be discussion on the use of core-shell particles in different types of liquid chromatography and examples of HPLC applications for the separation of various types of samples.

The introduction is concluded with a perspective on future development of core-shell particles in chromatography, including the limitations of the production method of such materials, the challenges currently faced by chromatographers and how the work undertaken in this research project plans to address these issues.

1.1.1 Monoliths

Monolithic columns were developed in the late 1980s and through the 1990s to be used as stationary phases in HPLC columns.[4-6] Porous monoliths, rather than discrete particles, can be thought of as a single rod of stationary phase that fills the entire column length. The material consists of large interconnected pores, shown in figure 1.1, resulting in high permeability and hence low back pressure, even at high flow rates.[7, 8] There are

generally two pore types; large macropores (>50 nm diameter) which run through the monolith structure and, in the case of silica monoliths, interconnecting mesopores (2-50 nm diameter) which are present in the silica walls.[7] Monoliths have been found to be a viable alternative to particle-packed columns for efficient separations in HPLC and satisfactory chromatographic performance has been achieved for a variety of samples.[9-13]

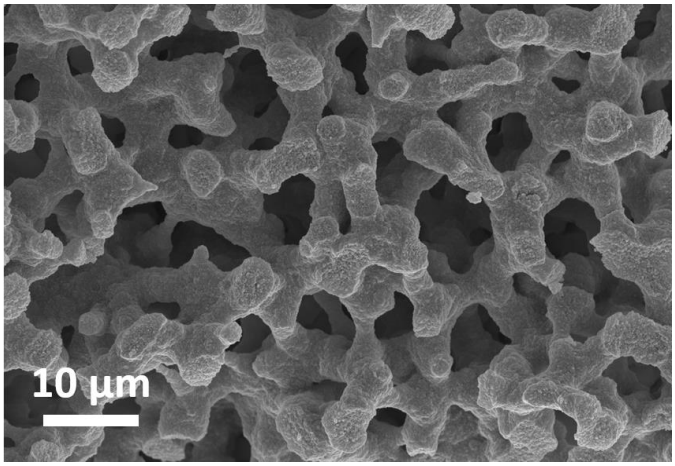

Figure 1.1 SEM image showing the porous structure of a silica monolith material.[14]

There are two main types of material used in monolithic columns; polymer or silica-based. Pioneering work in the preparation of polymer monoliths was performed by Hjertén *et al.* using hydrophilic gels,[5, 15] and by Svec *et al.* using hydrophobic gels.[16, 17] Polymer-based monoliths are generally prepared by in-situ polymerisation of organic monomers in a three step method, although in some cases the second step is the only one deemed necessary. Firstly the internal wall of the column is treated so that the later synthesised polymer will adhere strongly to it, stopping mobile phase flow between the wall and the polymer thus bypassing the bed and preventing separation. The second step involves the polymerisation of a mixture of reagents within the column, resulting in the precipitation of a high molecular weight polymer. The final step allows modification of the surface chemistry of the column bed, if necessary. There are many combinations of monomers and surface modifying reagents that allow for the tailoring of polymeric monoliths to a wide range of separations. For example, procedures to obtain materials suitable for ion exchange,[18, 19] hydrophobic interaction,[18] reversed phase[20] and narrow-bore columns[21] have been determined.

Silica-based monoliths are prepared using a sol-gel process in which an alkoxysilane solution forms a silica gel via hydrolysis and condensation.[22] Tetramethylorthosilicate (TMOS) and tetraethylorthosilicate (TEOS) are typical starting alkoxysilanes. The macropore formation within the silica sol-gel system is a competitive process involving phase separation and a sol-gel transition. A phase separation mechanism known as spinodal decomposition results in co-continuous structures of the two separated domains. There is composition fluctuation between two phase domains: a silica-rich domain (to be silica skeletons) and a solvent-rich domain (to be macropores).[23] A co-continuous, sponge-like domain structure develops and remains unbroken for a period of time, after which the phase domains continuously increase in size and finally result in fragmented domains and a continuous matrix. When gel formation and phase separation occur competitively, various co-continuous structures are permanently frozen in the network. In the case of silica monolith formation, the initially fluid reaction system turns into a continuous silica skeleton plus a fluid phase which fills the resultant pore structure. Removal of the fluid leaves behind open pores.

The size and volume of macropores in the structure can be controlled by various porogens such as water soluble polymers and surfactant templates which induce phase separation.[23] For example, the use of poly(ethylene glycol) (PEG) forms strong hydrogen bonds with the silanol groups of the growing silica structure. The phase separation tendency is determined mainly by the PEG to silica ratio, therefore adjusting the ratio allows control over the size of the silica skeleton and the size of the macropores. The volume fraction of the fluid phase which becomes the pore space after drying mainly depends on the volume fraction of solvent phase in the starting solution. Consequently, the size and volume of macropores can be controlled by adopting PEG as an additive. Silica monoliths may also contain pores in the skeleton wall which can be created by solvent exchange treatments to obtain a bimodal meso-macroporous pore size distribution.[24]

Monolithic silica columns can be prepared in a mould[25] (typically a glass tube up to 9 mm in diameter) to generate a rod, or in a fused silica capillary[23] using the sol-gel process. Preparation in a mould is accompanied by shrinkage of the structure, reducing the diameter of the resulting rod. The shrinkage causes detachment of the rod from the wall of the mould thus meaning it cannot be used directly as a HPLC column. Monolithic rods must therefore be recast, typically by covering with heat shrinking polytetrafluoroethylene (PTFE) tubing[6, 26] or clad in polyether ether ketone (PEEK)[25] before they can be utilised in chromatographic applications.

Columns have been prepared within 50-530 µm internal diameter (i.d.) fused-silica capillaries for use in HPLC and CEC.[25, 27-30] A small sized capillary is favourable to create covalent bonds between the wall and silica skeleton which overcomes the effect of shrinkage due to the large ratio of contact area to silica volume. For a larger sized capillary, shrinkage can be minimised by the use of a mixture of TMOS and methyltrimethoxysilane (MTMS) instead of TMOS alone.

The main obstacles for the wider use of monolithic columns are the reproducibility of the pore structure, shrinkage of the structure causing detachment from the column wall and the delicate cladding procedure to fit the monolith into a column. As a result, the analysis performance of monolithic columns may vary from batch to batch. Furthermore, the mechanical stability is generally weak for monolithic columns. There is an additional issue with polymer monoliths due to potential swelling problems in the presence of solvents.

1.1.2 Silica Microspheres

Although various polymer and ceramic microspheres have been used as packing materials, silica microspheres have been most extensively investigated and columns packed with these are by far the most commonly used. An example SEM image of 3 µm silica particles is shown in figure 1.2. Both non-porous and porous silica microspheres have been utilised as the stationary phase in HPLC columns. For non-porous particles, the separation occurs on the particle surface and band broadening is alleviated due to the extremely short diffusion path allowing fast mass transfer.[31] However, due to the low surface area, retention, selectivity and ultimately, resolution are limited. The loading capacity is also reduced. For porous silica microspheres, in addition to the external particle surface area the surface area within the pores provides more sites to interact with analytes. For liquid phase separation the pore size is typically required to be greater than 6 nm to allow access to analytes. For separation of large molecules and biomolecules greater than a few thousand kilodaltons (kDa), increased pore sizes of up to 100 nm are often required for efficient separation.[8]

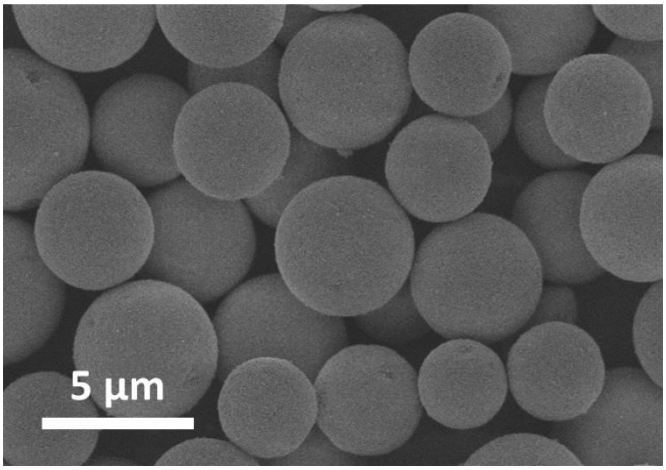

Figure 1.2 SEM image of classified 3 µm porous silica particles. Taken from own data.

The evolution of porous, spherical silica particles began in the early 1970s. Before this point sorbents were composed of irregularly shaped particles around 100 µm in size. Early chromatographic theory was developed in parallel with advances in gas chromatography in the 1950s and 1960s. This discussed the advantages of small particles in chromatography, predicting that the use of smaller and more uniform particles would result in increasingly efficient separations and faster optimum mobile phase velocities. The cost of using smaller particles however is a significant increase in operating pressure. Table 1.1 shows the advances in particle technology over the past 65 years, with a general trend of reducing particle diameter.

The size of silica particles and the packing quality significantly affect the performance of the packed columns. Silica particles with smaller diameters and narrow size distribution are employed by manufacturers to achieve high performance separation. However, back pressure is proportional to the square of the particle diameter[32] and while halving the particle size may double the separation performance in terms of theoretical plate numbers, it can also quadruple the back pressure.[8] Despite this, sub-2 µm microspheres are the current state of the art material on the market for porous silica microspheres. To achieve fast separation on silica microspheres of certain size, a straightforward approach is to increase the flow rate and therefore the pressure drop across the column. To run at this increased pressure, ultra-high pressure liquid chromatography (UPLC) has been developed and used. This technique places much stricter requirements on the pumping system and the whole flow system due to the very high

operating pressure. One alternative to sub-2 µm particles is the recently developed core-shell particles.

Table 1.1 Development of HPLC particles since the 1950s. As the particle diameter decreases, efficiency improves at the expense of increasing instrument pressure requirements.[1]

Year	Particle size (µm)	Pressure (bar)	Plates/metre
1950s	100, irregular	<10	1500
1967	50, pellicular	<10	6500
1972	10	15	40000
1976-1980	5	20-50	50000-100000
1980-1992	3	150	120000-150000
2000	2.5	200	160000
2003	<2	400	220000
2007	2.7, core-shell	100	210000

1.1.3 Core-Shell Particles

The concept of pellicular particles, a type of core-shell particle containing a glass bead or spherical polymer core, was initially suggested and used in the late 1960s.[3] It was noted by Horváth *et al.* that to achieve high speed and resolution in HPLC, long columns packed with small particles are required, operated at high mobile phase velocities resulting in high operating pressure. It was theorised that the available pressure drop is best exploited by using columns with low reduced plate heights in the practical range of mobile phase velocity. Pellicular particles were synthesised, meeting these requirements. Particles consisted of thin, uniform porous spherical shells supported by non-porous, mechanically strong glass spheres. The early generation of pellicular particles and shell particles were covered in the review by Guiochon *et al.*[33] At about the same time as Horváth, particles with a comparatively thicker shell were prepared by Kirkland.[34, 35] The spherical shape and

greater mechanical strength of these particles resulted in a higher column stability and a better reproducibility than columns packed with the irregularly shaped silica particles available at the time.

The development and use of core-shell particles became popular in the 1970s with materials produced by several brands, for example Zipax (Dupont), Corasil I and II (Waters) and Pellicosil (Macherey-Nagel). However, major improvements in the manufacture of fully porous particles also took place at the same time, which eventually led to the disappearance of core-shell particles altogether. More recently, requirements of improved analytical throughput have led to the need for greater column efficiency. In response to this, manufacturers have developed sub-2 µm totally porous particles; however these cannot be operated on conventional HPLC instruments which allow only moderate operating pressure. This has led to the rejuvenation of core-shell particles as an alternative.

The class of core-shell particles that are now widely used for chromatographic applications was initially developed by Agilent Technologies, who later synthesised and marketed these particles under the name Poroshell. The first "modern" core-shell material to be marketed however can be attributed to the 2.7 µm Halo material produced by Advanced Materials Technology (AMT).[36] The owners of AMT were later subject to a lawsuit filed by Agilent due to misappropriation of trade secrets after developing core-shell particles using confidential information they had learned while employed at Agilent.

Since their reintroduction, core-shell silica particles have been increasingly used for highly efficient separation with fast flow rate and relatively low back pressure.[33] The solid core plus the porous shell results in a larger particle diameter and significantly lower back pressure compared to sub-2 µm particles. The porous shell and small solid core may also provide higher surface area for the separation to occur. As an example, 2.7 µm core-shell silica particles with 1.7 µm core and 0.5 µm thick porous shell can yield efficiency close to that of sub-2 µm particles but with operation pressure similar to 3 µm particles.[37] The advantage with core-shell particles as packing materials is that the smaller pore depth drastically reduces the volume present for broadening from longitudinal diffusion (B term in the van Deemter equation). The shortened diffusion path length has also been shown to reduce the contribution of the C term due to fast mass transfer.[32, 38]

For chromatographic applications there are a number of core-shell particles commercially available in a variety of particle sizes, bonded phases and column dimensions. Examples include Poroshell (Agilent), Halo (AMT), Cortecs (Waters), Kinetex (Phenomenex),

Eiroshell (Glantreo), Accucore (Thermo Fisher Scientific) and Ascentis Express (Supelco). While all are marketed as core-shell materials and the specifications for a typical 2.7 µm material suggest similar particle diameters, there may be differences between the properties of the silica. For example the pore size, surface area, ratio of core:shell, % carbon loading and bonding density may vary, which should all be considered when selecting a column.

1.2 Preparation Methods for Core-Shell Particles

As the name suggests, core-shell particles are a class of particles comprised of a central core and surrounding shell. The two substituent parts can be composed of different materials, or the same materials with different structures. Figure 1.3 shows a schematic representation of different particle types with the core and shell(s) expressed in different colours. The core may be formed from a single sphere (Figure 1.3 A) or aggregation of several smaller spheres (Figure 1.3 B). It is possible to have a hollow shell with an internal sphere, described as a rattle-like or yolk-shell structure (Figure 1.3 C).[39] The shell structure can be a continuous layer (Figure 1.3 A-C), attachment of many smaller spheres onto a large core sphere (Figure 1.3 D and E)[40] or an aggregation of core spheres (Figure 1.3 F).[41]

Complex core-shell structures may also be made via incorporation of smaller spheres within the shell (Figure 1.3 G)[42] or with multiple shells (Figure 1.3 H).[43-45] Both the core and the shell can be composed of a non-porous material or have desirable and tuneable porous structures. The core-shell particles used in chromatography usually have both parts made from silica, but with a non-porous core and a porous shell (Figure 1.3 I). The size of the core particle, the shell thickness and shell porosity can be tuned to suit many different types of chromatographic applications. Core-shell particles are commonly synthesised via a multiple-step processes. The core particles are initially synthesised and the shell is then formed around this core using a variety of methods, depending on the type of core and shell materials and the desired morphology.[46]

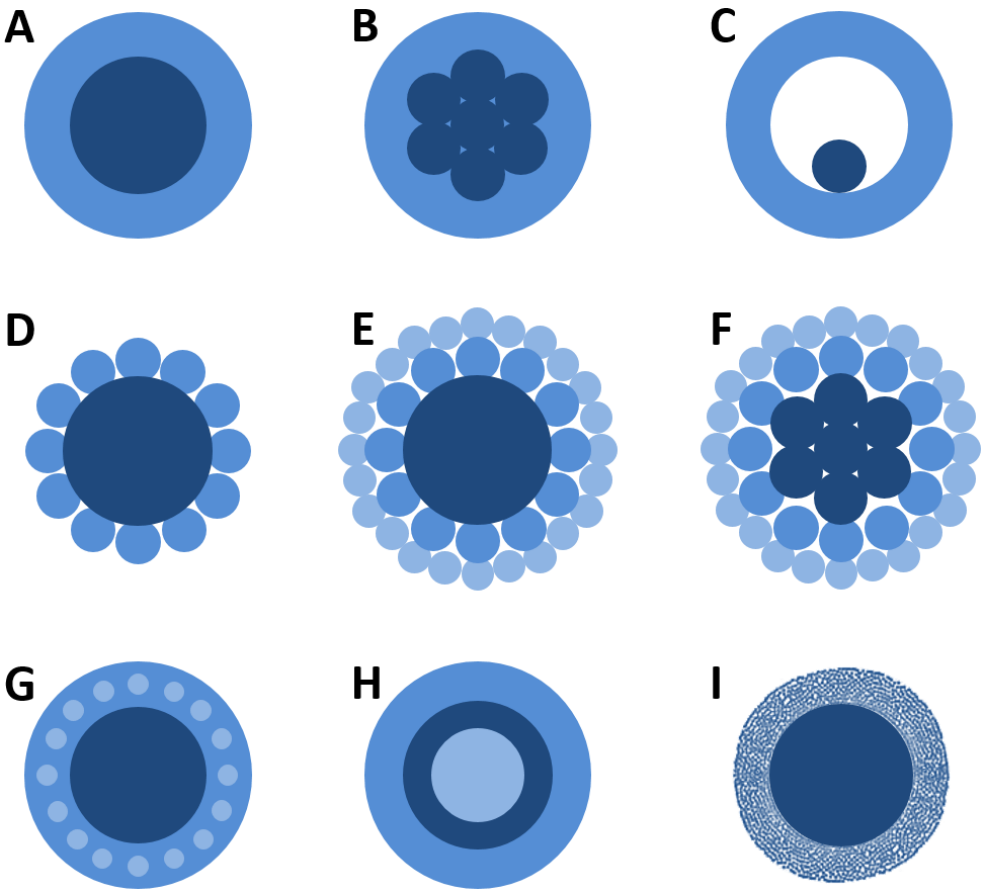

Figure 1.3 Schematic representation of different types of core-shell particles.[47]

Core-shell nanoparticles (<1 µm diameter) have been more extensively investigated compared to core-shell microspheres (1-1000 µm). The advantage of core-shell microspheres compared to nanospheres however is that they can be easily isolated by simple filtration or centrifugation. Silica core-shell microspheres are now routinely used as packing materials in HPLC because of the comparable size to existing spherical particles and the use of nanospheres would result in extremely high operating pressures.

The drive in the preparation of core-shell particles is to combine the desired properties of different materials and structures in order to offer a synergistic effect, to stabilise the active particles, or to provide biocompatible properties. For example, nanoparticles comprised of platinum-cobalt (Pt_3Co) intermetallic cores and a platinum shell with a thickness of 2-3 atomic layers could enhance their activity and stability as oxygen reduction electrocatalysts.[48] Nanoparticles are often coated with a layer of silica to improve stability in a water medium and provide biocompatibility for biomedical applications.[49, 50]

Many examples of core-shell microspheres have incorporated polymer microspheres such as polystyrene and poly(methyl methacrylate), or silica microspheres as the material for the core sphere.[51] The shells are commonly comprised of metal or oxide nanoparticles. After heat treatment or dissolution to remove the core, hollow spheres can be produced.[52] A rattle-like core-shell structure may be prepared this way when small spheres are present in the core spheres, provided that the small spheres cannot be removed or decomposed when the core spheres are removed.[53] There are numerous reported methods for preparing core-shell microspheres. The main focus in this section is on those methods used to prepare particles suitable for use in liquid chromatography.

1.2.1 Early Attempts

As mentioned earlier, the first generation of pellicular particles were introduced in the late 1960s by Horváth *et al*.[3] These particles were designed for use in liquid-liquid chromatography (LLC), acting as a support for a liquid stationary phase. Spherical glass beads around 50 µm in diameter were coated with a thin film of styrene, divinylbenzene and benzoyl peroxide. Polymerisation and crosslinking were carried out at 90 °C in an aqueous suspension of the coated beads. Organic chemical reactions could then be made on the aromatic rings of the coating to provide strong anion or cation exchangers by the bonding of sulfonic acid or quaternary ammonium ions. Impressive separations of a mixture of ribonucleosides were performed on a 2 m × 1 mm column packed with these particles.[54]

Kirkland *et al.* produced the first shell-type particles that can be likened to the modern core-shell particles used today, described as controlled porosity supports.[34] The material consisted of non-porous spherical core particles coated with a uniform porous shell of controlled thickness and porosity. Particle size was in the region of 40 µm. Synthesis of the shell was achieved by a layer-by-layer method (discussed later), where charged core spheres were treated with an organic colloidal material bearing the opposite charge. The excess organic material was removed, followed by immersion of the coated core particles into a dispersion of inorganic microparticles possessing an opposite charge to that of the organic layer. Repeating the process by alternating between organic colloid and inorganic microparticles resulted in the addition of multiple shell layers. Once the desired thickness had been achieved, the organic layer was removed by thermal treatment, leaving behind layers of the inorganic material.[55] The particles showed greater mechanical strength

compared to irregular packing materials available at the time, resulting in higher column stability and improved reproducibility. Several manufacturers later developed their own versions of these particles for use in LLC.

A second generation of core-shell particles was reported by Kirkland *et al.* in 1992. These were named Poroshell and composed of an ultra-pure non-porous silica core with a thin porous shell.[56] The core particles were prepared by sintering 7 µm porous silica Zipax particles at 1050 °C, reducing the surface area to less than 1 m^2/g. Following elutriation, this resulted in non-porous core particles around 5 µm in diameter. To form core-shell particles, co-spray-drying of an aqueous silica sol mixture and dense silica beads was performed so that a uniform porous shell of around 1 µm thickness formed around the core. Resultant particles were sintered then rehydroxylated for subsequent surface chemical modification. The Brunauer-Emmett-Teller (BET) surface area was measured by nitrogen adsorption to be 13 m^2/g, with a pore size of 30 nm. A disadvantage to the method was the formation of some totally porous microspheres that could not be effectively separated from the desired core-shell particles of the same size.

A coacervative approach was later employed to improve the quality of the Poroshell particles.[57] The core particles were again prepared by sintering 7 µm porous silica Zipax particles to form 5 µm non-porous core particles. These core particles were then coated with a urea-formaldehyde/silica sol coacervate film. Elimination of the urea-formaldehyde polymer by heating resulted in a layer of silica microparticles. Sintering was performed to increase particle strength and eliminate unwanted micropores, followed by rehydroxylation of the surface, simple classification by elutriation and bonding with a suitable stationary phase. Rapid separations of polypeptides, proteins, and DNA fragments were demonstrated under gradient conditions using a column packed with C18 functionalised particles.

More recently, an improved coacervative approach was developed by Chen *et al.* to produce core-shell particles for use in HPLC.[58, 59] A schematic of this method is shown in figure 1.4. In this method, solid silica spheres are modified with a proper functionality, such as a urea-formaldehyde polymer. These are then suspended in coacervation reaction mixtures of urea, formaldehyde, and colloidal silica sol under acidic conditions. A coacervate of urea-formaldehyde polymer and ultrapure silica sol particles is formed and is then coated on the solid cores. The urea-formaldehyde polymer is removed by burning in an oven and the particles are strengthened by sintering at high temperature. Particles

produced ranged 2.7 to 3.5 µm in diameter, depending on the size of the core particle and the shell thickness and were classified to produce a narrow size distribution.

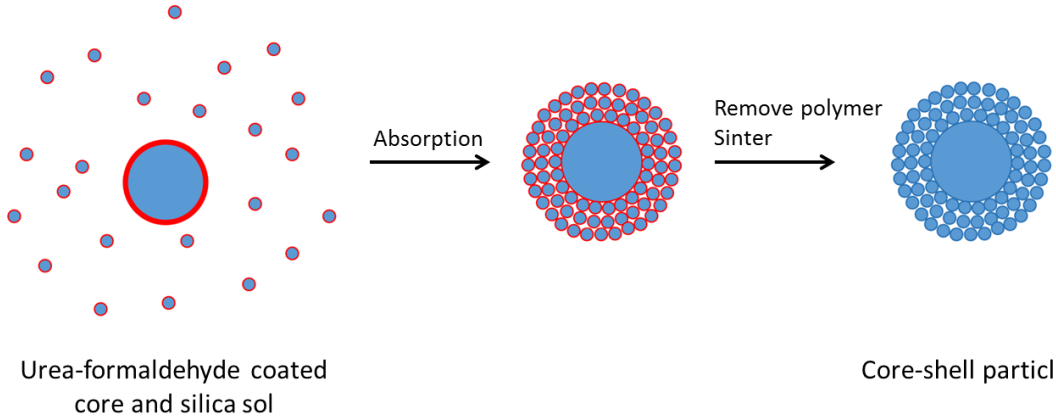

Figure 1.4 Schematic representation of coacervative method for synthesis of superficially porous particles.[59]

A dry blending method can be used to fix small particles onto larger particles when the ratio of the diameters is larger than 10:1. The binary mixture of particles is passed through a high-speed air stream and hit repeatedly by striking pins present on a rotor within a hybridiser. The small particles were fixed to the surface of the larger particles as a result of mechanical action.[60] In one example, core-shell composite microspheres of non-porous silica nanospheres on polyethylene beads were prepared by this approach.[60, 61] The diameters of the beads were 5, 10, and 20 µm, respectively. Separation of a protein mixture within 10 minutes was demonstrated by the column packed with these C18 bonded core-shell microspheres.[60] Similarly, a double-coating layer of silica and titania nanospheres on polyethylene beads was generated. When employed as a complex stationary phase for HPLC, the surface double layer caused a change in the surface acidity of the oxides, rather than just a mixture of two stationary phases. The separation of acidic and basic drugs was performed via a multiple retention mechanism.[62]

1.2.2 Layer-by-Layer Approach

The layer-by-layer (LbL) approach utilises electrostatic interaction (and also hydrogen bonding, covalent bonding and van der Waals interactions) between positively and negatively charged species to assemble multiple layers together. A schematic of this method is shown in figure 1.5. This technique has been widely used to prepare composites and microcapsules for biomedical applications.[63] Microparticles with suitable surface charges are used as the core and alternative layers of oppositely charged species, for example negatively surface-charged silica nanospheres and cationic polymer poly(diallydimethylammonium chloride), are built up onto the core particles. The removal of the core particles produces hollow capsules.

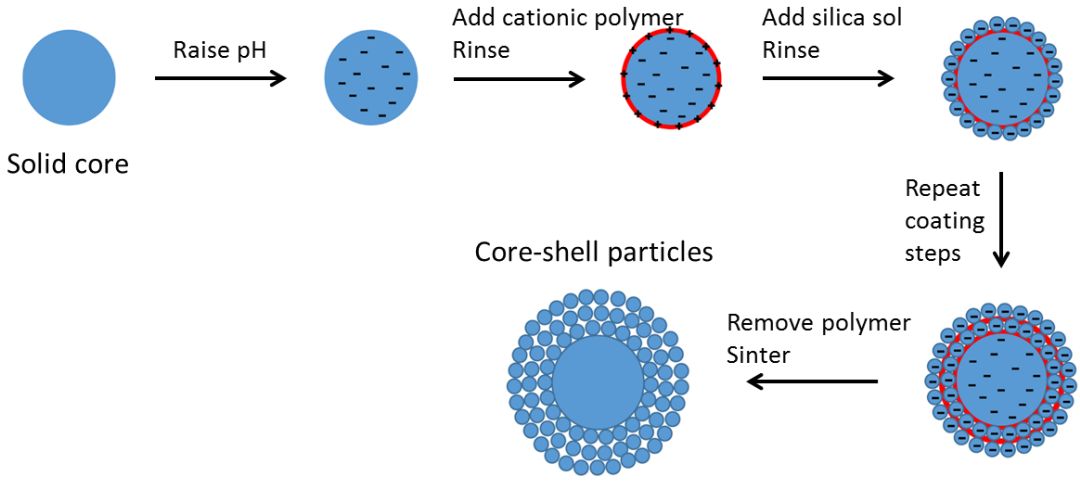

Figure 1.5 Schematic representation of the LbL process for synthesis of core-shell particles.[59]

A large percentage of core-shell silica particles available on the market for chromatographic use are now prepared by the LbL approach.[33] Using a method developed by Kirkland *et al.*, non-porous core particles are firstly treated with a polyelectrolyte, for example negatively charged silica particles bound with a cationic polymer. Excess polyelectrolyte is removed by rinsing. The coated core particles are then immersed in a dispersion of nanoparticles with charges opposite from those of the organic polyelectrolyte. This process is repeated by alternating immersions between the polyelectrolyte solution and the nanoparticle suspension until the desired shell thickness is achieved.[64] The resulting particles can then be treated thermally to remove the organic

polyelectrolyte and produce solid-core porous-shell particles. Figure 1.6 shows the scanning electron microscope (SEM) and transmission electron microscope (TEM) images of 2.7 µm Halo core-shell particles produced by this method.[65] The solid core and the porous shell structure can be clearly seen. Similar morphologies are observed for other types of core-shell particles, though these may vary in particle size, shell thickness, and pore size. These particle characteristics may be used to explain the difference in chromatographic performances of various manufacturers' core-shell columns.

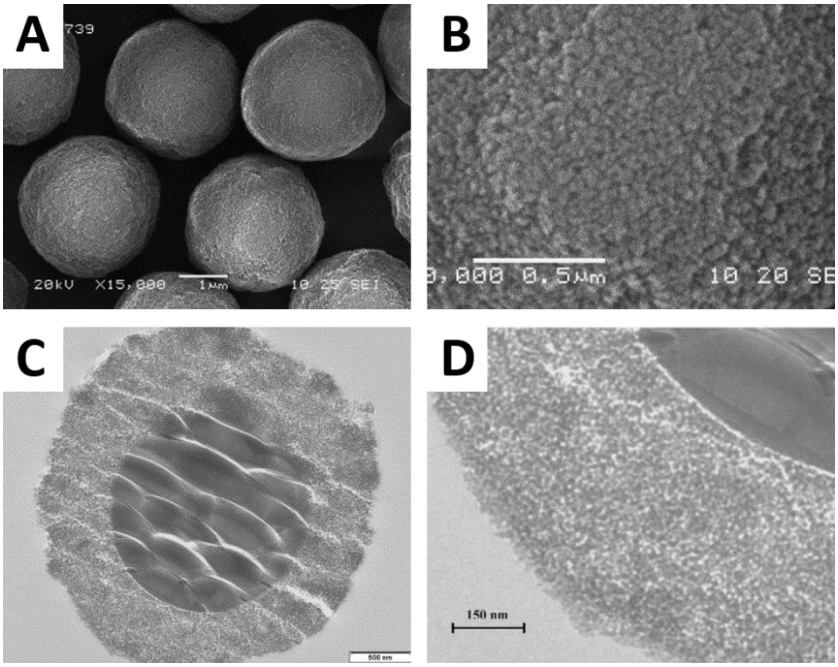

Figure 1.6 The morphology and pore structure of Halo 2.7 µm particles. SEM images (A and B) show the core-shell microsphere and the surface pore structure. TEM image (C) shows the solid core and porous shell structure. High resolution TEM image (D) shows the pore structure within the shell.[65]

Core-shell particles with quoted diameters of 1.6, 1.7, 2.5, 2.6, 2.7, 3.6 and 5 µm are currently available from several manufacturers. It should be noted that the size distributions may be obtained using different sizing methods, and by the use of either number or volume statistics. Additionally, physical properties may also differ between manufacturers; hence these particles are frequently evaluated together in comparison studies.

Recently developed 1.3 µm Kinetex core-shell particles have shown excellent chromatographic performance. These particles consisted of non-porous cores around 0.9 µm in diameter and porous shell 0.2 µm in thickness. The column packed with 1.3 µm particles gave peak capacity values that were 20-40% higher for the same analysis time than a reference column packed with 1.7 µm fully porous particles.[66] The obtained column efficiency, H_{min} = 1.95 µm, corresponds to a plate count of around 500000 plates/m, which is thought to be the lowest ever reported plate height value for a commercial column. The separation impedance of this column was also particularly low with E_{min} = 2000. It should be noted that the optimal linear velocity and hence the lowest possible H value could not be reached before exceeding the upper pressure limit of the UPLC instrument. It means that with such column, the major contribution to band broadening is longitudinal diffusion.[67] Comparison of 1.3, 1.7, 2.6 and 5 µm particles showed that the highest performance was achieved with the 1.3 µm material when a very short analysis time was required without the need for high resolution. The 5 µm material proved to be the best for high resolution separation if a longer run time was acceptable.

1.1 µm superficially porous particles with a 0.1 µm porous shell were synthesised by Blue *et al.*[68] 1 µm diameter non-porous silica spheres were heated at 1000 °C to produce 0.9 µm particles which were then rehydroxylated for the LbL coating of different sources of silica nanospheres. The particles were synthesised by alternating a layer of positively charged polyelectrolyte and negatively charged colloidal silica onto the non-porous silica core, using the Kirkland method.[64] The layers were alternated until the desired porous layer thickness was achieved. Resultant particles had narrow size distribution with a surface area of 52 m^2/g and pore diameter of 7.1 nm.

More complicatedly, chiral core-shell silica microspheres with a trans-(1R,2R)-diaminocyclohexane moiety bridged in the mesoporous shell were synthesised.[69] The chiral shell was formed by the co-condensation of N,N'-bis-[(triethoxysilyl)propyl]-trans-(1R,2R)-bis-(ureido)-cyclohexane (DACH-BS) and TEOS, using octadecyltrimethylammonium chloride and triblock poly(ethylene oxide)-b-poly(propylene oxide)-b-poly(ethylene oxide) copolymer as the templates. The chiral shell was attached via an alternative LbL method to that used by Kirkland. Non-porous core particles were added to a solution containing the templates, followed by addition of DACH-BS and TEOS to form a layer of mesoporous chiral nanospheres on the surface. The resultant particles were isolated, washed and the process repeated multiple times to build up the shell. The mean particle size was 2.3 µm, with a shell thickness of approximately 100 nm. The BET surface area of these particles was

measured by nitrogen adsorption to be 147 m^2/g, similar to that of commercial core-shell materials. When packed into HPLC columns the material provided fast enantioseparations of binaphthol, bromosubstituted binaphthol and biphenathrol.

Manufacturing core-shell silica particles with the LbL method is a time-consuming approach, offering low productivity. This is due to the numerous centrifugation and classification steps that are needed to remove any loosely bound species in each coating cycle to avoid particle aggregation. A multilayer-by-multilayer (MLbML) approach was developed to increase the process speed.[70] Silica core particles and silica nanoparticles were prepared by the Stöber process. The shell multilayers were assembled by repeated consecutive deposition of poly(diallyldimethylammonium chloride) (PDADMA) and silica nanoparticles. The polymer, depending on molecular weight, can absorb several layers of sol particles at a time. This allows for 5-10 layers of nanoparticles to be deposited per coating cycle, vastly improving the productivity of the synthesis. After five coatings, the surface area, pore volume, and average pore size of the core-shell particles were measured to be 255 m^2/g, 0.54 ml/g and 9.4 nm, respectively. The particles were also found to have a narrow size distribution. Resultant particles were around 900 nm in diameter which are perhaps too small for use in HPLC, however the layering process could be performed onto a larger diameter core particle.

Although fewer coating steps are required compared to the LbL method, the MLbML method is still a time-consuming approach due to the numerous centrifugation steps that are needed to remove the extra material and loosely bound species in each coating cycle. Each additional process step increases the variability of the process and decreases the yield.

Core-shell silica particles may be further coated with a layer of carbon. Carbon is interesting as it is chemically inert and highly stable for a range of test mixtures. Pre-formed commercial 2.7 µm core-shell silica particles were coated with carbon by firstly treating with aluminium.[71, 72] The amount of added aluminium corresponded to a full monolayer (assumed to be 8 $\mu mol/m^2$) of silanol groups on the silica surface. Chemical vapour deposition of carbon onto the aluminium surface was then conducted at 700 °C for 6 hours using hexane vapour as the carbon source. These carbon clad particles produced reasonable peak capacity values for the gradient separation of indole metabolites. During fast LC × LC analysis, the carbon-clad column also provided excellent focusing in the second dimension.

1.2.3 Shell Synthesis on Pre-Formed Cores

An alternative to the LbL approach is the formation of a shell onto the core particle by various synthetic methods. This method is most commonly used to prepare nanoparticles,[73, 74] however silica microspheres, polymer microspheres and other particles have been used as the cores in the preparation of a wide range of core-shell particles. For example silica-polymer core-shell particles by silica supported polymerisation,[75] core-shell hybrid particles and hollow structures by precipitation polymerisation,[76] silica-metal organic framework (MOFs) core-shell microspheres[77, 78] and shaped nanoparticle-shell nanospheres.[79] Hollow shell structures or capsules can be produced when the core polymer particles are removed by thermal treatment or washing.[52] Silica spheres are employed to prepare various inorganic or composite core-shell structures although silica can also be removed by acid etching or alkaline washing to produce hollow structures.

Silica is the main source for the core-shell particles used in chromatography. The Stöber reaction is a simple method commonly used to prepare uniform non-porous silica microspheres and nanospheres, where a tetraalkoxysilane is added to an excess of water containing a low mass alcohol, under basic conditions.[51] Most of the non-porous core particles used in the subsequent production of core-shell materials are synthesised by this method. The reaction can also be easily modified to produce uniform nanospheres in a variety of sizes that are commonly used as the substituent particles that make up the porous shell. The Stöber method can also be modified to produce mesoporous silica spheres via the introduction of a surfactant which can act as a template, for example cetyltrimethylammonium bromide (CTAB), Pluronic P123 or Pluronic F127.[80, 81]

Reactions based on the Stöber method have been frequently reported to form a silica coating on different types of particles, for example gold colloids and silica coated magnetite particles.[82, 83] In one example, the sol-gel process of TEOS and n-octadecyltrimethoxysilane was used to form a mesoporous shell onto previously prepared silica core spheres under basic conditions. The resultant particles were calcined to remove the porogen, after which porosity was found only in the outer shell. Particles sizes up to around 1 µm in diameter were produced. Depending on the amount of porogen in the reaction it was possible to obtain surface areas up to 350 m^2/g, with pore diameters up to 4 nm. The thermal stability and the high specific surface area make these silica beads suitable as adsorbents for various applications, such as capillary electrochromatography and ultrafast HPLC.[84]

In another example, preformed iron(II,III) oxide (Fe_3O_4) nanoparticles were coated with a thin layer of silica using a sol-gel approach to obtain non-porous silica-Fe_3O_4 composites. A surfactant templating approach was then applied, using CTAB as the template, to deposit a mesostructured CTAB/silica composite onto the silica-Fe_3O_4 microspheres. Finally the CTAB templates were removed to form a perpendicularly aligned mesoporous silica shell.[85] Li *et al.* produced monodisperse poly(styrene-co-acrylic acid) spheres by surfactant-free emulsion polymerisation, which were then used as core particles to form a silver nanoparticle shell via in-situ reduction of silver nitrate. The silver nanoparticle shell was stabilised by the formation of a silica layer using a sol-gel process. The shell was functionalised with reactive epoxides which could be further modified with amine or carboxylate groups for the derivatisation of biological molecules. These composite core-shell microspheres were used as high performance surface-enhanced Raman spectroscopy substrates and molecular barcode labels.[86]

1.2.4 One-Pot Synthesis and Spheres on Sphere Silica Particles

The core-shell silica particles intended for HPLC applications are usually prepared by a time-consuming LbL approach. A one-pot synthesis of core-shell particles suitable for packing into HPLC columns would be highly advantageous, offering potential benefits such as reduced reaction time, easier quality control, lower material costs, and process simplicity for scale-up. Han *et al.* reported that uniform core-shell nanospheres with a silver nanoparticle core and a thick mesoporous silica shell could be produced from a one-pot synthesis by subsequent addition of silver nitrate and TEOS with sodium hydroxide as a basic catalyst.[87] A one-step synthesis was also performed by Fuertes *et al.* to prepare SiO_2@resorcinol-formaldehyde resin nanospheres around 220 nm in diameter under Stöber conditions.[88] The reaction utilised the fast reaction rate of forming silica spheres and slow rate of forming resorcinol-formaldehyde spheres. There have however been very limited reports on the one-pot synthesis of core-shell silica microspheres which are suitable for HPLC.

Ahmed *et al.* reported a one-pot synthesis of a new type of core-shell silica from a single precursor, 3-mercaptopropyltrimethoxysilane (MPTMS).[40] These particles possessed a unique spheres on sphere (SOS) morphology composed of a solid microsphere core around 5.5 μm in diameter with a coating of nanospheres approximately 200 nm in size. Typically, an aqueous solution of poly(vinyl alcohol) (PVA) and CTAB was prepared.

Methanol, ammonium hydroxide and MPTMS were added sequentially with stirring. The reaction was stirred for 24 hours at room temperature and the resultant SOS silica particles collected.

In this one-pot synthesis, particles were formed in two stages, shown in figure 1.7. Silica nanoparticles were initially formed which grew to form the microsphere core within the first 30 minutes. In the second stage, at a reaction time of around 30 minutes, the silica nanosphere shell began to form on the core surface. After a reaction time of 180 minutes, the SOS particles were fully formed and the particle morphology did not change significantly beyond this point. It was found that the reaction time could be reduced to around 5 minutes by microwave heating at 40 °C.[89] Varying the preparation conditions, for example concentration of ammonium hydroxide, reagent concentration, stirring rate or solvent type, allowed a degree of control over the particle morphology, specifically core microsphere size, nanosphere size and density of nanospheres on the surface of the core. A HPLC column packed with functionalised SOS particles showed fast separation of a protein mixture with low back pressure.[40, 89] The early synthesis, properties and applications of SOS particles will be discussed in more detail in later chapters.

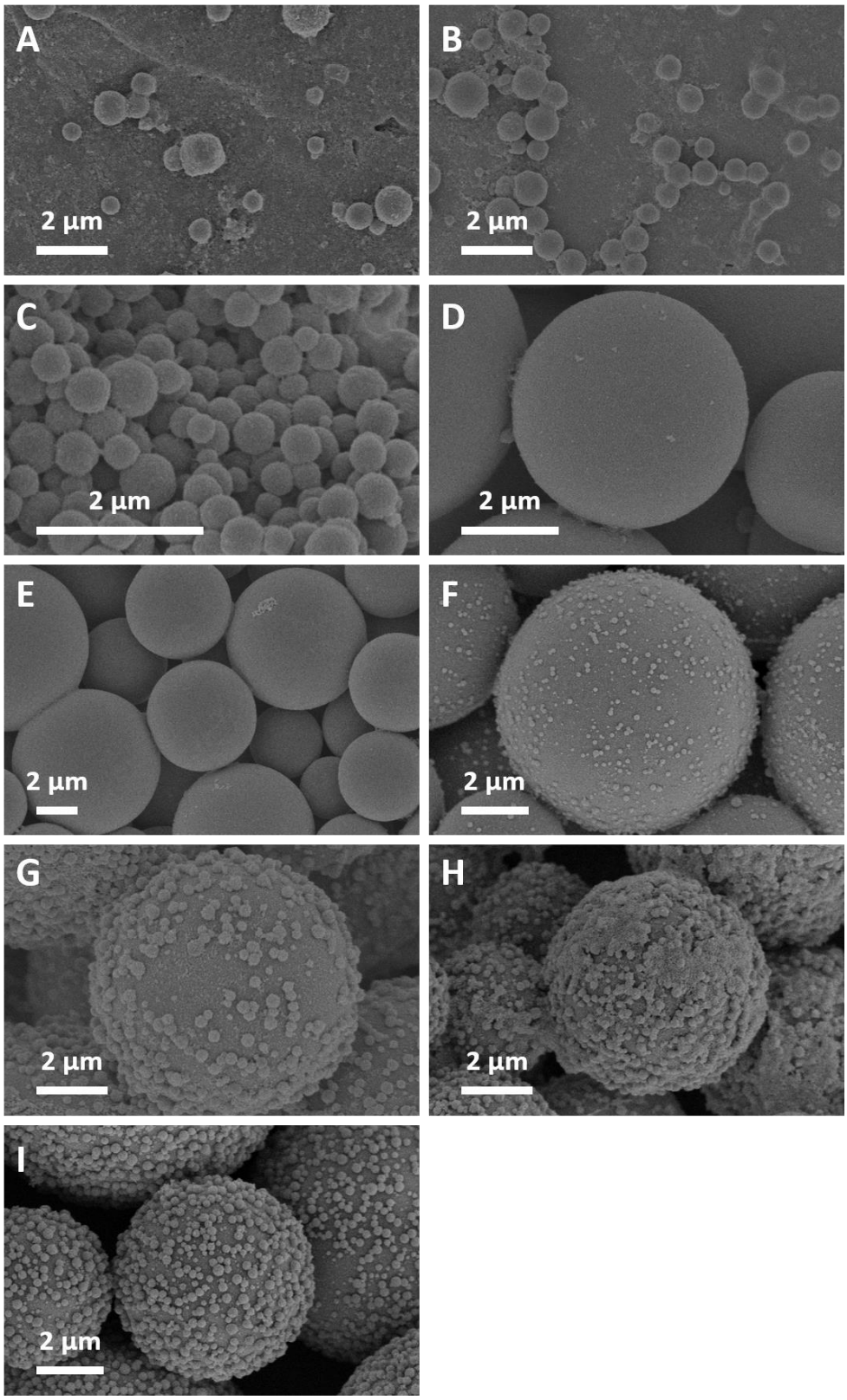

Figure 1.7 SEM images showing morphology evolution at different reaction times until the SOS particles are formed. Reaction time = 0.5 (A), 2 (B), 5 (C), 10 (D), 20 (E), 30 (F), 45 (G), 60 (H), 180 min (I).[40]

1.2.5 Droplet-Based Microfluidic Approach

Microfluidics is a highly interdisciplinary research area which involves physics, chemistry, engineering, materials science and biology. The technology utilises extremely small volumes (10^{-9} to 10^{-8} L) of fluids, using channels with dimensions from tens to hundreds of micrometres. The technique has been widely used to prepare extremely monodisperse emulsions, double emulsions and microspheres with complex morphologies and compositions.[90-92] Since monodisperse microspheres are thought to increase chromatographic performance by improvements in the packing quality, the microfluidic method could be very important in developing novel and high performance packing materials for chromatography. Conventional emulsification methods, for example stirring, homogenisation or sonication, typically produce polydisperse droplets that can be transformed into spherical microparticles through chemical or physical consolidation. The monodisperse emulsions produced by microfluidics can instead be used to yield highly uniform microspheres. Functionalised microspheres with complex morphologies, including core-shell structures, have been realised through shaping, compartmentalising, and microstructuring.[93]

Pickering emulsions, where the droplets are stabilised by small particles, are widely used to produce core-shell particles or capsules. An inside-out microfluidic approach was developed to produce monodisperse particle-stabilised emulsions and nanoparticle decorated microspheres. The nanoparticles are inducted in the droplet phase, thus minimising waste.[94] However, a double emulsion approach is probably more used in producing core-shell particles via the microfluidic approach. After forming a double emulsion, the droplets can be crosslinked or condensed to form dry core-shell particles. For example, poly(lactide-co-glycolide)-dichloromethane solution was injected through an inner capillary into a flow of aqueous alginate solution. The resulting oil in water emulsion droplets were then dispersed in a flow of toluene. The crosslinking of alginate and removal of dichloromethane produced PLG-alginate core-shell particles.[95]

A single emulsion method could also be used to prepare core-shell particles. As shown in figure 1.8, uniform droplets of silica sol prepared from TEOS were injected into a continuous oil phase containing tetrabutyl titanate (TBT), liquid paraffin, Span 80 and oleic acid, via a coaxial microfluidic device. As soon as the droplet was formed, due to water diffusion, the hydrolysis of TBT occurred at the water/oil interface to form a thin gel around the droplet. Titania-silica core-shell microspheres were obtained after calcination. The

dispersity and size of the microspheres could be controlled by changing the microfluidic flow parameters.[96]

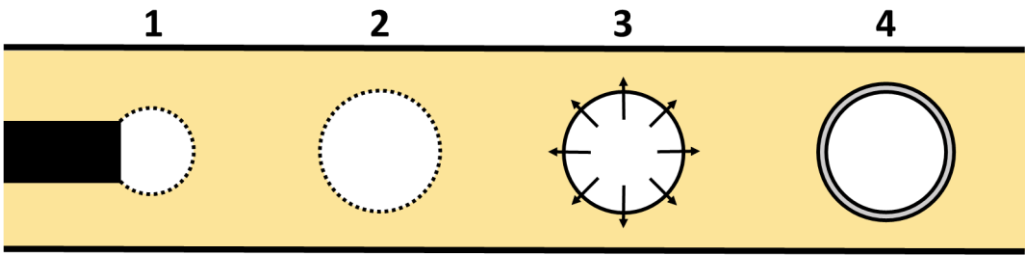

Figure 1.8 Scheme representing the preparation of silica-titania core-shell particles by a microfluidic approach.[96] Stages: 1) Silica sol droplet (white) is injected into the continuous oil phase (yellow). 2) TBT hydrolyses at the interface to form titanium hydroxide. 3) A thin shell forms around the silica sol droplet and water diffuses through the shell to the oil phase. 4) Growth of the shell.

A simple T-junction microfluidic device was also used to produce raspberry-like silica particles.[97] A silica sol formed from TEOS in ethanol and hydrochloric acid solution was pumped via one focusing inlet, while a sodium bicarbonate solution was pumped through a second inlet. Hexadecane containing a small amount of surfactant was used as the continuous phase, allowing the slow diffusion of ethanol from the silica sol precursor droplets. The surfactant acted as a stabiliser to the ethanol-rich droplets. Droplets were generated at a T-junction and travelled along a channel. By the time the droplets exited the device, a significant amount of ethanol had been removed via diffusion into the continuous phase, allowing formation of spherical, monodisperse silica gel particles. When solvent was fully removed from the gel particles by oven drying, the particle surface became corrugated and smaller particles grew outwards from the surface forming the raspberry-like morphology.

Although highly uniform particles can be produced from this method, the production rate is very slow due to the extremely small volumes involved. However, recent research at The University of Liverpool has led to a method of producing particles using an inkjet printer cartridge to produce uniform droplets of destabilised silica sol which were fed into liquid nitrogen. After the nitrogen had evaporated, monodisperse particles remained in the vessel. Using this method, up to 64000 particles could be produced per second.

1.3 The Fundamentals of Core-Shell Particles for HPLC

The underlying reasons for the advantages and performance benefits associated with solid-core porous-shell materials have been the subject of much debate. Initially the advantages were associated with the superior particle size distribution and the reduction in the resistance to mass transfer terms.[2, 31] Although there is an improvement in performance due to these physical parameters, the initial claims were not quite accurate. The combined effects from the monodisperse size distribution and reduced mass transfer effects due to the solid core are not as significant as for other contributing factors. In order to better understand how the morphology of core-shell particles improves the chromatographic performance, it is necessary to investigate the individual terms of the van Deemter equation[38] to determine the effect of the dispersion of the solute molecules within a packed bed environment. The equation is shown with a schematic van Deemter plot in figure 1.9, illustrating the effect of each of the three terms on the plate height.

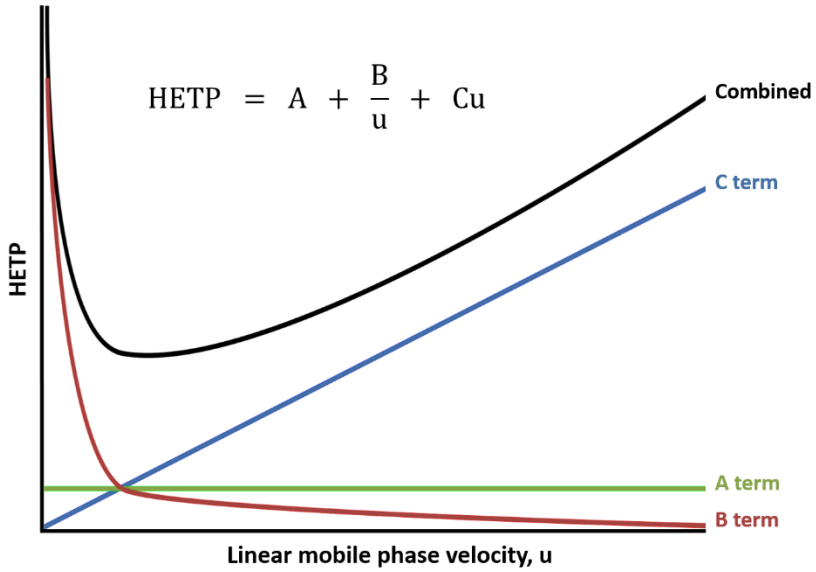

Figure 1.9 The van Deemter equation and plot, where HETP (H) is the height equivalent to a theoretical plate and u is the linear velocity of the mobile phase. A, B and C are numerical coefficients related to the parameters of the column.[38]

1.3.1 A Term

The first of the band broadening factors is the A term, eddy diffusion. A single analyte molecule within a band of analytes passing through a column can take one of many different paths. Multiple paths may arise from inhomogeneity in the column packing, hence the A term is often referred to as the packing term as it reflects the quality of the column bed. The multiple path effect makes analyte bands broader as they pass through the column. Particle diameter also has a pronounced effect on the diffusion. A larger particle size will deflect an analyte molecule a further distance compared to a smaller particle resulting in a longer path length and thus greater diffusion. The interpretation of the eddy dispersion term of the van Deemter equation has been of high interest to researchers and has improved substantially, although a certain degree of fitting of experimental data is still required to allow for optimisation of the postulated theory. The use of the Knox equation[98] relates an inverse cubic dependency of the linear velocity to the band broadening and has proved successful in the modelling of experimentally derived data.

The dispersion associated with the A term can be considered as an effect from both the diameter of the particles and the quality of the packed bed within the column. It has been shown that the packing density within a column varies radially as a result of the wall effect, which results in increased band broadening. This suggests two distinct components to the A term, one which relates to the short range packing effects associated with a regular packing of spheres, and the other being a long range effect which occurs due to radial inhomogeneity across the column.

It was suggested in some initial marketing literature of core-shell materials that many of the benefits arose simply because of the narrow particle size distribution, resulting in better packing of the particles. Although this is an easy concept to visualise, in practice the difference in size distribution that is quoted for fully porous and core-shell materials is simply not large enough to cause an adverse effect, and the concept is not applicable to the observed high efficiencies associated with core-shell materials. A typical core-shell particle will have $d^{90}/_{10}$ of 1.1 compared to a fully porous material with $d^{90}/_{10}$ of 1.5. It has been shown that this is not a significant enough change to allow for deterioration in the column performance.[99] In fact the data presented by Gritti *et al.* suggested that the performance of any form of sub-3 µm particles could be improved by the addition of small volume fraction of larger particles in the range 3-5 µm.

It is evident from experimental data however that core-shell materials do provide a benefit in terms of the A term. Since this parameter is dependent primarily on the particle size and the packing efficiency, the conclusion is that the column packing is better with core-shell materials than with fully porous materials. The morphology of core-shell particles provides a rougher surface than fully porous spherical particles. As a consequence, there is considerably more shear stress applied to the particles when they are packed. During the packing process, a solution containing a suspension of particles is compressed into the column under high pressure using a specialist packing pump. Once the column is packed, it undergoes a period of rest where this pressure is slowly released, after which the frits and other end fittings are attached. Although it is difficult to initially pack the core-shell material, once the column is packed the amount of shear stress required to overcome the frictional forces associated with the roughened surfaces is so great that bed expansion is virtually eliminated. By comparison, fully porous materials have a much smoother topography resulting in particles that are easier to pack. On consolidation of the bed however, the lack of a roughened surface means that these particles have much less frictional force between them and are able to slide over each other with relative ease compared to the core-shell materials. This results in bed expansion and the creation of bed heterogeneity.

Additionally, the shape of particles may play a part in the packing process. As shown in figure 1.6, core-shell particles are not truly spherical in shape and instead may be better described as slightly elliptic or irregular. As these particles are pumped into the column, the irregular shape experiences unequal force from the solvent flow and thus has the ability to rotate and fill any potential voids in the packed bed. Conversely, smooth spherical particles do not experience this flow difference as they are symmetrical and will therefore travel straight down the column. Voiding in the packed bed is more likely as particles have a tendency to stack, rather than rotate into place.

1.3.2 B Term

The second factor, the B term, is related to longitudinal diffusion and refers to the ability of molecules to undergo Brownian motion when placed in a fluid. In HPLC this is clearly undesirable, therefore it is important that analytes are not retained within the column for a longer amount of time than is necessary. This can be avoided by ensuring the capacity factor is kept at a reasonable amount and also by choosing an appropriate mobile

phase flow rate. A flow rate that is too low will result in excessive dispersion resulting in a broader peak. Simply increasing flow rate however has a negative effect on the C term and thus an optimum linear velocity must be established.

It is also necessary to consider the various zones within the column media that exist, since diffusion within these zones will be different. Diffusion can occur within the bulk media (interstices between particles, column dead volume) and also within the porous media (internal pore system of the particle). One of the biggest advantages to the use of core-shell materials is the reduction in the dead volume of the column. A fully porous material packed into a column will only occupy about a third of the column volume due to the extended pore system, whereas the amount of space occupied by the core-shell material is dramatically increased by about 20-30% due to the solid core.[100] This reduction in the accessible volume results in reduced longitudinal diffusion occurring within the column.

The Garnett-Torquato model can be applied to show the effect that the porous layer has on the effective diffusion.[101-103] The model is consistent with the structure of chromatographic beds made of core-shell particles randomly packed and immersed in a bulk eluent matrix. It takes into account both the geometry of the core-shell particles (the Garnett model) and their random spatial distribution inside the column (the Torquato model). The only approximation made in designing this composite model is that the diffusion hindrance caused by the presence of the partially permeable particles in the eluent bulk is ignored.[104] A plot can be made which shows the variation of the B term with respect to the retention of the analyte and also the internal porosity of the particle, which can be varied by altering the depth of the porous shell. Ω is the ratio of the effective diffusivity in the porous layer of the particle compared to that in the bulk, effectively giving an indication of the retention of a compound, with higher values being more applicable to more retentive compounds.

The minimal value for longitudinal diffusion is obtained when there is limited retention or when the particle does not have any porosity. The diagram in figure 1.10 demonstrates the advantages that reducing the volume of the column by increasing the ratio of solid core to the whole particle diameter (ρ) has on the longitudinal diffusion within the column. It can be seen that there is a significant reduction from B = 7.7 when Ω is 2, and ρ is 0 (high retention, totally porous particle), to B = 1.4 when Ω is 0, and ρ is 1 (low retention, non-porous particle). Although this is an extreme example, there is still an

appreciable change in the longitudinal diffusion when taking a more realistic value for Ω of 0.14.[100] It should be mentioned that the improvement in B term is important only in the low flow rate range. Generally around and above the optimal linear velocity, its impact is almost negligible.

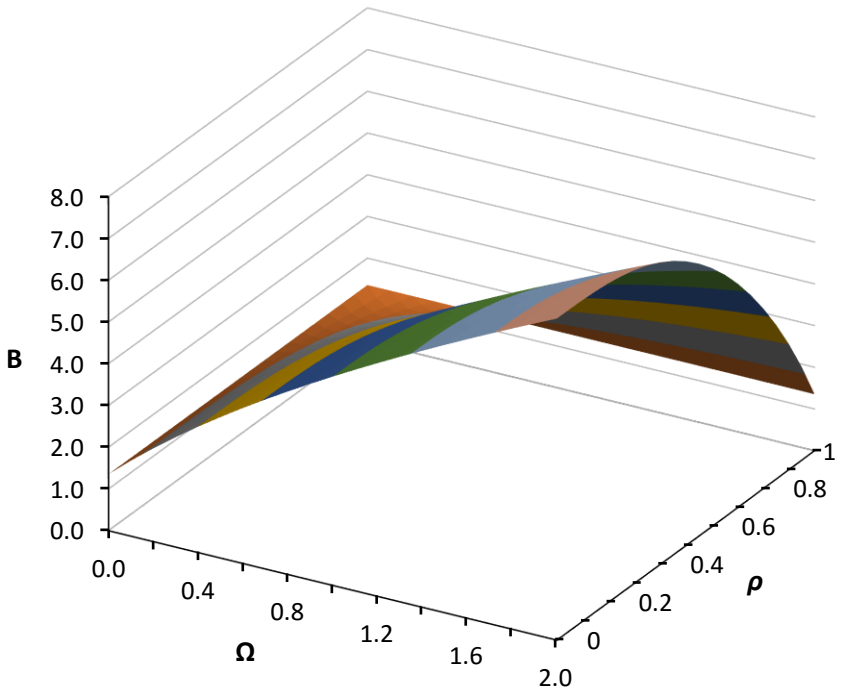

Figure 1.10 The minimal value for longitudinal diffusion (B) is obtained when either there is limited retention (Ω = 0) or when the particle does not have any porosity (ρ = 1).[47]

1.3.3 C Term

The final term to discuss is the C term, or resistance to mass transfer. One analyte molecule passing through the column may diffuse in and out of the porous stationary phase many times while another identical molecule may not necessarily spend as much time in the pore system and is thus eluted earlier. The rate at which analytes are able to diffuse in and out of the pore system dictates the amount of broadening that occurs. As an extreme example, one analyte may spend a long time within the pore structure while another is eluted almost immediately which would result in significant band broadening. It can therefore be seen that increasing the mobile phase velocity also leads to increased broadening of peaks. As with the other terms of the van Deemter model, the C term has

been reviewed and modified since the original publication,[38, 105] for example the inclusion of mass transfer effects due to different flow velocities within the mobile phase and not just within the stagnant regions of the pore structure.

Initially, many of the benefits of core-shell technology were thought to be associated with reduced mass transfer effects. It has since been shown by Gritti that for small molecules this is not the case.[106] The major contribution to the reduction in band broadening in core-shell materials is associated with the reduction in the A and B term dispersion processes through better packing and reduced column dead volume. Using the model proposed by Gritti,[106] it is possible to simulate large and small molecules and to determine the effect that altering the ratio of solid core to the whole particle diameter (ρ) will have on the overall chromatographic efficiency.

Figure 1.11 demonstrates that the porous layer has little effect on the overall H value for small molecules, whereas for larger molecules there is a more increased effect. The contribution of the B term is inversely proportional to the linear velocity and so does not contribute significantly to the overall band broadening at higher linear velocities. It can also be seen from figure 1.11 that although there is a difference in terms of the C term for small molecules when there are different porous shell thicknesses employed, in this case two extremes of ρ = 0.1 and ρ = 0.9 are shown. As an example of current core-shell particles, ρ = 1.7/2.7 = 0.63 for a 2.7 µm material with 0.5 µm shell.

Of greater interest though is the data shown which highlights the difference between the dispersion observed due to mass transfer effects for larger molecules where the diffusion coefficient is much lower. It is evident that the difference in C terms in this scenario is contributing significantly to a difference in the overall dispersion seen with a very thin porous layer compared to a virtually fully porous material. Thus it can be concluded that for large analytes such as proteins and other biomolecules, a thin porous layer should be employed to reduce dispersion effects.

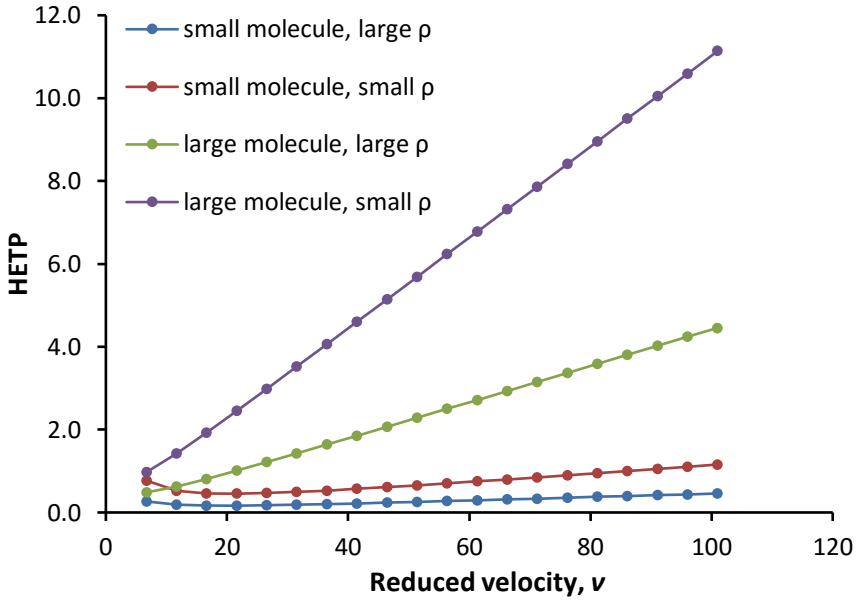

Figure 1.11 The plot shows the relationship of B and C terms of the van Deemter equation with reduced velocity. For large molecules where there is reduced diffusion, the C term has a significant effect as the solid core diameter is reduced. Data obtained from Thermo Scientific.

So far the dispersion associated with the use of monolithic columns has not been discussed, primarily because the dispersion models that are applicable to the treatment of packed bed columns are not directly transferable to monolithic structures. Silica monolithic columns consist of a continuous, porous rod that has a bimodal porosity.[7] These columns are made of a network of through-pores separated by a thin, porous silica skeleton, as seen in figure 1.1. The through-pores measured using mercury intrusion porosimetry were estimated to be 1.7 µm,[6] allowing for unrestricted movement of the mobile phase. Mesopores within the silica skeleton walls were measured by nitrogen adsorption to be 14 nm[107] and generate a large surface area that allows sufficient retention of analytes.

The large interconnected pores in monolithic columns account for their advantages over traditional packed columns[6, 7, 107, 108] since there is substantially less pressure required to obtain the optimal chromatographic efficiency. Due to the reduced pore depths associated with monolithic structures, there is also a reduction in the resistance to mass transfer term, which allows for use at elevated flow rates without loss of performance. However, the first generation monoliths suffer from a lack of radial homogeneity, caused by a few factors. The synthesis of a silica monolithic column involves an exothermic

condensation reaction, with the heat generated being evacuated radially through the monolith and thus generating a temperature gradient. Since the polycondensation reaction is temperature dependent, it will proceed faster in the column centre than at the walls, which can potentially affect the distribution of the porosity. Shrinkage occurs following the synthesis of the monolithic structure, meaning the rod has to be encapsulated by a heat-shrunk PEEK cladding before it can be used for chromatographic purposes.[14, 109] This encapsulation compresses the bed which may cause radial stress and strain. It is also feasible that during the polymerisation process the monolith is initially attached to the column wall, therefore some elastic deformation and breakage may occur as the monolith shrinks and detaches from the column wall.

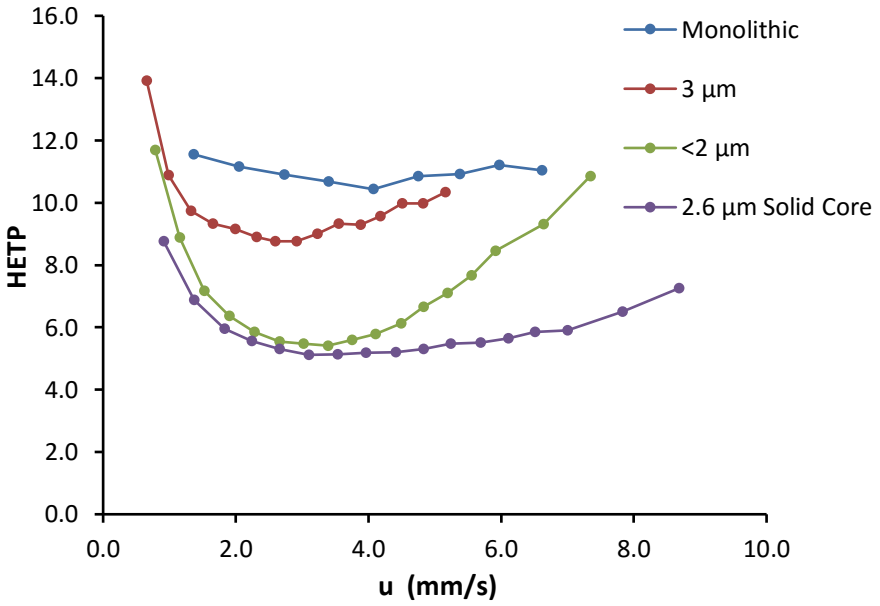

Figure 1.12 Comparison of efficiency using van Deemter plots for Accucore 2.6 µm core-shell microspheres, monolithic column, fully porous 3 µm microspheres and sub-2 µm microspheres. Data obtained from Thermo Scientific.

The radial heterogeneity has been shown to affect the radial distribution of analytes and also the chromatographic efficiency of the column. Indeed, some authors have demonstrated that the column efficiency can be improved by up to 100% by removing this effect.[107, 110] The band broadening process occurring within a monolithic column can be explained by the general rate model.[56, 57, 60, 61] It is therefore possible to produce a value for H, allowing for some comparisons with packed bed columns. Figure 1.12 shows an overlay

of H plotted against linear velocity for a 2.6 µm core-shell, 3 µm totally porous, sub-2 µm totally porous and monolithic column. It can be seen that the overall performance of the core-shell material is greater than the other columns under evaluation, providing the lowest minimum plate height and a relatively flat plot as the linear velocity is increased. The "worst" performance was obtained from the monolithic column, with a plate height of double that obtained for the core-shell column. However, this data does not take into account the amount of pressure required to drive such a separation. It should also be stressed that the van Deemter plot for the monolithic column is much flatter than the core-shell and fully porous materials.

1.3.4 Kinetic Plots

An area that needs further investigation is the concept that the back pressure generated by core-shell particles is lower than that of conventional, totally porous particles of the same column dimension. This is not correct, since the resistive forces exhibited by a bed packed with spherical beads are inversely proportional to the square of the particle diameter, in accordance with the Kozeny-Carmen model.[111]

$$\frac{\Delta P}{L} = \frac{P_0 \eta (1 - \varepsilon_T)^2 \mu_0}{\varepsilon_T^3 d_p^2}$$

Where ΔP is the pressure drop across the column, L is the length of the column, P_0 is a constant dependent on the topography of the column, η is the mobile phase viscosity, ε_T is the porosity of the packed column, μ_0 is the superficial velocity, and d_p is the particle diameter.

Pressure-driven flow through the pores in the shell structure does not occur as the diameters of the pores are too small relative to the interstitial spaces. Consequently, the resistive forces that are present are virtually the same whether the particle is porous or non-porous. Figure 1.13 demonstrates this point with the pressure drop obtained when using a 3 µm particle compared to that obtained when using a core-shell particle with a diameter of 2.6 µm. The observed pressure drop observed with a monolithic and sub-2 µm column is also included for completeness.

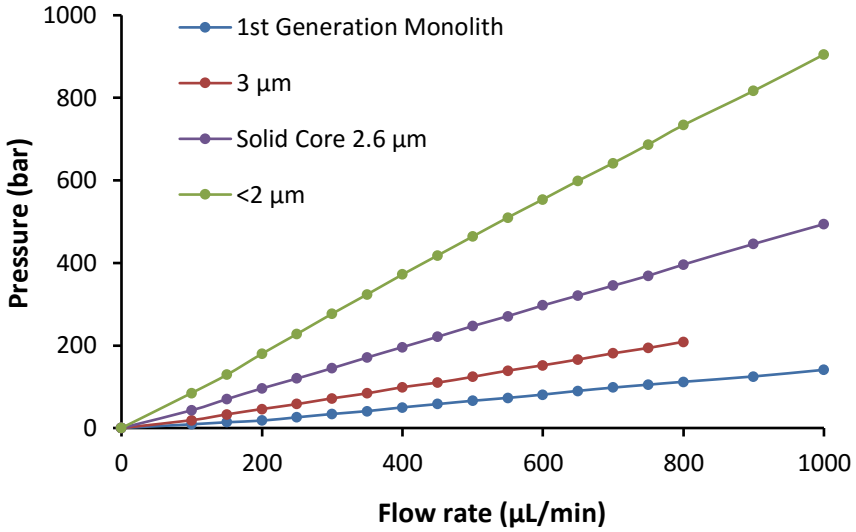

Figure 1.13 Comparison of back pressure for Accucore 2.6 µm core-shell microspheres, first generation monolithic column, fully porous 3 µm microspheres and sub-2 µm microspheres. Column dimensions 100 × 2.1 mm; mobile phase: acetonitrile/water (1:1); temperature 30 °C. Data obtained from Thermo Scientific.

In recent years, kinetic plots have become a highly useful tool by which different HPLC columns, particles, and particle sizes have been compared with each other. Kinetic plots are ideally suited to compare the performance of differently shaped or sized liquid chromatography supports, including monolithic supports which are traditionally difficult to compare against spherical particles. The use of kinetic or Poppe plots,[112-114] and specifically the use of impedance as devised by Knox and Bristow[115] demonstrate the performance of a column, accounting for the flow resistance or the permeability of the column. Impedance (E) is a term that defines the resistance encountered by a compound as it moves down the column, relative to the performance of said column. This gives a true measure of the performance of the column as it incorporates efficiency, time and pressure.

$$E = \frac{t\Delta P}{N^2 \eta}$$

Where t is the elution time of the test compound, ΔP is the pressure drop, N is the observed plate count and η is the mobile phase viscosity.[115]

Figure 1.14 demonstrates that the fully porous materials result in higher impedance, implying that more pressure is required to get an equivalent separation compared to core-shell and monolithic columns. From the data presented in figure 1.14 it is observed that the core-shell column provides the best separation per unit measure of pressure where a high efficiency is required. However, where a lower efficiency is acceptable then the monolithic column outperforms the other three columns.

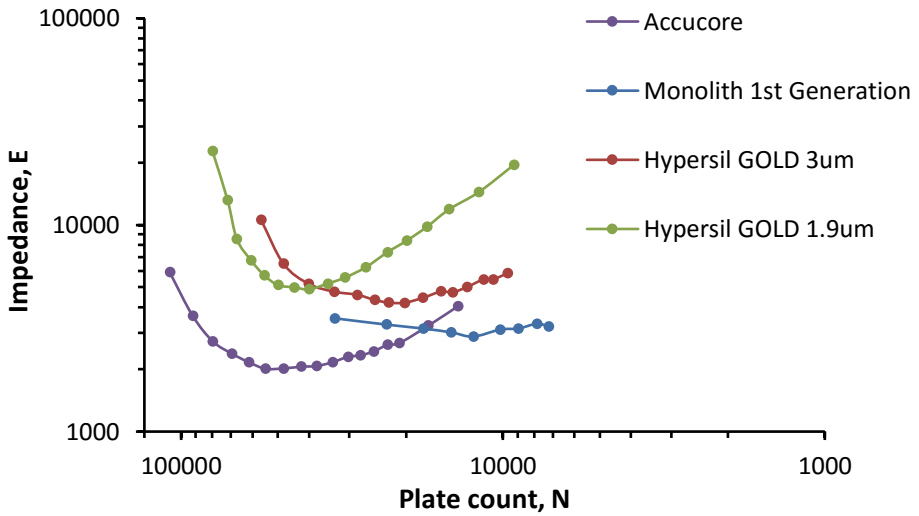

Figure 1.14 Impedance comparison of Accucore 2.6 µm core-shell microspheres, first generation monolithic column, fully porous 3 µm microspheres and sub-2 µm microspheres. Data obtained from Thermo Scientific.

The data when reviewing A, B and C terms illustrates that core-shell chromatographic supports exhibit less band broadening through eddy diffusion and resistance to mass transfer than fully porous chromatographic supports and monolithic columns. It has been demonstrated that variation of the porous shell can affect the overall chromatographic performance of the column and the importance of selecting the correct depth of porous layer to optimise the separation for small and large molecules has been highlighted. Through the use of kinetic plots and measurement of impedance, direct comparisons of the performance of various packed bed columns and, importantly, monoliths can also be achieved when a common scaling factor is introduced.[115]

1.4 Core-Shell Silica Microspheres in Liquid Chromatography

A major challenge in liquid chromatography is to attain fast, efficient separation. This can be achieved by reducing particle size and increasing flow rate, but at the expense of very high back pressure, placing a huge burden on HPLC instrumentation. 2.7 µm core-shell particles have shown comparable chromatographic performance to sub-2 µm particles while generating only slightly more back pressure than a 3 µm material. This can remove the need to use expensive UPLC equipment, while still attaining fast efficient separation.

Since the introduction of modern core-shell particles many other manufacturers have introduced their own core-shell products. A particle diameter of around 2.7 µm was initially the only size offered, however manufacturers have since expanded this class of particles and columns packed with particles ranging from 1.6 to 5 µm are now commercially available in a variety of dimensions. A large range of bonded phase chemistries are also available which allows for the use of core-shell particles in various modes of liquid chromatography. Some examples of the use of core-shell microspheres in liquid chromatography are discussed in this section.

1.4.1 Reversed Phase Chromatography

Reversed phase analysis is the most frequently used mode of HPLC. When looking at the core-shell columns offered by manufacturers, reversed phase bonded chemistries are the most abundant, with C18 phases being particularly common. A number of comparative studies have been performed to investigate the performance of different manufacturers' core-shell columns.

Comparing the efficiency of Kinetex C18 with Halo C18, it was reported that the Kinetex material resulted in superior performance in the separation of proteins with no loss in peak capacity with increasing mobile phase velocity.[116] It was concluded that the C term in the HETP plot for Halo particles was significantly larger. Another study indicated that this increase in performance could be a result of the difference in particles size between the Kinetex (2.6 µm) and Halo (2.7 µm).[117] The result confirmed the extremely flat HETP curve, the very low C term of the Kinetex column and its ability to successfully operate at high flow rates while experiencing less efficiency loss than other columns.[117]

A systematic evaluation was carried out by Oláh *et al.* to compare the kinetic performance on Kinetex and Ascentis Express columns by constructing van Deemter, Knox and kinetic plots using test mixture of estradiol, levonorgestrel, bicalutamide, and ivermectin.[118] These results indicated that the Kinetex column offered faster mass transfer with a flatter C term. It was suggested that this difference in performance was due to the Ascentis Express column having lower loading capacity and retention factor than even fully porous particles.

Columns packed with core-shell particles have been shown to provide high efficiencies with minimum reduced plate height values in the range of 1.7-1.5.[36, 119] For low molecular weight analytes up to 300 Da, minimum reduced plate heights as low as 1.1 were obtained using a Kinetex C18 column.[116]

DeStefano *et al.* reported fast, high resolution separation of naphthalene, virginiamycin, pesticides and explosives on Halo C18 and C8 columns.[36] The reduced plate height plots for virginiamycin obtained from both columns were significantly lower than 3 µm fully porous particles due to increased mass transfer. Guiochon *et al.* and others worked with the same type of columns, showing improved separation of large molecules such as proteins, moderate molecular weight peptides, and proteins digests of insulin, lysozyme, myoglobin, and bovine serum albumin.[117, 120-122]

Core-shell particles with a different range of pore sizes in the shell have been developed by manufacturers to suit different analytes. Particles with pore sizes in the range of 8-10 nm are adequate for the routine separation of small molecules.[123] Larger molecules require larger pores for efficient separation, for example particles with a pore size of 16 nm are useful for separating peptides and small proteins with molecular weights up to approximately 15 kDa.[124] Larger superficially porous particles with a pore size of 40 nm allow very large molecules of up to 500 kDa unrestricted access to the bonded phase and are optimised for protein separations.[125]

The relationship between the shell pore size and thickness was investigated to analyse diffusion of molecules.[126, 127] The pore size was found to be the major contributor toward restricted diffusion of large protein molecules of around 400 kDa, which was comparable to previous studies on the effect of pore size in fully porous particles.[127] The study involved the use of Halo C18 particles with pore sizes of 9, 16 and 40 nm for the separation of proteins such as myosin, ferritin, and β-amylase. Mass transfer kinetics can also be influenced by the shell thickness. When reducing the shell thickness from 350 to

150 nm, the A and B terms were both shown to be significantly reduced. Additionally, the analysis time of a reversed phase test mixture was almost halved by reducing shell thickness, while showing slightly improved efficiency.[126]

1.4.2 Hydrophobic Interaction Liquid Chromatography Separation

Unbonded silica phases and silica functionalised with diol, multiple hydroxyl or other polar groups can be used to increase retention of polar compounds such as carbohydrates, sugars, glycans, peptides and nucleic acids. This type of support would usually be classed as normal phase, however separation can instead be carried out under hydrophilic interaction liquid chromatography (HILIC) conditions.[128, 129] HILIC chromatography can potentially be used for many types of polar compound separations.

HILIC can be described as a variant of normal phase chromatography that partly overlaps with reversed phase. The stationary phase is hydrophilic but the method uses reversed phase type mobile phases with a small amount of aqueous content. The aqueous portion of the mobile phase forms a layer on the hydrophilic stationary phase, effectively creating a liquid/liquid extraction system in which analytes diffuse between the water deficient mobile phase and aqueous layer. Analytes are typically separated based on their polarity. More polar compounds have stronger interaction with the stationary layer and are thus retained for longer.

A Halo Penta-HILIC column demonstrated fast separation of a mixture of nucleosides and bases with excellent peak shapes and efficiency in less than 9 min.[130] It was also successfully used for the analysis of drugs of abuse such as cocaine, meperidine and methamphetamine. A comparative study with fully porous sub-2 µm and porous shell 2.7 µm was carried out under HILIC conditions. The core-shell column offered faster separation time and reduced the backpressure by half, but generated 30% lower efficiency than predicted.[131]

Core-shell particles can be also used in supercritical fluid chromatography (SFC) mode as it offers faster mass transfer and is environmentally friendly. Using supercritical CO_2 as the mobile phase, a Kinetex HILIC column was used to separate a low molecular weight test mix, consisting of a range of small drug-like molecules. When compared with 3 µm fully porous particles the core-shell column provided close to a 50% increase in efficiency and required only half the time to separate the test mix.[132]

1.4.3 Chiral Separation

Chiral separation accounts for the analysis of more than a third of marketed drugs. Around half of all marketed drugs are chiral and of these it is estimated that half of these exist as mixtures rather than single enantiomers. As enantiomers of a chiral drug may behave differently in vivo, it is advantageous to isolate the biologically active form for treatment.[133] There are a number of commercially available chiral phases such as polysaccharides,[134, 135] cyclodextrins,[136] and others,[137] although there are very few examples of core-shell particles used in this capacity.

One type of chiral core-shell material was discussed earlier, where 2.3 µm particles were synthesised with a 100 nm mesoporous shell of silica nanospheres bridged with a trans-(1R,2R)-diaminocyclohexane moiety.[69] Rapid chiral separation was demonstrated for the analysis of racemic binaphthyl derivatives. Another recent study reported the coating of 2.6 µm Kinetex particles with polysaccharide chiral selectors.[138] Particles were compared with a 3 µm totally porous material which had been coated using the same procedure. The columns were used for the enantiomeric separation of trans-stilbene oxide, benzoin and 2,2-dihydroxyl-6,6-dimethylbiphenyl.

The core-shell material displayed higher resolving ability compared to the totally porous material. This was observed for all three test compounds but was most pronounced in the case of trans-stilbene oxide. The core-shell column also resulted in significantly higher plate counts for all analytes. Although the core-shell material had slightly higher chiral selector content this cannot fully explain the observed improvement. An explanation could be that the chiral coating is more accessible to analytes when coated onto the material with superficial rather than deep through-pores.

1.4.4 Narrow Bore and Capillary HPLC

In recent years, column miniaturisation has been investigated and tested in order to achieve highly sensitive chromatography. Miniaturised columns are more suitable for handling minute or dilute samples, especially in areas such as forensic science and drug trials. The idea of miniaturisation is to provide higher sensitivity and peak capacity than standard columns with minimal dead volume for small sample amounts.[139] Although it is possible to use narrow bore columns of 1-2 mm i.d. on conventional HPLC systems, the instrument typically requires modification to reduce dead volume. This becomes much

more difficult when dealing with capillary columns as the pump needs to be adapted to accommodate low mobile phase flow valves. On-capillary sample injector and detection can be used to reduce dead volume. Studies on the efficiency between narrow bore and analytical type columns reveal the same column performance, due to the packing and wall effect.[140, 141] To overcome some of these issues various packing methods have been applied, such as dry packing,[142] high-pressure slurry packing,[143] and centripetal force packing.[144] The majority of studies have been performed using conventional 3-5 µm silica microspheres. Although improved chromatographic performance can be obtained by reducing particle size to 1.7 µm, this results in increased backpressure.[8] In this regard, core-shell particles may be utilised to improve separation efficiency and speed, negating the need to use very small particles.

Comparative studies have been performed to compare the efficiency of narrow bore core-shell columns (2.1 mm i.d.) with monolithic columns in the analysis of silybin diastereoisomers.[145] In the case of one analyte, silybin A, the core-shell Kinetex column provided markedly higher efficiency, h_{min} = 2.8, versus 5.6 for the Chromolith monolithic column. The resolution power was found to be comparable, but the Kinetex column required higher pressure to achieve the same separation. In contrast the monolith column displays higher permeability and significantly lower back pressure at high linear velocities. The large pore size also reduces the chance of clogging, which can be problematic during the separation of biological samples.

Omamogho *et al.* found that the performance of core-shell particles, particularly those with a thin shell, could be negatively affected by extra column band broadening when packed into narrow bore columns.[146] As an example, 2.6 µm Kinetex particles packed into 4.6 mm i.d. columns resulted in what is possibly the lowest ever measured reduced plate height of 1.1.[116] However, when packed into 2.1 mm i.d. columns the reduced plate height of 1.9 was the minimum achieved. This suggests that the packing of narrow bore columns does not provide comparable packed bed homogeneity to that of the standard bore columns. Any voiding in the packed bed within a narrow bore column would perhaps be more pronounced than in a standard bore column as it would represent a larger percent of the column volume. Gritti *et al.*[147] studied the mass transfer kinetics of the 1.7 µm Kinetex material packed in a 2.1mm i.d. column, and found the minimum reduced plate height was above 2.0. This suggests that the issue of packing narrow bore columns is compounded when the packing materials are finer, such as the sub-2 µm particles.

Gritti *et al.* also carried out systematic studies using different type of core-shell particles and investigated the effect of internal diameter of the column on efficiency.[148] The study showed that 4.6 mm i.d. columns provide larger column efficiencies than 2.1 mm i.d. columns packed with the same particle batch. This was the case for four different manufacturers' core-shell particles. Investigation of the mass transfer mechanism showed that the long range eddy dispersion HETP term is larger in narrow-bore than in wide-bore modern HPLC columns. This can be explained by the fact that radial excursion distance from the column centre to the wall is smaller in the case of the 2.1 mm column, hence the sample of interest reaches the column wall faster than in a 4.6 mm column. Therefore, the dispersive wall effects are smaller in 4.6 mm than in 2.1 mm columns because the former are operated in a dispersion regime that is closer to that of an infinite diameter column, free from wall and border effects.

Currently there are few studies published on the application of core-shell particles in capillary columns. Most of these involve capillary electrochromatography. Fanali *et al.* used 100 µm i.d. fused silica capillaries packed with 2.6 µm core-shell Kinetex C18 particles for the analysis of different brands of green and black tea constituents.[149] A method for the simultaneous separation of several polyphenols and methylxanthines in a single run, employing a nano-HPLC system, was developed. The core-shell material demonstrated retention factors and sample loading capacity slightly lower than those observed for the sub-2 µm column. However, similar efficiency separations, sharper peaks in the chromatogram and shorter analysis time were obtained. Accurate masses of the tea constituents were determined by coupling with mass spectrometry detection. Due to the use of the capillary column flow splitting was not required, resulting in better signal and sensitivity.

In another study, 2.6 µm phenyl-hexyl core-shell particles were packed into various sized capillary columns with internal diameters of 25, 50, 75, 100 and 150 µm. The kinetic performance of each was compared and also used to separate a mixture of aromatic hydrocarbons.[150] Higher plate counts were obtained with decreasing capillary diameter without significant decrease of efficiency, with the highest plate number observed for the 25 µm capillary. This appears to contradict the study by Gritti *et al.*,[148] which concluded that larger i.d. columns result in higher efficiency. However in nano-LC, with adequately prepared capillary columns, the effects of extra-column dead volumes are minimised due to on-capillary sample injection and detection. Indeed, the results indicated that extra band broadening observed with narrow bore columns was almost excluded in capillary columns.

This was particularly true for the 25 µm i.d. capillary which displayed a virtually flat HETP plot for n-butylbenzene, even at high linear velocities.

1.4.5 Capillary Electrochromatography

Capillary electrochromatography (CEC) is a separation technique in which the mobile phase is driven by an electro-osmotic flow rather than pressure. CEC combines the separation and selectivity of HPLC and the high efficiency of capillary electrophoresis.[151] The role of stationary phase has been investigated for improved separation. A variety of stationary phases has been tested such as silica and polymeric materials with different bonded phases.[151-153] Core-shell particles have shown a great success in conventional liquid chromatography however the use of these particles in CEC is so far rather limited.

Fanali *et al.* compared the performance of capillary columns packed with fully porous and core-shell silica particles for chiral separation in CEC mode.[154] The particles were coated with cellulose tris(4-chloro-3-methylphenylcarbanate), a polymer-based chiral selector. The capillary column packed with 2.8 µm core-shell particles showed baseline separation of warfarin and temazepam with excellent peak shapes compared to 3 µm fully porous particles. This study has shown that porous shell particles can perform in CEC mode without any loss of resolution or efficiency. It would be interesting if these particles can be expanded into separation of other mixtures.

1.4.6 Two Dimensional Liquid Chromatography

Two dimensional liquid chromatography (2D-LC) is a technique where the injected sample is analysed by the use of two separation stages. This is accomplished by injecting the eluent from the first column onto a second column. An example schematic of 2D-LC instrumentation is shown in figure 1.15. While applications exist which utilise a pair of identical phases, the two phases do not necessarily need to be the same. With an alternate (orthogonal) phase in the second dimension column, it becomes possible to separate analytes that are poorly resolved by the first column or to use the first dimension as a clean-up step. The main advantage of this method over conventional one-dimensional chromatography is the potential for a large increase in peak capacity. This can be achieved without requiring particularly efficient separations from either column as, under ideal

conditions, it is possible to obtain a total peak capacity equal to the product of the first and second separations.[155] The major disadvantage however is the long timescale involved in comprehensive 2D-LC. Gradient run times can exceed several hours, however theoretical peak capacities in the thousands can be achieved if a longer analysis time is acceptable.[156, 157]

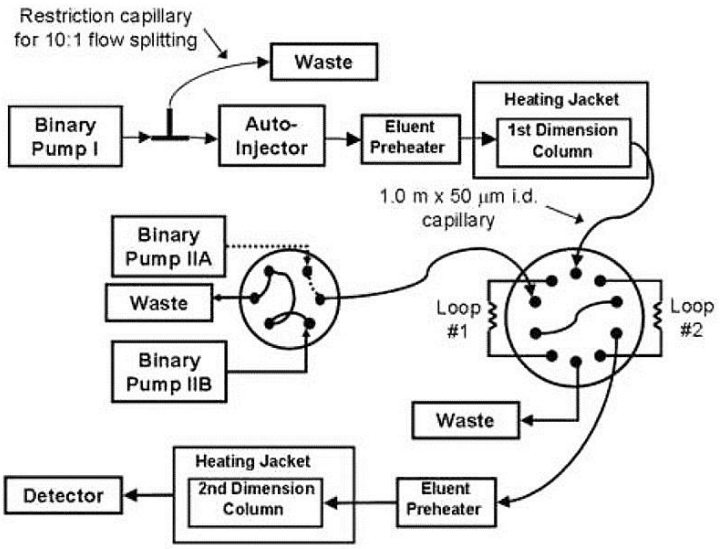

Figure 1.15 Schematic of instrumentation used for 2D-LC.[155]

Examples of the use of core-shell particles in 2D-LC include pharmaceutical and food analysis. In one study by Alexander *et al.*, the increased resolving power when using the reversed phase dual core-shell secondary columns confirmed the presence of minor components from the degradation of a drug compound.[158] This is particularly relevant for pharmaceutical applications as it addresses the problem of separating co-eluting impurities that may be hidden within a large peak of the active pharmaceutical ingredient, thus escaping detection. Very fast gradient separations were achieved at ambient temperature and reasonable operating pressure without compromising optimal first dimension sampling rates. The sensitivity of the interface was demonstrated in the analysis of a 1 mg/mL standard mixture containing 0.05% of a minor component.

In the analysis of pesticides in food, a fully porous HILIC column provided fast on-line clean-up of the samples in the first dimension, followed by analysis using either C18 core-shell or totally porous columns.[159] The combination of HILIC and reversed phase chromatography provided high orthogonality and was shown to be capable of analysing

over 300 compounds with good sensitivity and robustness. For the majority of compounds, no significant differences were observed between the second dimension columns. Small variations were found for the retention times but not for peak shape or signal intensity. The core-shell material produced the best performance in this second dimension, providing narrow, well separated peaks and also the best sensitivity.

1.5 Applications of Core-Shell Particle Columns

Some applications have already been covered in the previous section when discussing the types of liquid chromatography employing core-shell particles columns. This section will provide further example applications. Although not an exhaustive list, it intends to show that columns packed with core-shell particles are routinely used for analysing a large variety of samples in different fields.

1.5.1 Proteins, Peptides and Biomolecules

Kirkland *et al.* published an overview describing the range of Halo core-shell particles and their optimisation in separating particular groups of compounds based on their size and properties.[130] The first Halo core-shell particles developed by AMT were 2.7 µm in diameter with a 0.5 µm shell, 9 nm pores and a surface area of 135 m^2/g. These were developed mainly for separation of small molecules. Due to the poor diffusion by larger analytes into the pore system, core-shell particles with 16 nm pores were later introduced which were more suitable for the separation of peptides and small proteins up to around 15 kDa.[160] A test mixture of five proteins (6-14 kDa) was analysed on two C18 core-shell columns with pore diameters of 9 and 16 nm. As shown in figure 1.16 A, the 16 nm material resulted in much sharper peak shapes for all analytes.

Most recently, core-shell particles with even wider pores were introduced for the analysis of large proteins and biomolecules.[161] Analytes up to around 400 kDa were efficiently separated using this column without observing any restrictive diffusion that would hinder the chromatographic performance. When compared with fully porous particles, the column packed with core-shell particles provided better chromatographic performance in the analysis of carbonic anhydrase (29 kDa). The van Deemter plot in Figure 1.16 B shows higher efficiency for the core-shell column at the minimum plate height and

the also a far smaller increase in plate height as the mobile phase velocity was increased. This is a result of the superior mass transfer and reduced C term, facilitated by the thin, highly porous shell.[123]

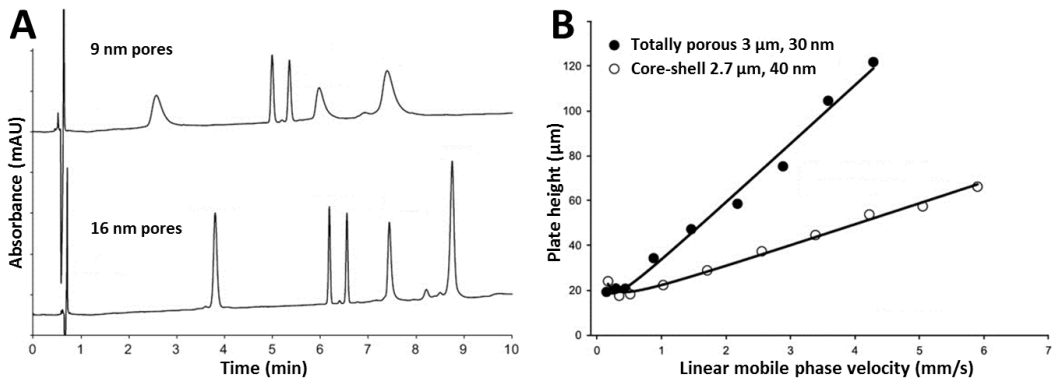

Figure 1.16 Effect of increasing pore size from 9 nm to 16 nm on the separation of a protein test mix containing ribonuclease A, bovine insulin, human insulin, cytochrome c and lysozyme (A).[160] Comparative van Deemter plots for 40 nm core-shell and 30 nm totally porous particles for the analysis of carbonic anhydrase (B).[123]

Wagner *et al.* systematically investigated the effects of particle size, pore size, shell thickness and bonded phase effects on the analysis of biomolecules.[127] By altering the physical properties of the particles they were able to optimise these parameters to produce particles capable of delivering fast, efficient separation of specific molecular sizes. A comparison between the stationary phases with differing pore size in figure 1.17 shows restricted diffusion for larger molecules such as ribonuclease A (14 kDa) and insulin (6 kDa) on the 9 nm C18 phase, and that increasing the pore size to 16 and 40 nm improves the peak shape and resolution. The effect is most apparent for the largest analyte, ribonuclease A. In a study on shell thickness, 2.7 µm overall diameter particles with 0.35 µm shell thickness and 3.4 µm overall diameter particles with 0.2 µm shell were compared, both of which had a wide pore size of 40 nm.[127] Unusual results were obtained when van Deemter plots were produced for the proteins studied, where the larger diameter particle showed a smaller plate height, especially at higher mobile phase velocity, which was attributed to the reduced shell thickness. When compared with 3 µm totally porous particles, the superior mass transfer of the core-shell particles resulted in faster protein separation and improved resolution.

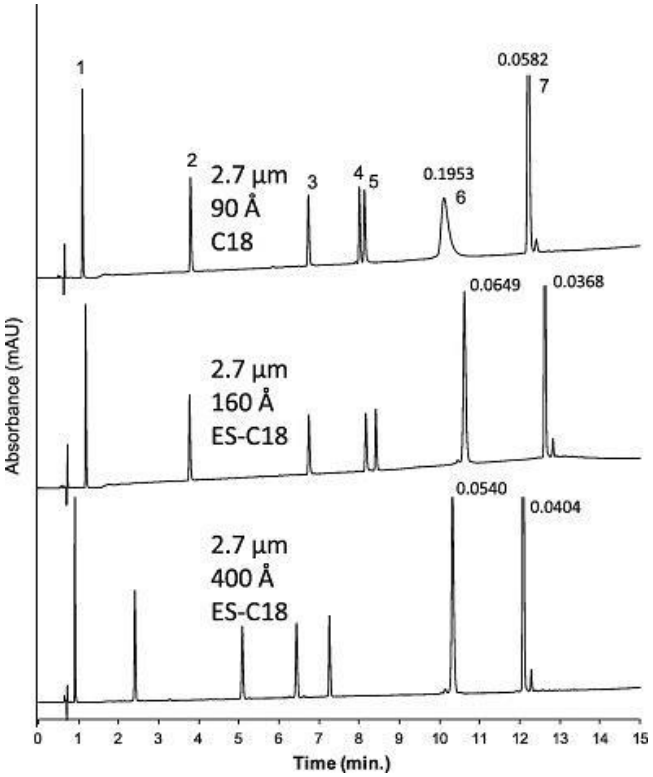

Figure 1.17 Effect of pore size on peak width and resolution of a protein/peptide test mixture. Peak identities: 1) Gly-Tyr, 2) Val-Tyr-Val, 3) methionine enkephalin, 4) angiotensin II, 5) leucine enkephalin, 6) ribonuclease A, 7) insulin. Peak widths in minutes measured at 50% height.[127]

Staub *et al.* made comparisons between totally porous sub-2 µm and sub-3 µm core-shell particles for the analysis of peptides, proteins and protein digests.[162] Chromatographic performance was found to be similar between the two types of silica. Analysis of a test mixture containing six peptides using a selection of C18 core-shell and C18 sub-2 µm columns showed comparable results for all in terms of resolution and peak capacity. The overlaid chromatograms are shown in figure 1.18. All columns were able to fully separate the mixture within 3.5 min. However, the core-shell columns generated little more than half the back pressure compared with the sub-2 µm column. Each column was also tested using a tryptic digest of four proteins, equivalent to approximately 160 peptides, with a goal of improving peak capacity and resolution. Again, the results were comparable between the four columns and all yielded close to the target number of peaks.

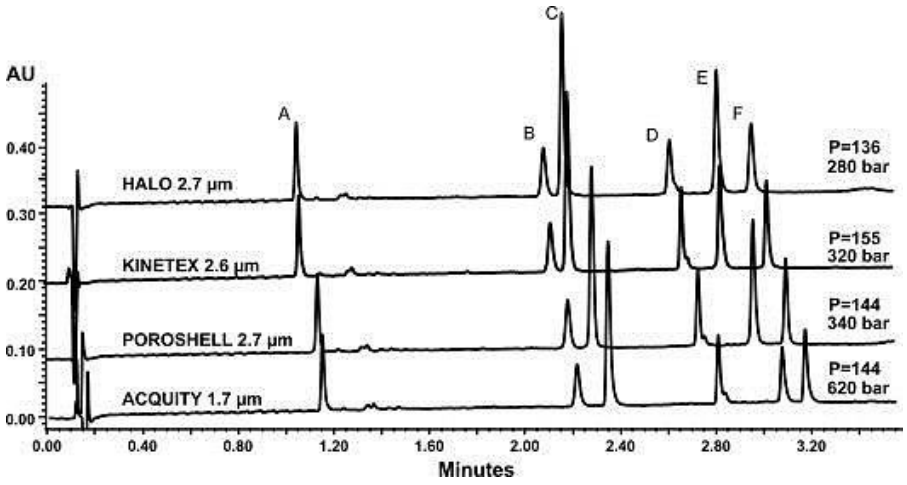

Figure 1.18 Overlaid chromatograms of peptide test mix separated on three core-shell columns: Halo C18, 2.7 µm; Poroshell 120 EC-C18, 2.7 µm; Kinetex C18, 2.6 µm and one totally porous column: Acquity C18 BEH 120, 1.7 µm. All column dimensions 50 × 2.1 mm.[162]

Ruta *et al.* evaluated the performance of core-shell particles for the separation of a range of pharmaceutical compounds.[163] A test mixture of 13 analytes including basic drugs and acidic compounds was investigated using columns packed with a variety of core-shell and sub-2 µm particles. An identical elution order was seen on the four columns tested under acidic conditions, as any residual silanols on the surface of the stationary phase were neutral at pH 2.7 and a reversed phase mechanism should govern the retention. There were some changes observed in selectivity between columns, but with some small adjustments it should be possible to transfer a method developed for the sub-2 µm column to a core-shell column. Under neutral conditions, surface silanols were deprotonated and changes in retention time and selectivity were observed due to differing silanol activity between columns. Peaks found to be tailing under acidic conditions showed improved width and asymmetry at neutral pH. Selectivity between columns was similar, though there were certain peaks where one type of particle provided superior resolving power than the other, highlighting the potential for method transfer.

Fekete *et al.* described the use of 1.3 µm core-shell particles for separation of small molecules and peptides.[164] Looking at the kinetic properties of these small particles, the van Deemter plot was extremely flat over the entire range of mobile phase velocity. In isocratic mode, the new core-shell 1.3 µm particles provided excellent efficiency for peptides as the column could be run at the optimal flow rate thus minimising longitudinal

diffusion. When analysing peptides in the gradient elution mode, the 1.3 µm particles offered the fastest separation up to a peak capacity of 700.

1.5.2 Food Analysis

As the use of core-shell particles is a comparatively recent trend in chromatography, their use in fields such as food analysis is still emerging. Some examples include the determination of toltrazuril and its metabolites,[165] corticosteroids,[166] chloramphenicol,[167] and flavonoids[168] in foodstuffs and the detection of neonicotinoids in beeswax.[169] The latter described a new method to detect a total of 7 neonicotinoids in beeswax using liquid chromatography coupled to electrospray ionisation mass spectrometry (ESI-MS).[169] Initial stock solutions were tested to develop the method before samples taken from 30 apiaries located close to fruit orchards were analysed. In total 11 samples were found to show neonicotinoid residues at low levels (11-153 µg/kg). The method demonstrated consistent and reliable results and optimisation of the preparation method allowed for good recoveries at different concentrations.

Another important use of core-shell columns is in the detection of contaminants originating from food packaging, such as the migration of compounds.[170] One application is concerned with detecting bisphenol compounds in soft drinks and canned foods using a liquid chromatography-tandem mass spectrometry method (LC-MS/MS).[171] Epoxy-based laquers are commonly used as a coating on the inside of food containers to reduce food spoilage and prevent degradation of the container itself. Some coatings are based on polymerisation of bisphenol A-diglycidyl ether (BADGE) or bisphenol F-diglycidyl ether (BFDGE) which can release these compounds and derivatives into the packed foods. As well as this, hydrolysed and chlorinated derivatives such as BADGE·H_2O, BADGE·$2H_2O$, BFDGE·H_2O, BFDGE·$2H_2O$, BADGE·HCl, BADGE·2HCl and BADGE·HCl·H_2O can also be produced, especially when the coating is thermally treated or comes into contact with acidic and aqueous contents. Current LC-MS/MS methods of analysis use conventional 3-5 µm particles, leading to long analysis times when detecting both BADGE and BFDGEs in the same run. The aim was to develop a faster method using LC-MS/MS. In this study a core-shell 2.7 µm Ascentis Express C18 column was chosen over a sub-2 µm column as the lower back pressure generated (200 versus 513 bar at 600 µL/min) enabled a longer column length of 150 mm to be utilised.[171] Efficient separation of detected BADGEs in asparagus was achieved using the core-shell column, with a run time of under 5 min. Figure 1.19

shows the chromatograms in which BADGE·H_2O, BADGE·$2H_2O$, BADGE·HCl, BADGE·2HCl and BADGE·HCl·H_2O were detected.

A further investigation by the same group was concerned with analysis of bisphenols in canned soft drinks.[172] Bisphenol A (BPA) is widely used in the production of the resin coating of drinks cans, therefore contents may be expected to contain traces of BPA derivatives. As there is an abundance of toxicity data for BPA, limits are in place on migration limits from coating to food as well as tolerable daily intake. Due to these restrictions, other bisphenol compounds are being considered for use in place of BPA, however there is significantly less published data on these alternatives and for most, no limits have yet been proposed. An online solid phase extraction (SPE) LC-MS/MS method was developed using the same core-shell column as in the previous example. The SPE LC-MS/MS method was then used for the analysis of bisphenols in eleven canned soft drinks. BPA was detected in most samples and bisphenol F found in only two. The rest of the bisphenol compounds were not identified. The use of a SPE clean-up step allowed the analysis of bisphenols at concentrations lower than 100 ng/L and the method was shown to be robust and sensitive enough for routine analysis of these compounds.

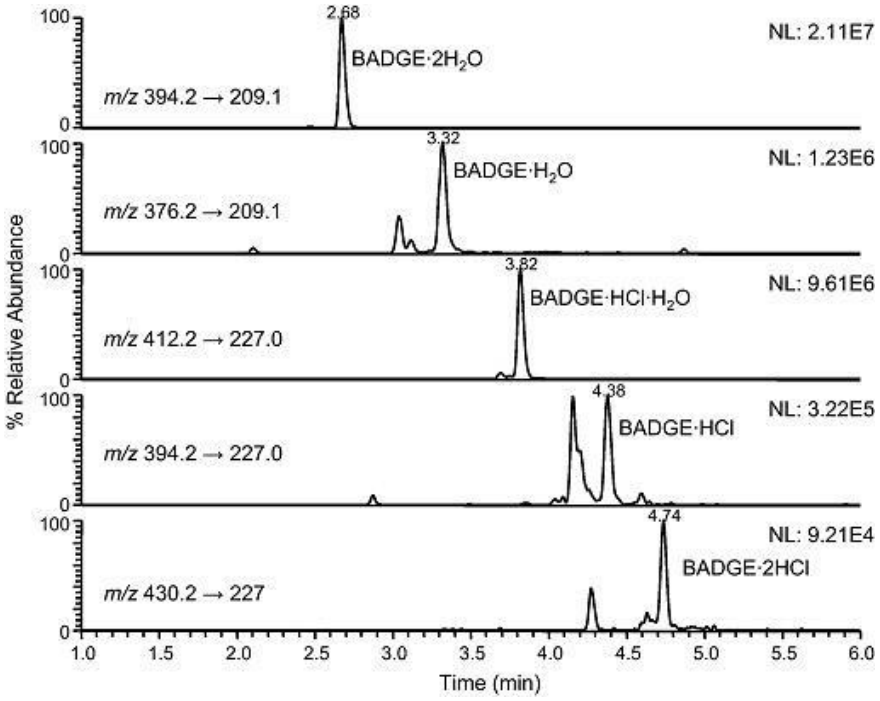

Figure 1.19 LC-MS/MS chromatogram in SRM acquisition mode for the analysis of BADGEs in asparagus.[171]

1.5.3 Environmental

Core-shell technology has also found its way into the analysis of water samples, including drinking water, surface water and sewage. Various techniques are used for the detection of antibiotics,[173] drugs of abuse,[174-176] oestrogens,[177] bisphenols,[178] pharmaceuticals,[179] herbicides, and pesticides. Pesticides are widely used in agriculture to protect crops from threats such as weeds, disease and insects, however they can also cause environmental pollution in water and wildlife as well as serious health effects in human beings. As such, maximum contamination values in drinking water for a number of pesticides have been established by several legislative bodies.

As pesticides are usually detected at low concentrations, highly sensitive techniques are required to analyse them. Off-line SPE followed by gas or liquid chromatography coupled to mass spectrometry (GC-MS or LC-MS) is the most common approach. The downside is that off-line SPE methods are time consuming and typically require high sample volumes. Hurtado-Sánchez *et al.* developed a fast, sensitive method utilising on-line SPE coupled with HPLC and tandem mass spectrometry (SPE-LC-MS/MS).[180] The method was initially optimised and validated by spiking water samples with a known concentration of a number of pesticides to assess the precision and linearity of the method, as well as establish detection limits. Matrix effects were also studied and for most compounds were found to be diminished by dilution of samples with pure water. Real life surface water samples were then collected and analysed for polar pesticides using this method. A 50 × 4.6 mm column packed with 2.7 µm Poroshell 120 EC-C18 particles was used. Among the samples tested, the highest number of pesticides were detected in irrigation waters from agricultural sources. Six compounds were found at trace levels above the detection limit. Additionally during the validation of the method, three compounds that were found not to be retained with off-line SPE were also successfully analysed. The method was shown to be highly effective and suitable for use in routine analysis.

Another study by Zhang *et al.* presented an alternative SPE and LC-MS/MS method to analyse a range of herbicides in environmental water.[181] The method was validated by addition of target herbicides into water samples at two concentrations. The recoveries of 31 compounds were monitored, the majority of which achieved acceptable values of recovery and repeatability. As part of the method validation, limits of detection were calculated to be less than 10 ng/L for the majority of compounds. The method was then applied to the analysis of storm water samples. 24 of the 31 monitored herbicides were

detected in a wide range of concentrations. Comparison of the 2.6 µm Kinetex core-shell column to a 5 µm totally porous material showed an improvement in efficiency and the run time was halved.

Chocholouš *et al.* looked at the advantages of core-shell technology in the determination of phenolic acids using a sequential injection chromatography (SIC) method.[182] These compounds are hydroxylated derivatives of benzoic or cinnamic acid and are commonly found in plants. Phenolic acids have attracted considerable interest in the past few years because of their potential health benefits. They are powerful antioxidants which show antibacterial, antiviral, anti-carcinogenic, anti-inflammatory and vasodilatory action. Typical stationary phases used in SIC are monolithic sorbents with C18 or surfactant functionalisation. By contrast, core-shell particles are available with many different chemistries. The use of alternative phases allows for extended selectivity by increasing the number of interactions between the analytes and the stationary phase. Separation conditions were optimised for three core-shell columns with alternate functionalisation and their ability to separate a total of seven phenolic acids was compared. Using a reversed phase amide column provided the highest chromatographic resolution and allowed for complete baseline separation of protocatechuic, syringic, vanillic, ferulic, sinapinic, p-coumaric and o-coumaric acids. Phenyl-hexyl and C18 columns were unable to completely separate the tested mixture, with some co-elution observed. The work demonstrated fast chromatographic separation as well as a simple, fast and low-cost analysis.

Vinci *et al.* developed a liquid chromatography method to determine polycyclic aromatic hydrocarbons (PAHs) in rainwater.[183] Many PAHs are considered as carcinogens, benzo[a]pyrene for example has been categorised as a human carcinogen since 1987. In general PAHs are not detected individually, but in mixtures. 16 have been monitored by the United States Environmental Protection Agency (EPA) and listed as priority organic pollutants due to their environmental effects. The method was optimised by testing a standard mixture containing all 16 EPA-PAHs which gave fast separation of all compounds with good resolution and sensitivity. Chromatographic performance was comparable to columns packed with a 1.8 µm totally porous material in terms of retention time and solvent consumption, but with the advantage of far lower operating pressure.[184] When applied to the analysis of rainwater samples, PAHs were detected in each that were analysed and the method was shown to be viable for trace analysis of environmental water samples.

1.6 Summary

It has been shown that core-shell particles can possess many different structures and morphologies. Core-shell particles, particularly nanospheres, have been widely investigated in materials science and are exploited for a very wide range of applications. For the majority of chromatographic applications, core-shell microspheres are utilised. This literature review has identified different types of core-shell particles and explained their preparation methods. The main focus has been on those methods used to produce core-shell microspheres for chromatographic use.

The LbL approach is the main method for the preparation of core-shell microspheres for use as the packing materials for HPLC columns. However there are limitations to this method, mainly the time-consuming multiple-synthesis and classification steps. It has been shown that a monodisperse size distribution is typically preferred for packing materials. The microfluidic approach is very effective in producing monodisperse particles and therefore may have potential for use in chromatography. The versatility and low productivity of this approach have limited its application for production of HPLC packing materials so far. To address the time-consuming procedures in the LbL approach, a one-pot synthesis method has been developed resulting in the formation of SOS core-shell particles. Columns packed with SOS silica have shown promising performance in the separation of certain mixtures, although further optimisation is required to achieve comparable performance to commercial core-shell columns.

It has been argued that the excellent performance and low back pressure from core-shell particle columns is a result of the monodisperse size distribution. This chapter has shown that, although a desirable quality, this is unlikely to be the single reason. It has been discussed and evidenced with test data, how these particles perform by means of A, B and C terms in the van Deemter equation and kinetic plots. The performance of core-shell particles has been compared with that of monolithic columns and totally porous silica microspheres, particularly current state of the art sub-2 µm materials. Columns packed with core-shell particles are now routinely used in reversed phase HPLC for a wide variety of applications. Examples have been discussed where both successful and potential method transfer from totally porous particles can be implemented, with comparable or improved performance and reduction in operating pressure. Indeed, columns packed with core-shell particles have been shown to be an ideal alternative to achieve fast, efficient separation. This is especially useful where UPLC instrumentation is not available. Applications in

different separation modes have also been discussed, for example HILIC and chiral separation, demonstrating the increasingly wide use of core-shell particles in HPLC.

There is no doubt that core-shell particles will be continuously evaluated and investigated for highly efficient separation of new and complex mixtures. The challenges lie in the separation of isomers or molecules with very similar structures or properties, chiral separation and complex samples from biological, life sciences and proteomics. Researchers and manufacturers will need to carefully consider and adjust particle size, shell thickness, pore size, porosity and the surface functionalities to address various and specific separation needs. It is also vitally important to optimise the packing methods and instrumentation to allow the separations to be performed under optimal conditions. 2D-LC in particular is currently a fast-growing area of chromatography and it is important that core-shell particles play a significant role in this.

1.7 Thesis Overview

The work presented in this thesis is focused on developing SOS particles for use in the HPLC separation of large molecules such as proteins. The experimental work aims to produce near monodisperse particles from the one-pot process without the need for classification, which would represent a vast reduction in production time compared to current core-shell materials. Resultant particles will then be bonded and the chromatographic performance assessed using HPLC.

Chapter 2 describes the production of SOS particles, initially observing the effects of changing reagent type and concentration on the resultant morphology. This is followed up by optimisation work to produce near monodisperse particles with a complete shell of nanoparticles surrounding the core. Chapter 3 explores the possibility of using microwave irradiation as the heating source for the functionalisation of SOS particles. Although microwave equipment for scientific use has been available since the 1980s, there are very few literature examples where microwave heating has been utilised specifically for producing bonded silica materials for chromatographic purposes. In chapter 4 the chromatographic performance of SOS particles is assessed by HPLC, particularly for the analysis and separation of intact proteins. Finally, chapter 5 discusses a number of interesting particle morphologies which have also been discovered during the SOS development, through various modifications to the synthesis method.

1.8 References

1. L. R. Snyder, J. J. Kirkland and J. W. Dolan, *Introduction To Modern Liquid Chromatography*, John Wiley & Sons, 2011.
2. S. Fekete, E. Oláh and J. Fekete, *Journal of Chromatography A*, 2012, **1228**, 57-71.
3. C. Horvath and S. R. Lipsky, *Journal of Chromatographic Science*, 1969, **7**, 109-116.
4. T. B. Tennikova, B. G. Belenkii and F. Svec, *Journal of Liquid Chromatography*, 1990, **13**, 63-70.
5. S. Hjertén, J.-L. Liao and R. Zhang, *Journal of Chromatography A*, 1989, **473**, 273-275.
6. H. Minakuchi, K. Nakanishi, N. Soga, N. Ishizuka and N. Tanaka, *Analytical Chemistry*, 1996, **68**, 3498-3501.
7. G. Guiochon, *Journal of Chromatography A*, 2007, **1168**, 101-168.
8. K. K. Unger, R. Skudas and M. M. Schulte, *Journal of Chromatography A*, 2008, **1184**, 393-415.
9. F. Svec, *Journal of Chromatography A*, 2010, **1217**, 902-924.
10. R. Bandari, W. Knolle, A. Prager-Duschke, H.-J. Gläsel and M. R. Buchmeiser, *Macromolecular Chemistry and Physics*, 2007, **208**, 1428-1436.
11. J. H. Smith and H. M. McNair, *Journal of Chromatographic Science*, 2003, **41**, 209-214.
12. N. Ishizuka, H. Kobayashi, H. Minakuchi, K. Nakanishi, K. Hirao, K. Hosoya, T. Ikegami and N. Tanaka, *Journal of Chromatography A*, 2002, **960**, 85-96.
13. N. Tanaka, H. Kobayashi, N. Ishizuka, H. Minakuchi, K. Nakanishi, K. Hosoya and T. Ikegami, *Journal of Chromatography A*, 2002, **965**, 35-49.
14. K. Cabrera, *Journal of Separation Science*, 2004, **27**, 843-852.
15. S. Hjertén, *Industrial and Engineering Chemistry Research*, 1999, **38**, 1205-1214.
16. F. Svec and J. M. J. Frechet, *Analytical Chemistry*, 1992, **64**, 820-822.
17. F. Svec and C. G. Huber, *Analytical Chemistry*, 2006, **78**, 2100-2107.
18. J.-L. Liao, R. Zhang and S. Hjertén, *Journal of Chromatography A*, 1991, **586**, 21-26.
19. D. Sýkora, F. Svec and J. M. J. Fréchet, *Journal of Chromatography A*, 1999, **852**, 297-304.
20. C. Ericson, J.-L. Liao, K. i. Nakazato and S. Hjertén, *Journal of Chromatography A*, 1997, **767**, 33-41.
21. A. Maruška, C. Ericson, Á. Végvári and S. Hjertén, *Journal of Chromatography A*, 1999, **837**, 25-33.

22. L. L. Hench and J. K. West, *Chemical Reviews*, 1990, **90**, 33-72.
23. N. Tanaka, H. Kobayashi, K. Nakanishi, H. Minakuchi and N. Ishizuka, *Analytical Chemistry*, 2001, **73**, 420 A-429 A.
24. K. Nakanishi, H. Minakuchi, N. Soga and N. Tanaka, *Journal of Sol-Gel Science and Technology*, 1997, **8**, 547-552.
25. N. Tanaka, H. Nagayama, H. Kobayashi, T. Ikegami, K. Hosoya, N. Ishizuka, H. Minakuchi, K. Nakanishi, K. Cabrera and D. Lubda, *Journal of High Resolution Chromatography*, 2000, **23**, 111-116.
26. H. Minakuchi, K. Nakanishi, N. Soga, N. Ishizuka and N. Tanaka, *Journal of Chromatography A*, 1997, **762**, 135-146.
27. H. Zou, X. Huang, M. Ye and Q. Luo, *Journal of Chromatography A*, 2002, **954**, 5-32.
28. M. Motokawa, H. Kobayashi, N. Ishizuka, H. Minakuchi, K. Nakanishi, H. Jinnai, K. Hosoya, T. Ikegami and N. Tanaka, *Journal of Chromatography A*, 2002, **961**, 53-63.
29. M. Motokawa, M. Ohira, H. Minakuchi, K. Nakanishi and N. Tanaka, *Journal of Separation Science*, 2006, **29**, 2471-2477.
30. H. Kobayashi, W. Kajiwara, Y. Inui, T. Hara, K. Hosoya, T. Ikegami and N. Tanaka, *Chromatographia*, 2004, **60**, S19-S25.
31. J. E. MacNair, K. C. Lewis and J. W. Jorgenson, *Analytical Chemistry*, 1997, **69**, 983-989.
32. N. Wu and A. M. Clausen, *Journal of Separation Science*, 2007, **30**, 1167-1182.
33. G. Guiochon and F. Gritti, *Journal of Chromatography A*, 2011, **1218**, 1915-1938.
34. J. J. Kirkland, *Analytical Chemistry*, 1969, **41**, 218-220.
35. J. J. Kirkland, *Journal of Chromatographic Science*, 1969, **7**, 7-12.
36. J. J. DeStefano, T. J. Langlois and J. J. Kirkland, *Journal of Chromatographic Science*, 2008, **46**, 254-260.
37. R. W. Brice, X. Zhang and L. A. Colón, *Journal of Separation Science*, 2009, **32**, 2723-2731.
38. J. J. van Deemter, F. J. Zuiderweg and A. Klinkenberg, *Chemical Engineering Science*, 1956, **5**, 271-289.
39. J. Liu, S. Z. Qiao, J. S. Chen, X. W. Lou, X. Xing and G. Q. Lu, *Chemical Communications*, 2011, **47**, 12578-12591.
40. A. Ahmed, H. Ritchie, P. Myers and H. Zhang, *Advanced Materials*, 2012, **24**, 6042-6048.

41. X.-l. Zhang, H.-y. Niu, W.-h. Li, Y.-l. Shi and Y.-q. Cai, *Chemical Communications*, 2011, **47**, 4454-4456.
42. N. Insin, J. B. Tracy, H. Lee, J. P. Zimmer, R. M. Westervelt and M. G. Bawendi, *ACS Nano*, 2008, **2**, 197-202.
43. X. Lai, J. Li, B. A. Korgel, Z. Dong, Z. Li, F. Su, J. Du and D. Wang, *Angewandte Chemie International Edition*, 2011, **50**, 2738-2741.
44. H. H. Park, K. Woo and J.-P. Ahn, *Scientific Reports*, 2013, **3**, 1497.
45. R. Gui, A. Wan and H. Jin, *Analyst*, 2013, **138**, 5956-5964.
46. R. Ghosh Chaudhuri and S. Paria, *Chemical Reviews*, 2012, **112**, 2373-2433.
47. R. Hayes, A. Ahmed, T. Edge and H. Zhang, *Journal of Chromatography A*, 2014, **1357**, 36-52.
48. D. Wang, H. L. Xin, R. Hovden, H. Wang, Y. Yu, D. A. Muller, F. J. DiSalvo and H. D. Abruña, *Nature Materials*, 2013, **12**, 81-87.
49. D. Ling and T. Hyeon, *Small*, 2013, **9**, 1450-1466.
50. J. Della Rocca, D. Liu and W. Lin, *Accounts of Chemical Research*, 2011, **44**, 957-968.
51. W. Stöber, A. Fink and E. Bohn, *Journal of Colloid and Interface Science*, 1968, **26**, 62-69.
52. T.-S. Deng and F. Marlow, *Chemistry of Materials*, 2012, **24**, 536-542.
53. S. Wang, M. Zhang and W. Zhang, *ACS Catalysis*, 2011, **1**, 207-211.
54. C. G. Horvath, B. A. Preiss and S. R. Lipsky, *Analytical Chemistry*, 1967, **39**, 1422-1428.
55. *US Pat.*, US3505785 A, 1970.
56. J. J. Kirkland, *Analytical Chemistry*, 1992, **64**, 1239-1245.
57. J. J. Kirkland, F. A. Truszkowski, C. H. Dilks Jr and G. S. Engel, *Journal of Chromatography A*, 2000, **890**, 3-13.
58. *US Pat.*, US7846337 B2, 2010.
59. W. Chen, K. Jiang, A. Mack, B. Sachok, X. Zhu, W. E. Barber and X. Wang, *Journal of Chromatography A*, 2015, **1414**, 147-157.
60. F. Honda, H. Honda and M. Koishi, *Journal of Chromatography A*, 1992, **609**, 49-59.
61. H. Honda, M. Kimura, F. Honda, T. Matsuno and M. Koishi, *Colloids and Surfaces A: Physicochemical and Engineering Aspects*, 1994, **82**, 117-128.
62. F. Honda, H. Honda, M. Koishi and T. Matsuno, *Journal of Chromatography A*, 1997, **775**, 13-27.
63. W. Tong, X. Song and C. Gao, *Chemical Society Reviews*, 2012, **41**, 6103-6124.

64. *US Pat.*, US20090297853 A1, 2009.
65. F. Gritti, I. Leonardis, J. Abia and G. Guiochon, *Journal of Chromatography A*, 2010, **1217**, 3819-3843.
66. A. C. Sanchez, G. Friedlander, S. Fekete, J. Anspach, D. Guillarme, M. Chitty and T. Farkas, *Journal of Chromatography A*, 2013, **1311**, 90-97.
67. S. Fekete and D. Guillarme, *Journal of Chromatography A*, 2013, **1308**, 104-113.
68. L. E. Blue and J. W. Jorgenson, *Journal of Chromatography A*, 2011, **1218**, 7989-7995.
69. X. Wu, L. You, B. Di, W. Hao, M. Su, Y. Gu and L. Shen, *Journal of Chromatography A*, 2013, **1299**, 78-84.
70. H. Dong and J. D. Brennan, *Chemical Communications*, 2011, **47**, 1207-1209.
71. C. Paek, A. V. McCormick and P. W. Carr, *Journal of Chromatography A*, 2011, **1218**, 1359-1366.
72. C. Paek, Y. Huang, M. R. Filgueira, A. V. McCormick and P. W. Carr, *Journal of Chromatography A*, 2012, **1229**, 129-139.
73. M. Shao, F. Ning, J. Zhao, M. Wei, D. G. Evans and X. Duan, *Journal of the American Chemical Society*, 2012, **134**, 1071-1077.
74. F. Hu, S. Chen and R. Yuan, *Sensors and Actuators B: Chemical*, 2013, **176**, 713-722.
75. J. Moraes, K. Ohno, T. Maschmeyer and S. Perrier, *Chemistry of Materials*, 2013, **25**, 3522-3527.
76. G. L. Li, H. Mohwald and D. G. Shchukin, *Chemical Society Reviews*, 2013, **42**, 3628-3646.
77. S. Sorribas, B. Zornoza, C. Tellez and J. Coronas, *Chemical Communications*, 2012, **48**, 9388-9390.
78. A. Ahmed, M. Forster, R. Clowes, D. Bradshaw, P. Myers and H. Zhang, *Journal of Materials Chemistry A*, 2013, **1**, 3276-3286.
79. J. Y. Sun, Z. K. Wang, H. S. Lim, S. C. Ng, M. H. Kuok, T. T. Tran and X. Lu, *ACS Nano*, 2010, **4**, 7692-7698.
80. S.-H. Wu, C.-Y. Mou and H.-P. Lin, *Chemical Society Reviews*, 2013, **42**, 3862-3875.
81. A. Ahmed, R. Clowes, E. Willneff, H. Ritchie, P. Myers and H. Zhang, *Industrial & Engineering Chemistry Research*, 2009, **49**, 602-608.
82. C. Graf, D. L. J. Vossen, A. Imhof and A. van Blaaderen, *Langmuir*, 2003, **19**, 6693-6700.
83. W. Li and D. Zhao, *Advanced Materials*, 2013, **25**, 142-149.

84. G. Büchel, K. K. Unger, A. Matsumoto and K. Tsutsumi, *Advanced Materials*, 1998, **10**, 1036-1038.

85. Y. Deng, D. Qi, C. Deng, X. Zhang and D. Zhao, *Journal of the American Chemical Society*, 2008, **130**, 28-29.

86. J.-M. Li, W.-F. Ma, C. Wei, J. Guo, J. Hu and C.-C. Wang, *Journal of Materials Chemistry*, 2011, **21**, 5992-5998.

87. L. Han, H. Wei, B. Tu and D. Zhao, *Chemical Communications*, 2011, **47**, 8536-8538.

88. A. B. Fuertes, P. Valle-Vigon and M. Sevilla, *Chemical Communications*, 2012, **48**, 6124-6126.

89. A. Ahmed, W. Abdelmagid, H. Ritchie, P. Myers and H. Zhang, *Journal of Chromatography A*, 2012, **1270**, 194-203.

90. W. Wang, M.-J. Zhang and L.-Y. Chu, *Accounts of Chemical Research*, 2014, **47**, 373-384.

91. J. I. Park, A. Saffari, S. Kumar, A. Günther and E. Kumacheva, *Annual Review of Materials Research*, 2010, **40**, 415-443.

92. J.-T. Wang, J. Wang and J.-J. Han, *Small*, 2011, **7**, 1728-1754.

93. J. H. Kim, T. Y. Jeon, T. M. Choi, T. S. Shim, S.-H. Kim and S.-M. Yang, *Langmuir*, 2014, **30**, 1473-1488.

94. Z. Nie, J. I. Park, W. Li, S. A. F. Bon and E. Kumacheva, *Journal of the American Chemical Society*, 2008, **130**, 16508-16509.

95. J. Wu, T. Kong, K. W. K. Yeung, H. C. Shum, K. M. C. Cheung, L. Wang and M. K. T. To, *Acta Biomaterialia*, 2013, **9**, 7410-7419.

96. W. Lan, S. Li, J. Xu and G. Luo, *Langmuir*, 2011, **27**, 13242-13247.

97. C.-X. Zhao and A. P. J. Middelberg, *RSC Advances*, 2013, **3**, 21227-21230.

98. J. H. Knox, *Journal of Chromatography A*, 1999, **831**, 3-15.

99. F. Gritti, T. Farkas, J. Heng and G. Guiochon, *Journal of Chromatography A*, 2011, **1218**, 8209-8221.

100. F. Gritti and G. Guiochon, *Journal of Chromatography A*, 2011, **1218**, 3476-3488.

101. J. C. M. Garnett, *Colours in Metal Glasses and in Metallic Films*, 1904.

102. S. Torquato, *Random Heterogeneous Materials: Microstructure and Macroscopic Properties*, Springer, New York, 2002.

103. S. Torquato, *Journal of Applied Physics*, 1985, **58**, 3790-3797.

104. F. Gritti and G. Guiochon, *Chemical Engineering Science*, 2011, **66**, 3773-3781.

105. J. H. Knox and H. P. Scott, *Journal of Chromatography A*, 1983, **282**, 297-313.

106. F. Gritti, *Chromatography Today*, 2012, **May/June**, 4.

107. K. S. Mriziq, J. A. Abia, Y. Lee and G. Guiochon, *Journal of Chromatography A*, 2008, **1193**, 97-103.

108. N. Vervoort, P. Gzil, G. V. Baron and G. Desmet, *Journal of Chromatography A*, 2004, **1030**, 177-186.

109. F. C. Leinweber, D. Lubda, K. Cabrera and U. Tallarek, *Analytical Chemistry*, 2002, **74**, 2470-2477.

110. A. Soliven, D. Foley, L. Pereira, G. R. Dennis, R. A. Shalliker, K. Cabrera, H. Ritchie and T. Edge, *Journal of Chromatography A*, 2014, **1334**, 16-19.

111. P. C. Carman, *Transactions, Institution of Chemical Engineers*, 1937, **15**, 150-166.

112. H. Poppe, *Journal of Chromatography A*, 1997, **778**, 3-21.

113. G. Desmet, D. Clicq and P. Gzil, *Analytical Chemistry*, 2005, **77**, 4058-4070.

114. G. Desmet, D. Clicq, D. T. T. Nguyen, D. Guillarme, S. Rudaz, J.-L. Veuthey, N. Vervoort, G. Torok, D. Cabooter and P. Gzil, *Analytical Chemistry*, 2006, **78**, 2150-2162.

115. P. Bristow and J. Knox, *Chromatographia*, 1977, **10**, 279-289.

116. F. Gritti, I. Leonardis, D. Shock, P. Stevenson, A. Shalliker and G. Guiochon, *Journal of Chromatography A*, 2010, **1217**, 1589-1603.

117. F. Gritti and G. Guiochon, *Journal of Chromatography A*, 2010, **1217**, 1604-1615.

118. E. Oláh, S. Fekete, J. Fekete and K. Ganzler, *Journal of Chromatography A*, 2010, **1217**, 3642-3653.

119. J. J. Kirkland, T. J. Langlois and J. J. DeStefano, *American Laboratory*, 2007, **39**, 18-21.

120. K. Kaczmarski and G. Guiochon, *Analytical Chemistry*, 2007, **79**, 4648-4656.

121. N. Marchetti and G. Guiochon, *Journal of Chromatography A*, 2007, **1176**, 206-216.

122. N. Marchetti, A. Cavazzini, F. Gritti and G. Guiochon, *Journal of Chromatography A*, 2007, **1163**, 203-211.

123. J. J. DeStefano, S. A. Schuster, J. M. Lawhorn and J. J. Kirkland, *Journal of Chromatography A*, 2012, **1258**, 76-83.

124. S. A. Schuster, B. E. Boyes, B. M. Wagner and J. J. Kirkland, *Journal of Chromatography A*, 2012, **1228**, 232-241.

125. S. A. Schuster, B. M. Wagner, B. E. Boyes and J. J. Kirkland, *Journal of Chromatography A*, 2013, **1315**, 118-126.

126. J. O. Omamogho, J. P. Hanrahan, J. Tobin and J. D. Glennon, *Journal of Chromatography A*, 2011, **1218**, 1942-1953.
127. B. M. Wagner, S. A. Schuster, B. E. Boyes and J. J. Kirkland, *Journal of Chromatography A*, 2012, **1264**, 22-30.
128. A. J. Alpert, *Journal of Chromatography A*, 1990, **499**, 177-196.
129. J. Pesek and M. T. Matyska, *LCGC North America*, 2007, **25**, 480-490.
130. J. J. Kirkland, S. A. Schuster, W. L. Johnson and B. E. Boyes, *Journal of Pharmaceutical Analysis*, 2013, **3**, 303-312.
131. B. Chauve, D. Guillarme, P. Cléon and J. L. Veuthey, *Journal of Separation Science*, 2010, **33**, 752-764.
132. T. A. Berger, *Journal of Chromatography A*, 2011, **1218**, 4559-4568.
133. J. McConathy and M. J. Owens, *Primary Care Companion to The Journal of Clinical Psychiatry*, 2003, **5**, 70-73.
134. A. Cavazzini, L. Pasti, A. Massi, N. Marchetti and F. Dondi, *Analytica Chimica Acta*, 2011, **706**, 205-222.
135. E. Yashima, *Journal of Chromatography A*, 2001, **906**, 105-125.
136. X. Lai, W. Tang and S.-C. Ng, *Journal of Chromatography A*, 2011, **1218**, 5597-5601.
137. T. J. Ward and K. D. Ward, *Analytical Chemistry*, 2012, **84**, 626-635.
138. K. Lomsadze, G. Jibuti, T. Farkas and B. Chankvetadze, *Journal of Chromatography A*, 2012, **1234**, 50-55.
139. T. Takeuchi, *Analytical and Bioanalytical Chemistry*, 2003, **375**, 26-27.
140. S. Bruns, J. P. Grinias, L. E. Blue, J. W. Jorgenson and U. Tallarek, *Analytical Chemistry*, 2012, **84**, 4496-4503.
141. R. G. Avery and J. D. F. Ramsay, *Journal of Colloid and Interface Science*, 1973, **42**, 597-606.
142. L. A. Colón, T. D. Maloney and A. M. Fermier, *Journal of Chromatography A*, 2000, **887**, 43-53.
143. R. J. Boughtflower, T. Underwood and C. J. Paterson, *Chromatographia*, 1995, **40**, 329-335.
144. A. M. Fermier and L. A. Colón, *Journal of Microcolumn Separations*, 1998, **10**, 439-447.
145. P. Marhol, R. Gažák, P. Bednář and V. Křen, *Journal of Separation Science*, 2011, **34**, 2206-2213.
146. J. O. Omamogho and J. D. Glennon, *Analytical Chemistry*, 2011, **83**, 1547-1556.

147. F. Gritti and G. Guiochon, *Journal of Chromatography A*, 2010, **1217**, 5069-5083.

148. F. Gritti and G. Guiochon, *Journal of Chromatography A*, 2014, **1333**, 60-69.

149. C. Fanali, A. Rocco, Z. Aturki, L. Mondello and S. Fanali, *Journal of Chromatography A*, 2012, **1234**, 38-44.

150. S. Fanali, S. Rocchi and B. Chankvetadze, *Electrophoresis*, 2013, **34**, 1737-1742.

151. M. G. Cikalo, K. D. Bartle, M. M. Robson, P. Myers and M. R. Euerby, *Analyst*, 1998, **123**, 87R-102R.

152. D. Wistuba, *Journal of Chromatography A*, 2010, **1217**, 941-952.

153. H. Lu and G. Chen, *Analytical Methods*, 2011, **3**, 488-508.

154. S. Fanali, G. D'Orazio, T. Farkas and B. Chankvetadze, *Journal of Chromatography A*, 2012, **1269**, 136-142.

155. D. R. Stoll, X. Li, X. Wang, P. W. Carr, S. E. G. Porter and S. C. Rutan, *Journal of Chromatography A*, 2007, **1168**, 3-43.

156. J. N. Fairchild, K. Horváth and G. Guiochon, *Journal of Chromatography A*, 2009, **1216**, 1363-1371.

157. D. R. Stoll, X. Wang and P. W. Carr, *Analytical Chemistry*, 2008, **80**, 268-278.

158. A. J. Alexander and L. Ma, *Journal of Chromatography A*, 2009, **1216**, 1338-1345.

159. S. Kittlaus, J. Schimanke, G. Kempe and K. Speer, *Journal of Chromatography A*, 2013, **1283**, 98-109.

160. S. A. Schuster, B. M. Wagner, B. E. Boyes and J. J. Kirkland, *Journal of Chromatographic Science*, 2010, **48**, 566-571.

161. S. Fekete, R. Berky, J. Fekete, J.-L. Veuthey and D. Guillarme, *Journal of Chromatography A*, 2012, **1236**, 177-188.

162. A. Staub, D. Zurlino, S. Rudaz, J.-L. Veuthey and D. Guillarme, *Journal of Chromatography A*, 2011, **1218**, 8903-8914.

163. J. Ruta, D. Zurlino, C. Grivel, S. Heinisch, J.-L. Veuthey and D. Guillarme, *Journal of Chromatography A*, 2012, **1228**, 221-231.

164. S. Fekete and D. Guillarme, *Journal of Chromatography A*, 2013, **1320**, 86-95.

165. A. Martínez-Villalba, E. Moyano, C. B. Martins and M. Galceran, *Analytical and Bioanalytical Chemistry*, 2010, **397**, 2893-2901.

166. Á. Tölgyesi, V. K. Sharma and J. Fekete, *Journal of Chromatography B*, 2011, **879**, 403-410.

167. Y. Lu, Q. Shen, Z. Dai and H. Zhang, *Analytical and Bioanalytical Chemistry*, 2010, **398**, 1819-1826.

168. D. Šatínský, K. Jägerová, L. Havlíková and P. Solich, *Food Analytical Methods*, 2013, **6**, 1353-1360.

169. K. P. Yáñez, J. L. Bernal, M. J. Nozal, M. T. Martín and J. Bernal, *Journal of Chromatography A*, 2013, **1285**, 110-117.

170. H. Gallart-Ayala, O. Núñez and P. Lucci, *TrAC Trends in Analytical Chemistry*, 2013, **42**, 99-124.

171. H. Gallart-Ayala, E. Moyano and M. T. Galceran, *Journal of Chromatography A*, 2011, **1218**, 1603-1610.

172. H. Gallart-Ayala, E. Moyano and M. T. Galceran, *Analytica Chimica Acta*, 2011, **683**, 227-233.

173. S. Bayen, X. Yi, E. Segovia, Z. Zhou and B. C. Kelly, *Journal of Chromatography A*, 2014, **1338**, 38-43.

174. P. Vazquez-Roig, C. Blasco and Y. Picó, *TrAC Trends in Analytical Chemistry*, 2013, **50**, 65-77.

175. N. Fontanals, R. M. Marcé and F. Borrull, *Journal of Chromatography A*, 2011, **1218**, 5975-5980.

176. M. Pedrouzo, F. Borrull, E. Pocurull and R. M. Marcé, *Journal of Separation Science*, 2011, **34**, 1091-1101.

177. L. Ciofi, D. Fibbi, U. Chiuminatto, E. Coppini, L. Checchini and M. Del Bubba, *Journal of Chromatography A*, 2013, **1283**, 53-61.

178. H. Gallart-Ayala, E. Moyano and M. T. Galceran, *Journal of Chromatography A*, 2010, **1217**, 3511-3518.

179. W. Peysson and E. Vulliet, *Journal of Chromatography A*, 2013, **1290**, 46-61.

180. M. C. Hurtado-Sánchez, R. Romero-González, M. I. Rodríguez-Cáceres, I. Durán-Merás and A. G. Frenich, *Journal of Chromatography A*, 2013, **1305**, 193-202.

181. P. Zhang, A. Bui, G. Rose and G. Allinson, *Journal of Chromatography A*, 2014, **1325**, 56-64.

182. P. Chocholouš, J. Vacková, I. Šrámková, D. Šatínský and P. Solich, *Talanta*, 2013, **103**, 221-227.

183. G. Vinci, M. L. Antonelli and R. Preti, *Journal of Separation Science*, 2013, **36**, 461-468.

184. G. Purcaro, S. Moret, M. Bučar-Miklavčič and L. S. Conte, *Journal of Separation Science*, 2012, **35**, 922-928.

2 Synthesis of Spheres on Sphere Silica Particles

2.1 Introduction

As has been discussed in the introduction, core-shell particles for use in HPLC are typically prepared by a time-consuming LbL approach. A simpler synthetic process or a one-pot reaction would be highly advantageous, offering a reduction in reaction time, easier quality control and lower material costs. The particles should also have ideal properties for use in HPLC, namely spherical microspheres with narrow particle size distribution (PSD). The recent discovery of spheres on sphere (SOS) particles[1] offers a route to a new type of core-shell morphology obtained from a fast, one-pot reaction.

This chapter will discuss SOS particles, describing the synthesis and morphology. The reaction is based around the Stöber method of producing silica spheres,[2] therefore it will also be important to consider the basis of this reaction and alkyl orthosilicate precursors in general within the literature review.

The aim of the experimental work in this chapter is to investigate the synthetic procedure, observing the morphology changes from varying experimental parameters and to optimise the reaction conditions to produce SOS particles suitable for chromatographic use.

2.2 Literature Review

2.2.1 Alkyl Orthosilicate Precursors

Many of the silica particles used in chromatography are produced from alkyl orthosilicate precursors. Alkyl orthosilicates have the structure $Si(OR)_4$, where R is an alkyl chain typically ranging up to five carbon atoms in length. Tetraethyl orthosilicate (TEOS) is frequently used in the synthesis of silica particles.[2-5] Alkyl orthosilicates are produced from the dropwise addition of silicon tetrachloride ($SiCl_4$) to an anhydrous alcohol.[6] The alcohol must be present in a 10% excess to ensure completion of the reaction and $SiCl_4$ chilled to 0 °C to control the reaction. Most of the residual hydrochloric acid is removed by sparging the reaction product with dry nitrogen gas, however calcium oxide may also be required to minimise the content of acid in the final product.[7] Further purification can be achieved through vacuum distillation.

Silica materials are produced from alkyl orthosilicates firstly via hydrolysis of the orthosilicate to orthosilicic acid (H_4O_4Si), followed by condensation into further higher silicic acids with the general formula $[SiO_x(OH)_{4-2x}]_n$.[8] The reaction proceeds slowly under neutral conditions, and may instead be catalysed by the use of acidic or basic conditions. Under acidic conditions (figure 2.1), a hydrogen ion attacks oxygen in the orthosilicate allowing a water molecule to attack the silicon atom.[9, 10] This results in the formation of a Si-OH group and the removal of the alkyl group in the form of an alcohol. Under basic conditions (figure 2.2), a hydroxide ion attacks the silicon atom directly, allowing a water molecule to attack the alkyl group. Again, this results in the removal of the alkyl group in the form of an alcohol, plus a new hydroxide ion.[5, 9, 10] The net reaction is given as:

$$n\ Si(OR)_4 + 2n\ H_2O \rightleftharpoons (SiO_2)_n + 4n\ ROH$$ [11]

Hydrolysis

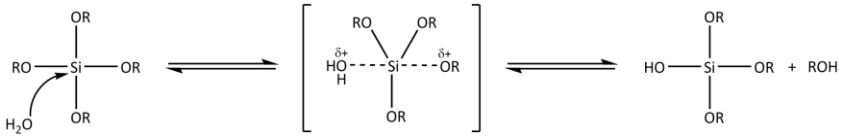

Condensation

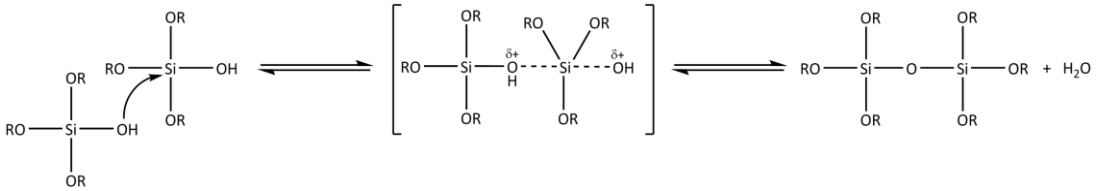

Figure 2.1 Acid catalysed hydrolysis and condensation.[10]

Hydrolysis

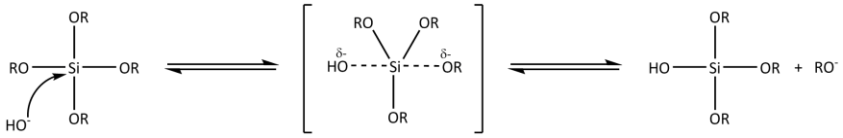

Condensation

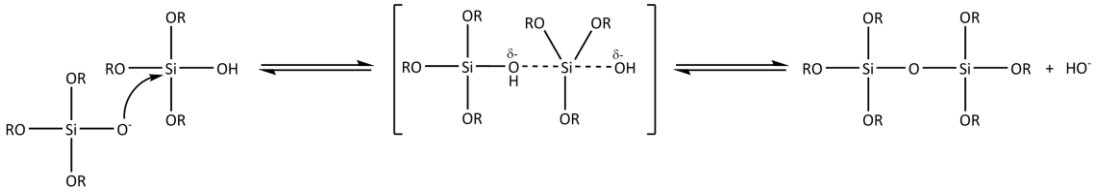

Figure 2.2 Base catalysed hydrolysis and condensation.[10]

2.2.2 Stöber Particle Synthesis

The Stöber process is a commonly reported synthesis of solid monodisperse silica spheres.[2] This reaction utilises alkyl orthosilicates as the silica precursor, added to a solution containing water, a low molecular weight alcohol and is catalysed by a base. The reaction scheme is shown in figure 2.2. A key advantage to using basic over acid catalysed reactions is the tendency to form monodisperse spheres. Stöber systematically studied the reaction and found the resultant particle diameter could be varied between 50 nm and 2 µm, depending on choice of silica precursor, choice of alcohol and the volume ratios of reagents. The reactions were performed at room temperature with constant agitation. The use of sonication, shaking and magnetic stirring were all found to be effective at keeping particles in suspension during formation. The total amount of solution in each experiment was in the range of 50-110 mL, although the reaction volume was increased to 2 L for one experiment to assess any change in particle morphology. The scaled up reaction yielded identical results to an 80 mL reaction, using the same concentration of reagents.

The alcohols investigated were methanol, ethanol, n-propanol and n-butanol. The reaction rate was found to be fastest when using methanol, which also resulted in the smallest particle size. The reaction rate was slowest with n-butanol and led to the largest particle size. A broad PSD was also observed when using larger alcohols; however a 1:1

mixture of methanol and n-butanol provided more uniform large particles. A similar relationship between reaction rate and particle size was observed when changing the carbon chain length of the orthosilicate. The alkyl orthosilicates used were tetra methyl orthosilicate, tetra ethyl orthosilicate, tetra n-propyl orthosilicate, tetra n-butyl orthosilicate and tetra n-pentyl orthosilicate, which were redistilled before use. The fastest reaction and smallest particle size were again obtained when using tetra methyl orthosilicate while the slowest reaction and largest particle size was observed with tetra n-pentyl orthosilicate. The PSD was also broadened as the particle size was increased.

An investigation into the influence of the concentration of water, ammonia and alkyl orthosilicate was made using ethanol and TEOS in the reaction.[2] Ammonia had a large influence on the morphology and created spherical particles whenever it was present during the reaction. In the absence of ammonia, irregularly shaped particles were formed. An increase in ammonia concentration led to the formation of larger particles. The largest spheres were obtained when the reaction mixture was saturated with ammonia (8 M). When the water concentration was varied, a maximum particle size of around 800 nm was reached when the concentration of water was around 6 M. Different concentrations of TEOS did not have a significant influence on particle size.

The work was extended by Bogush *et al.*, who established the ranges of reagent concentrations that would result in the production of monodisperse silica particles from the reaction composed of water, ethanol, ammonia and TEOS.[3] Concentration ranges were reported as 0.1-0.5 M for TEOS, 0.5-17 M for water and 0.5-3M for ammonia. The reaction volume was varied between 150 mL and 4 L without significant variation in final particle size and reactions were left to stir at room temperature for 3-8 hours. The maximum particle size achieved was again found to be around 800 nm, which was obtained when using concentrations of 0.3 M TEOS, 7 M water and 2 M ammonia. The particle size was found to go through a maximum as both water and ammonia concentration were increased.

Additionally, the study established a relationship between the final particle size and the initial reagent concentrations. The resultant expression was determined from experimental observations of around 100 samples. D_P is the average diameter in nm and reagent concentrations are shown in mol/L.

$D_P = A[H_2O]^2 \exp(-B[H_2O]^{½})$

$A = [TEOS]^{½} (82 - 151[NH_3] + 1200[NH_3]^2 - 366[NH_3]^3)$

$B = 1.05 + 0.523[NH_3] - 0.128[NH_3]^2$

The predicted diameters plotted against the experimentally observed diameters found that the majority of the data falls within 20% deviation. Likewise, the resultant particle size obtained experimentally from varying water and ammonia concentration provide very close values to those predicted by the above relationship.

Although it is possible to achieve monodisperse particles from the water, ethanol, ammonia and TEOS reaction, the maximum diameter appears to be limited to around 800 nm. Several strategies have been suggested to increase the particle size. Stöber *et al.* performed the reaction with alternative alcohols and alkyl orthosilicates.[2] The synthesis of particles up to 2 μm in size was reported in this case, however the PSD was significantly broadened. Alternative methods are to increase the ionic strength of the reaction,[12] or to perform the reaction at reduced temperature. For example, when conducting the synthesis at -20 °C particles around 1.9 μm in diameter were produced, compared to 0.5 μm at room temperature.[13]

Another method is to use seeded growth. Bogush *et al.* conducted experiments where a seed suspension is initially prepared using normal Stöber reaction conditions.[3] The size of the seed was not found to influence the PSD of the final product and was selected on the basis of the desired final size. Additional TEOS and water were added to the seed suspension in a 1:2 molar ratio after the seed suspension had stopped reacting. Up to twice the original amount of TEOS was added in each subsequent addition at an interval of 8 hours for up to 10 additions. Particles up to 1 μm in diameter were produced using this method.

Similarly, Giesche described the preparation of monodisperse silica particles by a controlled growth process.[7] Mixtures of TEOS/ethanol and ammonia/water/ethanol were added continuously to a suspension of seed particles, with the addition rate controlled by a pair of peristaltic pumps. Monodisperse particles up to 3.6 μm in diameter were produced by this method. The equipment used however was highly complex and required the TEOS to be vacuum distilled and further treated with calcium oxide to remove any residual

hydrochloric acid from the synthesis. Additionally it was important to avoid any reaction in the TEOS/ethanol droplets before they reached the seed suspension as any pre-hydrolysis can result in secondary nucleation. The TEOS/ethanol inlet was therefore adjusted to obtain free falling droplets which were added in a flow of dry air to keep any ammonia present in the gas phase away from the inlet.

As another example of continuous seeded growth, Unger *et al.* described the formation of monodisperse silica particles with mean particle diameters between 0.05-10 µm.[14] The particles were produced by a two-step process. Initially a suspension of seed particles was prepared, followed by controlled addition of an alkyl orthosilicate until the desired particle size was achieved. Of the examples stated in the patent, the largest diameter was 3.1 µm. The number of initial seed particles defined the total number of spheres produced. No new particles were synthesised from the secondary addition of the silica precursor, instead the rate of addition was controlled to the extent that only growth upon the initial seeds was observed.

2.2.3 Surfactant Templated Silica

The particles produced from the Stöber reaction are typically non-porous and therefore have low surface area. In many applications, particularly chromatography, porosity is important to facilitate retention and efficient separation of analyte molecules. Porous materials can be classified into three groups according to their pore size: microporous (<2 nm), mesoporous (2-50 nm) and macroporous (>50 nm).[15] Porosity may be generated by the use of templates present during the synthesis reaction. Micropores and mesopores are typically formed by the use of ionic surfactants,[16, 17] or block copolymers.[18] Macropores require larger templates and can be formed by emulsion templating,[19, 20] colloidal templating,[21, 22] or polymer gel templating.[23-25]

Surfactants are organic compounds that are amphiphilic, consisting of a hydrophilic head (typically a polar group) and a hydrophobic tail (typically a hydrocarbon chain). They are classified according to the polar head group. They may be described as non-ionic, anionic, cationic or zwitterionic, depending on the overall charge and functionality present on the head. The amphiphilic nature means that they have a tendency to assemble at interfaces,[26] reducing the system free energy. The surface tension varies strongly with the concentration of surfactant and subsequently surfactants are induced to aggregate into

micelles. In 1913 McBain described the basic ideas for spherical colloidal micelles, termed "colloidal ions", prepared in soaps and detergents.[27] This later led to the introduction of the concept of critical micelle concentration (CMC).

The CMC is an important characteristic of a surfactant. This is defined as the surfactant concentration above which micelle formation occurs. In the micelle structure, the hydrophobic tails of the surfactant molecules are contained within roughly spherical aggregates, while the head portions form an outer layer around which water molecules are present.[28] Beyond the CMC, self-assembly occurs to form micellar rods.[29] Increasing the concentration further leads to agglomeration into hexagonal, lamellar or cubic liquid crystal structures, depending on concentration and temperature.[30] These liquid crystal phases may be used as templates to form porous materials.

There has been extensive interest in the synthesis of mesoporous silica materials since the discovery of the M41S materials by the Mobil group in 1992.[16, 31] Notable examples include MCM-41, MCM-48 and MCM-50, which possess hexagonal, cubic and lamellar mesostructures, respectively. The abbreviation MCM refers to Mobil Composition of Matter. The synthetic procedure utilised aggregates of surfactant molecules in the form of a liquid crystalline phase as structure directing agents. This led to the assembly of an ordered mesostructured composite around which the condensation of silica precursors was performed under basic conditions. Materials with narrow pore size distribution, high surface area and high ordering of mesopores were then obtained by removal of the surfactant by calcination or acid extraction. The pore size can be directly controlled by the choice of surfactant. Cetyltrimethylammonium bromide (CTAB), containing a C16 hydrophobic tail, is commonly used in the formation of mesoporous silica materials. Beck *et al.* reported the use of surfactants with shorter tails (C14, C12 and C8), noting that reducing the chain length led to the production of MCM-41 with smaller mesopores which correlated directly with the size of the micelle.[31] Achievable pore sizes were in the range of 2-15 nm.

Two mechanisms have been proposed to describe the formation of the M41S materials. One possibility is a true liquid crystal templating mechanism, shown in figure 2.3. In this case, the concentration of surfactant (CTAB) forms a lyotropic liquid crystalline phase without requiring the addition of a silica source (TEOS).[32] The silica source, once added, then undergoes condensation around the hexagonal CTAB template. Alternatively, the second method proposes that addition of TEOS to a CTAB solution induces ordering of

silicate-encased surfactant micelles simultaneously, and that micelle formation requires the presence of the silicate.

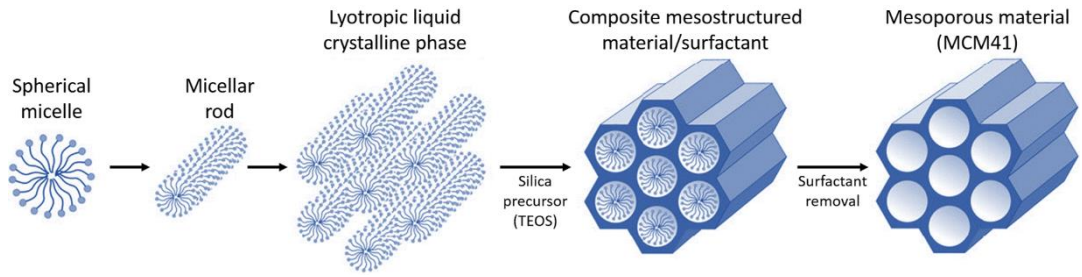

Figure 2.3 Formation of the mesoporous silica material MCM-41 via a true liquid crystal templating mechanism.[32]

The initial studies into the M41S family of materials led to other research groups developing alternative synthetic methods to obtain mesoporous silica materials. One alternative is the Santa Barbara Amorphous (SBA) class of silica materials, synthesised under acidic conditions.[18, 33] This class of materials, particularly SBA-15, have also earned much attention due to their excellent thermal stability, variable pore size, and tailored particle morphology. The pore system consists of a mesoporous network formed as a result of a liquid crystal template arrangement, using the amphiphilic, non-ionic triblock copolymer poly(ethylene oxide)-b-poly(propylene oxide)-b-poly(ethylene oxide) as the structure directing agent.[34] Pore sizes from 30-100 nm could be obtained via this templating method.[18]

2.2.4 Spheres on Sphere Particles

Ahmed *et al.* described a method of producing uniform porous silica microspheres from TEOS, using a modified Stöber reaction.[35] The addition of CTAB to the reaction was found to introduce porosity into the particles. A hydrophilic polymer, poly(vinyl alcohol) (PVA), was also introduced which stabilised the particles, prevented aggregation and facilitated the production of uniform and well-dispersed particles with high surface area. The average pore size of the particles was measured to range from 2.5-3.5 nm when using CTAB as the templating agent, depending on the type and concentration of polymer used.

While small pores are suitable for catalysis, sensors and controlled delivery, silica particles for use HPLC typically require mesopores in the range of 6-50 nm to achieve efficient separation.[36] Ahmed found that the pore size could be increased up to 6.5 nm by the use of swelling agents and hydrothermal treatment. The monodisperse PSD and resultant mesoporous structure would make them ideal for chromatographic use, however the small diameter of the particles, typically less than 1 µm, meant that high backpressure would likely prove problematic when packed into HPLC columns and subsequently they were not used for this purpose.

Following on from this work led to the discovery of SOS particles.[1] This is a new type of core-shell particle produced from an alternative modified Stöber reaction using the silica precursor 3-mercaptopropyl trimethoxysilane (MPTMS). Again, CTAB and PVA were present in the reaction to act as a template and stabilising agent respectively. Particles were formed in a one-pot reaction and were composed of a large core surrounded by a single layer of nanospheres up to 200 nm in diameter. The mean particle diameter was around 5.5 µm with a broad PSD. Analysis by nitrogen adsorption found the SOS material to be microporous, with surface area of around 200 m^2/g and peak pore sizes of 0.91 and 1.54 nm after calcination in air at 600 °C. The SEM image and nitrogen adsorption data are shown in figure 2.4.

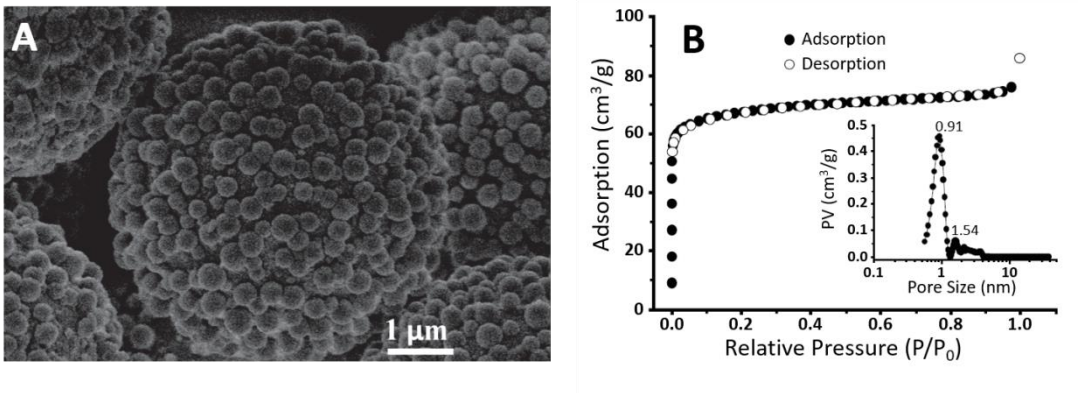

Figure 2.4 Scanning electron microscope (SEM) image of SOS particles (A). Nitrogen adsorption data (B) and pore size data (B, inset).[1]

The formation of SOS particles was discussed briefly in the introduction. In a time study, the morphology of particles produced at various intervals during the synthesis was imaged by SEM. As shown in figure 1.7 in chapter 1, it was found that particles are produced via a two-stage nucleation. In the first stage, formation of smooth silica microspheres (core particles) occurs within 30 minutes. In the second stage, nucleation of nanospheres to form the single layer shell occurs on the surface of the microspheres. No further growth was observed after 180 minutes, at which point fully-formed SOS particles could be isolated.

When using TEOS as the silica precursor, the introduction of CTAB to the modified Stöber reaction was found to produce mesoporous particles.[35] The SOS material produced from MPTMS however was found to be microporous, indicating that CTAB templates were absent in the particles. The formation of micropores was instead attributed to the removal of residual mercaptopropyl groups during calcination at 600 °C. It was noted however that the presence of CTAB was essential to obtain the SOS morphology, as omission of surfactant led to the formation of smooth microspheres only. Despite the microporous nature of particles, the unique single-layer shell morphology leads to the formation of interstitial macropores between the surface nanospheres when packed into a HPLC column.[37] Initial HPLC testing showed promising results from a range of surface functionalities including reverse-phase (C4, C8, C18), normal-phase (silica, diol) and HILIC (diol) phases.[38] The relatively large particle size and microporous nature resulted in very low operating pressure.

SOS particles were further used as supports onto which an additional layer of metal-organic framework (MOF) nanocrystals was synthesised.[39] MOFs are a type of crystalline porous materials formed via the linkage of metal ions and organic ligands.[40] Most MOFs exhibit microporous structures, although great effort has been made to prepare mesoporous MOFs, for example by ligand extension or combining the synthesis with surfactant templating. The pore size, pore shape, and pore surface functionality are very well defined in MOFs, making them suitable for highly selective separation of gases or small molecule liquids.[40, 41]

MOFs have previously been packed into columns for liquid phase separation,[42] however low separation efficiency and poor column stability are often observed for such columns. An explanation for this is that MOFs are normally prepared as irregularly shaped microparticles. The packing of such particles is very difficult, often leading to an unstable

packing bed, crushed particles and high back pressure. To address this problem, MOF nanocrystals could be synthesised onto silica microsphere supports as a new type of packing material. HKUST-1, a thermally stable cubic MOF with a channel pore size of 1 nm formed by the ligand 1,3,5-benzenetricarboxylic acid and copper(II) acetate ($Cu_2(OAc)_4$) units, was used in the study.[39] HKUST-1 nanocrystals were formed onto SOS microspheres which had been functionalised with surface carboxylate groups. The silica support was non-porous. The presence of microporous HKUST-1 was confirmed by nitrogen adsorption analysis. SEM images and nitrogen adsorption data are shown in figure 2.5. Compared to the packed HKUST-1 particles, the composite core-shell column showed fast separation of xylene isomers. Similarly, another type of MOF (ZIF-8) shell consisting of nanocrystals was formed onto commercially available 3 µm silica microspheres with carboxylic modification. The packed columns showed high column efficiency for the separation of endocrine disrupting chemicals and pesticides.[43]

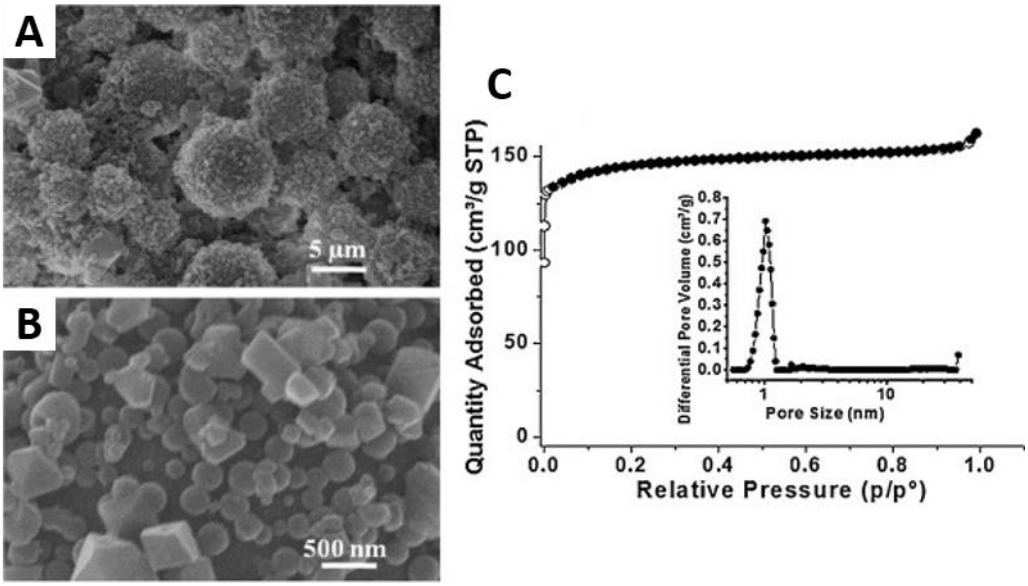

Figure 2.5 HKUST-1 nanocrystals synthesised onto SOS silica particles. The resultant particles (A) and the surface morphology (B) are shown by SEM imaging. The nitrogen adsorption data (C) shows a microporous material with pore size of around 1 nm.[39]

2.2.5 Aims

The aim of the experimental work in this chapter is to establish optimal conditions to obtain reproducible SOS particles from the modified Stöber reaction. It will also be important to gain a degree of control over the particle morphology, specifically the particle diameter, PSD and coverage of surface nanospheres. Previous studies have suggested that this may be achievable through choice of reagent and concentration.

There are several experimental parameters that can be altered in the SOS reaction which will be described in turn, along with the resultant morphology changes. The aim is to understand the effect each reagent has on the reaction to ultimately be able to control the particle morphology. The SOS material produced should have properties that are desirable for use in HPLC; spherical, particle diameter between 2-5 µm and narrow PSD. Previously, synthesis has typically been performed on a small scale. Once a reproducible production method has been established, scale-up should also be assessed.

It has been discussed in chapter 1 that reducing the thickness and porosity of the shell of core-shell particles leads to improved chromatographic performance, particularly for large molecules, due to a reduction in B and C terms of the van Deemter equation. Indeed, the HPLC column prepared by Ahmed *et al.* displayed promising performance in the separation of a protein test mix.[1, 38] The SOS particles will therefore be prepared with the intended application of peptide, protein and large molecule analysis.

2.3 Experimental

There are five components that can be varied in the synthesis reaction of SOS particles: base, surfactant, polymer, solvent and silica precursor. The experimental work in this chapter aims to modify each of these reagents in turn, observing the resultant morphology changes. Both the choice and concentration of reagent will be assessed, with the aim to produce SOS particles with a complete shell of nanospheres and narrow PSD. Particles will be characterised by particle sizing, SEM imaging, nitrogen adsorption, mercury intrusion and thermogravimetric analysis (TGA).

2.3.1 Chemicals

Ammonium hydroxide (28-30%, NH_3 basis), cetyltrimethylammonium chloride (CTAC, 25% in water), CTAB (≥98%), MPTMS (95%), n-butanol (>99%), Poly(ethylene glycol) (PEG, M_W = 10k), Poly(methyl vinyl ether) (PMVE, 50% in water), PVA (M_W = 2k, 9-10k, 16k, 22k, 31-50k), polyvinylpyrrolidone (PVP, M_W = 10k, 29k, 40k, 55k), Sodium dodecyl sulfate (SDS, 95%), sodium hydroxide (≥98%), tannic acid (ACS reagent), triethylamine (≥99%), TWEEN 20 and TWEEN 80 were purchased from Sigma-Aldrich. Acetone (GPR), ethanol (ABS), methanol (AR) and isopropanol (HPLC grade) were obtained from Fisher Scientific. All chemicals were used as received. Deionised water was prepared in the laboratory.

2.3.2 The Standard Reaction

A set of standard conditions is described which will be referred to when modifying further reactions. This reaction results in well-defined spherical SOS particles with a dense, but incomplete surface coverage of nanospheres, shown in figure 2.6. Particles produced by this method typically have a mean particle size of 3-4 µm in diameter and a broad PSD, with a $d^{90}/_{10}$ ratio between 1.8 and 2.2. All reactions were performed at room temperature on an IKA 15-position magnetic stirrer plate. Stirring was performed using Teflon coated stirrer bars. The speed was kept constant at setting 8 (approximately 800 rpm) for all reactions and was sufficient to keep resultant particles suspended in the solution.

The standard conditions are as follows: PVA (0.25 g) and CTAB (0.1 g) were dissolved in deionised water (5 mL) with gentle heating to aid dissolution. The concentrations of polymer and surfactant were 5% and 2% weight based on water. Methanol (8 mL) was added, followed by diluted ammonium hydroxide (2 mL, 5.6%). The solution was stirred for 15 minutes before addition of MPTMS (500 µL). The reaction was stirred overnight. SOS particles were collected on a sintered glass filter and washed with distilled water (5 x 20 mL), then methanol (5 x 20 mL) before drying under vacuum at 60 °C. Typically 0.35 g of particles were produced.

Reactions were performed in new glassware each time. Significant variation in particle diameter of Stöber spheres was observed by Ahmed with repeated use of glassware, even following a thorough cleaning procedure.[44] It is thought that the harsh basic conditions in the reaction have a detrimental effect on the walls of the glass vessel

and that a reaction occurs at the terminal silanol sites. It was observed in these studies that the areas of glassware exposed to the reaction solution became cloudy during the synthesis, even at the lowest base concentration, indicating that a reaction does occur on the surface and some particles may be attached to the vessel wall. When reusing glassware, even after thorough cleaning, some of the previous particles may still be present on the walls of the vessel. It is thought that these can act as a seed, promoting growth of larger particles and thus accounting for the variation in the diameter.

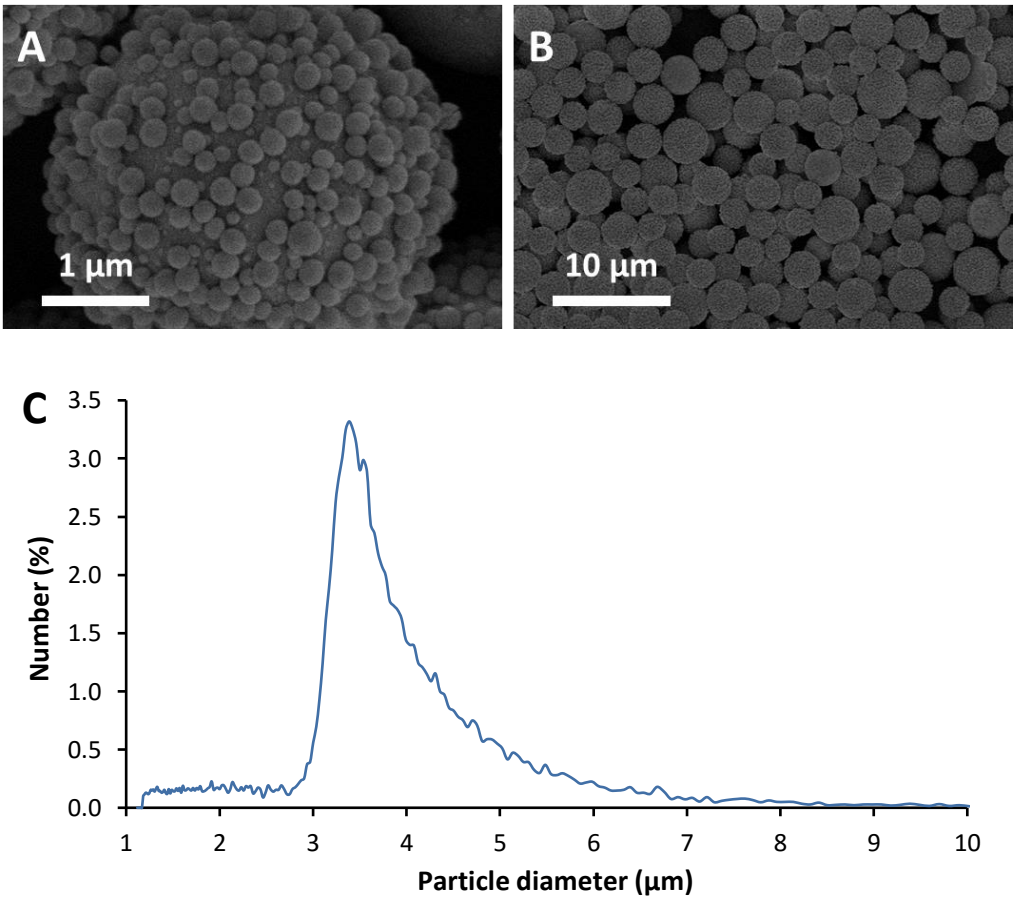

Figure 2.6 SOS particles produced from the standard reaction. Particle morphology (A) and dispersity (B) are shown by SEM imaging, along with the PSD (C).

2.3.3 Characterisation

Following drying under vacuum, SOS particles were calcined in a furnace (Carbolite CWF1200) to remove the residual mercaptopropyl groups and any components left over from the particle synthesis. Conditions: heat in air at 1 °C/min, hold at set temperature for 12 hours, then allow to cool to room temperature. Particles were calcined between 450 and 1000 °C for 12 hours to assess the effect on physical properties. The results in table 2.1 show that sample mass and surface area are reduced as the furnace temperature is increased, with the steepest drop in surface area observed between 550-650 °C. There is also a small decrease in particle diameter as the furnace temperature is increased.

Table 2.1 Effect of calcination temperature on physical properties of SOS particles.

Temperature (°C)	% mass loss	Surface area (m^2/g)	Particle diameter (µm)
450	48.1	288	2.27
500	49.2	256	2.21
550	49.9	233	2.30
600	52.3	138	2.22
650	54.0	18	2.14
700	54.4	6.0	2.15
750	54.7	5.1	2.16
800	54.7	4.8	2.12
850	54.8	4.0	2.08
900	55.2	4.8	2.05
950	55.2	4.4	2.07
1000	55.4	3.9	2.04

Particle sizing was performed using a Beckman Coulter Multisizer 3 at Thermo Scientific, using an electrical zone sensing method based on the Coulter principle.[45] In a Coulter counter instrument, a tube with a small aperture on the wall is filled with an electrolytic solution and immersed in a vessel containing particles that are dispersed at low concentration in the same electrolytic solution. Two electrodes are inserted into the solution, one inside and one outside the aperture tube. An electric field is applied to form a current path provided by the electrolyte, and the impedance between the electrodes is measured. Particles pass through a sensing zone provided by the aperture when the suspension is drawn from the vessel, and a volume of the electrolyte equivalent to the immersed volume of the particle is displaced from the sensing zone. This causes a short term change in the resistance across the aperture which is measured as a voltage pulse or a current pulse. By measuring the number of pulses and their amplitudes, it is possible to collect information about the number of particles and the volume of each individual particle. The number of pulses counted during measurement relates to the number of particles measured and the amplitude of the pulse is proportional to the volume of the particle. From this data it is possible to construct the PSD.[46] In this study the number distribution is used throughout, where each particle has equal weighting within the PSD regardless of the diameter. Alternatively, volume statistics may be used where particles with a larger diameter and therefore volume represent a greater proportion of the PSD. Measurement of number distribution is preferred here as the mean diameter of SOS particles is typically less than 5 µm.

Different size apertures can be used depending on the size range of interest. A range of aperture sizes are available, typically from 20-2000 µm. Each aperture can be used to measure particles within a size range of 2 to 80% of its nominal diameter. Therefore, the measurement of particle sizes ranging of 0.4 to 1600 µm is possible.[46, 47] However, it should be noted that the ability of analysing particles is limited to those particles that can be suitably suspended in an electrolyte solution. The selection of the most suitable aperture size is also dependent upon the particles to be measured. For example a 50 um diameter aperture can measure a particle size range of 1-40 µm.

Samples in this study were prepared by dispersing in Isoton II electrolyte and analysed using a 30 or 50 µm diameter aperture for 30000 counts at a current of 800 µA. The PSD, defined by the $d^{90}/_{10}$ ratio, was measured from the sizing data. The value for d90 is the particle size measured at the 90th percentile of the cumulative PSD, similarly the d10

is the particle size measured at the 10th percentile. Division of d90 by d10 gives an indication of dispersity, with a smaller value indicating a narrower PSD.[48]

Particle morphologies were imaged with a Hitachi S4800 scanning electron microscope (SEM). The maximum useful magnification achievable with a conventional optical microscope is around 1000×. When imaging samples such as micron-sized particles, particularly when the surface morphology is of interest, this level of magnification is insufficient. For increased resolution and higher useful magnification, the wavelength of the imaging radiation must be decreased.[49] The SEM is a type of microscope that utilises a focused beam of high energy electrons to generate a variety of signals though interaction with the sample of interest. This allows much higher magnification, up to 500000×, and provides resolution down to the nanometre scale.[50-52] Although SEM is most commonly used to provide images of the sample morphology, characterisation may also be performed.[53]

Samples were prepared for SEM by depositing a thin film of SOS particles onto an aluminium SEM stud. This was achieved either by a placing a drop of a dilute suspension of particles in methanol onto the stud and allowing the solvent to evaporate, or by placing a small amount dried powder onto double-sided carbon tape and removing the loosely held excess. For imaging, the sample must be electrically conductive and grounded to avoid accumulation of charge at the surface which may result in scanning faults. SOS samples were made conductive by coating in gold using an Emitech K550X sputter coater for 2 minutes at 25 mA.

Measurement of Brunauer-Emmett-Teller (BET) surface area[54] was performed by nitrogen adsorption at 77 K, using a Micromeritics ASAP 2420 adsorption analyser. Where only surface area measurement was required, a Quantachrome NOVA 4200e adsorption analyser was used. The pore diameter was calculated from Barrett-Joyner-Halenda (BJH) desorption data.[55] Samples were degassed overnight at 120 °C before analysis.

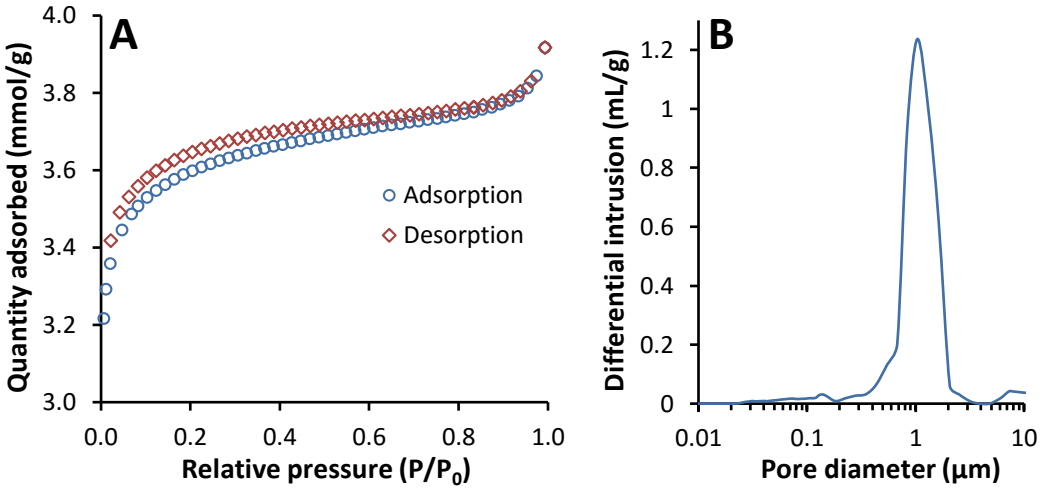

Figure 2.7 Nitrogen isotherm plot (A) and mercury intrusion plot (B) for SOS particles prepared from the standard reaction.

The nitrogen isotherm for the SOS particles obtained from the standard reaction is shown in figure 2.7 A. The BET surface area was measured to be 240.4 m^2/g, with an average pore diameter of 2.2 nm. The plot suggests a type I isotherm, which is normally observed for microporous silica. As the measurement of pore size using nitrogen adsorption is limited to around 100 nm, the interstitial pore size between particles was measured by mercury intrusion porosimetry[56] using a Micromeritics Autopore IV 9500. The non-wetting property and high surface tension of mercury means that it does not intrude into the pores without external pressure. From the pressure versus intrusion data, the instrument can generate pore size distributions using Washburn's equation.[57] The mercury intrusion plot is shown in figure 2.7 B, indicating a pore size of around 1 µm.

TGA is a thermal analysis method in which the mass of a substance is monitored as either a function of increasing temperature with constant heating rate, or as a function of time with constant mass loss or constant temperature.[58] A typical instrument consists of a sample pan that is supported by a precision balance. The pan resides within a furnace and is heated or cooled while the change in mass is monitored. A purge gas which may be reactive or inert controls the sample environment. Additionally, instruments may also have means to analyse the volatile components that are produced from the decomposition of samples.

SOS particles were analysed using a TA Instruments Q500 to assess the percent mass loss with increasing temperature. The differential thermogravimetric curve, shown in

figure 2.8, displays an initial step between 200 and 300 °C due to removal of residual PVA and CTAB from the synthesis reaction, accompanied by loss of mercaptopropyl groups up to 700 °C. There is limited mass loss beyond 700 °C, above which a maximum value of 54% loss is reached. This is consistent with the results obtained in table 2.1. CHNS analysis of as-prepared SOS particles showed the material to contain 20.44% carbon, 5.51% hydrogen, 0.75% nitrogen and 23.61% sulfur due to the presence of mercapto groups and residual surfactant. After calcination at 1000 °C these values were reduced to zero, indicating the organic content had been removed.

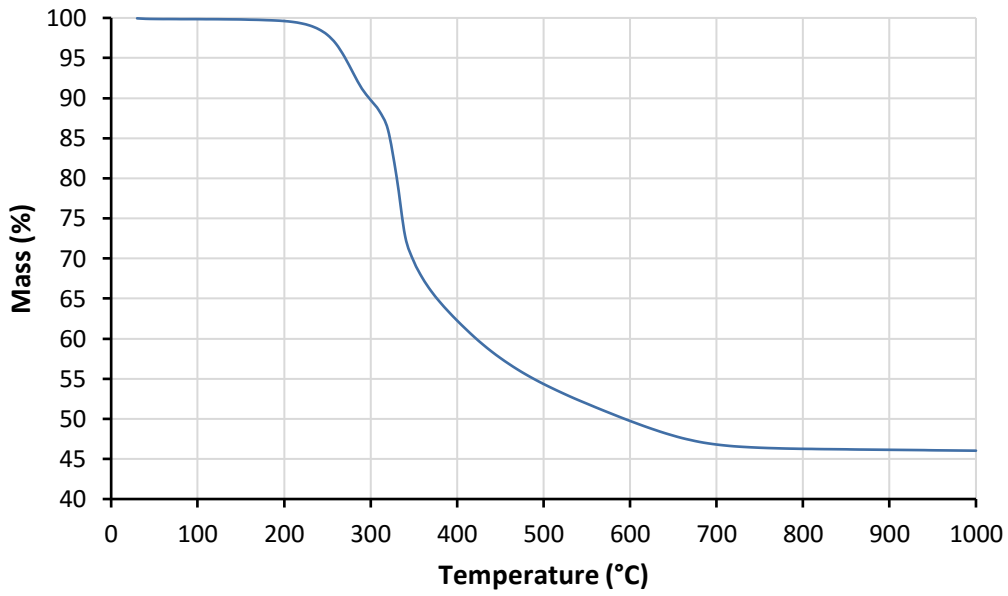

Figure 2.8 Differential thermogravimetric curve for SOS silica particles.

2.4 Results and Discussion

Initially, each of the components in the standard reaction were investigated. The resultant changes in particle morphology were assessed by changing each component in turn. The concentration of each reagent was considered, as well as alternative chemicals. The reaction conditions were then modified further by combining the positive effects of each reagent change, with the aim of producing monodisperse particles with a complete single shell of nanospheres on the surface. The results section will describe the modifications to reaction parameters and the numerous particle morphologies generated from this.

2.4.1 Effect of Base

The standard reaction was performed using as-bought ammonium hydroxide solution diluted to 5.6% with distilled water. Firstly, an investigation was carried out to determine the influence of ammonia concentration on the morphology of the SOS particles. It has been shown that as the pH in the Stöber reaction is altered, there is a change in particle diameter, with increasing pH leading to larger particles.[2, 3] The method used to synthesise SOS particles is based on the Stöber reaction with additional components and it has previously been shown that ammonia concentration can have a large effect on the resultant SOS particle morphology.[1] The concentrations of ammonium hydroxide used in this study are described in table 2.2 along with the resultant values for surface area, particle diameter and PSD. All other parameters were unchanged.

Particles from each of the reactions were imaged using SEM to observe the morphology changes. The images are shown in figure 2.9. It is clearly shown that as the ammonia concentration is reduced, the density of nanoparticles on the surface increases. There is a significant difference between 28% (undiluted, reaction solution pH = 11.8) which shows barely any surface particles, and 0.7% (reaction solution pH = 10.5) which displays a near-complete shell. Another observation made after MPTMS addition was the time taken for the solution to turn cloudy, the point at which microspheres (core particles) are produced. As ammonia concentration was increased, a shorter time was taken for the reaction to display cloudiness. For example, the reaction with 28% ammonia displayed cloudiness within 1 minute, but when reducing the concentration to 0.7%, the time increased to 20 minutes.

There is a clear link between reaction pH and surface nanoparticle density. As the pH is increased, the density of nanoparticles is much lower. An explanation for this is that at high pH particle growth proceeds quickly, driven by base concentration, meaning there is less opportunity for nanosphere growth. Less secondary nucleation is observed as the silica precursor is rapidly converted to form microspheres, thus resulting in a less densely packed shell. At lower pH however, the reduced reaction rate allows for greater nucleation and growth of nanospheres, leading to a denser coverage on the surface. Despite the difference in morphology, the size of nanoparticles on the surface remained in the range of 50-200 nm for all samples. This suggests that ammonia concentration can be used to control particle diameter and nanoparticle density, but not nanoparticle size.

Surface area measured using nitrogen adsorption was found to be in the region of 190-240 m^2/g for all samples following calcination at 550 °C, with an average value of 207 m^2/g. Despite the various morphologies all samples were found to have pore size around the 2 nm microporous boundary, where measured, with a maximum average diameter of 2.35 nm observed. The similar values for surface area measured for the various morphologies makes it difficult to determine how much additional surface area is gained from having a denser layer of surface nanoparticles.

Table 2.2 Influence of ammonia concentration on physical properties.

Ammonia concentration (%)	Surface area (m^2/g)	Pore diameter (nm)	Particle diameter (µm)	$d^{90}/_{10}$
28	216	2.18	3.90	2.07
14	190	2.25	3.49	1.80
7	193	2.30	3.78	1.84
5.6	240	2.25	3.85	1.82
2.8	209	*	3.93	1.58
1.4	206	2.35	4.02	1.92
0.7	194	*	4.11	1.66

* not measured

The mean diameter for all SOS products produced was in the range of 3.4-4.2 µm. With the exception of one sample, the particle size displayed a trend of increasing particle diameter as the reaction pH was decreased. This is consistent with the results obtained by Ahmed *et al.* in the synthesis of SOS particles[1] and also the studies on the Stöber reaction by Bogush *et al*.[3] An explanation is that when ammonia concentration is higher, the rate of both hydrolysis and condensation are increased. Particle formation and precipitation are therefore faster resulting in a smaller diameter. Observed values for PSD ($d^{90}/_{10}$) were quite broad, typically above 1.8, although this represents a significantly narrower PSD than silica particles manufactured from a sol-gel reaction before they have undergone any classification. Following classification a typical core-shell material has a $d^{90}/_{10}$ ratio of <1.15,

and totally porous particles <1.5. The SOS reaction ideally needs to be controlled and improved to obtain particles with a narrow PSD, ideally with a $d^{90}/_{10}$ ratio better than that of classified totally porous particles, which would remove the need for a time-consuming and inefficient classification process.

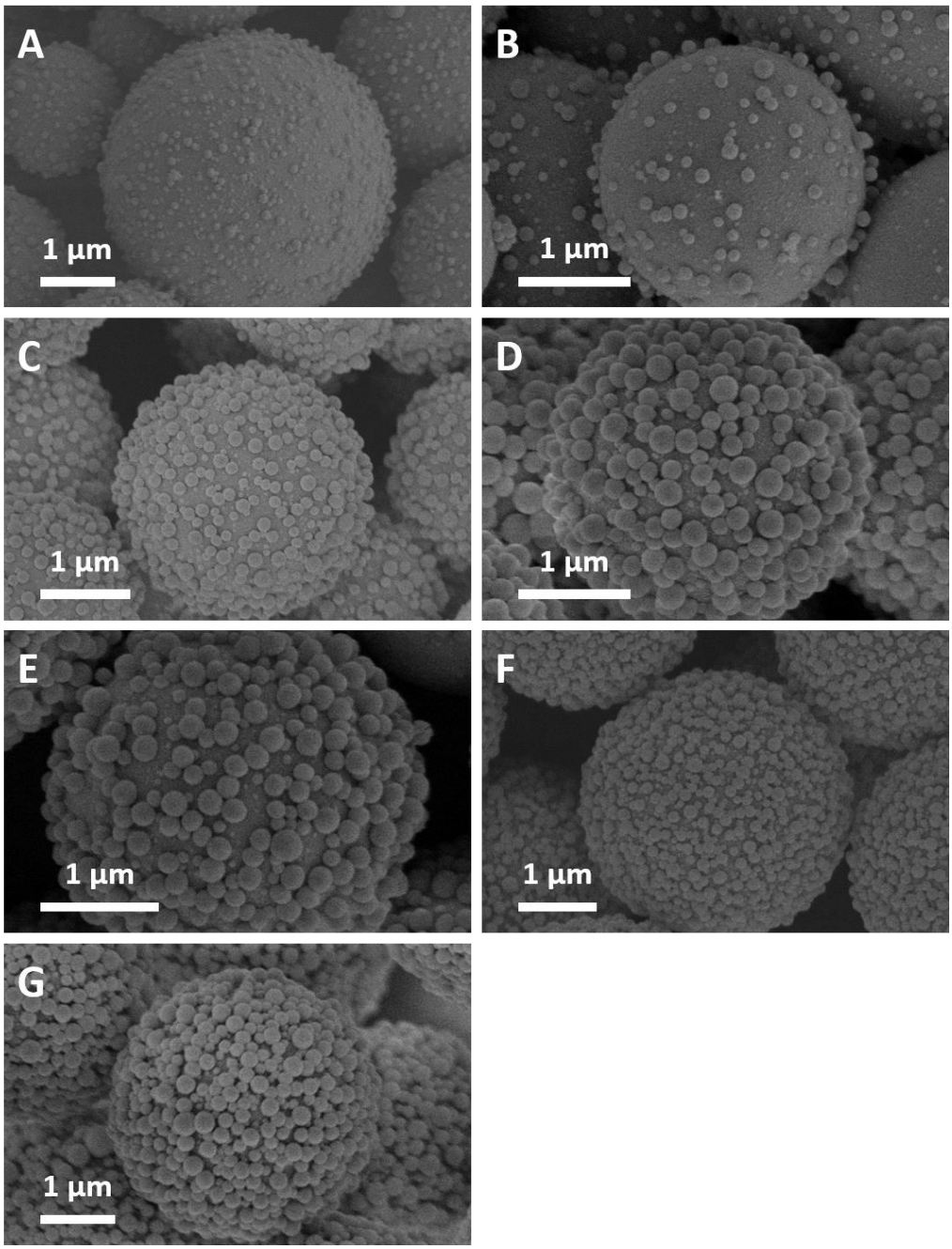

Figure 2.9 SEM images showing the resultant particle morphology when varying ammonia concentration in the standard reaction. 28% (A), 14% (B), 7% (C), 5.6% (D), 2.8% (E), 1.4% (F), 0.7% (G). Values based on dilution of as-bought 28% ammonium hydroxide.

In one study, homogenisation of the reaction mixture was performed in an effort to improve the PSD. It was thought that this would distribute reagents more evenly within the solution, leading to the formation of uniform particles. This was performed both before and after MPTMS addition. Homogenisation (5 minutes, setting 3, approximately 15000 rpm) before MPTMS addition led to the formation of SOS particles that were very similar in morphology to those from the standard conditions. Homogenisation immediately after MPTMS addition (same time and settings) was found to reduce the time taken to form a cloudy solution and resultant particles had less surface spheres. No improvement in PSD was observed in either case.

Alternative bases were substituted into the reaction in place of ammonia. The use of 0.1 M sodium hydroxide (2 mL) led to the formation of particles that displayed partial SOS morphology with a layer of very small nanoparticles, shown in figure 2.10 A. However, a significant proportion of the resultant material was present as aggregates, both attached and free from the particles. It is also preferable to avoid the use of reagents containing sodium in the reaction, as its presence in the final product can adversely affect chromatographic results. The use of triethylamine (2 mL) led to the formation of smooth spheres with a broad PSD and included a number of broken particles, shown in figure 2.10 B. It is apparent that ammonia provides the best results for SOS formation and altering the concentration allows for an excellent degree of control over the nanoparticle layer.

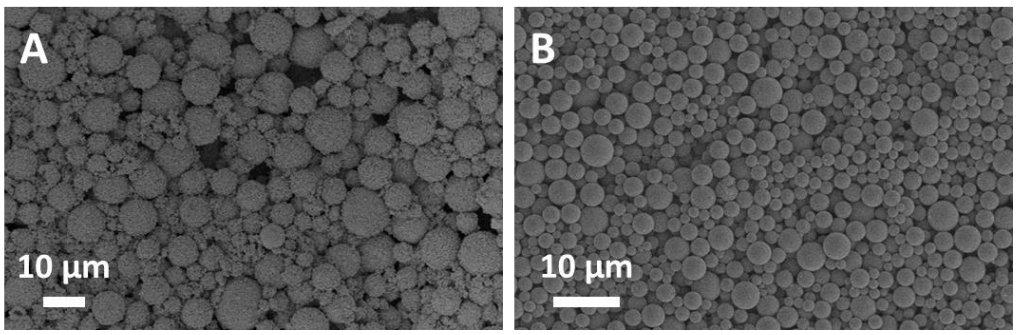

Figure 2.10 SEM images of particles produced when using sodium hydroxide (A) and triethylamine (B) as the base in the standard reaction.

2.4.2 Effect of Polymer

In the standard reaction, PVA with average molecular weight of 9-10k was used in 5% concentration, based on the initial amount of water. The use of alternative molecular weights of 2k and 16k also resulted in the formation of SOS particles with similar sized nanospheres on the surface. However, fewer surface spheres were observed compared to particles obtained from the standard reaction. SEM images are shown in figure 2.11 A and B. Increasing the molecular weight further, using 22k and 31-50k PVA (figure 2.11 C and D), saw a significant decrease in the number of surface particles. The use of even higher molecular weights led to difficulties in dissolving the polymer in a 5% solution and were not used in this study.

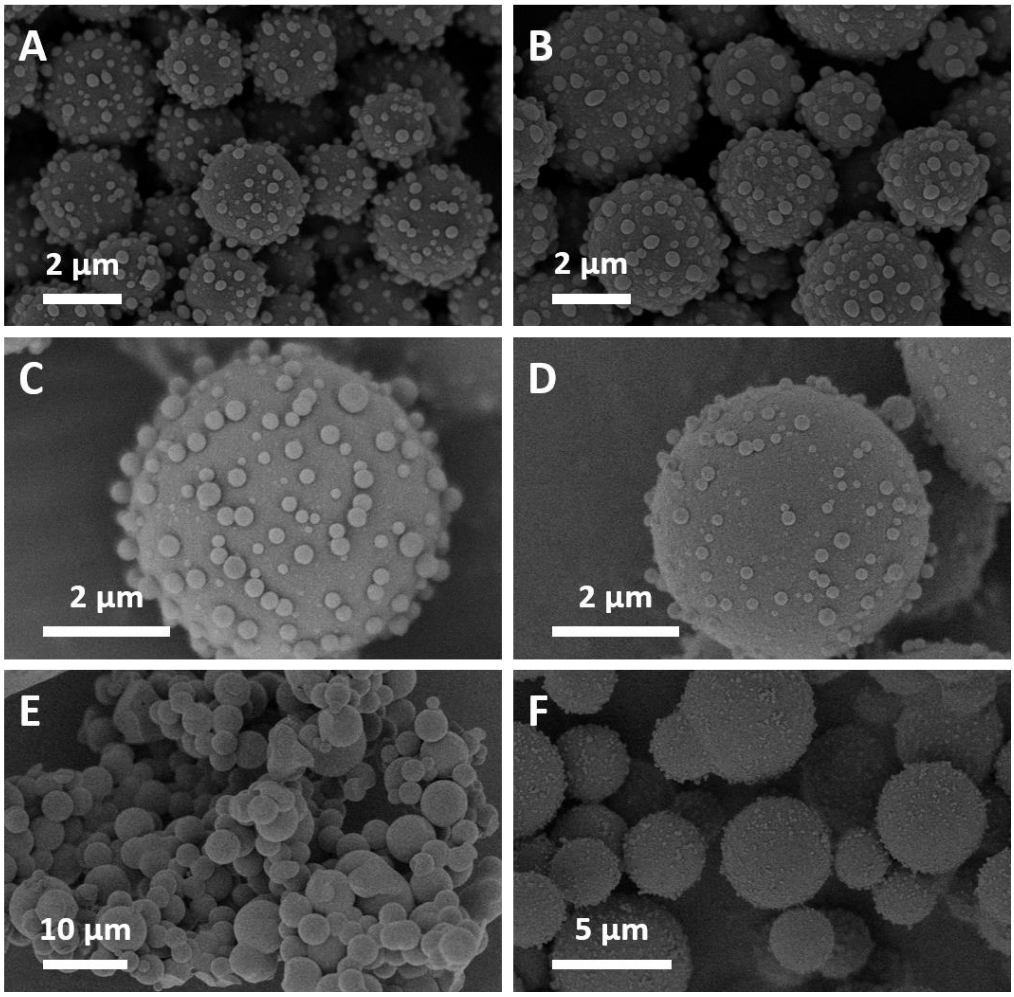

Figure 2.11 SEM images of particles produced when varying molecular weight and concentration of PVA. M_W = 2k (A), 16k (B), 22k (C), 31-50k (D). Concentration = 0% PVA (E), 10% PVA (F).

The role of PVA was to stabilise the SOS particles during synthesis and prevent growth of aggregates. It was observed that omitting the polymer from the reaction led to the formation of large aggregates that were fused together. Increasing the concentration of 9-10k PVA to 10% led to the formation of SOS with only a low coverage of small surface nanoparticles. SEM images are shown in figure 2.11 E and F. The presence of PVA is essential in the reaction to produce SOS particles, however if the concentration is too high this can have a detrimental effect on the surface topography of particles.

When replacing PVA with PVP (10k) in 5% concentration in the standard reaction, smooth spheres were produced with smaller diameter and narrower PSD. Likewise, the use of alternative molecular weight PVP (29, 40 and 55k) in further reactions did not result in the formation of an SOS product, instead smooth particles or spheres with small protrusions were obtained, again with improved PSD. SEM images are shown in figure 2.12. It appears that PVP provides a better stabilising effect in terms of PSD, however the SOS morphology is lost when simply replacing the polymer without changing any other parameters.

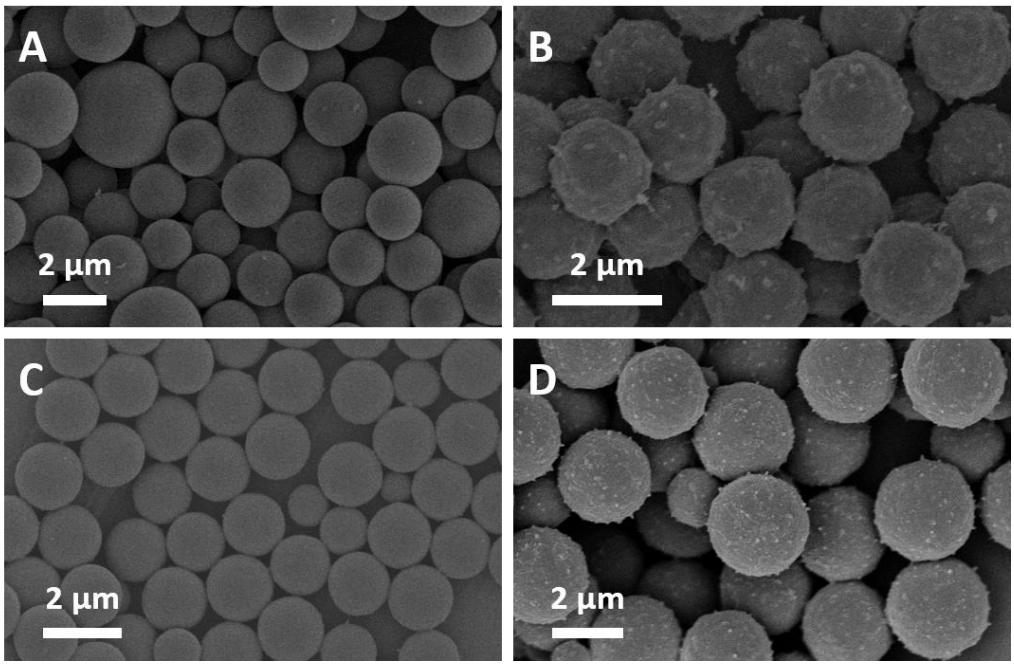

Figure 2.12 SEM images showing the effect of PVP molecular weight on particle morphology. M_W = 10k (A), 29k (B), 40k (C), 55k (D).

While replacing PVA with PVP does not produce SOS particles, it does provide an improvement in PSD. The $d^{90}/_{10}$ ratio of the particles produced when using PVP (10k) was 1.57. An investigation was undertaken using a mixture of PVA and PVP (both 10k) to see if this would combine the effects of the two polymers, creating SOS particles with narrower PSD in a one-pot process. CTAB was present in each reaction in 2% concentration. The use of a 1:1 (by weight) PVA:PVP ratio did not lead to the formation of spherical particles, rather a layer of half-formed and fused spheres. Raising the ratio to 4:1 produced spherical particles displaying SOS morphology, though the surface nanoparticle size was much smaller (20-100 nm) and the PSD showed no improvement. However, when using a PVA:PVP ratio of 1:2, partial SOS morphology and a slight improvement in dispersity was observed, though surface nanoparticles were still small.

A second approach was attempted, where two separate polymer solutions were premade and mixed into the required ratio before use in the reaction. The PVA solution contained 2% CTAB, while the PVP solution contained no surfactant. The overall concentration of polymer remained at 5%, based on water. The ratios used are shown in table 2.3. At the highest concentration of PVP, the particles formed did not show any SOS morphology and the PSD was poor. Increasing SOS character was observed as the ratio of PVA:PVP was increased above 40:60, with the greatest nucleation observed when using the highest concentration of PVA.

Table 2.3 Ratio of PVA (9-10k):PVP (10k) and particle sizing data.

PVA solution	PVP solution	Particle diameter (μm)	$d^{90}/_{10}$
5	95	2.86	1.90
10	90	4.19	1.97
40	60	3.99	1.64
50	50	2.73	1.43
60	40	2.77	1.62
90	10	2.76	2.48
95	5	2.86	1.90

The PSD at both extremes of PVA and PVP concentration was found to be poor. An ideal ratio appears to be between 40 and 60% PVA solution, where a minimum value of the $d^{90}/_{10}$ ratio is obtained. Within this range, formation of SOS particles is observed and the narrowest PSD is achieved. This method has shown promising results in terms of a one-pot reaction yielding spheres on sphere particles with narrow PSD.

Alternative polymers were substituted into the reaction in place of PVA at 5% concentration. The use of PMVE, which differs in structure to PVA by having a methoxy group rather than a hydroxyl group, resulted in oval-shaped smooth particles. These were less than 1 µm in size with broad PSD. This indicates that a polar group is necessary for effective stabilisation of the reaction and formation of SOS or discrete spherical particles as seen with PVA or PVP. The use of PEG led to aggregated, irregular spheres. Despite the terminal hydroxyl groups, it is likely that the main chain of the polymer does not provide the same stabilising effect as the repeating polar hydroxyl group present in PVA. The chemical structures are shown in figure 2.13.

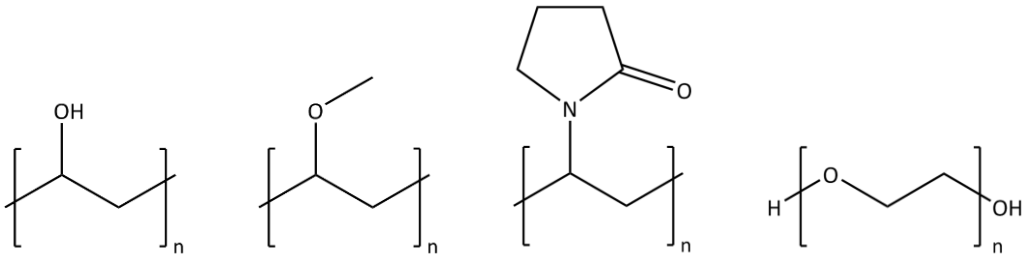

Figure 2.13 Chemical structure of polymers studied in the SOS reaction. From left to right; PVA, PMVE, PVP and PEG.

2.4.3 Effect of Surfactant

In previous studies, the surfactant CTAB has been utilised as a templating agent to form mesoporous silica microspheres.[16, 17] However in the formation of SOS, the nitrogen adsorption data following calcination indicates the presence of micropores, not mesopores. This suggests that the CTAB template is not incorporated into the SOS particles and instead micropores are formed from the removal of mercaptopropyl groups, present in the final product due to the use of the MPTMS precursor.

It is shown in the SEM images in figure 2.14 that the concentration of CTAB has a significant effect on the particle morphology. At high concentration (5 and 10% weight solution) SOS type particles were produced, although the density of the nanoparticle layer was low and the diameter of surface spheres was very small. In the case of 10% some fusing of particles was also observed. When CTAB was present at low concentration (≤0.1%) or omitted entirely from the reaction, small smooth spheres were produced, indicating that the presence of surfactant is essential to form SOS particles. The reaction begins to produce SOS particles when CTAB is present in ≥0.25% concentration, however the best results are observed at a concentration of 1-2%.

As the concentration of CTAB is reduced, a smaller particle diameter is observed, with improved PSD. An explanation could be that the reaction solution is becoming more alike to the conditions in an unmodified Stöber reaction when less surfactant is present, which would typically lead to the preparation of smaller, uniform smooth spheres. Indeed when omitting both polymer and surfactant from the standard SOS reaction, uniform smooth spheres were produced that were around 1.5 μm in diameter.

Cetyltrimethylammonium is a cationic surfactant consisting of a C16 chain attached to a quaternary ammonium group which is balanced by an anion, typically bromide (CTAB), chloride (CTAC) or hydroxide (CTAOH). Replacing CTAB with 2% CTAC in the standard method led to the formation of SOS particles which were very similar in terms of morphology and dispersity to those produced when using 1% CTAB. The SEM image is shown in figure 2.14 H. As CTAC is supplied as a 25% solution it is preferred to use CTAB (supplied in powder form) as the weight can be more accurately measured, particularly in the case of the low concentration examples.

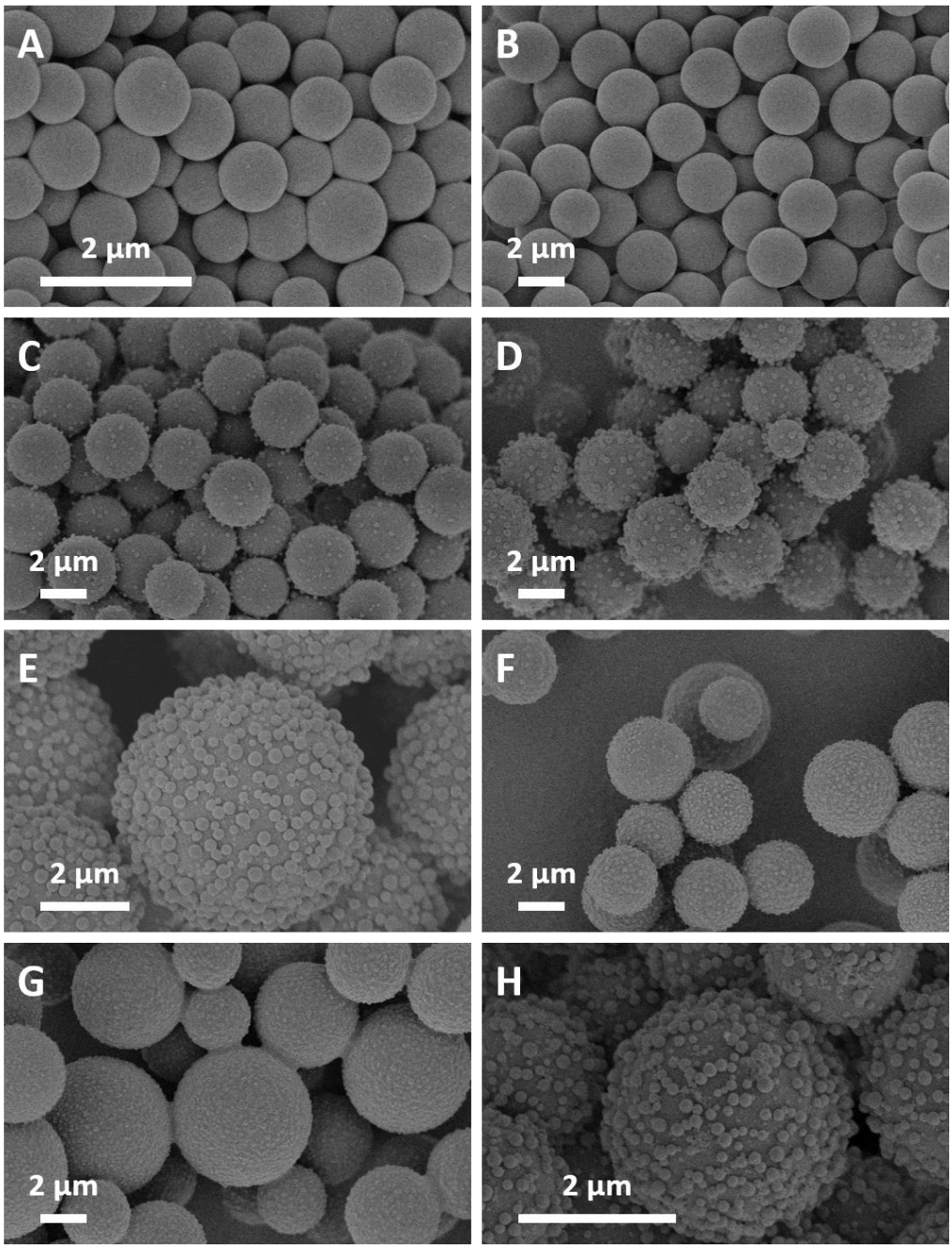

Figure 2.14 SEM images showing resultant morphology from changing concentration of CTAB. Concentration = 0% (A), 0.1% (B), 0.25% (C), 0.5% (D), 1% (E), 5% (F), 10% (G), 2% CTAC (H).

TWEEN 20 is a non-ionic polysorbate surfactant. When used as a replacement for CTAB at 2% weight in solution, smooth polydisperse spheres were produced. Decreasing the amount of surfactant to 0.5% weight however led to protrusions upon the surface of the core particles. These did not grow further to form spheres on the surface even after

allowing to stir for 48 hours. Reducing the concentration to 0.25% and 0.1% led to greater roughness of the particle surface, although again no SOS morphology was produced. Images of the particles are shown in figure 2.15. As observed for CTAB, the PSD improved significantly as the concentration of TWEEN 20 was reduced. This agrees with the theory that reducing the amount of surfactant has a positive effect on the PSD. TWEEN 80 was also used in the same study using identical concentrations to TWEEN 20, however no rough surface was observed, with all particles having a smooth spherical morphology.

Other surfactants were tested as replacements for CTAB without success. The anionic, amphiphilic surfactant SDS was used at concentrations of 2, 1, 0.5 and 0.25% weight in solution, however each of these reactions resulted in smooth spheres which were fused together. Likewise, the use of tannic acid in the same concentrations as SDS led to the formation of smooth spherical particles, which also included a large amount of aggregated pieces.

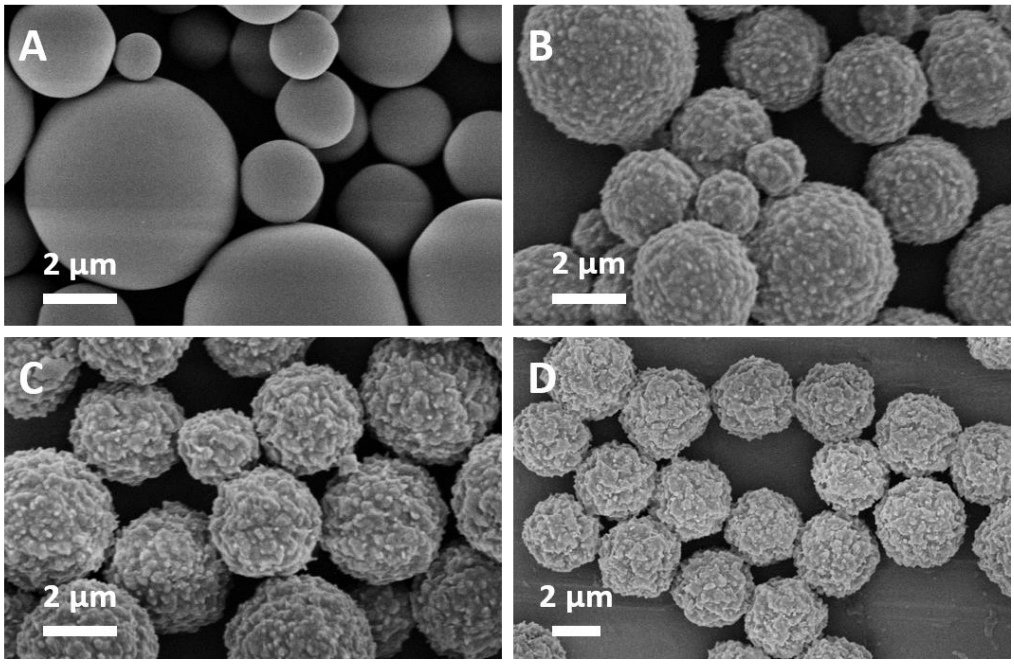

Figure 2.15 SEM images showing resultant morphology from changing concentration of TWEEN 20. Concentration = 2% (A), 0.5% (B), 0.25% (C), 0.1% (D).

2.4.4 Concentration of Silica Precursor

The MPTMS concentration in the reaction was found to have a significant effect on particle size. The volume of MPTMS was varied between 10 and 250 µL while keeping the amounts of all other reagents constant. It can be seen from the SEM images in figure 2.16 that as the precursor volume is reduced a smaller particle size is obtained. The images show that the resultant particle size was less than 500 nm when adding 10 and 20 µL MPTMS. Despite this very small size, particles were roughly spherical and not smooth, instead displaying a small amount of growth from the surface. In the case of 20 µL some irregular structures were also formed. Particle size increased further when adding 30 µL MPTMS, although the resultant particles were cluster-like rather than displaying core-shell morphology. When 50 µL is added, discrete particles with clear SOS morphology were produced. The particle size from this reaction is in the region of 1 µm. The SOS morphology is retained when increasing the MPTMS amount further, again with an increase in particle size as shown by the images from the addition of 100 and 250 µL.

It has been shown in this study that well-formed SOS particles of various size can be produced when the amount of MPTMS used is equal to or greater than 50 µL. It also appears that a two-step formation process is still followed, regardless of the volume of MPTMS added. It is interesting that the particle size is reduced, rather than forming fewer numbers of larger SOS particles. This suggests that the shell nanoparticles are formed at a precursor concentration where the remaining amount of unreacted MPTMS is not present in sufficient quantity to form more core spheres.

Increasing the amount of MPTMS to 600, 700 and 800 µL led to the formation of SOS particles which were very similar to those obtained from the standard reaction in terms of particle diameter and surface nanoparticle density. However, when increasing the amount to 1000 and 2000 µL, fewer, smaller nanoparticles were formed on the surface, suggesting that the other reagents were not present in high enough concentration to fully stabilise the reaction. Another observation was that no significant increase in particle diameter was observed for of the reaction when MPTMS addition was increased beyond 500 µL.

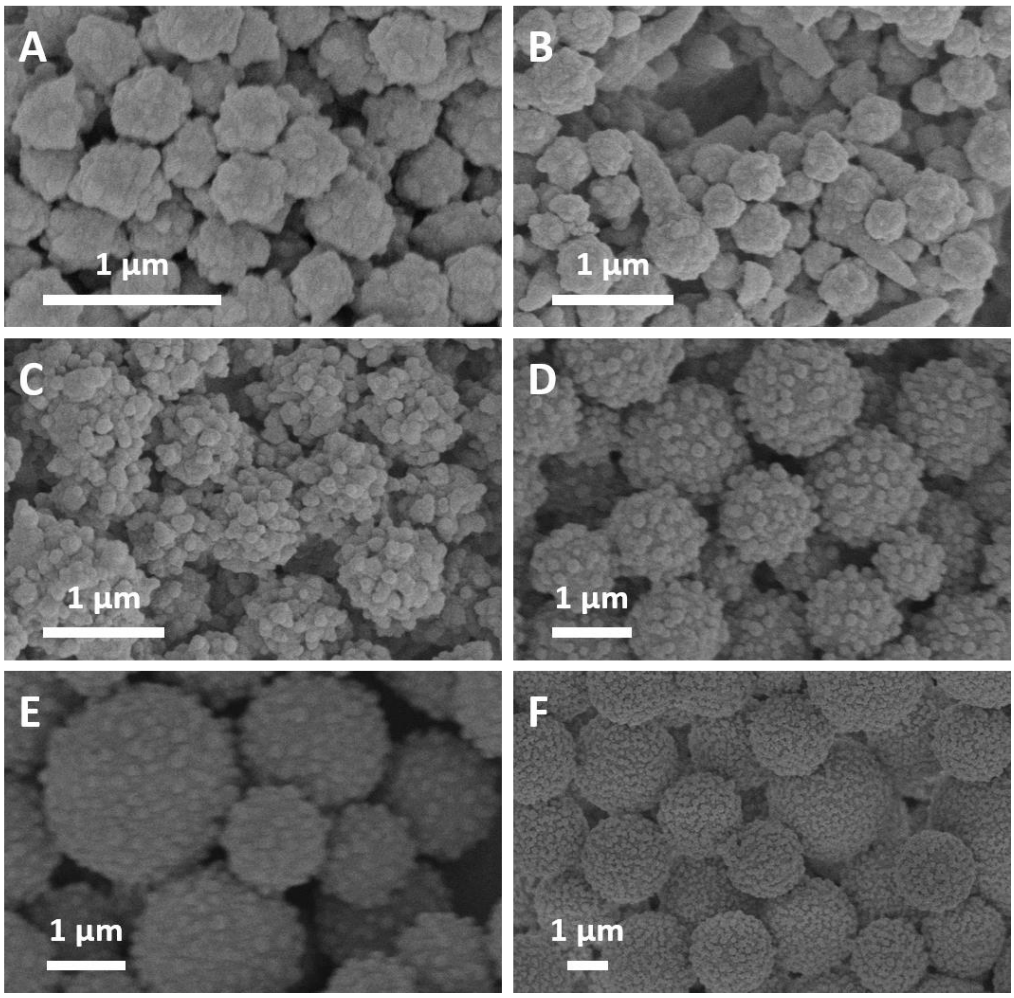

Figure 2.16 SEM images showing morphology changes when varying the amount of MPTMS added to the standard reaction conditions. Addition volume = 10 µL (A), 20 µL (B), 30 µL (C), 50 µL (D), 100 µL (E), 250 µL (F).

2.4.5 Effect of Solvent

The ratio of methanol and water in the standard reaction was investigated to assess the effect on particle morphology. In previous studies of the Stöber reaction the water content has been shown to have an effect on the particle diameter.[2, 3] In one study, a peak particle size of 600 nm was obtained when the amount of water comprised 13% of the reaction volume.[59] The particle size was rapidly reduced when either increasing or decreasing the percentage, instead forming very small nanoparticles.

The ratio of methanol:water in the standard SOS reaction was 8:5, with a combined volume of 13 mL. The total reaction volume was 15.5 mL, containing 44% water (including that of the ammonia solution). In this study the total reaction volume was kept constant while varying the ratio of methanol:water. As PVA is insoluble in methanol the ratios of 13:0 and 12:1 (12.2 and 18.6% water respectively) were achieved by initially dissolving PVA in the ammonia solution, however these conditions both led to the formation of large, polydisperse smooth spheres. The only ratio in this study that produced SOS particles was 10:3 (31.5% water) which resulted in well-formed spheres that were very similar in morphology to those obtained from the standard 8:5 ratio, although some particles had patches where no nanoparticles were present on the surface. The SEM images are shown in figure 2.17.

Increasing the proportion of water resulted in the loss of SOS morphology. Ratios of 5:8, 3:10 and 0:13 (63.8, 76.7 and 96.1% water) all produced smooth spheres. Bimodal size distributions were observed when the volume of water is increased. For the 5:8 and 3:10 ratio reactions, microspheres between 2-3 µm are produced along with a large number of sub-1 µm particles. When omitting methanol from the reaction, the size of the smaller particles is reduced to approximately 300 nm. The SEM images are shown in figure 2.17.

It was observed that the time taken for the reaction to turn cloudy was longest at the lowest concentration of water, which also produced the largest particles. It was noted by Stöber that the condensation rate depends strongly upon the water content of the reaction,[2] however no data was provided in the article detailing the effects. As the amount of water in the SOS reaction was increased, the time was shortened and smaller particles were obtained. This is similar to the effect seen when adjusting ammonia concentration, which produced the smallest particles at the fastest reaction rate.

The choice of alcohol was also found to be important to produce SOS particles. Ethanol, isopropanol and n-butanol were tested as replacements for methanol, however full SOS morphology was not observed in any case. The use of ethanol led to very few nanoparticles attached to the surface of polydisperse microspheres. Isopropanol formed smooth microspheres only and n-butanol resulted in large numbers of highly fused spheres which were around 1 µm in diameter. The PSD was poor for all reactions.

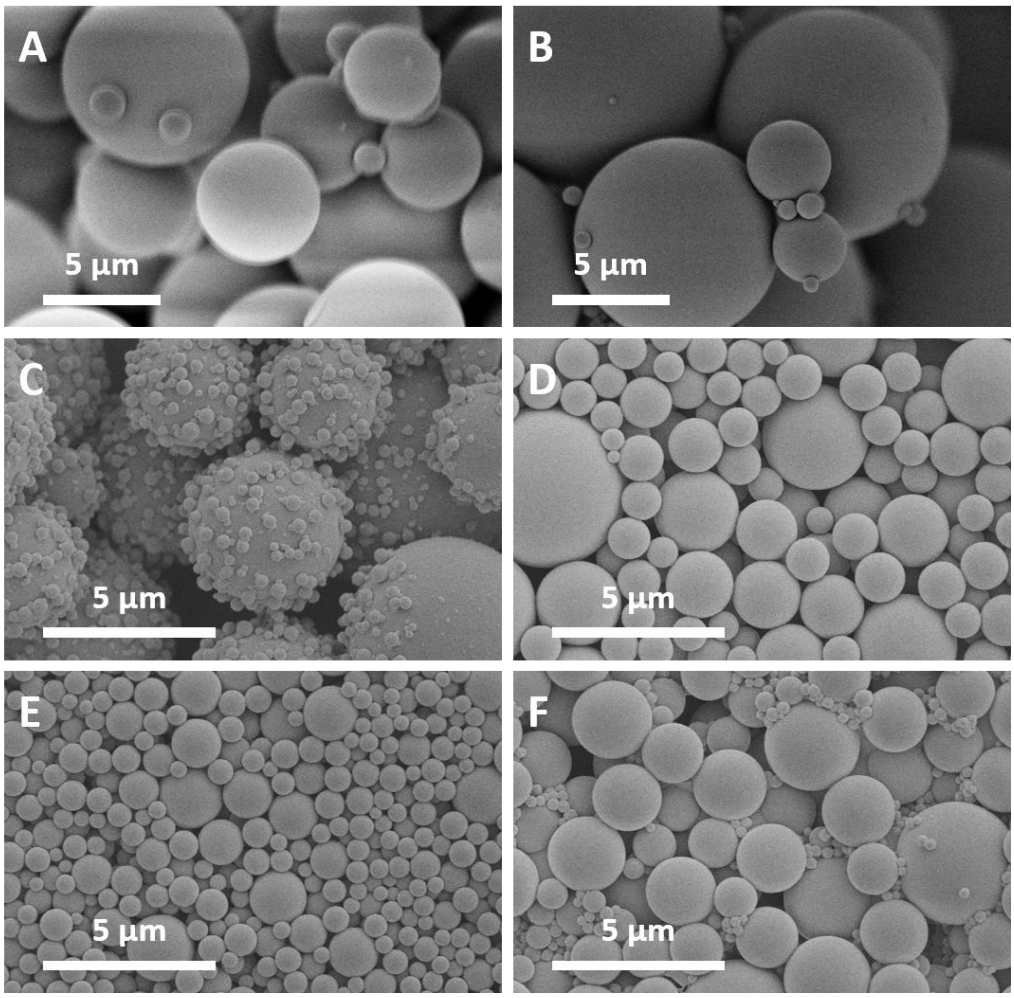

Figure 2.17 SEM images showing the effect of the ratio of methanol:water on particle morphology. Ratio = 13:0 (A), 12:1 (B), 10:3 (C), 5:8 (D), 3:10 (E), 0:13 (F).

2.4.6 Monodisperse Spheres on Sphere Particles

So far it has been shown that modifying the reaction conditions can have a pronounced effect on resultant particle morphology. It is also clear that the reaction is very sensitive to the concentration of reagents. For example the SOS morphology is lost when the concentration of PVA or CTAB is increased or decreased outside of the optimal range. It is possible to individually control particle diameter, nanoparticle density and PSD by changing type and concentration of reagents. It should therefore be possible to combine the effects and hence control all of these physical properties by changing two or more parameters in the reaction.

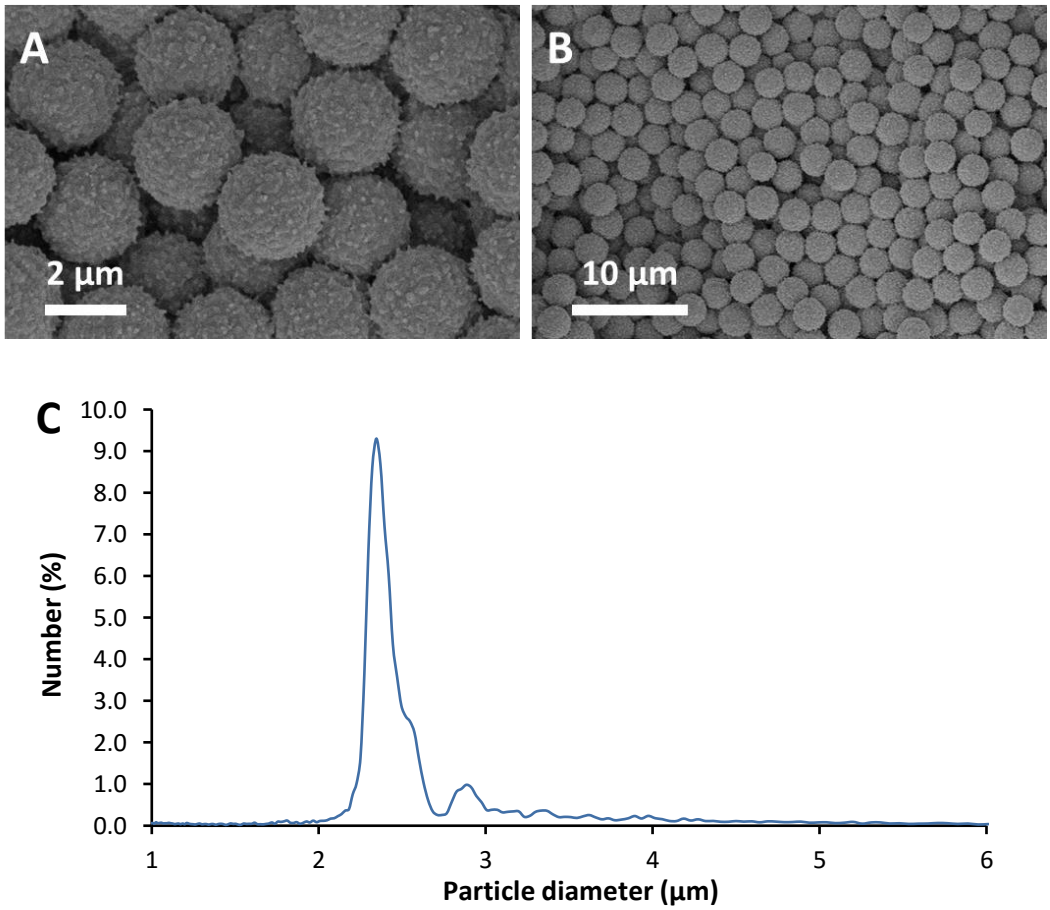

Figure 2.18 Particles obtained from the reaction using PVP (10k) in the absence of CTAB. Particle morphology (A) and dispersity (B) are shown by SEM imaging, along with the PSD (C).

Despite not forming an SOS product, the use of 10k PVP in 5% concentration in the standard reaction does provide a narrow PSD. Likewise, reducing the amount of CTAB in the reaction also improves the PSD. The combination of these yields interesting results. When using 5% PVP in the absence of CTAB, spherical particles are produced with a rough, irregular surface. The mean diameter was 2.60 µm with a modal size of 2.36 µm. PSD was further improved with the $d^{90}/_{10}$ ratio measured to be 1.40. SEM images and a plot of the PSD are shown in figure 2.18. When introducing CTAB into this reaction, partial SOS morphology is formed as the surface protrusions instead begin to form nanospheres. CTAB is required in very low concentration in this case. The greatest surface growth was observed when using 0.25% CTAB, with less SOS character shown as the concentration is increased. Beyond 2% concentration, the SOS morphology is almost completely lost and smooth spheres are produced. The SEM images are shown in figure 2.19.

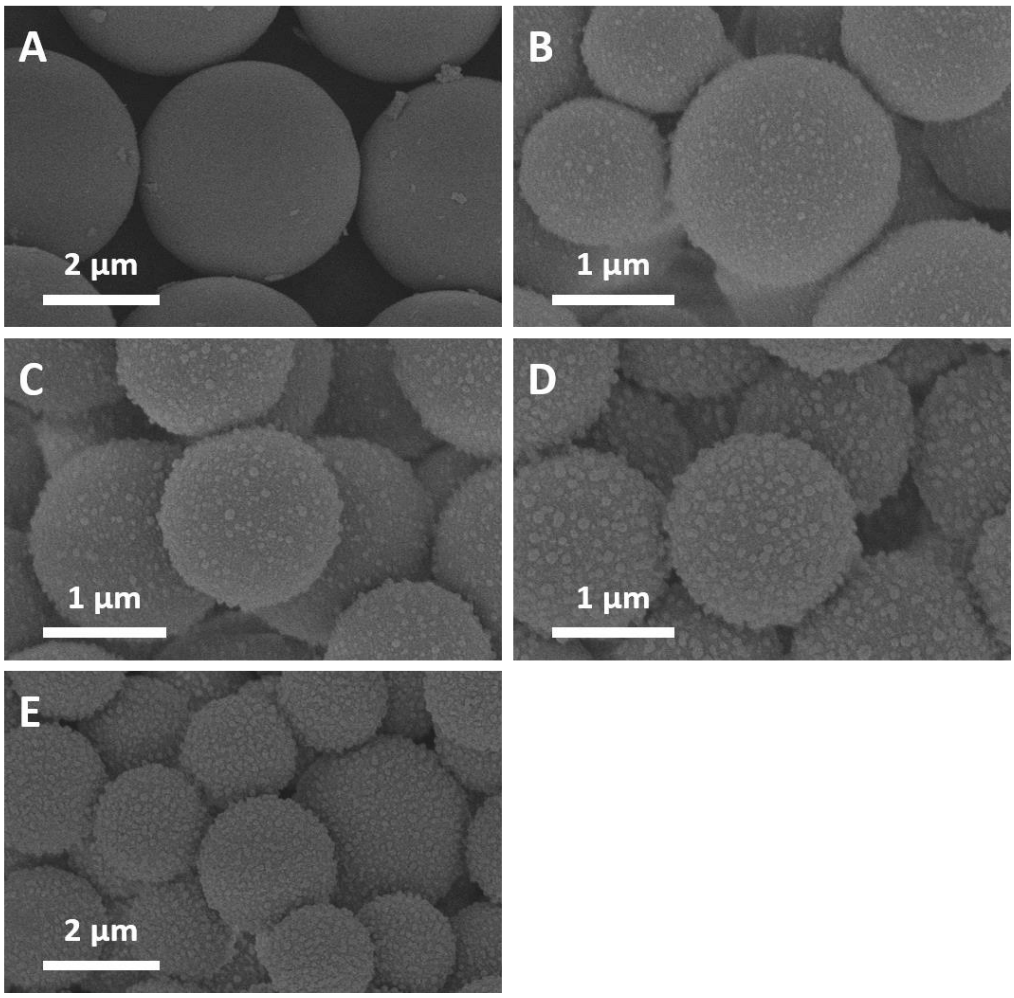

Figure 2.19 SEM images of particles produced when varying the concentration of CTAB in the reaction with 5% PVP (10k). Concentration = 4% (A), 2% (B), 1% (C), 0.5% (D), 0.25% (E).

The variation of PVP and CTAB concentration has resulted in particles possessing two out of the three desired properties; narrow PSD and a mean diameter ideal for use in HPLC. The fact that rough particles were obtained, rather than smooth spheres, indicates that surface growth proceeds using these conditions and therefore the formation of nanoparticles on the surface should be possible. It has been shown in the individual studies that reducing the concentration of ammonia in the reaction lead to much greater nucleation on the surface of the resultant SOS particles. This provides a potential route to the formation of nanoparticles rather than just surface roughness.

Reducing the ammonia concentration to 2.8, 1.4 and 0.7% in the reactions where 5% PVP is present with either 2% or omission of CTAB again led to particles which had

rough protrusions from the surface, much alike to those in figure 2.18. As previously observed, the PSD was much narrower when omitting CTAB from the reaction compared to 2% concentration.

As shown in figure 2.19, the greatest surface nucleation when using 5% PVP and ammonia at a concentration of 5.6% was observed when using 0.25% CTAB. When reducing the concentration of ammonia to 1.4% in this reaction, there is much more time for secondary nucleation to occur and leads to the formation of well-defined SOS particles with a complete single shell of nanoparticles on the surface. The amount of MPTMS was also varied in this reaction, with the best results observed when 400 µL was added. These conditions will be referred to as the optimised reaction. SEM images and sizing plot are shown in figure 2.20.

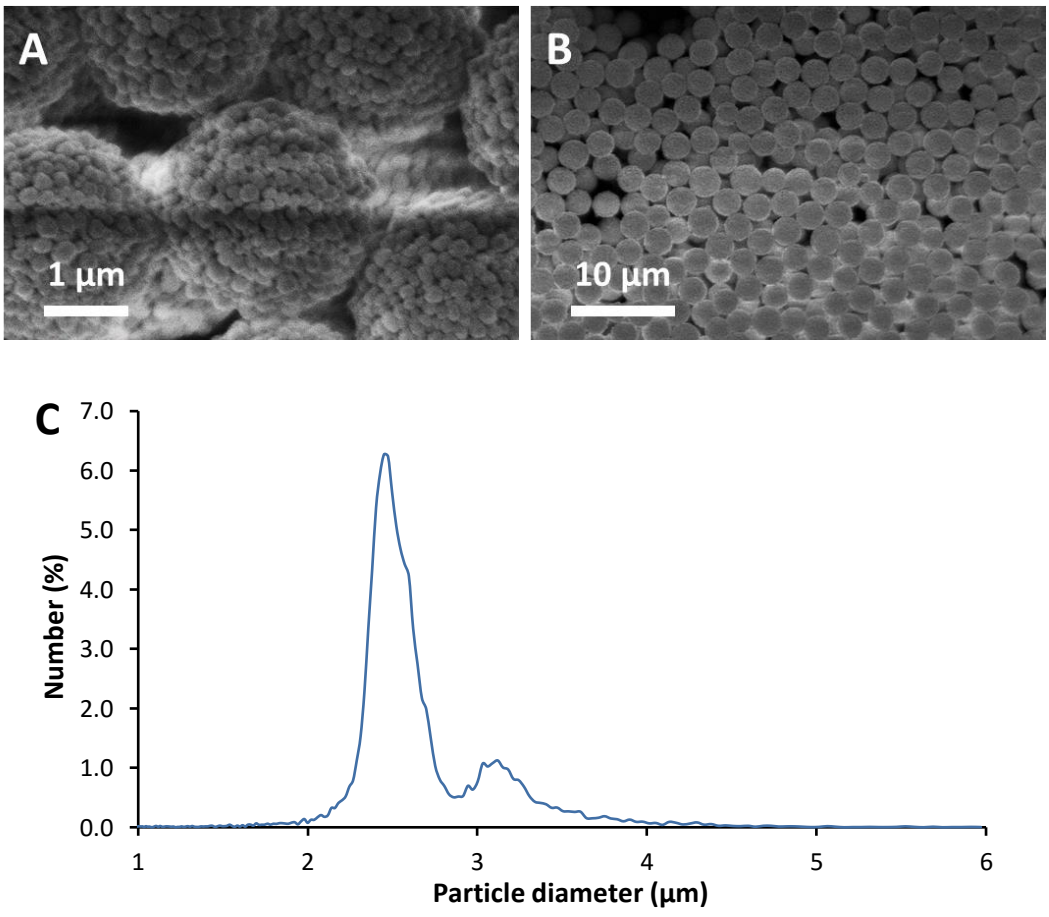

Figure 2.20 SOS particles obtained from the optimised reaction using 5% PVP, 0.25% CTAB and 1.4% ammonia concentrations, with the addition of 400 µL MPTMS. Particle morphology (A) and dispersity (B) are shown by SEM imaging, along with the PSD (C).

The mean particle diameter was 2.83 µm, with a modal size of 2.51 µm. Additionally the particles displayed very narrow PSD, with a $d^{90}/_{10}$ ratio of 1.31. The size and dispersity show that these particles have ideal physical properties for use in HPLC columns. BET surface area was measured to be 209 m^2/g by nitrogen adsorption and the interstitial pore size was measured using mercury intrusion with an indicated diameter of around 0.9 µm. These values are consistent with standard SOS materials. Nitrogen isotherm and mercury intrusion plots are shown in figure 2.21.

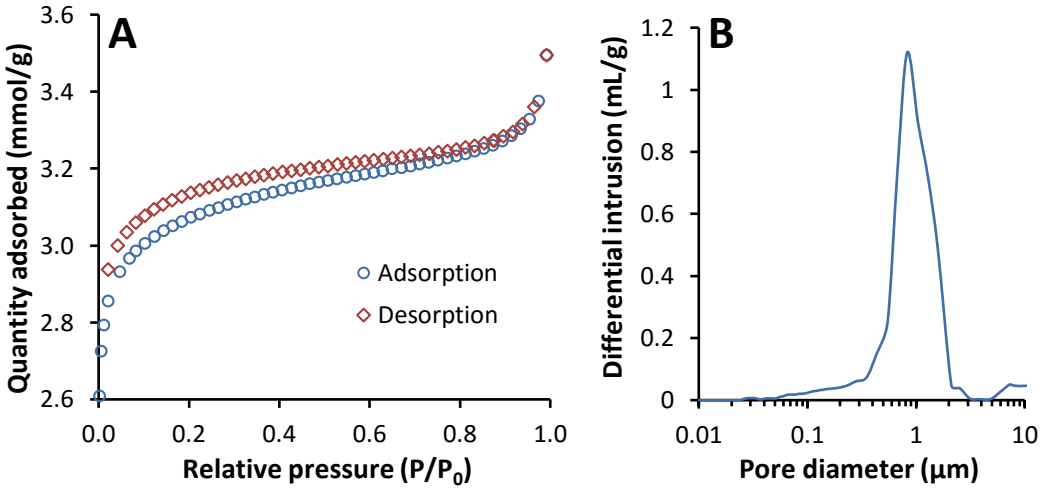

Figure 2.21 Nitrogen isotherm plot (A) and mercury intrusion plot (B) for SOS particles prepared from the optimised reaction.

2.4.7 Large Scale Reaction

So far, all of the reactions described have been performed on a small scale of approximately 15.5 mL, depending on the amount of MPTMS used. Following calcination at 550 °C, 0.12-0.15 g of material could be produced from the optimised reaction described previously. If these particles are to be used in chromatographic applications, clearly the yield from such a small reaction will be insufficient and the required number of reactions impractical where batches of silica are needed. The optimised reaction conditions were therefore scaled up to assess any changes in particle morphology and physical properties. The total reaction volume was 770 mL (50 times scale up). The reaction was performed at room temperature on a magnetic stirrer plate. Stirring was performed using a Teflon coated stirrer bar at a speed of 240 rpm. Brand new glassware was used.

PVP (12.5 g) and CTAB (0.625 g) were dissolved in deionised water (250 mL). The concentrations of polymer and surfactant were 5% and 0.25% based on water. Methanol (400 mL) was added, followed by diluted ammonium hydroxide (100 mL, 1.4%). The solution was stirred for 15 minutes, before addition of MPTMS (20 mL) in 2 mL aliquots at even intervals over 10 minutes. The reaction was stirred overnight. SOS particles were collected on a sintered glass filter and washed with distilled water (5 x 100 mL), then methanol (5 x 100 mL) before drying under vacuum at 60 °C. 14.8 g of particles were produced, which was reduced to 7.2 g following calcination at 550 °C for 12 hours.

The mean particle diameter was 3.02 µm, with a modal size of 2.90 µm. As in the small scale reaction a narrow PSD was obtained, with a $d^{90}/_{10}$ ratio of 1.24. The SEM images and sizing plot are shown in figure 2.22. BET surface area was measured to be 205 m^2/g by nitrogen adsorption.

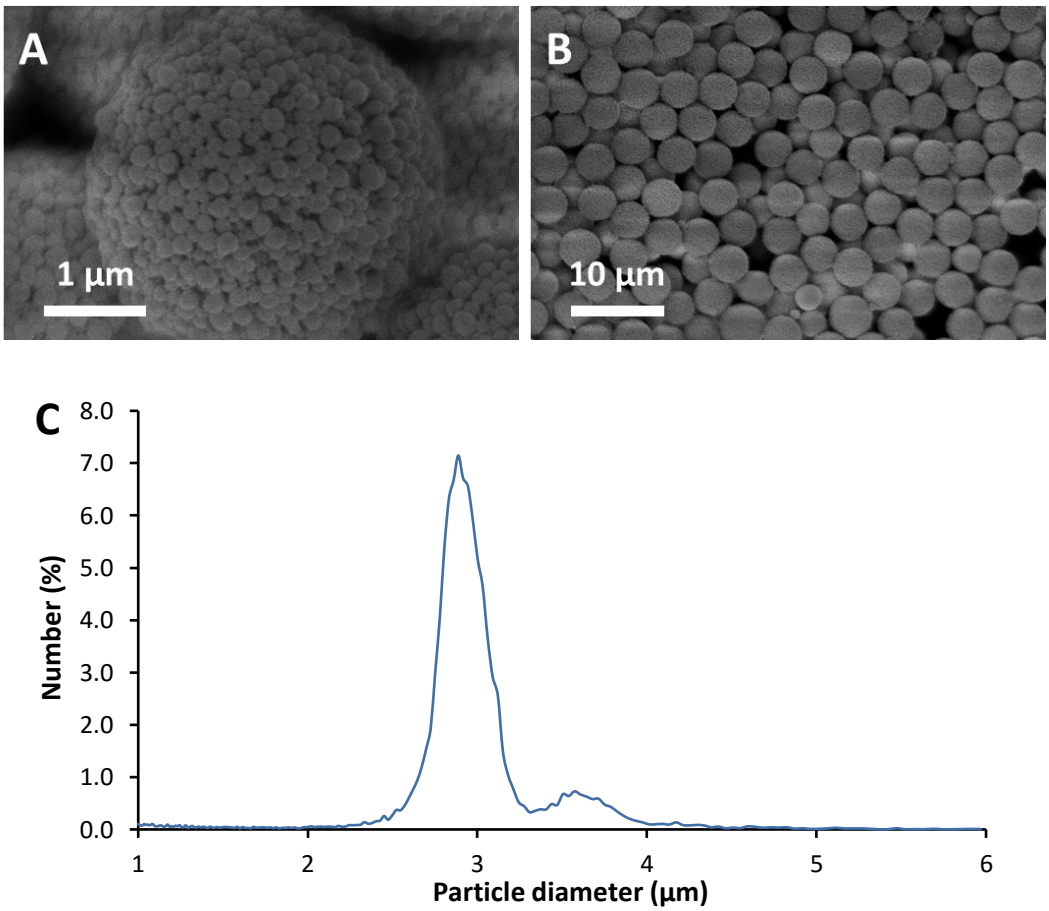

Figure 2.22 SOS particles obtained from the scaled up optimised reaction. Particle morphology (A) and dispersity (B) are shown by SEM imaging, along with the PSD (C).

As shown in the SEM images for the small and large scale reactions in figures 2.21 and 2.22, the particle morphologies do not display any significant differences. Both have a complete single shell of particles around the core with nanoparticles in the region of 100-200 nm. The mean particle diameter shows a small increase of 200 nm in the case of the scaled up reaction which may be caused by the addition of a larger amount of MPTMS. As the size of the surface nanoparticles is the same, this suggests a larger core microsphere. The addition of MPTMS was completed in stages over 10 minutes, which introduced an appreciable amount of precursor each time. Although the stirring rate was sufficient to keep resultant particles in suspension, the reaction mixture does not reach a homogenous state immediately after MPTMS addition. It was observed that the precursor accumulates at the bottom of the vessel for several seconds before mixing fully into the reaction volume. This is likely to result in areas within the reaction volume where the MPTMS concentration is initially much higher than expected. It has previously been shown that increasing the amount of MPTMS in the reaction forms larger particles, therefore it can be assumed that these initial areas of higher concentration may lead to the formation of slightly larger microspheres. Once the reaction reaches a homogenous state, the reaction proceeds normally and the size and density of nanospheres is as expected.

The standard reaction conditions with reduced ammonia concentration were also scaled up by the same amount and the resulting particles classified by a settling method to obtain a narrow PSD. Again, the reaction was performed in brand new glassware at room temperature on a magnetic stirrer plate with stirring provided by a Teflon coated stirrer bar at a speed of 240 rpm. PVA (12.5 g) and CTAB (5 g) were dissolved in deionised water (250 mL). Methanol (400 mL) was added, followed by diluted ammonium hydroxide (100 mL, 1.4%). The solution was stirred for 15 minutes, before addition of MPTMS (25 mL) in 2.5 mL aliquots at even intervals over 10 minutes. The reaction was stirred overnight. SOS particles were collected on a sintered glass filter and washed with distilled water (5 x 100 mL), then methanol (5 x 100 mL) before drying under vacuum at 60 °C. 18.2 g of particles were produced, which was reduced to 9.0 g following calcination at 550 °C for 12 hours.

The calcined particles were classified by a settling method. This is a classification process that works on the basis that larger, heavier particles (heavies) will drop out of solution faster than smaller, lighter ones (fines). Particles are suspended in solution for each classification step. The suspension is allowed to settle for a certain amount of time, after which the solution containing the remaining fines is decanted off, leaving the heavies

fraction at the bottom of the vessel. Lengthening the settle time allows more heavies to elute and leaves fewer fines in the solution, likewise shortening the settle time leads to a smaller heavy fraction. Additionally very long or very short settle times allow a smaller cut out of the heavy or fine end of the PSD.

Pre-classification SOS particles had mean particle size of 3.19 µm. However the PSD was quite broad, with a $d^{90}/_{10}$ ratio of 1.88. 9.0 g of unclassified particles were suspended in 1.8 L of 1% weight SDS solution and allowed to settle for 1 hour to remove the largest particles and any aggregates. The resultant solution was decanted into a second vessel, particles resuspended with stirring and allowed to settle for 6 hours. This step is required to remove the smallest particles, for example any nanospheres that are not attached to larger particles. Only one classification step was required to remove the fines (<2 µm) from the PSD. The solution was decanted, removing the remaining waste fines that were still suspended and leaving the required heavies at the bottom of the beaker.

The heavy fraction from the 6 hour step was suspended in 1.8 L of fresh SDS solution and 1, 2 and 3 hour settling steps performed to take cuts out of the heavy end of the PSD. Resultant particles were isolated by filtration and washed thoroughly with water, water/acetone (1:1 V/V), then acetone to remove the residual SDS, before drying under vacuum at 60 °C. After classification the resultant mean particle diameter was 2.79 µm, with a modal size of 2.51 µm. A narrow PSD was obtained, with a $d^{90}/_{10}$ ratio of 1.24. SEM images of the classified particles and the overlaid sizing plots from before and after classification are shown in figure 2.23. BET surface area was measured to be 195 m^2/g by nitrogen adsorption.

Although the diameter and PSD of the classified material are ideal, the yield of particles was significantly reduced due to the classification process. 4.8 g of particles were obtained following classification, indicating that 53% of the starting material was removed as waste. Another disadvantage is the length of time required to perform the settling. The method requires particle sizing after each settling step to assess the effect on PSD. Additionally, each step is not guaranteed to provide the desired effect on the PSD and may therefore need to be resettled for an alternative length of time. The method described above required almost 12 hours settling time in total. This does not include the time in the preparative steps such as preparation of SDS solution, sample preparation, particle sizing and isolation from the suspension solution by filtration. It is therefore advantageous to

synthesise SOS particles from the one pot reaction where an equivalently narrow PSD can be obtained.

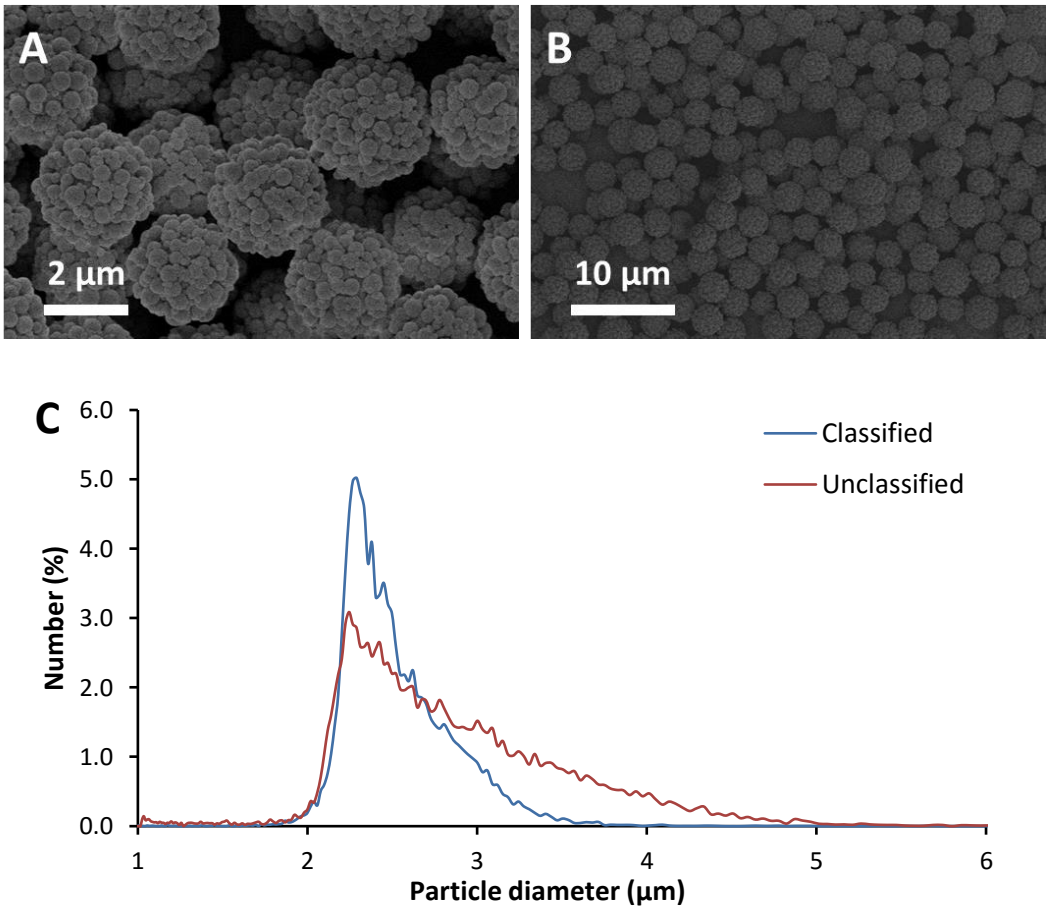

Figure 2.23 SOS particles obtained from the standard reaction using 1.4% ammonia concentration. Morphology (A) and dispersity (B) of classified particles are shown by SEM imaging, along with the PSD before and after classification (C).

2.4.8 Controlled Precursor Addition

In the synthesis methods so far, the entire volume of MPTMS has been added in one step for small scale reactions or stepwise over 10 minutes for large scale studies. Addition of MPTMS was performed by pipette in the case of the large scale reactions with the rate kept as constant as possible, although steps such as refilling of the pipette leads to some variation.

Previous studies of the Stöber reaction have made use of controlled addition of the silica precursor to good effect. For example Giesche *et al.* devised a complex reactor system which allowed continuous addition of TEOS into a seed solution, enabling synthesis of large Stöber particles with controllable diameter and excellent PSD.[7] Similarly, Unger used a continuous addition method to grow seeded particles.[14] Although these examples describe methods intended to facilitate particle growth beyond the 800 nm limit, the SOS reaction may also benefit from controlled addition of the silica precursor. In the previously described large scale reactions MPTMS has initially accumulated at the bottom of the vessel. Although this has not appeared to have a detrimental effect on dispersity, with a continuous addition method the reaction volume would remain in a homogenous state, leading to highly reproducible particle diameter and morphology.

Initial thoughts were to add the precursor using a HPLC pump. The extremely high accuracy would allow excellent control over the addition rate. This method was not attempted however due to possible compatibility issues of pump parts with MPTMS, particularly the piston seals. Contamination of the tubing and pump internals would also be inevitable due to direct contact with the precursor. Additionally, despite the high accuracy, the fastest rate of addition would be limited to 2 mL/min, the highest setting of the pump. A syringe pump was instead used (Harvard Apparatus 22) as this avoided direct contact of any pump parts with MPTMS while still allowing accurate addition over an extended range of flow rates, from 0.002 µL/hour to 55 mL/min.

Reaction solutions were made up in the same concentrations as the scaled up optimised method in section 2.4.7. Each reaction volume was 770 mL. All reactions were performed in new glassware at room temperature on a magnetic stirrer plate. Stirring was performed using a Teflon coated stirrer bar at a speed of 240 rpm. A total of 20 mL MPTMS was added directly into the reaction at various flow rates: 8.0, 6.0, 4.0, 2.0, 1.0, 0.75, 0.5 and 0.25 mL/min. This equated to addition times ranging between 2.5 and 80 minutes. The SEM images for each are shown in figure 2.24.

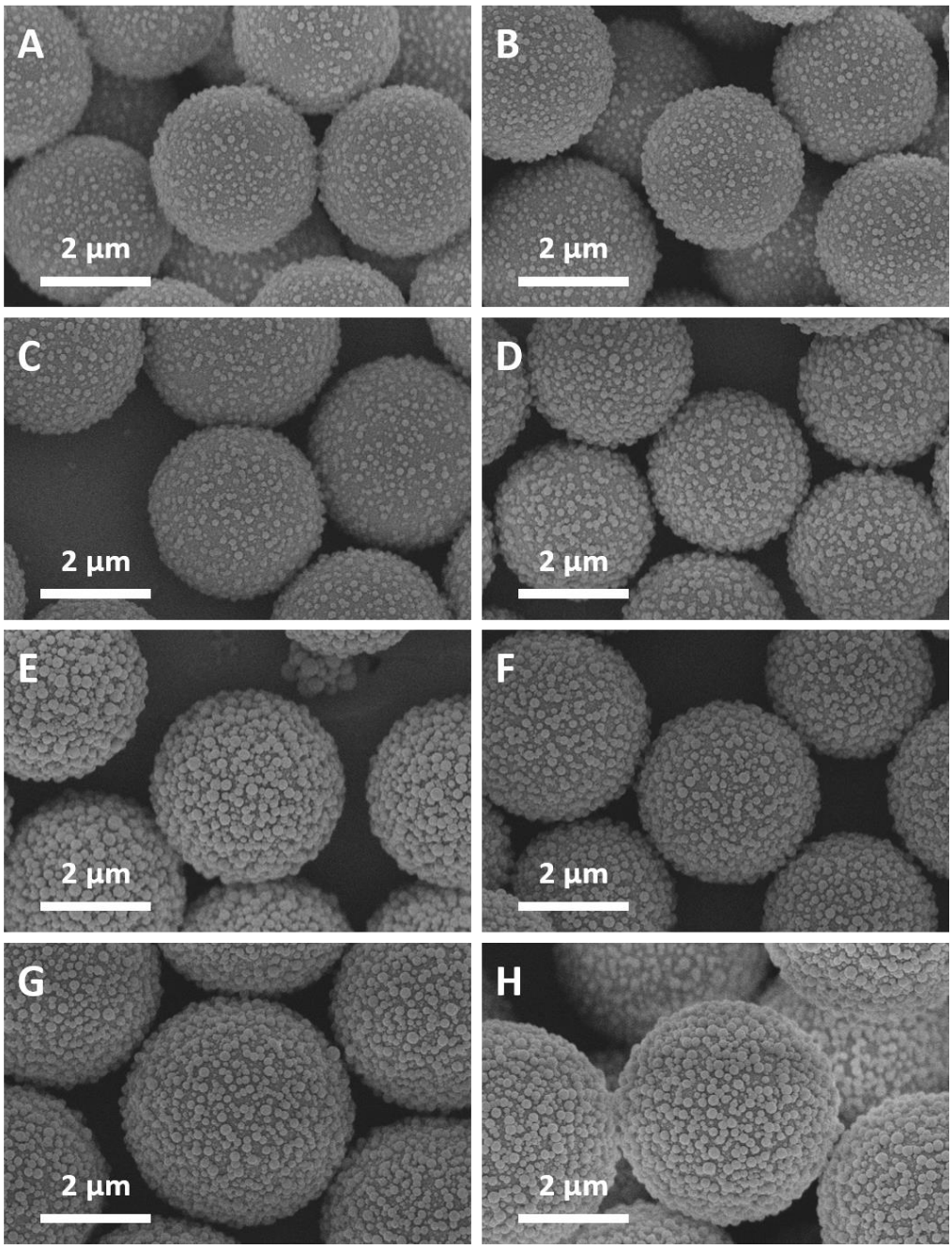

Figure 2.24 SEM images of particles produced when changing the addition rate of MPTMS into the reaction using a syringe pump. Addition rate (mL/min) = 8.0 (A), 6.0 (B), 4.0 (C), 2.0 (D), 1.0 (E), 0.75 (F), 0.5 (G), 0.25 (H).

Discrete SOS particles were obtained from all of the reactions, with various amounts of surface aggregation observed. Each of the reactions in this study led to the synthesis of similar sized particles to the previous optimised reaction, around 3 µm, with narrow PSD. As shown in the SEM images, the slowest addition rates (≤1 mL/min) produced

the greatest amount of surface aggregation and also the largest surface nanospheres. The length of addition time in this case (≥20 min) was sufficient to form core microspheres while MPTMS was still being added, which can then promote further growth of shell particles. Increasing the rate of addition led to a reduction in both the number and size of surface nanospheres as the concentration of MPTMS is much higher during the core formation stage and no further MPTMS is added once the core particles have been formed. Additionally, when measuring the BET surface areas of the particles, a range of 62-230 m^2/g was obtained. In general, the slower addition rates led to reduced surface area. This may suggest that pore filling is occurring as MPTMS is still being added after core particles have been formed, however some samples do not fit this pattern and it can not be stated for certain that there is a trend.

None of the SOS particles produced in this study had a full shell of nanospheres. However in the scaled up optimised reaction in section 2.4.7, where the addition rate was approximately 2 mL/min, a full shell was obtained. In this case, addition of MPTMS was performed in 2 mL steps each time rather than continuous addition suggesting that an initial amount of MPTMS may be required to facilitate faster formation of the core particles.

A second method was attempted, which was more alike to the seeded growth study by Giesche *et al*.[7] An initial amount of MPTMS was added, immediately followed by further addition via syringe pump. The reactions in this study were based on the optimised synthesis method in section 2.4.6, scaled up by 10 times to a total volume of 155 mL. The total amount of MPTMS added was 4 mL. All reactions were performed in new glassware at room temperature on a magnetic stirrer plate. Stirring was performed using a Teflon coated stirrer bar at a speed of 200 rpm.

Experimental conditions were studied in which the initial amount of MPTMS and flow rate were both varied. 0.5, 1 and 2 mL were chosen as the initial volumes and added instantly using a pipette. In the first study the remaining amount of MPTMS (3.5, 3 and 2 mL) was added by syringe pump at a rate of 0.125 mL/min. The pump was started as the initial volume was added, ensuring constant addition. The conditions equated to addition times that varied between 16 and 28 minutes. In the second study the addition rate via syringe pump was reduced to 0.065 mL/min. These conditions equated to addition times that varied between 30 and 55 minutes.

The particles produced when using a faster addition rate of 0.125 mL/min were very similar to the SOS material previously prepared from the optimised reaction, with narrow PSD. The SEM images are shown in figure 2.25 A, C and E. The reactions where 0.5 and 1 mL MPTMS was initially added displayed a full shell of nanoparticles around 250 nm in diameter. However, when 2 mL MPTMS was initially added SOS particles with only a partial shell were obtained. This reaction had the shortest addition time of 16 minutes and only 2 mL secondary addition. Based on previous observations, the shorter addition time combined with the smaller secondary volume of MPTMS is likely to be the cause of this morphology difference.

When the rate of secondary addition was reduced to 0.065 mL/min, highly uniform SOS particles were produced which showed significant morphology differences to those previously observed. The SEM images are shown in figure 2.25 B, D and F. The reactions where 0.5 and 1 mL MPTMS was initially added displayed a full shell of nanoparticles around 300 nm in diameter, additionally further nanoparticles up to 100 nm in size were found to grow upon the shell particles. These particles have been termed fractal SOS, due to the self-similar properties of the surface topography. When 2 mL MPTMS was initially added, regular SOS particles were obtained and secondary nucleation upon the shell particles was not observed.

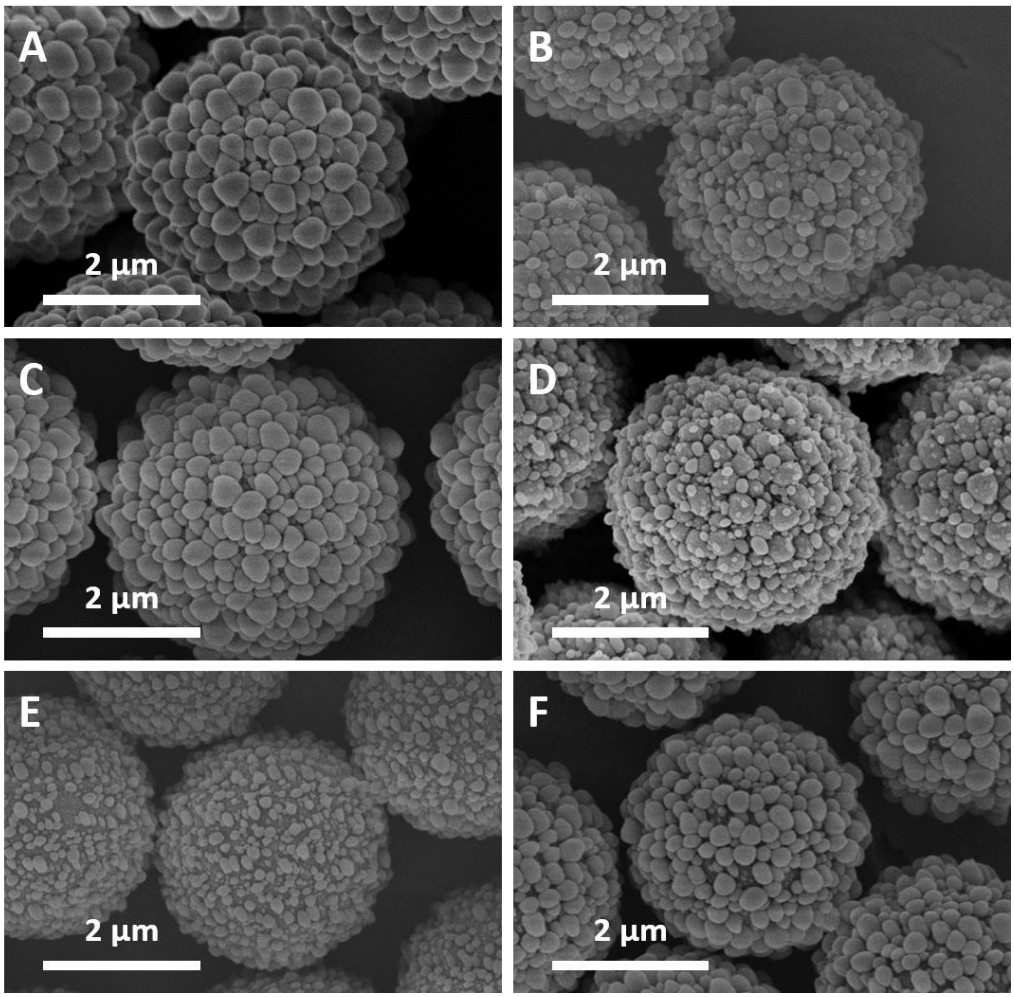

Figure 2.25 SEM images of particles produced using syringe pump addition at 0.125 mL/min after addition of 0.5 (A), 1 (C) and 2 mL (E) MPTMS; and using syringe pump addition at 0.065 mL/min after addition of 0.5 (B), 1 (D) and 2 mL (F) MPTMS. Total MPTMS addition was 4 mL for all reactions.

The reaction condition where 1 mL of MPTMS was initially added, followed by secondary addition at 0.065 mL/min was investigated further, as this method produced what appear to be the most uniform particles plus the greatest surface aggregation. Alternative addition rates for the secondary step were studied. 3 mL MPTMS was added via syringe pump at flow rates of 0.06, 0.04 and 0.02 mL/min, equating to addition times of 50, 75 and 150 minutes. SOS particles with very narrow PSD were obtained from all three reactions, with partial fractal morphology observed for the particles. The SEM images and overlaid sizing plots are shown in figure 2.26.

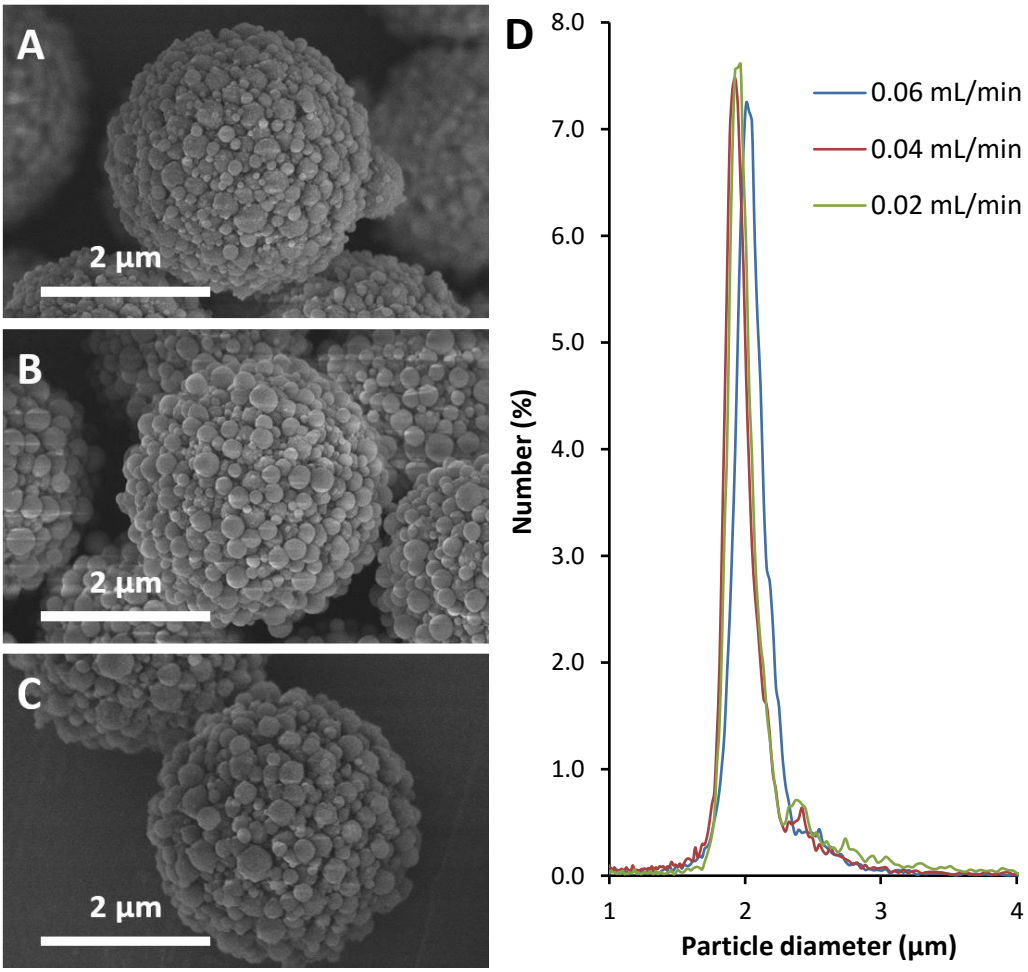

Figure 2.26 Fractal SOS particles obtained via initial MPTMS addition volume of 1 mL, followed by syringe pump addition at 0.06 (A), 0.04 (B) and 0.02 mL/min (C) to a total volume of 4 mL are shown by SEM imaging, along with the overlaid PSD (D).

Table 2.4 Physical data for particles shown in figure 2.26.

Addition rate (mL/min)	Surface area (m^2/g)	Particle diameter (µm)	$d^{90}/_{10}$
0.06	179	2.06	1.21
0.04	117	2.01	1.23
0.02	62	2.09	1.24

The physical data in table 2.4 shows that particle diameter and PSD appear to be unaffected by the addition rate, however the surface area is significantly reduced at lower addition rates. This may be due to pore-filling by MPTMS as the precursor is still being added after the point where particles have already been formed. The particle diameters were measured to be around 2 µm, with $d^{90}/_{10}$ ratios approaching that of core-shell materials (<1.15). Although the particle diameters in this study were smaller than those obtained from the optimised reaction in section 2.4.6 and 2.4.7, there was a small improvement in PSD observed, indicating that controlled addition appears to be beneficial to facilitate the synthesis of monodisperse particles.

2.4.9 Alternative Morphologies

The experimental work in this chapter has concentrated on the development of the synthesis reaction of the SOS material to obtain particles with ideal morphology, diameter and PSD. The work so far has described these attempts only, however many alternative and unexpected morphologies were also observed when changing reagent type and concentration in the reaction. For example the synthesis of fractal SOS particles, which display further surface aggregation when compared to regular SOS particles, has been described in the previous section and will be further discussed later in this thesis.

One particularly interesting outcome from the modified synthesis is the possibility of forming highly uniform microspheres. If the concentration of ammonia in the optimised reaction (section 2.4.6) is increased to 14%, SOS morphology is lost and smooth spherical particles with mean diameter of around 3 µm are produced with narrow PSD. The synthesis may provide a fast, simple alternative to the current methods of producing spherical, mesoporous silica particles for chromatographic use, which typically require many classification steps to achieve an acceptable PSD. The diameter and physical properties make these particles potentially useful for use in routine HPLC separation of small molecules. The synthesis and modification of these particles will also be discussed later.

2.5 Conclusion

In this chapter, each of the reagents in the SOS synthesis method has been investigated, with the aim of forming SOS particles with a complete shell of nanoparticles and narrow PSD. A range of concentrations and alternative reagents have been discussed, and their effects on the resultant particle morphology recorded.

It is apparent that the synthesis of SOS particles is very sensitive to changes in the reaction conditions. If reagents are present outside of an optimal concentration range the SOS morphology is either reduced or lost completely. This was observed when modifying the concentration of polymer and surfactant. It was found that omitting PVA from the standard reaction led to the formation of aggregated smooth particles. Although the polymer is required to stabilise the reaction, in too high a concentration it was found to be detrimental to the SOS morphology, with very few nanoparticles formed on the surface. A reduction in the concentration of CTAB was shown to improve the PSD, but its omission led to the formation of uniform smooth spheres only. It is thought that the reduction in concentration of these two reagents results in a reaction solution which is more alike to an unmodified Stöber synthesis,[2] which typically results in the formation of smooth, uniform microspheres. A study of the SOS reaction without the addition of polymer or surfactant was also found to produce smooth, uniform spheres around 1.5 µm in diameter, which supports this theory.

The concentration of ammonia was shown to provide a large effect on the resultant surface topography. It was found that the density of surface nanoparticles could be controlled by changing the concentration. The amount of aggregation is directly related to the rate of reaction, with an increasing amount of surface particles observed as the concentration of ammonia is reduced. An explanation is that at higher concentration the reaction rate is much faster, therefore particle growth proceeds quickly and there is less opportunity for nanoparticle growth. Reducing the ammonia concentration reduces the reaction rate, providing more time for secondary nucleation to occur and resulting in a denser shell coverage. The concentration of ammonia also had an effect on the particle diameter with the smallest particles formed at the highest concentration. This is consistent with the observations of both Ahmed[1] and Bogush,[3] where decreasing pH led to an increase in particle size. This is again linked to the reaction rate, with the higher pH providing faster particle formation and precipitation, and thus a smaller particle diameter.

The ratio of methanol:water was also found to have a large effect on the resultant particle morphology, with an optimal ratio of 8:5 required to produce SOS particles. Previous studies of the Stöber reaction have found the water content to have an effect on the particle diameter and rate of condensation,[2] with a significant reduction in particle size obtained either side of an optimum volume.[59] In this study however the particle size was found to increase when reducing the water content, with loss of the SOS morphology. Large, polydisperse smooth spheres were instead formed. Increasing the water content also led to the loss of the SOS structure. However, the particle diameter was reduced in this case, with a bimodal size distribution observed. The rate at which the reaction turned cloudy was found to be longest at the lowest concentration of water, which also resulted in the formation of the largest particles. Increasing the amount of water led to smaller particles and shortened reaction time. This is similar to the effect seen when adjusting ammonia concentration, which produced the smallest particles at the fastest reaction rate.

Through a combination of effects from changing reagent type and concentration, SOS particles around 3 µm in diameter with a complete single layer of nanoparticles were successfully synthesised. Additionally, the PSD was significantly improved over the standard SOS method, with a $d^{90}/_{10}$ ratio of 1.31. Scale up of this reaction was performed with resultant particles found to have similar mean diameter and identical surface morphology. The $d^{90}/_{10}$ ratio of 1.24 also showed a slight improvement. The particle diameter and PSD of these particles potentially make this material ideal for chromatographic use. The use of new glassware for each reaction may contribute to obtaining a narrow PSD. It has been shown previously that large variation in Stöber particle diameter occurs with repeated use of glassware, even after a thorough cleaning procedure,[44] due to possible seeded growth from residual particles present on the glassware wall from previous syntheses.

The optimised method allows the formation of SOS particles in a one-pot reaction that have comparable diameter and PSD to standard SOS particles that have undergone classification via a settling method. The classification process in this work required around 12 hours of settling time and resulted in 53% mass loss. Other classification methods that could be considered to improve the PSD of standard SOS particles include elutriation or air classification, however these would also result in mass loss and possibly even longer process times to complete. The one-pot method is therefore highly advantageous as it removes the need for numerous time-consuming classification steps and leads to a much higher yield.

Once optimal conditions had been determined, the controlled method of MPTMS addition via syringe pump was found to improve the PSD further. The lowest $d^{90}/_{10}$ ratio of 1.21 is approaching that of commercial core-shell materials (≤1.15). It was found that an initial addition of MPTMS was required to begin particle formation, followed by constant addition using the syringe pump. The best results were obtained from an initial volume of 1 mL followed by further addition of 3 mL at 0.065 mL/min. A new type of SOS structure with increased amounts of surface aggregation was obtained from these conditions, which will be discussed later in this thesis.

Aside from the rough surface due to the shell layer, the SOS particles discussed in this chapter are highly spherical in nature. This is particularly apparent when comparing to core-shell materials produced by the LbL method, for example those shown in figure 1.6, chapter 1. As the SOS particles are produced in a one-pot method, the single-layer shell is uniform over the whole particle surface, resulting in a highly spherical product. By contrast, LbL synthesis adds numerous layers in multiple steps. This inevitably leads to areas of uneven coverage and the final product is not spherical. The combination of rough surface, high sphericity and narrow PSD of SOS particles may facilitate high quality packing of HPLC columns due to ideal packing of spheres and shear effects locking particles in place.

Further investigation of the optimised SOS reaction should include larger scale up of the reaction volume, followed by assessment of the morphology and physical properties. The largest reaction described in this chapter was 770 mL total volume, producing 7.2 g of material after calcination. This would provide enough material for around 12 HPLC columns with dimensions of 100 × 2.1 mm. By contrast, a typical batch size for commercial core-shell particles can exceed 500 g, although particles may not necessarily all be produced from a single reaction and could instead be composed of blends of several batches.

There has been some interest into SOS silica materials from other university research groups and industry, particularly manufacturers of HPLC columns. Although it has not been possible to supply material to all who have requested, there are several ongoing collaborations with a number of institutions including Thermo Scientific, Novo Nordisk, ePrep, the University of Geneva and the University of Dundee.

2.6 References

1. A. Ahmed, H. Ritchie, P. Myers and H. Zhang, *Advanced Materials*, 2012, **24**, 6042-6048.
2. W. Stöber, A. Fink and E. Bohn, *Journal of Colloid and Interface Science*, 1968, **26**, 62-69.
3. G. H. Bogush and C. F. Zukoski, *Journal of Colloid and Interface Science*, 1991, **142**, 1-18.
4. A. Van Blaaderen and A. Vrij, *Langmuir*, 1992, **8**, 2921-2931.
5. A. van Blaaderen and A. Vrij, *Journal of Colloid and Interface Science*, 1993, **156**, 1-18.
6. A. W. Dearing and E. E. Reid, *Journal of the American Chemical Society*, 1928, **50**, 3058-3062.
7. H. Giesche, *Journal of the European Ceramic Society*, 1994, **14**, 205-214.
8. N. N. Greenwood and A. Earnshaw, *Chemistry of the Elements*, Elsevier Science, 2012.
9. L. L. Hench and J. K. West, *Chemical Reviews*, 1990, **90**, 33-72.
10. A. E. Danks, S. R. Hall and Z. Schnepp, *Materials Horizons*, 2016.
11. R. K. Iler, *The Chemistry of Silica: Solubility, Polymerization, Colloid and Surface Properties and Biochemistry of Silica*, Wiley, 1979.
12. A. Van Blaaderen, J. Van Geest and A. Vrij, *Journal of Colloid and Interface Science*, 1992, **154**, 481-501.
13. C. G. Tan, B. D. Bowen and N. Epstein, *Journal of Colloid and Interface Science*, 1987, **118**, 290-293.
14. *US Pat.*, US4775520 A, 1988.
15. K. S. W. Sing, D. H. Everett, R. A. W. Haul, L. Moscou, R. A. Pierotti, J. Rouquerol and T. Siemieniewska, *Reporting Physisorption Data for Gas/Solid Systems*, Wiley-VCH Verlag GmbH & Co. KGaA, 2008.
16. C. T. Kresge, M. E. Leonowicz, W. J. Roth, J. C. Vartuli and J. S. Beck, *Nature*, 1992, **359**, 710-712.
17. G. S. Attard, J. C. Glyde and C. G. Goltner, *Nature*, 1995, **378**, 366-368.
18. D. Zhao, Q. Huo, J. Feng, B. F. Chmelka and G. D. Stucky, *Journal of the American Chemical Society*, 1998, **120**, 6024-6036.
19. H. Zhang, G. C. Hardy, M. J. Rosseinsky and A. I. Cooper, *Advanced Materials*, 2003, **15**, 78-81.

20. A. Imhof and D. J. Pine, *Nature*, 1997, **389**, 948-951.
21. O. D. Velev and E. W. Kaler, *Advanced Materials*, 2000, **12**, 531-534.
22. M. L. K. Hoa, M. Lu and Y. Zhang, *Advances in Colloid and Interface Science*, 2006, **121**, 9-23.
23. D. Walsh, L. Arcelli, T. Ikoma, J. Tanaka and S. Mann, *Nature Materials*, 2003, **2**, 386-390.
24. J. H. Schattka, D. G. Shchukin, J. Jia, M. Antonietti and R. A. Caruso, *Chemistry of Materials*, 2002, **14**, 5103-5108.
25. J. Zhou, M. Zhou and R. A. Caruso, *Langmuir*, 2006, **22**, 3332-3336.
26. M. J. Rosen and J. T. Kunjappu, *Surfactants and Interfacial Phenomena*, Wiley, 2012.
27. J. W. McBain, *Transactions of the Faraday Society*, 1913, **9**, 99-101.
28. G. S. Hartley, *Kolloid-Zeitschrift*, 1939, **88**, 22-40.
29. F. Reiss-Husson and V. Luzzati, *The Journal of Physical Chemistry*, 1964, **68**, 3504-3511.
30. G. J. T. Tiddy, *Physics Reports*, 1980, **57**, 1-46.
31. J. S. Beck, J. C. Vartuli, W. J. Roth, M. E. Leonowicz, C. T. Kresge, K. D. Schmitt, C. T. W. Chu, D. H. Olson and E. W. Sheppard, *Journal of the American Chemical Society*, 1992, **114**, 10834-10843.
32. F. Hoffmann, M. Cornelius, J. Morell and M. Fröba, *Angewandte Chemie International Edition*, 2006, **45**, 3216-3251.
33. Q. Huo, D. I. Margolese and G. D. Stucky, *Chemistry of Materials*, 1996, **8**, 1147-1160.
34. A. Monnier, F. Schüth, Q. Huo, D. Kumar, D. Margolese, R. S. Maxwell, G. D. Stucky, M. Krishnamurty, P. Petroff, A. Firouzi, M. Janicke and B. F. Chmelka, *Science*, 1993, **261**, 1299-1303.
35. A. Ahmed, R. Clowes, E. Willneff, H. Ritchie, P. Myers and H. Zhang, *Industrial & Engineering Chemistry Research*, 2009, **49**, 602-608.
36. J. Nawrocki, C. Dunlap, A. McCormick and P. W. Carr, *Journal of Chromatography A*, 2004, **1028**, 1-30.
37. G. Guiochon and F. Gritti, *Journal of Chromatography A*, 2011, **1218**, 1915-1938.
38. A. Ahmed, W. Abdelmagid, H. Ritchie, P. Myers and H. Zhang, *Journal of Chromatography A*, 2012, **1270**, 194-203.

39. A. Ahmed, M. Forster, R. Clowes, D. Bradshaw, P. Myers and H. Zhang, *Journal of Materials Chemistry A*, 2013, **1**, 3276-3286.
40. H.-C. Zhou, J. R. Long and O. M. Yaghi, *Chemical Reviews*, 2012, **112**, 673-674.
41. K. A. Cychosz, R. Ahmad and A. J. Matzger, *Chemical Science*, 2010, **1**, 293-302.
42. Z. Y. Gu, C. X. Yang, N. Chang and X. P. Yan, *Accounts of Chemical Research*, 2012, **45**, 734-745.
43. Y.-Y. Fu, C.-X. Yang and X.-P. Yan, *Chemistry – A European Journal*, 2013, **19**, 13484-13491.
44. A. Ahmed, PhD thesis, University of Liverpool, 2012.
45. *US Pat.*, 2656508A, 1953.
46. Beckman Coulter Inc., www.beckmancoulter.com.
47. T. Allen, *Particle Size Measurement*, Springer Netherlands, 2012.
48. Horiba Ltd., www.horiba.com.
49. K. D. Vernon-Parry, *III-Vs Review*, 2000, **13**, 40-44.
50. D. C. Joy and J. B. Pawley, *Ultramicroscopy*, 1992, **47**, 80-100.
51. D. C. Joy and D. G. Howitt, *Scanning Electron Microscopy*, Academic Press, New York, 2003.
52. D. C. Joy, *Ultramicroscopy*, 1991, **37**, 216-233.
53. D. C. Joy, *Current Opinion in Solid State and Materials Science*, 1997, **2**, 465-468.
54. S. Brunauer, P. H. Emmett and E. Teller, *Journal of the American Chemical Society*, 1938, **60**, 309-319.
55. E. P. Barrett, L. G. Joyner and P. P. Halenda, *Journal of the American Chemical Society*, 1951, **73**, 373-380.
56. H. M. Rootare, *A Review of Mercury Porosimetry*, Springer US, 1970.
57. E. W. Washburn, *Physical Review*, 1921, **17**, 273-283.
58. A. W. Coats and J. P. Redfern, *Analyst*, 1963, **88**, 906-924.
59. R. Sato-Berrú, J. M. Saniger, J. Flores-Flores and M. Sanchez-Espíndola, *Journal of Materials Science and Engineering. A*, 2013, **3**, 237.

3 Microwave Assisted Bonding

3.1 Introduction

While a great deal of interest is shown by manufacturers and researchers in the synthesis of new types of silica particles and introduction of new bonded phases, there appears to be much less focus on the bonding techniques used to functionalise the particles for chromatographic use.

Until the 1970s the majority of liquid chromatography columns contained a hydrophilic stationary phase such as unfunctionalised silica. On this type of column analytes are retained based on their affinity for the polar silanol groups on the surface of the stationary phase, a method which was later termed normal phase chromatography (NPC).[1] While this type of interaction is suitable for polar compounds, for non-polar and biological samples selectivity is poor and the high organic content of the mobile phase is incompatible with many compounds of interest, particularly pharmaceuticals. An alternative method is therefore required.

Reversed phase chromatography (RPC) was introduced in 1950 by Howard and Martin[2] and was further developed through the 1960s and 70s, the name derived from having an opposite "reversed" retention mechanism to NPC. The stationary phase in RPC is typically a silica that has been modified with a hydrophobic functional group.[3, 4] This allows a much greater selection of surface chemistries and many more applications than NPC, as such it is now the most routinely used HPLC method.

The literature review will discuss the various chemical reactions that have been employed in the silanisation of silica and the use of traditional/conventional heating methods for these reactions. This is followed by discussion about the use of microwave irradiation as a heating source for synthesis and the option to perform microwave assisted bonding onto silica particles for chromatographic use.

3.2 Literature Review

There are several reactions that have been used to modify the silica surface with functional groups which in turn allow control of the chromatographic properties. As early as 1957, studies had been undertaken into the modification of silica powders with aliphatic

alcohols via an esterification reaction to produce a hydrophobic surface.[5] A detailed investigation of this reaction was later published.[6] The first attempt to functionalise silica gel for chromatographic purposes however was made by Halasz and Sebastian.[7] Short-chain alkoxy groups were attached to the surface, again via an esterification reaction, resulting in the formation of a Si)-O-C bond. The bracket denotes a surface silicon atom. The reaction overview can be seen in figure 3.1 A.

One shortcoming of the esterification method is that the silicon-oxygen-carbon link is susceptible to hydrolysis, especially in the case of RPC which uses aqueous mobile phase. The bonded phase can be readily removed from the surface, leading to regeneration of the original silanol groups. Around the same time, an alternative bonding method was introduced by Kirkland, involving the use of chlorosilane reagents.[8] The chlorosilane reacts with a silanol on the silica surface, leading to the formation of a much more stable Si)-O-Si-C link, shown in figure 3.1 B.

Methoxy or ethoxy silanes can be substituted for the chloro derivative under similar reaction conditions. When using chlorosilanes, a base such as imidazole or 2,6-lutidine is included, which acts as both a catalyst for the reaction and a scavenger for the hydrochloric acid produced. This has the effect of shifting equilibrium to the product side.[9] Two molecules of base are required to activate the organosilane Si-Cl bond to form a reactive intermediate and hydrochloric acid.[10] The intermediate then reacts with a hydroxyl group present on the silica surface, attaching the alkylsilane ligand and reforming a molecule of base. The reaction scheme is shown in figure 3.2. Bases such as imidazole are also able to form intermediates with the organosilane, forming a pentacoordinate silicon atom. This has the effect of lengthening the Si-Cl bond, making it more susceptible to nucleophilic attack.[9] The use of organosilanes forms the basis of most silanisation reactions today due to the stable Si-C bond and wide range of reagents to choose from.

A different approach is the formation of a direct Si)-C linkage to the silica surface. This can be achieved by initial chlorination of the silica surface, followed by treatment with a Grignard reagent or organolithium compound, shown in figure 3.1 C.[11-13] Another option is via reduction of the silanol groups to Si)-H, followed by hydrosilation, shown in figure 3.1 D.[14] The resulting Si)-C bond is very stable at low pH where an organosilane bonded phase would perhaps begin to see stripping of the functional groups from the silica. The ease of the organosilane reaction however makes it the preferred choice for manufacturers,

especially as the majority of HPLC applications are performed within the pH operating range of their materials.

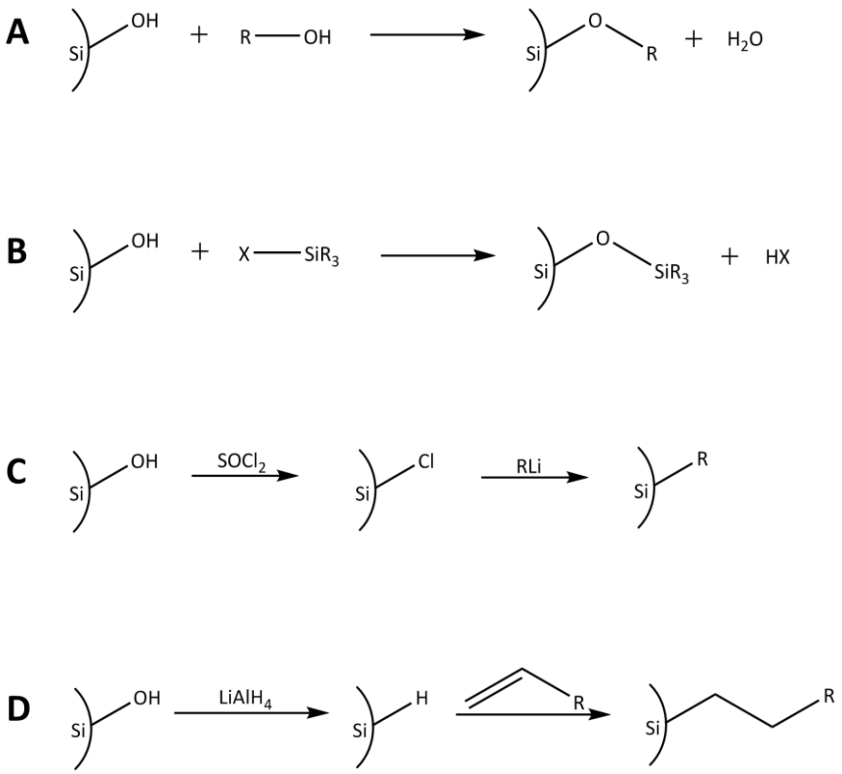

Figure 3.1 Bonding methods onto the Si-OH surface. Esterification reaction (A); organosilane reaction, where X = Cl, OMe, OEt (B); via chlorination and Grignard reagent (C); via reduction and hydrosilation (D).

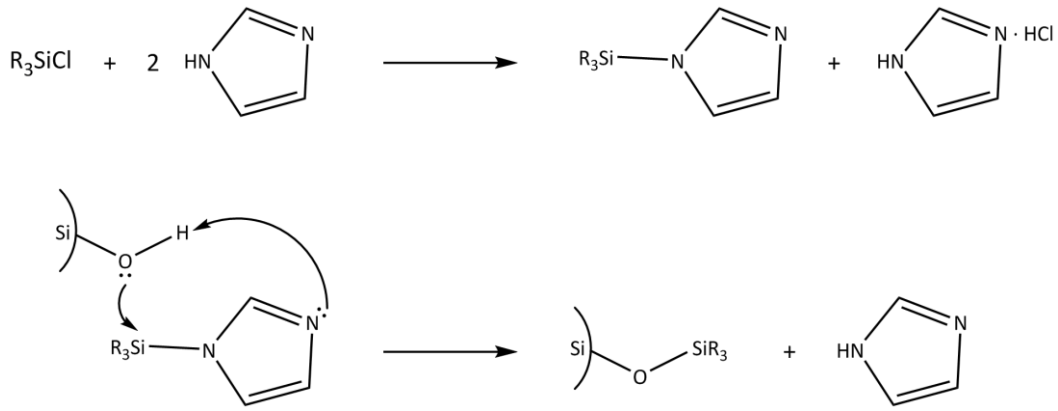

Figure 3.2 The role of base in the silanisation reaction.[9]

Residual silanol groups have been shown to be a cause of peak tailing, reduced chromatographic performance and mechanical instability in the column packing.[15, 16] The concentration of silanol groups on the silica surface may range up to a theoretical maximum of 8 μmol/m^2, depending upon the type of silica and if any treatment has been performed to rehydroxylate the surface.[17-19] Depending on the size of ligand being added, maximum achievable bonding densities are far lower than this due to steric hindrance between the attached groups.[20-22] One very high bonding density of 5.43 μmol/m^2 was reported, which was achieved by the attachment of a small trimethylsilane group.[23] However, to achieve sufficient analyte retention and selectivity, HPLC columns are typically bonded with longer alkyl chains (up to 30 carbon atoms) or other bulky ligands, hence the maximum density for these is lower. It is therefore apparent that many residual silanols will be present, even after an efficient bonding process. It is essential that the number of remaining hydroxyl groups is reduced to the greatest degree possible. This is achieved by the attachment of a small organosilane ligand, using reagents such as bis(dimethylamino)dimethylsilane (BMMS), trimethylsilylimidazole (TMSI) or hexamethyldisilazane (HMDS), and is referred to as the endcapping step. These ligands can be attached via the same bonding methods as the original ligand. The small size of the groups allows the maximum possible amount of residual silanols to be converted, although in practice some will remain on the surface.

The use of traditional reflux methods are employed by most manufacturers when producing their bonded phases. Typically the heating is performed by a heating mantle, oil bath or hot plate. While this is generally seen as an acceptable form of heating, there are a number of drawbacks. The method of heating is slow and inefficient due to initial heating of the vessel, dependency on convective currents, thermal loss to the surrounding area, and thermal conductivity of the reagents and materials to be heated. The maximum achievable temperature is also dictated by the boiling point of the solvent meaning long, energy intensive reaction times ranging from 6 up to 24 hours are often required.

In conventional methods the vessel is exposed to the heating source and the heat is then transferred to the reactants by convection. The walls of the vessel often experience higher temperatures than the bulk of the reaction solution. This can lead to localised overheating, bumping and possible degradation or decomposition of reaction components. The bonding method clearly has a very large influence on the batch to batch reproducibility of the bonded phase silica.[4] Variation in the reaction conditions can cause significant issues

when quality control (QC) testing, especially in the case of carbon loading and bonding density. Lower than expected results for percent carbon can often lead to reduced chromatographic performance and therefore rework of the silica to bring it into required specification, costing further time and energy.

Although microwave technology has been available since the 1950s, it was not until 1986 that the technology was used in a scientific capacity.[24] Early microwave "reactors" were often domestic kitchen appliances which did not allow stirring of reactions, monitoring of temperature, control over the amount of power applied or direction of the microwave field. As a result reproducibility was often very poor and the method proved to be very hazardous with explosions reported.[25] By contrast, modern laboratory microwave reactors allow the user to safely and accurately control the reaction conditions. Temperature and stirrer controls are incorporated, as well as pressure monitoring systems for sealed vessel methods. Microwaves are directed at the sample using a single mode cavity, designed for the length of a single wave. This wave generates high electromagnetic field intensity with homogenous energy distribution within the cavity where the synthesis takes place, ideal for reproducible heating.

Unlike traditional heating, microwave irradiation heats the sample by direct coupling of the microwave energy to the molecules present in the reaction mixture via dipole rotation and ionic conduction. This method of heating has the benefits of extremely efficient energy transfer to the reaction mixture instead of the vessel, and reaction components are heated at the same rate throughout the vessel.[26]

When irradiated, dipoles in the mixture will align themselves in the direction of the applied electric field. As the field oscillates, the dipoles in the sample will attempt to realign themselves to the alternating electric field releasing energy as heat due to molecular friction and dielectric loss. The amount of heat generated depends on how effectively dipoles can align to the field. If they align themselves too quickly (irradiation frequency too low) or too slowly (frequency too high) then no heating will occur. Microwave reactors used for scientific purposes have an allocated frequency of 2.45 GHz which allows enough time for realignment, but not enough to follow the field precisely. In ionic conduction, ionic molecules in the reaction mixture oscillate under the influence of the magnetic field causing collisions with neighbouring atoms and thus creating heat. This effect provides greater heat generation than the dipole rotation mechanism.

Microwave synthesis is now a common method in the laboratory and there are a great number of publications describing its use to drive chemical reactions.[27-30] Despite this, examples where microwave irradiation has been used for the silanisation of silica are still quite limited, and no commercial chromatography column exists where this technology has been utilised.

Procopio *et al.*[31, 32] described a method of attaching alkylsulfonates onto mesoporous silica achieving good coverage and short reaction time, however there was no comparison with conventional heating methods. Both Garcia *et al.*[33] and Fukuya *et al.*[34] performed comparison studies between microwave and reflux heating methods onto silica, fully characterising the resultant particles. Both publications concluded that a significantly increased reaction rate is observed when using microwave bonding. Reaction rate was found to be highly dependent upon the length of alkyl group being attached, the leaving group of the alkoxysilane and choice of reaction solvent. Percent carbon values were comparable between heating methods, although some unexplained structural differences in the bonded layer were observed in the NMR characterisation. There is speculation that there may be some non-thermal effects occurring when using microwave heating,[35] but this has been attributed to the method of temperature measurement[36] and inhomogeneity of the reaction solution resulting in thermal effects.[37-39] Nevertheless, the topic of non-thermal effects is still hotly debated.[40, 41]

There is currently only a single publication describing a comparison that also includes chromatographic data. Mignot *et al.* assessed different grafting methods onto core-shell silica along with comprehensive characterisation.[42] Bonding of a C18 phase was performed onto the same silica using both conventional reflux and microwave irradiation. Once packed into columns the bonded phases were assessed with the Tanaka test protocol[43] alongside three commercial core-shell C18 materials.

It was found that bonding via microwave irradiation resulted in slightly lower maximum values for percent carbon (9.5 versus 10.1%) and hence surface coverage when compared with conventional heating. However, the reaction time was significantly shortened; 30 minutes versus 5 hours. The precise microwave method, specifically details of the reaction temperature and vessel type (open or closed), was not disclosed. It is therefore difficult to say if the coverage could be improved upon by modification of the procedure, either by increasing the reaction temperature or superheating in a sealed vessel. The maximum obtained coverage of 3.6 μmol/m^2 from the microwave reaction is

slightly lower than the theoretical maximum of between 4 and 4.7 µmol/m^2, and indicates that the process could potentially be improved, although this value still indicates a highly efficient bonding process.

Assessment with the Tanaka test mixtures showed comparable results between three different commercial C18 columns and the silica samples bonded via the two heating methods. The results from each column can be seen overlaid in figure 3.3. The microwave and conventional C18 columns were not endcapped and produced higher values for hydrogen bonding capacity (HBC) and ion exchange at pH 7.6 (IEX 7.6). This is likely caused by residual silanol groups. Other differences in the chromatographic performance between all columns in the study may be attributed to the type of silica used and the exact bonding process followed. Importantly, the two samples bonded in-house displayed nearly identical values for all test parameters, indicating that microwave irradiation would appear to be a viable alternative to traditional heating.

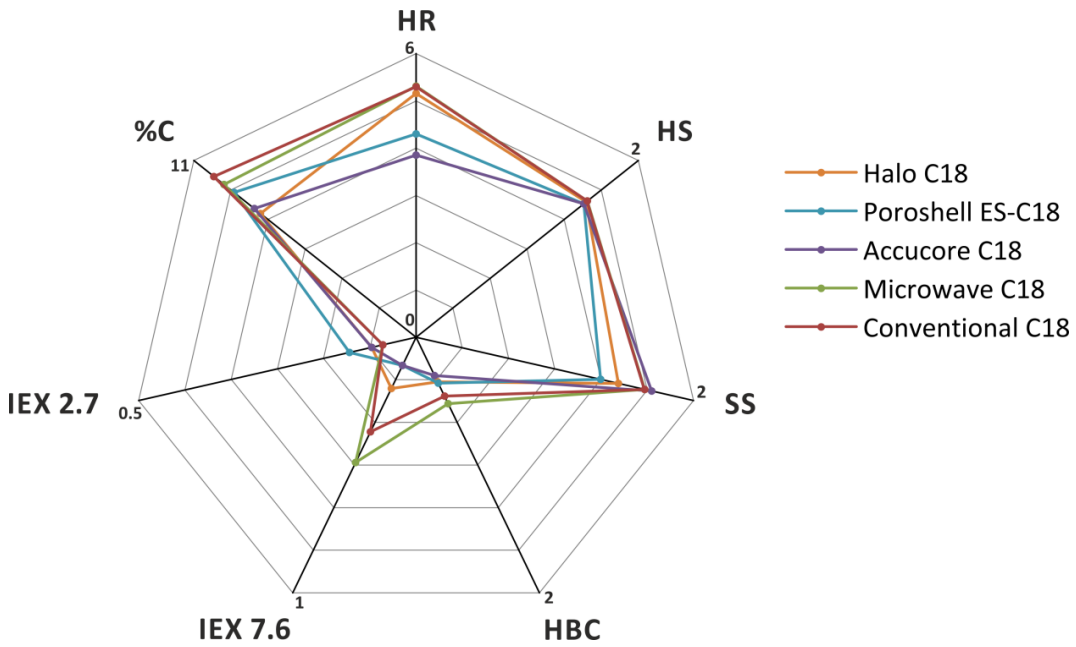

Figure 3.3 Radar plot of Tanaka test results and carbon loading for commercial, microwave and conventional C18 phases. Figure produced from chromatographic data by Mignot *et al.*[42] Parameters: HR - hydrophobic retention; HS - hydrophobic selectivity; SS - steric selectivity; HBC - hydrogen bonding capacity; IEX 7.6 - ion exchange capacity at pH 7.6; IEX 2.7 - ion exchange capacity at pH 2.7; %C - percent carbon loading.

This chapter aims to study the suitability of microwave irradiation as a heating method for the silanisation of SOS silica. It will firstly be necessary to determine optimal reaction conditions to achieve fast and consistent coverage with the attached functional group. It will be important to ensure reproducibility of the bonded phases and to compare the results from the microwave method with traditional heating. The performance of HPLC columns packed with functionalised SOS particles prepared by microwave and traditional bonding methods will also be compared.

3.3 Experimental

SOS silica particles for use in this chapter were produced from the reactions described in section 3.3.2. Functionalisation of SOS silica was performed following calcination at 550 or 600 °C. Particles were acid washed following calcination to reactivate the surface silanol groups. Surface areas of SOS samples were in the range of 68 to 240 m^2/g, and particle diameter 2.9 to 4.0 µm. No classification steps were performed to modify the size distribution, which ranged from $d^{90}/_{10}$ of 1.24 to 2.31.

The method of bonding via microwave irradiation was optimised and the results compared with conventional heating by reflux on an oil bath. The chromatographic performance of HPLC columns packed with SOS-C4 particles was then assessed with the separation of a protein test mixture. Alternative bonding solvents are also investigated.

3.3.1 Chemicals

1-(trimethylsilyl)imidazole (TMSI, ≥98%), ammonium hydroxide (28-30%, NH_3 basis), carbonic anhydrase, CTAB (≥98%), dimethylformamide (DMF, >99%), imidazole (≥99%), limonene (97%), lysozyme, MPTMS (95%), myoglobin, nitric acid (ACS reagent, 70%), ovalbumin, PVA (M_W = 9-10k), PVP (M_W = 10k) and trifluoroacetic acid (TFA, 99%) were purchased from Sigma-Aldrich. Butyl(chloro)dimethyl silane (C4 reagent, >97%) was purchased from Tokyo Chemical Industry. Acetone (GPR), acetonitrile (HPLC), chloroform (AR), dichloromethane (DCM, AR), isopropanol (HPLC), methanol (HPLC) and toluene (HPLC) were obtained from Fisher Scientific. Deionised water and Milli-Q water (18 MΩ) were prepared in the laboratory.

3.3.2 Particle Synthesis

Method 1: PVA (5.0 g) and CTAB (2.0 g) were dissolved in deionised water (100 mL). Methanol (160 mL) was added with stirring, followed by diluted ammonium hydroxide (5.6%, 40 mL). The solution was stirred for 15 minutes before addition of MPTMS (10 mL). The reaction was stirred overnight. SOS particles were collected on a sintered glass filter and washed with distilled water (5 x 50 mL), then methanol (5 x 50 mL) before drying under vacuum at 60 °C. Typically 6 g of particles were produced.

Method 2: PVP (5.0 g) and CTAB (0.25 g) were dissolved in deionised water (100 mL). Methanol (160 mL) was added with stirring, followed by diluted ammonium hydroxide (1.4%, 40 mL). The solution was stirred for 15 minutes before addition of MPTMS (8 mL). The reaction was stirred overnight. SOS particles were collected on a sintered glass filter and washed with distilled water (5 x 50 mL), then methanol (5 x 50 mL) before drying under vacuum at 60 °C. Typically 5 g of particles were produced.

Method 1 describes the standard method of producing SOS particles. This results in well-defined spherical SOS particles with a relatively dense, though not complete surface coverage of nanospheres, shown in figure 3.4 A. Particles produced by this method typically have a mean particle size of 3-4 µm in diameter but with broad size distribution, $d^{90}/_{10}$ ratio between 1.8 and 2.4. Method 2 describes the optimised synthesis of SOS particles, discussed in the previous chapter. This method typically produces particles around 3 µm in diameter with narrow size distribution, $d^{90}/_{10}$ ratio <1.4 and a complete single shell of nanospheres surrounding the core, shown in figure 3.4 B.

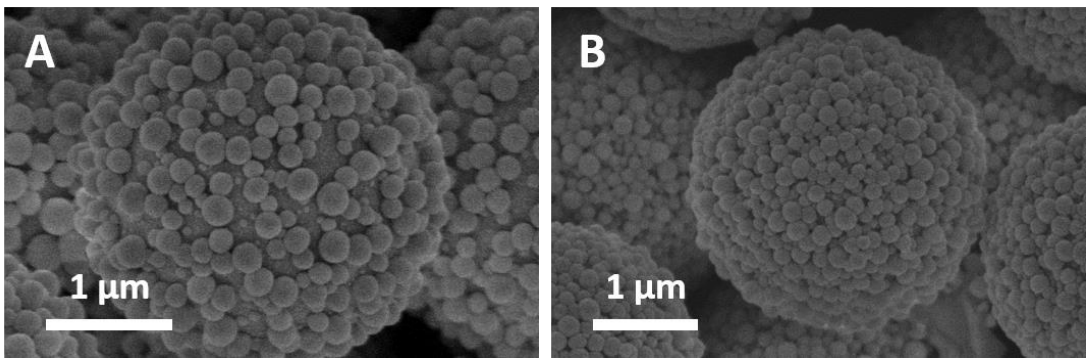

Figure 3.4 SEM images showing surface morphology of SOS particles. Particles produced from method 1 (A). Particles produced from method 2 (B).

3.3.3 Silica Pre-Treatment

SOS silica samples were calcined in a furnace (Carbolite CWF1200) to remove the residual mercapto groups and any organic components left over from the particle synthesis. Average mass loss was 53%. Conditions: heat in air at 1 °C/min, hold at 550 or 600 °C for 12 hours, then allow to cool to room temperature.

SOS samples were then acid washed to rehydroxylate the surface. For 1 g of silica, 10 mL of 0.02 M nitric acid was added and the resulting slurry heated with stirring at 90 °C for 3 hours. Treatment of fully porous, spherical silica would typically use 0.1 M acid, but these conditions were found to adversely affect the SOS morphology resulting in loss or damage to some surface nanospheres. The acid treated silica was washed on a sintered glass filter with five 30 mL aliquots of deionised water so that no trace of acid remained. Particles were then washed with methanol followed by acetone and dried under vacuum at 80 °C. Before bonding, silica was dried at 150 °C under vacuum for 16 hours to remove all traces of water and activate the surface silanol groups.

3.3.4 Bonding Using Microwave Irradiation

All microwave reactions were performed on a CEM Explorer microwave reactor, shown in figure 3.5. The associated computer software enables the user to create a heating profile allowing complete control over the reaction conditions. The reactor is fitted with an autosampler, allowing high throughput of up to 48 (35 mL) or 96 (10 mL) vessels to be sequentially run. This is particularly useful for optimising the bonding method as many alternative conditions can be quickly assessed. Another advantage of the microwave reactor over conventional reflux is the option to use a closed vessel method where specialised glass reaction vessels are sealed with venting caps which are designed to release pressure instead of the glass vessel failing in the event of excessive pressure. This enables the user to have the reaction proceed at a temperature above the boiling point of the solvent, a process known as superheating.[28]

For C4 silanisation of SOS particles all glassware was washed with deionised water, then acetone and dried at 150 °C before use. 1 g of acid treated silica was dispersed in toluene (7.5 mL) with sonication in a 35 mL reaction vessel. A rare earth stirrer bar, imidazole (0.1 g) and C4 reagent (0.4 g) were added and the vessel sealed. Reagent

amounts were adjusted according to the mass of silica starting material, the ratio was kept constant. Typical microwave instrument parameters were as follows:

Reaction type	Dynamic closed vessel method
Reaction temperature	120 °C
Maximum pressure	17 bar
Maximum power setting	300 W
Stir speed	High
Pre-stirring	1 minute
Reaction time	20 minutes

Figure 3.5 CEM Explorer microwave reactor with autosampler.

A high stir speed was applied due to the nature of the SOS material to settle quickly in solution. Resultant SOS-C4 particles were washed on a sintered glass filter with toluene (30 mL), methanol (30 mL), methanol/water (1:1 V/V, 30 mL) and methanol (30 mL). Particles were first dried in air on the filter for 1 hour, then under vacuum at 80 °C overnight. Endcapping was performed using the same method with TMSI in place of the chlorosilane and the omission of imidazole.

3.3.5 Carbon Analysis

The carbon content of functionalised SOS particles was analysed with a Thermo FlashEA 1112 Elemental Analyser. All reported percent carbon values are after the endcapping stage. The percent carbon value was used in conjunction with BET surface area data to calculate the bonding density of the silica stationary phase using the Berendsen-de Galan equation.[44]

$$\alpha = \frac{\%C \times 10^6}{M_C n_C S_{BET} \left[100 - \left\{\left(\frac{\%C}{M_C n_C}\right) M_L\right\}\right]}$$

Where α is the bonding density in μmol/m^2, %C is the percent carbon of the bonded material, M_C is the atomic weight of carbon, n_C is the total number of carbon atoms in the ligand, S_{BET} is the surface area of the silica and M_L is the molecular weight of the attached ligand.

3.3.6 Column Packing

As was discussed in chapter 1, core-shell particles exhibit a very stable packing bed in the column due to shear force and the rough surface locking particles in place. The packing procedure of core-shell particles however is more difficult than for smooth spherical particles as this shear force must initially be overcome. Optimisation of the packing method was therefore required to pack SOS particles into the HPLC column. Early methods of column packing with very large particles (10-30 μm) were to simply pour the dry silica media into the column, allow to settle, and repeat until the column was filled before adding the end fittings.[45] For particles less than 10 μm this method is generally not suitable and a slurry method is typically used.[46, 47]

To pack a column with the slurry method, the silica material is firstly dispersed in a suitable slurry solvent using sonication. It is important for particles to be well dispersed to ensure bed homogeneity in the packed column.[48] A small excess of the material is required to ensure the column is completely filled. Common packing solvents include acetone,

chloroform, heptane, isopropanol, methanol, toluene or a mixture of a number of these. This is not an exhaustive list and many alternatives may also be used provided they are compatible with the bonded phase. The choice of solvent makes a surprisingly large contribution to the quality of the packed column.[48] Different bonded phases, morphologies and even particle sizes often require different slurry solutions to achieve the best possible packing. An appreciable amount of work goes into developing column packing procedures and column manufacturers do not generally disclose their packing methods.

An example of equipment used to pack HPLC columns is depicted in figure 3.6. The column hardware with outlet frit and end fitting attached is connected to a pre-column which in turn is connected to a slurry reservoir. The prepared silica slurry solution, made up to the appropriate volume to completely fill this reservoir, is poured into the reservoir and the pump adapter attached. A specialised air-driven packing pump is then used to pump solvent (the push solvent) through the system at a chosen pressure until a pre-determined amount has passed through the column. The push solvent is normally an organic solvent, although again this depends on the bonded phase being packed.

A typical packing pump is capable of up to 1000 bar output pressure and high flow rates of up to 1 L/min. As the push solvent is being pumped through the system, the porous frit within the HPLC column outlet retains the compressed silica material producing a packed structure similar to close-sphere packing. Once the required amount of solvent has passed through the column, the pump is switched off and the system allowed to equilibrate back to atmospheric pressure. The packed column can then be removed from the pre-column and the inlet frit and end fitting attached.

As well as the choice of solvent, the reservoir size also contributes to the quality of the packed column. During QC testing, a column may produce peaks which are not symmetrical (Gaussian) across the whole chromatogram. Manufacturer specification will allow for some variation in this parameter, but in cases where asymmetry is slightly out of specification the reservoir size can be adjusted to compensate for this. If peaks are fronting (asymmetry <1) it indicates that the column has packed too slowly and that a smaller reservoir size should be used. Conversely if peaks are tailing (asymmetry >1), it indicates the column may have packed too quickly and the reservoir size should be increased.

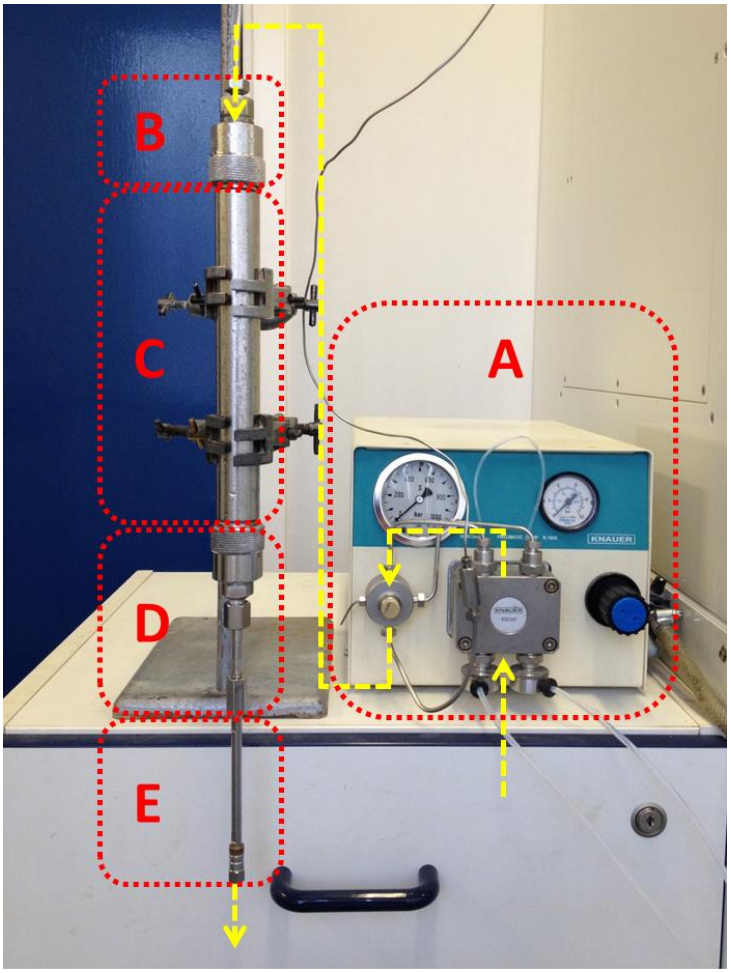

Figure 3.6 Column packing equipment, composed of packing pump (A), pump adapter (B), slurry reservoir (C), pre-column (D) and column to be packed (E). Direction of solvent flow is shown by the yellow arrows.

The parameters were carefully considered for packing SOS particles into HPLC columns. C4 functionalised SOS particles were packed into 50 or 100 mm stainless steel narrow bore columns with 2.1 mm internal diameter, sealed with 0.5 µm porous titanium frits. The SOS material has a tendency to settle quickly in organic solvents with low density and/or viscosity. This was apparent when attempting to use methanol (d = 0.79 g/mL, η = 0.545 mPa·s) as the slurry solvent as the initially dispersed particles dropped rapidly to the bottom of the measuring cylinder. To address this, a mixed slurry solvent containing methanol, chloroform (d = 1.48 g/mL) and isopropanol (η = 1.96 mPa·s) was used to increase the density and viscosity. A silica suspension was prepared by dispersing 0.25 g (50 mm column) or 0.5 g (100 mm column) of the functionalised particles in a solution of 72:8:20 chloroform:methanol:isopropanol (V/V/V). Experimentation using 15, 30 and 60 mL

reservoir sizes found the ideal reservoir size to be 30 mL. This allowed a relatively quick packing time of around 30 minutes and resulted in the best peak shape. To pack the silica slurry, 60 mL methanol was pumped through the column at 600 bar.

3.4 Results and Discussion

3.4.1 Optimisation of Microwave Reaction Conditions

Firstly a study was performed to observe the difference between heating at 110 °C and superheating at 120 °C. Toluene is a non-polar solvent with a boiling point of 110.6 °C, and is virtually transparent to the microwave field. The reaction is driven by the dipole rotation mechanism, with microwave energy applied directly to the reagents possessing a dipole moment, namely the hydroxyl groups on the surface of SOS silica, N-H group present in imidazole and the Si-Cl bond in the C4 reagent.

The SOS silica was produced from the reaction described in method 1, section 3.3.2 and calcined at 550 °C. The surface area was measured by nitrogen adsorption to be 197 m^2/g. The reaction was held at temperature for 20 minutes and performed in triplicate for bonding and endcapping stages. Results for percent carbon and bonding density are shown in table 3.1. Despite using a sealed vessel, the pressure remained below 0.5 bar even at the higher temperature of 120 °C, safely within the limit of the vessel and equipment.

Table 3.1 Effect of superheating on carbon loading and bonding density.

Bonding method	Ligand	% C	α (µmol/m^2)
Toluene Microwave 110 °C	C4	2.57	1.89
		2.45	1.80
		2.32	1.70
Toluene Microwave 120 °C	C4	3.01	2.23
		2.75	2.03
		3.05	2.26

Superheating at 120 °C resulted in percent carbon loading (% C) and bonding densities that were on average 0.49% and 0.38 µmol/m^2 greater than those obtained from the reaction at 110 °C. It was decided that all toluene-based microwave reactions should be performed at the higher temperature. The superheating method achieved bonding densities that are less than those of commercially available C4 columns, typically 2.5-4.0 µmol/m^2 (where manufacturer data is made available). The values therefore seem lower than expected for the SOS material, however it is very likely that the microporous structure is not fully accessible to all of the bonding reagents and that only the accessible surface area is functionalised. By contrast, commercial particles have larger mesopores which allow access to reagents and hence bonding over a greater proportion of the particle surface.

A batch of SOS silica was synthesised via method 1 to assess the effect of reaction time on the carbon loading values when using the microwave reactor. Particles were again calcined at 550 °C and surface area was measured by nitrogen adsorption to be 180 m^2/g. Particle size was not obtained. Five reactions were performed using identical amounts of silica and reagents. The same conditions were applied to each: reaction performed at 120 °C using a closed vessel method, high stir speed and 300 W maximum power. The reaction hold time was varied between 10 to 120 minutes. The same reaction times were also repeated for the endcap stage. Results are shown in table 3.2. It was found that there was no benefit in terms of carbon loading by increasing the reaction time beyond 20 minutes, unless the duration was increased to 120 minutes. As a shorter reaction time is favoured, the optimised method used for further study was decided to be a 20 minute reaction performed at 120 °C.

Table 3.2 Effect of microwave reaction time on carbon loading and bonding density.

Bonding method	Ligand	Reaction time (min)	% C	α (µmol/m^2)
Toluene Microwave 120 °C	C4	10	2.43	1.95
		20	2.57	2.07
		40	2.50	2.01
		60	2.56	2.06
		120	2.76	2.23

3.4.2 Comparison of Microwave and Conventional Heating

There is currently very little in the literature that directly compares the use of microwave irradiation with traditional heating methods. The optimised microwave method was therefore performed alongside a reflux reaction using an oil bath as the heating source to assess any difference in percent carbon content and bonding density.

Heating with the oil bath was performed by refluxing for 16 hours in a 50 mL round-bottom flask. The microwave bonding was performed in a 35 mL closed vessel at 120 °C. Both methods used the same amounts of reagents. Two batches of SOS silica were prepared via method 2, designated 1 and 2. Surface areas were measured by nitrogen adsorption to be 148 and 122 m^2/g respectively, after calcination at 550 °C. The mean particle size was 3.0 µm for both, with a $d^{90}/_{10}$ ratio of 1.24 (batch 1) and 1.36 (batch 2). Reactions using both heating methods were performed in triplicate on each batch of silica. The prefixes MB- and OB- refer to microwave bonding and oil bath bonding. Results are shown in table 3.3.

Percent carbon results for the three samples of each batch were very consistent for the microwave method, with relative standard deviation (RSD) of 3.68% (MB-1) and 1.40% (MB-2) between each trio. The first set of oil bath samples had higher RSD of 3.81% (OB-1), while the second set (OB-2) included a low result which did not allow a representative comparison, giving 12.20%. The percent carbon value typically increases with larger surface area simply because there are more silanol sites where bonding can occur. The bonding density (α) is therefore a better comparison between different batches of silica as it takes into account the effect of surface area. In the case of the microwave method the average values were identical for both batches, with a measurement of 2.11 $\mu mol/m^2$. The RSD between all six results was 2.57%, compared with 3.57% from the oil bath reaction (calculated from five results, 8.38% with low result included).

Table 3.3 Comparison of bonding results obtained from microwave and reflux heating methods.

Silica	Ligand	Bonding method	% C	α (µmol/m^2)
MB-1	C4	Microwave 120 °C 20 min	2.26	2.20
			2.17	2.10
			2.10	2.03
OB-1	C4	Oil bath Reflux 16 hours	2.45	2.39
			2.28	2.22
			2.42	2.36
MB-2	C4	Microwave 120 °C 20 min	1.78	2.08
			1.80	2.11
			1.83	2.14
OB-2	C4	Oil bath Reflux 16 hours	1.65	1.93
			2.07	2.44
			2.04	2.40

The samples from the microwave method show slightly lower carbon loading than those obtained from the oil bath, typically around 0.2%. However the results show improved consistency which can be explained by the high degree of reaction control and uniform heating provided by the microwave reactor, with energy being applied directly to the reactants rather than the vessel. As was discussed earlier, the carbon loading can potentially be increased by extending the heating time in the microwave reactor. A 120 minute reaction still represents a massive reduction in reaction time over a 16 hour reflux.

A sample from each of MB-1 (% C = 2.17%, α = 2.10 µmol/m^2) and OB-1 (% C = 2.42%, α = 2.36 µmol/m^2) was selected for packing into a HPLC column to assess and compare the chromatographic performance of microwave and conventionally bonded media in the separation of large molecules. The column dimensions were 100 × 2.1 mm and particles were packed using the method described in section 3.3.6. A test mixture of four

proteins was prepared, containing carbonic anhydrase (65 µg/mL), lysozyme (65 µg/mL), myoglobin (65 µg/mL) and ovalbumin (75 µg/mL), made up in Milli-Q water.

The protein test mixture was separated using a linear gradient method. Mobile phase A: water + 0.1% TFA; B: acetonitrile + 0.1% TFA; gradient: 30-65% B in 6 minutes (5.83 %/min); flow rate 400 µL/min; temperature: 50 °C; detection: 220 nm; injection volume: 20 µL. Maximum back pressure was 176 bar (MB-1) and 180 bar (OB-1). The overlaid chromatogram for both columns is shown in figure 3.7. The retention times for both columns were virtually identical and both produced narrow, well resolved peaks separated within 5 minutes.

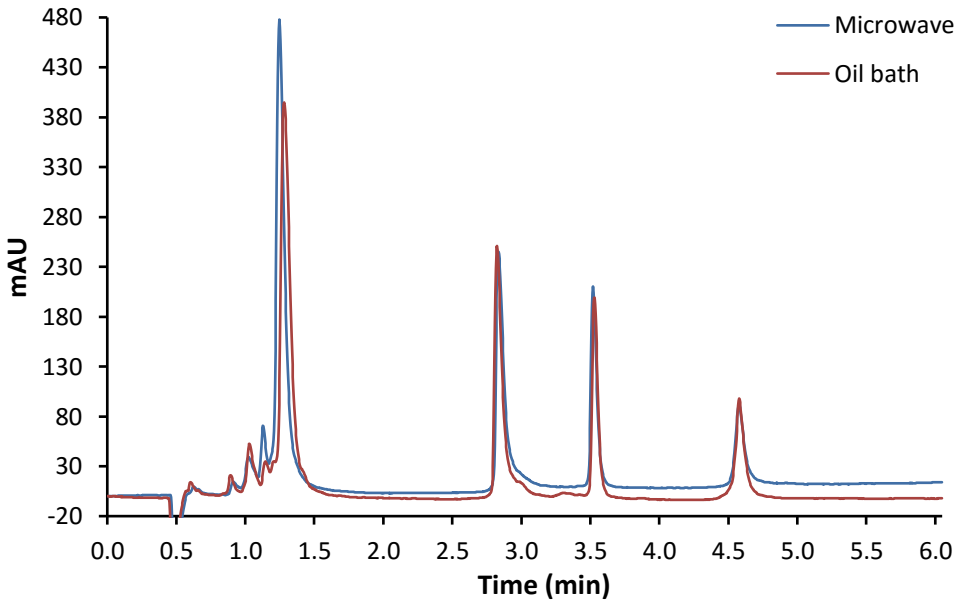

Figure 3.7 Overlaid chromatogram of protein test mixture separation on microwave and oil bath bonded columns. Elution order: lysozyme, myoglobin, carbonic anhydrase, ovalbumin.

Values for peak capacity (P_C) were determined from gradient time (t_g), unretained peak time (t_0) and peak width at 50% height ($W_{50\%}$) using the following equation.[49]

$$P_C = 1 + \frac{(t_g - t_0)}{1.7 \times W_{50\%}}$$

Inclusion of the unretained peak time in the equation accounts for the fact that no component in the test mixture can elute before a time equivalent to the column void volume (dead volume). For fast analysis, this time can represent a significant proportion of the analysis time, and omission leads to an over estimate of the peak capacity.

The peak width at 50% height was preferred to avoid any imprecision associated with width measurement at the baseline for proteins which often contain closely related variants. Measurement at 50% height ensures the value is not affected by any impurities that are partially resolved from the main component. Peak width at the baseline is achieved by extrapolation, which assumes that peaks are Gaussian in shape.[50] Peak width at 50% height is defined as 2.35σ, where σ is the standard deviation, and the baseline value at 13.4% height as 4.0σ. The peak width at 50% height is therefore multiplied by a factor of 1.7 (4 ÷ 2.35) to give an estimate of baseline width.

The value for peak capacity is unitless as gradient time and peak width are both measured in minutes. The calculated value provides an indication of the number of analytes that can be resolved by the column within the gradient run time. A larger number is preferable as this indicates narrower peak widths and hence better performance, theoretically allowing more compounds to be analysed during the same run, dependant on their relative retention times. Peak capacity results were very similar for both columns, with an almost identical average value of 58 (MB-1) and 57 (OB-1), suggesting comparable performance between the two.

A commercial core-shell column, Thermo Scientific Accucore 150-C4 (2.6 µm, 100 × 2.1 mm), was also used to separate the protein test mixture. This material has a pore size of 15 nm and is optimised for the separation of biomolecules, particularly proteins and larger peptides. The HPLC gradient was adjusted to match the elution time of the final peak to that of the SOS columns. The Accucore column provided longer retention hence the

gradient steepness was increased to reduce the run time. The modified gradient used was 30-68.5% B in 6 minutes which allowed a direct comparison of peak capacity with the SOS columns. All other conditions were identical.

Under these gradient conditions both SOS columns provided slightly better performance than the Accucore column, which resulted in an average peak capacity of 54. The lower value can be partly explained by the longer unretained peak time of the Accucore material (t_0 = 0.67 min) due to the thick, highly porous shell. By comparison the SOS material (t_0 = 0.49 min) has a shallow shell depth with much less accessible porosity and therefore fewer possible paths through the column, leading to a shortened unretained peak time. Additionally, higher back pressure of 205 bar was seen for the Accucore column compared to a maximum of 180 bar for the SOS column.

It is interesting to note when comparing the two materials the Accucore column resulted in a narrower peak width for the first analyte, lysozyme (14 kDa), whereas the SOS columns produced narrower peak widths for the two largest proteins, carbonic anhydrase (30 kDa) and ovalbumin (45 kDa), indicating that the shallow shell depth and interstitial macroporosity provides improved mass transfer as the analyte size is increased. Peak widths for myoglobin (17 kDa) were virtually identical for all three columns.

3.4.3 Batch to Batch Reproducibility

Small differences in the physical properties of batches of silica media are unavoidable due to the numerous stages involved in the method of making an amorphous product. Particle diameter, size distribution and surface area are controlled as best as possible to produce a consistent product, however some variation will always occur. Likewise, bonding reactions will always result in some variation in terms of the final product carbon loading, and the column packing process also has a large effect on column performance. In HPLC it is vital that the results are repeatable, therefore it is essential that the entire process is controlled as best as possible and that any differences between individual batches of silica do not cause excessive variation in chromatographic performance.

To assess the batch to batch reproducibility of the microwave bonding method, three batches of SOS silica were prepared via method 1, designated MB-3, MB-4 and MB-5,

followed calcination at 550 °C. Physical properties (surface area, mean particle size, $d^{90}/_{10}$) were as follows. MB-3: 226 m^2/g, 3.9 µm, 2.31; MB-4: 240 m^2/g, 2.9 µm, 1.82; MB-5: 200 m^2/g, 4.0 µm, 2.06. Each batch of SOS was split into three sub-reactions, all of which were functionalised with a C4 group using microwave irradiation. As before, the reaction was performed in toluene at 120 °C for 20 minutes and the reaction was repeated for the endcapping stage. Results are summarised in table 3.4.

For the three reactions within each batch, values for carbon content and bonding density are closely matched, with the exception of one slightly lower result for MB-5, reaction 2. RSD of the percent carbon values from each batch were as follows: MB-3, 1.45%; MB-4, 2.74%; MB-5, 3.54%. This indicates that the method is highly reproducible for samples within each batch.

Comparison of bonding density between all nine reactions also reveals highly consistent results with RSD of 4.56%, indicating that the batch to batch bonding results would be acceptable to pass a typical 5% manufacturer specification. Once again this highlights the reproducible nature of the microwave bonding method and potential to replace conventional heating in a manufacturing capacity.

Table 3.4 Bonding results from batch to batch reproducibility study.

Batch	Ligand	Reaction	% C	α (µmol/m^2)
MB-3	C4	1	3.19	2.06
		2	3.10	2.00
		3	3.16	2.04
MB-4	C4	1	3.53	2.16
		2	3.60	2.21
		3	3.41	2.09
MB-5	C4	1	2.52	2.02
		2	2.36	1.89
		3	2.50	2.01

Each of the nine samples from the reproducibility study were packed into a 50 × 2.1 mm HPLC column using the method described in section 3.3.6. The shorter column length was used due to the limited amount of available bonded material from each batch.

The chromatographic performance of each column was compared in the separation of the same protein test mixture described in section 3.4.2, containing carbonic anhydrase, lysozyme, myoglobin and ovalbumin, made up in Milli-Q water. The protein test mixture was again separated using a linear gradient method. Mobile phase A: water + 0.1% TFA; B: acetonitrile + 0.1% TFA; gradient: 30-65% B in 6 minutes (5.83 %/min); flow rate 400 µL/min; temperature: 40 °C; detection: 220 nm; injection volume: 10 µL. Overlaid chromatograms of the three columns from each batch are shown in figures 3.8 (MB-3), 3.9 (MB-4) and 3.10 (MB-5).

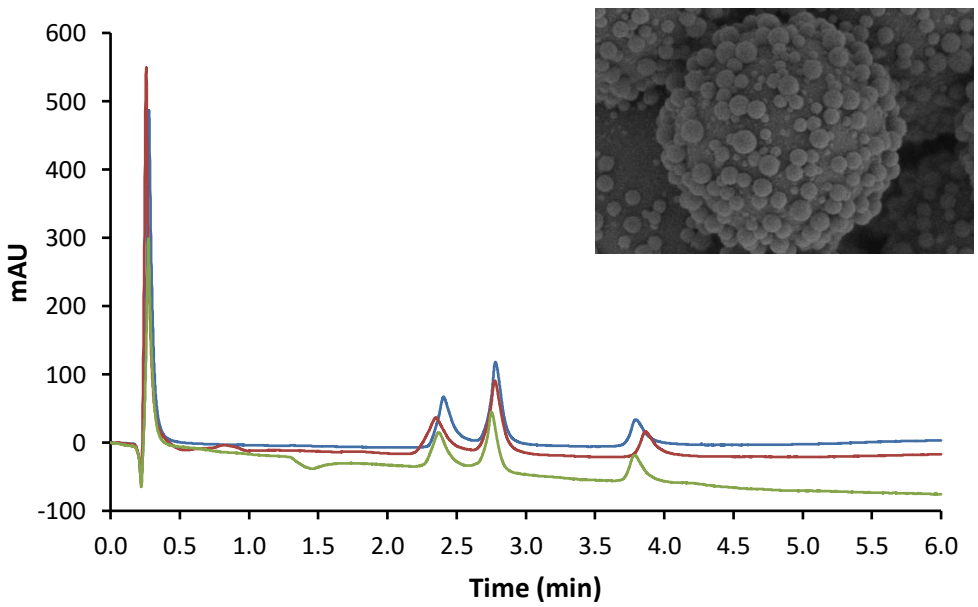

Figure 3.8 Overlaid chromatogram of protein test mixture separation on three columns from batch MB-3. Inset: SEM image of base silica.

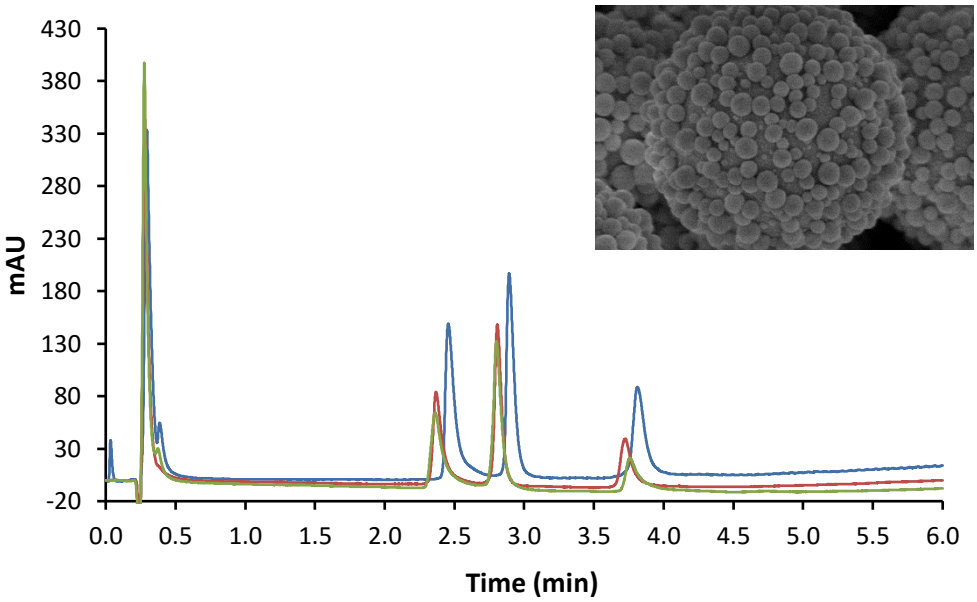

Figure 3.9 Overlaid chromatogram of protein test mixture separation on three columns from batch MB-4. Inset: SEM image of base silica.

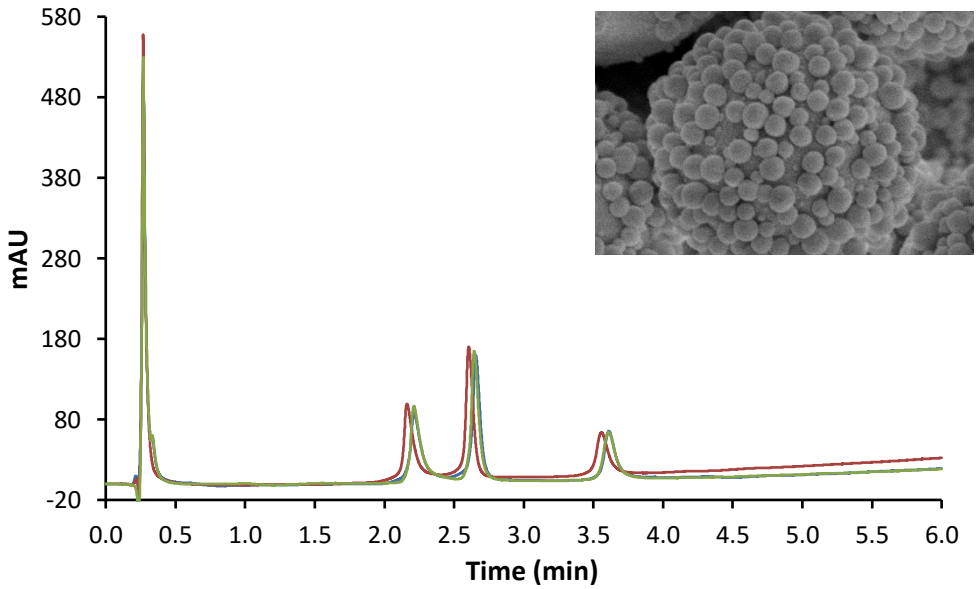

Figure 3.10 Overlaid chromatogram of protein test mixture separation on three columns from batch MB-5. One trace (blue) is partially hidden due to similar retention. Inset: SEM image of base silica.

The protein text mixture was fully resolved in less than 4 minutes for all nine columns, all of which showed identical selectivity. Elution order was lysozyme, myoglobin, carbonic anhydrase and ovalbumin. A comparison of retention times for all columns is shown in table 3.5. Between the three columns within each batch, very low values for RSD were obtained when comparing retention times for all analytes, indicating comparable performance. Comparison of retention times between batches displays some differences, particularly for MB-5 where the analysis resulted in shorter retention for peaks 2, 3 and 4. However assuming a ±5% specification set around the average, all columns would pass quality check. The overlaid chromatogram showing the test mixture separation on the first column of each batch is shown in figure 3.11.

Table 3.5 Comparison of retention times for analytes on each column. Peak identities: 1) lysozyme, 2) myoglobin, 3) carbonic anhydrase, 4) ovalbumin.

Batch	Peak	Retention time (min)			RSD (%)
		Column 1	Column 2	Column 3	
MB-3	1	0.28	0.27	0.27	2.11
	2	2.41	2.35	2.37	1.29
	3	2.78	2.77	2.75	0.55
	4	3.80	3.86	3.79	0.99
MB-4	1	0.29	0.28	0.28	2.04
	2	2.46	2.37	2.36	2.30
	3	2.89	2.81	2.80	1.74
	4	3.81	3.73	3.76	1.07
MB-5	1	0.27	0.27	0.27	0.00
	2	2.21	2.16	2.21	1.32
	3	2.66	2.60	2.64	1.16
	4	3.61	3.56	3.61	0.80

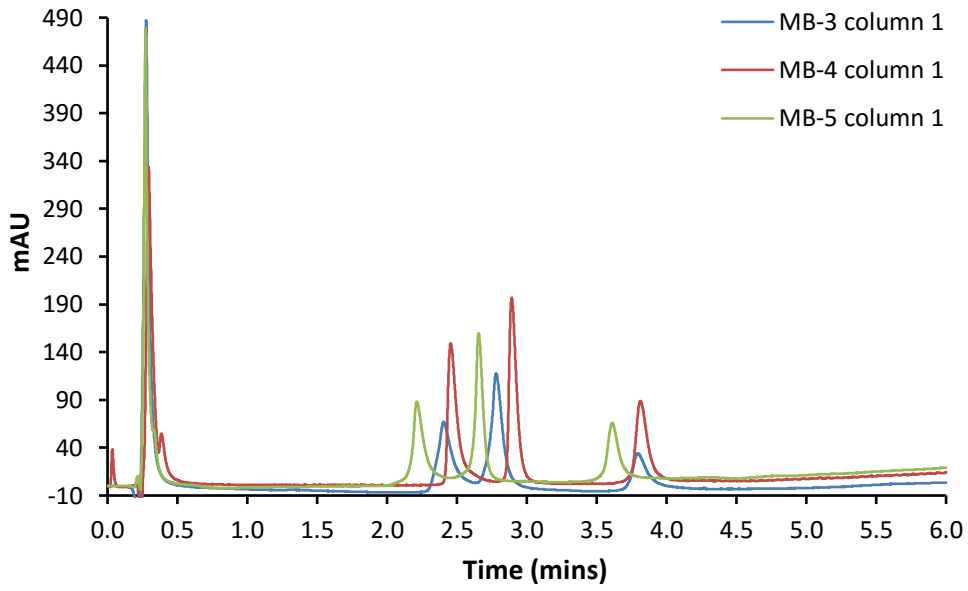

Figure 3.11 Overlaid chromatogram of protein test mixture separation on the first column from each batch.

The use of a 50 mm column length led to a shorter gradient time (t_g-t_0) compared to the 100 mm columns in section 3.4.2. Average peak capacity values were calculated as before, though the first peak (lysozyme) was omitted from this calculation due to elution close to the unretained peak (t_0 = 0.25 min). This did not allow accurate measurement of the peak width. This led to the conclusion that 100 mm columns should be used for future study. The average peak capacity values calculated from the final three peaks were 32 (MB-3), 40 (MB-4) and 39 (MB-5).

Since the bonding density values were very similar for all nine columns, an explanation for the lower peak capacity for batch MB-3 is likely to be caused by the silica media rather than an issue with the bonding process. The sizing data shows this batch to have the broadest size distribution. SEM images taken of the three batches, shown inset in figures 3.8, 3.9 and 3.10, also show there to be fewer surface nanospheres for MB-3 compared to the other two batches. The conclusion is that these physical properties will have an effect on the quality of column packing and hence the column performance. This agrees with the theory discussed earlier where shear force due to the rough surface holds particles in place when packed into the column, preventing bed expansion and that a narrower particle size distribution aids in providing ideal close-packing of spheres.

3.4.4 Alternative Bonding Solvents

Although toluene has been used throughout the studies in this chapter, alternative solvents were also assessed for microwave assisted bonding of SOS particles. The dielectric constant of the solvent must be taken into account when using the microwave reactor, as energy is supplied via interaction of the electromagnetic field with reagents which can potentially lead to high operating pressures within the vessel. Some pressure build up in the sealed vessel is inevitable and normal, particularly when working with polar solvents, hence the glass reaction vessels are designed to safely withstand up to 30 bar and are sealed with a pressure-venting cap. A list of recommended maximum reaction temperatures for solvents is also provided by the microwave manufacturer.[51]

Kinkel and Unger studied the role of solvent in the bonding of fully porous silica with n-octadecyl (C18) groups, using a conventional reflux method.[9] Tetrahydrofuran, DMF, benzene, diethyl ether, DCM and acetonitrile were included. It was found that the best results were obtained when using DCM or DMF, both of which resulted in high bonding densities of >3 μmol/m^2 after a 28 hour reflux. It should be noted that toluene was not included in this study due to the use of benzene, however it is now commonly used in many bonding methods as a replacement for benzene as it is much less hazardous to health.

Four solvents were chosen for comparison in the C4 bonding of SOS particles: toluene, DCM, limonene (dipentene) and DMF. The first three are non-polar and virtually transparent to the microwave field, with energy supplied directly to the SOS silica and other reagents. DMF is an aprotic polar solvent and therefore the entire reaction volume will experience direct heating. The use of protic solvents was avoided as hydroxyl or amine groups can compete with the surface silanol groups for the ligand being attached, leading to lower than expected surface functionality and undesired by-products. Limonene was included to demonstrate a potentially greener and safer alternative to toluene.

A batch of SOS silica was prepared via method 2. Particles were calcined at 600 °C which resulted in a reduction of surface area compared to samples calcined at 550 °C due to closure of the pore system. The surface area was measured by nitrogen adsorption to be 68 m^2/g. Due to the number of required experiments the microwave bonding method described in section 3.3.4 was run on a reduced scale. The batch was split between twelve 10 mL reaction vessels, 0.2 g silica into each. 1.5 mL of comparison solvent, 20 mg

imidazole and 80 mg C4 reagent were added to each vessel. Each solvent was run in triplicate. Identical microwave reaction parameters to previous studies in this chapter were followed: 20 minute reaction at 120 °C (80 °C for DCM) using a closed vessel method. The results for carbon loading and surface coverage are shown in table 3.6.

The best results were observed when using limonene and toluene, both of which resulted in bonding densities of ≥3.35 µmol/m^2. This value is comparable to commercially available C4 materials. This indicates that although the total surface area has been reduced compared to particles calcined at 550 °C, the bonding density is increased as a larger proportion of the surface area is accessible to bonding reagents. The use of DCM resulted in significantly lower values, however the set of reactions were run at a reduced temperature of 80 °C due to the low boiling point. Reactions with DCM may therefore require the heating time to be extended to achieve equivalent bonding density.

Table 3.6 Comparison of bonding results when using various reaction solvents.

Solvent	Ligand	Temperature	% C	α (µmol/m^2)
Toluene	C4	120 °C	1.60	3.35
			1.63	3.42
			1.60	3.35
Dichloromethane	C4	80 °C	1.15	2.39
			1.15	2.39
			1.10	2.28
Limonene	C4	120 °C	1.63	3.42
			1.67	3.50
			1.67	3.50
Dimethylformamide	C4	120 °C	1.48	3.09
			1.49	3.11
			1.44	3.01

The use of DMF provided values slightly lower than those from the toluene and limonene reactions. The polar nature of the solvent however resulted in extremely rapid heating, typically reaching required temperature in around 45 seconds, equating to a heating rate of 125 °C/min. The required amount of microwave power to maintain the reaction temperature was also reduced. After initial heating, approximately 6 W was required compared to 30-40 W for the three non-polar solvents. Despite this, the observed pressure within the vessel did not exceed 5 bar, safely within the limit of the equipment.

The lower bonding densities observed for DMF may be explained by not achieving superheating conditions due to the higher boiling point of 153 °C. As discussed earlier in the chapter, superheating in toluene at 120 °C versus 110 °C results in higher carbon loading, therefore the same approach was applied to DMF. Although superheating was not possible as the boiling point of DMF is greater than that of the C4 reagent (138 °C), the reaction temperature could still be increased to 135 °C. The elevated temperature resulted in carbon loading comparable to that of the toluene reactions, with % C of 1.61% and α = 3.39, indicating that DMF is also a viable solvent for the functionalisation of SOS particles using microwave heating.

3.5 Conclusion

The suitability of microwave irradiation as the heating source for the silanisation of SOS silica has been assessed. A microwave bonding method has been developed which facilitates rapid, reproducible C4-functionalisation of SOS silica media, providing a considerable reduction in reaction time compared to traditional reflux.

Heating by microwave irradiation was compared to traditional reflux to assess any difference in bonding density. It was firstly found that superheating in toluene at 120 °C using the microwave reactor led to carbon loading and bonding density values greater to those at 110 °C, therefore all further microwave-based experiments were performed at this temperature. The 20 minute microwave reaction in toluene at 120 °C consistently led to bonding densities between 2.0-2.1 µmol/m^2. The results were slightly lower than obtained from a 16 hour reflux which typically produced bonding densities between 2.2-2.4 µmol/m^2, however the latter displayed higher variation between these values.

Although there were some differences in the carbon loading and bonding density, the SOS-C4 materials produced from both microwave and reflux silanisation methods have shown almost identical performance in the HPLC separation of a protein test mixture. High values were obtained for peak capacity, which exceeded that of a commercial C4 column optimised for protein separation.

In an assessment of batch to batch reproducibility, three batches of SOS-C4 particles were prepared. In total, nine columns were tested using the same protein test mixture. A small amount of variation was observed in the retention, however if a typical manufacturer specification of ±5% was set around the average value for retention time all nine columns would be within this limit. One of the batches resulted in lower values for peak capacity, however this is attributed to the morphology of the SOS particles rather than the bonding process. The SOS synthesis has since been optimised to produce much more consistent particles. It was also noted that the shorter column dimension of 50 × 2.1 mm resulted in reduced retention and did not allow accurate measurement of the first peak width. This has been addressed by using 100 × 2.1 mm columns in future experiments.

A major advantage of the microwave reactor is the vast reduction in experiment time. A 20 minute reaction represents a 98% reduction in heating time compared to a 16 hour reflux. This does not include the time taken to heat the vessel to the required temperature, nor the time to cool. The microwave reactor is capable of extremely rapid heating, around 45 °C/min for toluene based reactions and as high as 125 °C/min for DMF, which again provides a further time advantage. Further investigation shows there to be no benefit from increasing the microwave heating time beyond 20 minutes until at least 120 minutes. Samples tested from the increased microwave reaction time show bonding density values similar to that of reflux heating. This lengthened microwave reaction still represents an 88% reduction in heating time.

Due to the shortened reaction time the microwave reactor also provides a large reduction in power consumption. Although the maximum output power of the microwave is 300 W, consumption close to this is only required briefly during the initial heating stage. As little as 6 W (DMF) is required to maintain constant temperature. By contrast, a hot plate rated at 600 W running constantly for 16 hours uses a great deal more electricity. While this is perhaps not an important factor in this research project, it may be of more interest to manufacturers who are looking to speed up their bonding processes and reduce costs.

After calcination at 550 °C, lower bonding densities for SOS have been observed for both heating methods compared to commercially available core-shell materials. Even despite the homogenous heating effect of the microwave reactor which provides energy to the entire silica particle, including the internal pores, the microporous properties mean that some or all of the bonding reagents cannot penetrate into the pore system and silanisation only occurs upon the accessible surface area. This is not necessarily a disadvantage of the SOS material, as analytes are also unable to access the pore system and the bonding density of the accessible surface area may well be comparable to that of commercial materials, although this cannot be directly measured.

In the investigation into alternative bonding solvents, SOS particles were calcined at 600 °C. This had the effect of reducing the total surface area by closing up some of the pores. It is presumed that the accessible surface area was not significantly reduced as higher bonding densities were measured which were more comparable to that of commercial C4 materials. For example the toluene and limonene-based reactions gave an average of 3.37 and 3.48 µmol/m^2 respectively, compared to 3.5 µmol/m^2 for the Accucore 150-C4 material.

In the study conducted by Kinkel *et al.*,[9] DCM and DMF were found to provide the best results as the solvent for the C18 silanisation of silica. In the microwave study, the use of limonene or toluene was found to provide the greatest bonding density. It should be noted however that DCM was heated at a lower temperature and that a longer reaction time is likely required to increase the value. A reaction time of 28 hours was used in the tests conducted by Kinkel *et al*. When using DMF, increasing the reaction temperature to 135 °C provided bonding density values comparable to toluene. The study has shown that, if required, alternative solvents can be utilised in the functionalisation of the SOS material.

The results obtained in this chapter indicate that microwave bonding is capable of producing bonded phases that are comparable with those obtained from conventional reflux. The microwave method has the additional benefits of improved consistency of the carbon loading and bonding density values, significantly reduced reaction time and associated reduction in energy consumption. A number of column manufacturers have expressed interest into the use of microwave irradiation as the driving force to produce their bonded phases, it is expected that commercial columns produced using this technology will be introduced in the near future.

3.6 References

1. W. T. Cooper, *Normal Phase Chromatography*, John Wiley & Sons, Ltd, 2006.
2. G. A. Howard and A. J. P. Martin, *Biochemical Journal*, 1950, **46**, 532-538.
3. W. J. Lough, *Reversed Phase Liquid Chromatography*, John Wiley & Sons, Ltd, 2006.
4. J. G. Dorsey and W. T. Cooper, *Analytical Chemistry*, 1994, **66**, 857A-867A.
5. W. Stöber, G. Bauer and K. Thomas, *Justus Liebigs Annalen der Chemie*, 1957, **604**, 104-110.
6. C. C. Ballard, E. C. Broge, R. K. Iler, D. S. S. John and J. R. McWhorter, *The Journal of Physical Chemistry*, 1961, **65**, 20-25.
7. I. Halász and I. Sebestian, *Angewandte Chemie International Edition in English*, 1969, **8**, 453-454.
8. J. J. Kirkland and J. J. DeStefano, *Journal of Chromatographic Science*, 1970, **8**, 309-314.
9. J. N. Kinkel and K. K. Unger, *Journal of Chromatography A*, 1984, **316**, 193-200.
10. R. J. P. Corriu and C. Guerin, *Journal of Organometallic Chemistry*, 1980, **198**, 231-320.
11. J. J. Pesek and S. A. Swedberg, *Journal of Chromatography A*, 1986, **361**, 83-92.
12. D. C. Locke, J. T. Schmermund and B. Banner, *Analytical Chemistry*, 1972, **44**, 90-92.
13. O.-E. Brust, I. Sebestian and I. Halász, *Journal of Chromatography A*, 1973, **83**, 15-24.
14. J. E. Sandoval and J. J. Pesek, *Analytical Chemistry*, 1991, **63**, 2634-2641.
15. J. Köhler, D. B. Chase, R. D. Farlee, A. J. Vega and J. J. Kirkland, *Journal of Chromatography A*, 1986, **352**, 275-305.
16. J. Köhler and J. J. Kirkland, *Journal of Chromatography A*, 1987, **385**, 125-150.
17. S. A. Wise and W. E. May, *Analytical Chemistry*, 1983, **55**, 1479-1485.
18. S. C. Antakli and J. Serpinet, *Chromatographia*, 1987, **23**, 767-769.
19. L. T. Zhuravlev, *Langmuir*, 1987, **3**, 316-318.
20. G. E. Berendsen and L. d. Galan, *Journal of Liquid Chromatography*, 1978, **1**, 561-586.
21. H. Hemetsberger, P. Behrensmeyer, J. Henning and H. Ricken, *Chromatographia*, 1979, **12**, 71-76.
22. K. K. Unger, N. Becker and P. Roumeliotis, *Journal of Chromatography A*, 1976, **125**, 115-127.

23. D. Corradini, E. Eksteen, R. Eksteen, P. Schoenmakers and N. Miller, *Handbook of HPLC*, CRC Press, 2011.
24. R. Gedye, F. Smith, K. Westaway, H. Ali, L. Baldisera, L. Laberge and J. Rousell, *Tetrahedron Letters*, 1986, **27**, 279-282.
25. R. J. Giguere, T. L. Bray, S. M. Duncan and G. Majetich, *Tetrahedron Letters*, 1986, **27**, 4945-4948.
26. B. L. Hayes, *Microwave Synthesis: Chemistry at the Speed of Light*, CEM Publishing, Matthews, NC, 2002.
27. S. Caddick and R. Fitzmaurice, *Tetrahedron*, 2009, **65**, 3325-3355.
28. C. O. Kappe and D. Dallinger, *Molecular Diversity*, 2009, **13**, 71-193.
29. R. Hoogenboom and U. S. Schubert, *Macromolecular Rapid Communications*, 2007, **28**, 368-386.
30. S. Barlow and S. R. Marder, *Advanced Functional Materials*, 2003, **13**, 517-518.
31. A. Procopio, G. Das, M. Nardi, M. Oliverio and L. Pasqua, *ChemSusChem*, 2008, **1**, 916-919.
32. A. Procopio, G. De Luca, M. Nardi, M. Oliverio and R. Paonessa, *Green Chemistry*, 2009, **11**, 770-773.
33. N. García, E. Benito, J. Guzmán, R. de Francisco and P. Tiemblo, *Langmuir*, 2010, **26**, 5499-5506.
34. N. Fukaya, H. Yamashita, H. Haga, T. Tsuchimoto, S.-y. Onozawa, T. Sakakura and H. Yasuda, *Journal of Organometallic Chemistry*, 2011, **696**, 825-828.
35. M. R. Rosana, Y. Tao, A. E. Stiegman and G. B. Dudley, *Chemical Science*, 2012, **3**, 1240-1244.
36. C. O. Kappe, B. Pieber and D. Dallinger, *Angewandte Chemie International Edition*, 2013, **52**, 1088-1094.
37. N. Kuhnert, *Angewandte Chemie International Edition*, 2002, **41**, 1863-1866.
38. M. H. C. L. Dressen, B. H. P. v. d. Kruijs, J. Meuldijk, J. A. J. M. Vekemans and L. A. Hulshof, *Organic Process Research & Development*, 2007, **11**, 865-869.
39. M. A. Herrero, J. M. Kremsner and C. O. Kappe, *The Journal of Organic Chemistry*, 2008, **73**, 36-47.
40. G. B. Dudley, A. E. Stiegman and M. R. Rosana, *Angewandte Chemie International Edition*, 2013, **52**, 7918-7923.
41. C. O. Kappe, *Angewandte Chemie International Edition*, 2013, **52**, 7924-7928.

42. M. Mignot, A. Tchapla, O. Mercier, N. Couvrat, S. Tisse, P. Cardinael and V. Peulon-Agasse, *Chromatographia*, 2014, **77**, 1577-1588.
43. K. Kimata, K. Iwaguchi, S. Onishi, K. Jinno, R. Eksteen, K. Hosoya, M. Araki and N. Tanaka, *Journal of Chromatographic Science*, 1989, **27**, 721-728.
44. G. E. Berendsen, K. A. Pikaart and L. d. Galan, *Journal of Liquid Chromatography*, 1980, **3**, 1437-1464.
45. S. Pryde and M. T. Gilbert, *Applications of High Performance Liquid Chromatography*, Springer Netherlands, 1979.
46. H. P. Keller, F. Erni, H. R. Linder and R. W. Frei, *Analytical Chemistry*, 1977, **49**, 1958-1963.
47. M. Broquaire, *Journal of Chromatography A*, 1979, **170**, 43-52.
48. J. J. Kirkland and J. J. DeStefano, *Journal of Chromatography A*, 2006, **1126**, 50-57.
49. S. A. C. Wren, *Journal of Pharmaceutical and Biomedical Analysis*, 2005, **38**, 337-343.
50. J. M. Miller, *Chromatography: Concepts and Contrasts*, Wiley, 1988.
51. CEM Corporation, www.CEM.com.

4 Spheres on Sphere Particles for Chromatography

4.1 Introduction

The optimised synthesis and functionalisation of SOS particles by microwave irradiation, followed by preliminary HPLC analysis has been discussed in the previous two chapters. The experimental work in this chapter will focus on the chromatographic performance and applications of functionalised SOS particles that have been packed into HPLC columns. If these columns are found to provide comparable performance to commercial materials, the SOS synthesis and bonding methods would represent a vast reduction in the time, labour and energy required to produce near monodisperse core-shell particles for chromatographic use. The performance of fractal particles is also discussed and compared to the SOS material.

HPLC is a widely used technique and an essential analysis tool in laboratories, owing to its universal applicability and high assay precision.[1] The challenges in HPLC are to obtain fast, efficient separation, preferably with low back pressure. The literature review will provide a background on early chromatography, the evolution of liquid chromatography (LC) leading to modern day HPLC, efficiency in LC and the concept of fractal chromatography.

4.2 Literature Review

4.2.1 Early Chromatography

Liquid chromatography was first developed in the late 1890s by the Russian botanist Mikhail Tswett as a technique to separate and isolate plant pigments.[2] Using calcium carbonate as adsorbent and petroleum ether/ethanol mixtures as eluent, separation of chlorophyll and carotenoids was achieved. This kind of separation is now regarded as liquid-adsorption chromatography, where the affinities of compounds for the stationary phase determine their retention. It was predicted by Tswett that chlorophyll was held to the plant tissue by adsorption, and that stronger solvents were necessary to overcome this adsorption. This was demonstrated by the extraction of carotene using non-polar solvents, followed by the use of polar solvents to extract chlorophyll.

Unfortunately, Tswett's work was not generally accepted, partly due to the publication only being available in Russian meaning it was not readily accessible to the majority of chemists, but mainly due to subsequent research by Willstätter and Stoll who were unable to reproduce his results.[3] Warnings by Tswett not to use aggressive adsorbents went unheeded, leading to decomposition of the chlorophylls and ultimately the experiments failed. As a consequence, the published results rejecting Tswett's original work impeded the development of chromatography by 20 years.

In the late 1930s Martin and Synge developed a liquid-liquid separation technique known as partition chromatography.[4] Hydrophilic silica gel was packed into a column as a support for the stationary phase, in this case water. An organic solvent acted as the mobile phase, flowing through the column. It was found that polar analytes diffuse into the stationary phase and are retained. The separating power was demonstrated by the separation of acetyl amino acids, where the stronger the interaction between analyte and stationary phase the longer the elution time. It was also observed that increasing the polarity of the mobile phase resulted in a decrease in retention time.

Their publication recommended the replacement of the liquid mobile phase with a suitable gas which should accelerate the transfer between phases and provide more efficient separation.[4] This formed the concept of gas chromatography (GC). In the same paper it was also predicted that the use of small particles and high pressure in LC columns would improve efficiency and separation. This was a key factor in the development of modern HPLC.

One of the most important developments in liquid chromatography was the introduction of reversed phase chromatography (RPC) by Howard and Martin in 1950.[5] This technique requires the mobile phase to be more polar than the stationary phase and was used to solve the problem of separating long-chain fatty acids. Normal phase chromatography (NPC) was the only available option at the time, however analytes were found to favour the less polar mobile phase and could not be separated by this approach. Their solution was to decrease the polarity of the stationary phase. This was achieved by the treatment of kieselguhr (diatomaceous earth) with hydrophobic groups, rendering the surface unwettable for aqueous mobile phases. The rapid development of RPC continued, as it was found to allow a much greater selection of surface chemistries and many more applications than NPC. As such it is now the most routinely used HPLC method.

4.2.2 Evolution of Liquid Chromatography

Despite the suggestions of Martin and Synge who (correctly) suggested that smaller particle size and higher pressure would provide improved LC separation, the development of LC was largely overlooked until the 1960s due to the favoured technique of GC. Following on from the work of Martin and Synge, it was predicted by Giddings,[6] Huber[7] and others that LC could be operated in the high efficiency mode by reducing the packed particle diameter substantially below the typical size of 150 µm at the time, and using pressure to increase the mobile phase velocity.[8] Extensive experimentation into the improvement of column packings was performed throughout the 1960s and 70s[9] and has continued to the present day with the introduction of sub-2 µm and core-shell materials.[10] The evolution of packed particles has been described in table 1.1, chapter 1. Reducing the particle size places increasingly larger demands on the LC equipment due to higher operating pressures, as the pressure drop is inversely proportional to the particle diameter.[11] As such, the development of HPLC instrumentation has had to keep pace to meet these pressure requirements, particularly for sub-2 µm particles, resulting in the modern HPLC and UPLC systems available today, some of which are designed to operate at pressures of up to 1500 bar.

A typical modern HPLC system consists of a pump, mobile phase degasser, autosampler, injection system, column compartment and detector. The pump is capable of extremely high precision over a large range of flow rates which may extend up to 10 mL/min in some cases. The pump may have a single channel (isocratic), or multiple channels (binary, ternary, quaternary) which allows the user to easily change mobile phase composition and also perform gradient separation. The autosampler and injection system is automated and designed to quickly and accurately load samples to be analysed using the LC system. The autosampler compartment may hold as many as 1000 sample vials under controlled temperature conditions, facilitating high throughput analysis.

The column compartment allows control over the operating temperature of the column, which can have a large effect over the retention time and behaviour of samples, particularly for large biomolecules.[12, 13] The latest LC systems allow control of the temperature over a range of 10 °C below ambient to 120 °C with accuracy and stability stated as ±0.5 °C. The column compartment may also allow pre-heating of the mobile phase and various methods of temperature control, for example still air or forced air mode,

depending on the application. Despite this precise control, the use of temperature programming is still an underused variable in HPLC analysis.

Sample detection may be performed by many techniques including refraction,[14] fluorescence,[15] conductivity,[16] electrochemistry[17] and light-scattering.[18] The most common type of detector used in HPLC is the ultra violet (UV) detector, first introduced in the 1960s,[19] which provides high sensitivity for light absorbing compounds. The UV detector operates at a single wavelength over the range of 195-370 nm, and can be adjusted to suit the compounds of interest. Most detectors now provide wider wavelength selection, covering both the UV and visible spectrum (195-700 nm), and are therefore named UV/VIS detectors. The photo diode array (PDA) detector works on the same principle, but is able to scan the entire spectrum during analysis. This is convenient to determine the most suitable wavelength without repeat analysis.[20]

Mass spectrometry may also be used as a detection technique when coupled to the LC system,[21] and has been developed as such since the introduction of electrospray ionisation in the late 1980s.[22] Liquid chromatography-mass spectrometry (LC-MS) is now a routinely used analytical technique, competing with conventional LC detection due to the high sensitivity, specificity and the ability to analyse complex mixtures.[23]

4.2.3 Efficiency in Liquid Chromatography

In their 1941 paper, Martin and Synge adopted the theory of theoretical plates to describe the efficiency of a chromatographic column.[4] This was taken from comparison to a distillation column which divides the total length into a number of layers, each of which is equivalent to one theoretical plate.[24] The higher the plate number, the more efficient the column. In HPLC the number of theoretical plates (plate count, N) can be determined by the retention time (t_R) and the peak width at the base (W_B) of an analyte peak in the chromatogram using the equation:[25]

$$N = 16 \left(\frac{t_R}{W_B}\right)^2$$

From this equation it can be seen that high efficiency is dependent upon narrow peak widths throughout the chromatogram. As an analyte passes through the packed column it experiences dispersion effects resulting in broadening of the detected peak. Band broadening effects have been discussed by van Deemter[26] who described a relationship between dispersive effects in the column and the height equivalent to a theoretical plate (HETP or H), calculated from column length (L) and plate count (N) using the equation:

$$H = \frac{L}{N}$$

van Deemter described three terms responsible for band broadening: A term, eddy diffusion; B term, longitudinal diffusion; and C term, resistance to mass transfer. The effects of each have been discussed in chapter 1. The three effects are related to H using the van Deemter equation:[26]

$$H = A + \frac{B}{u} + Cu$$

A plot of H versus the mobile phase linear velocity (u) results in a van Deemter curve, shown in figure 4.1. The minimum point on the curve, known as the minimum plate height (H_{min}), is where the highest efficiency is obtained and can also be used to determine the optimum linear velocity at which the highest efficiency can be achieved.

The van Deemter plot has some limitations however, as it does not account for analysis time or operating pressure and therefore does not consider the flow resistance or permeability of the column. Kinetic plots provide an alternative method of plotting the same data, taking into account the permeability of the material from a measure of column length, mobile phase viscosity and maximum pressure drop across the column.[27-29] As was briefly discussed in chapter 1, kinetic plots are very useful when comparing the performance of differently sized and shaped stationary phases, providing information such as efficiency per unit time or efficiency per unit length of column.

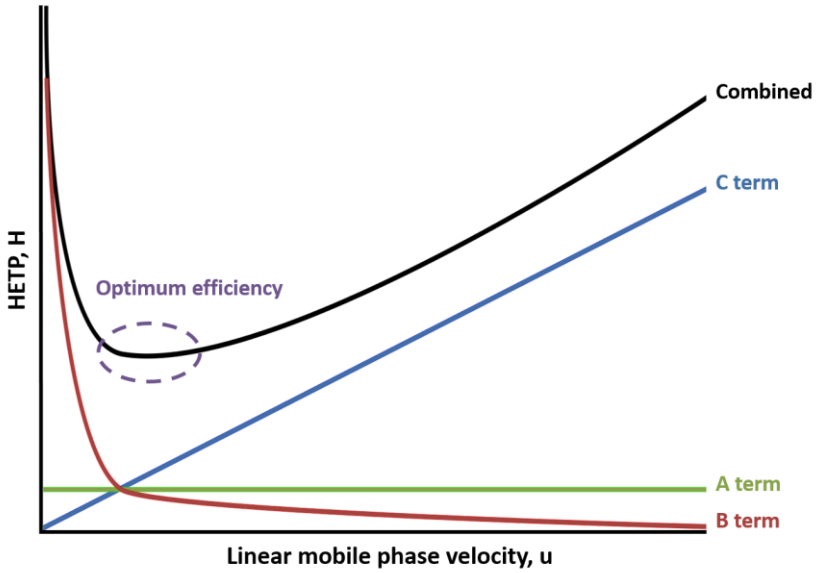

Figure 4.1 van Deemter plot showing the contribution of individual terms to band broadening and the area where optimum efficiency is obtained.

One type of kinetic plot, devised by Bristow and Knox,[12] plots impedance against efficiency to demonstrate the performance of a column. Impedance (E) defines the resistance encountered by a compound as it passes through the column relative to the performance of the column. This gives a true measure of the chromatographic performance as it incorporates efficiency, time and pressure. Impedance can be calculated using the following equation:

$$E = \frac{t\Delta P}{N^2 \eta}$$

Where t is the elution time of the test compound, ΔP is the pressure drop, N is the observed plate count and η is the mobile phase viscosity.[12]

In isocratic study, where the composition of the mobile phase remains constant during the analysis, plate height or plate count are used as measures of chromatographic performance. This is not applicable to gradient elution, where the composition of the mobile phase is changed continuously or stepwise during the analysis. Instead, an

alternative measure of efficiency, peak capacity is used. This is a concept first introduced by Giddings[30] and represents the number of component peaks that can be resolved within the chromatographic run time. Values for peak capacity (P_C) can be calculated using gradient time (t_g) and baseline peak width (W_B) using the following equation:[31]

$$P_C = 1 + \frac{t_g}{W_B}$$

The equation can be modified to include the unretained peak time (t_0), accounting for the fact that no component in a test mixture can elute before this time.[32] For fast gradient analysis, t_0 may represent a significant proportion of the analysis time, and its omission leads to overestimation of the peak capacity. Additionally, peak width at 50% height ($W_{50\%}$) is commonly used in the peak capacity calculation when analysing biomolecules. As discussed in chapter 3, this avoids imprecision associated with measuring the width at the baseline, for example in the analysis of proteins which may contain closely related variants that are partially resolved from the main component. Peak width at 50% height is defined as 2.35σ, where σ is the standard deviation. The peak width at the baseline is defined as 4.0σ. The peak width at 50% height is multiplied by a factor of 1.7 (4 ÷ 2.35) to give an estimate of baseline width. The equation therefore becomes:

$$P_C = 1 + \frac{t_g - t_0}{1.7 \times W_{50\%}}$$

For the analysis of peptides and proteins this equation will be used throughout the chapter to measure peak capacity.

For the HPLC analysis of large molecules such as proteins and other biomolecules, gradient elution is almost exclusively used. The behaviour of such samples is often complex with common effects such as changes in molecular conformation,[33] sample carryover[34] and peak tailing observed, particularly in reversed phase mode.[35] Although the chromatographic theory developed for small molecules (<500 Da) may be applied to large

molecules, the isocratic retention of the latter is extremely sensitive to changes in the mobile phase composition and elution strength.[36, 37] The isocratic separation of proteins and biomolecules is therefore difficult,[35] and there are few reports found in the literature describing the isocratic study of large molecules.[38-40] The HPLC analysis of peptides and proteins in this chapter will therefore be performed using gradient elution.

4.2.4 Fractal Chromatography

In recent years there has been a renewed interest in particle technology for both HPLC and UPLC, due to the introduction of solid core technology.[41] Prior to this there was little novel development in particle morphology since the changes related to reducing the particle diameter from 5 and 3 µm down to sub-2 µm,[10] or the introduction of hybrid phases to aid pH stability.[42, 43] The patents associated with solid core technology have resulted in manufacturers and researchers having a much greater level of interest in the basic production of silica particles, particularly since the current manufacturing processes are known to be fairly time consuming.

This has led to the development of SOS particles; a completely new type of core-shell silica material which is manufactured using a one-step synthesis.[44] Using an optimised synthesis method developed in chapter 2, near-monodisperse particles can be produced without the need for further modification or classification. The morphology of the particle has been designed to deliver the real advantages of the core-shell particles, with a range of synthesis parameters allowing control over the particle morphology.

Investigation of some of the morphologies produced reveals that the structure of the SOS particles closely resembles a true fractal structure. Fractal structures have been associated with chromatographic media for some time, although they have been more associated with the concept of a fractional dimension rather than having a degree of self-similarity. A fractional dimension compares how detail in a pattern changes with the scale at which it is measured. A commonly used example describes how the measured length of a coastline changes depending on the length of the measuring stick used, with a smaller measuring stick able to more accurately follow the coastline. The fractional dimension quantifies how the number of measuring sticks required to measure the coastline changes with the scale applied to the stick.

SOS particles demonstrate not only a fractional dimension, but also a degree of self-similarity, creating the possibility of having a surface topography which is essentially homogeneous to solute molecules. This potentially eliminates one of the issues associated with traditional porous structures in which individual analyte molecules do not experience the same surface topography, resulting in a larger C-term in the van Deemter equation.[26] This is particularly relevant for large molecules where diffusional processes related to the different pore depths can result in poor peak shape, either through equilibration effects or because molecules effectively get stuck between the walls of the pores.

The concept of fractals was first introduced in the 17th century by Leibniz, who was investigating the possibility of repeating self-similarity. The concept of fractals was not followed for another century until it was studied by Weierstrass,[45] Cantor,[46] Klein,[47] Poincaré[48] and Koch[49] who developed the first mathematical understanding in terms of self-similarity and the concept of a fractional dimension. Koch also presented the first illustrative representations of a fractal shape, in particular the Koch curve shown in figure 4.2. Soon after, the first mathematical models were developed which involved the use of mapping of complex number systems by Julia and Fatou.[50, 51] This was extended further by Mandelbrot,[52] with the discovery of the Mandelbrot mapping function and the resulting fractal pattern that this generated.[53]

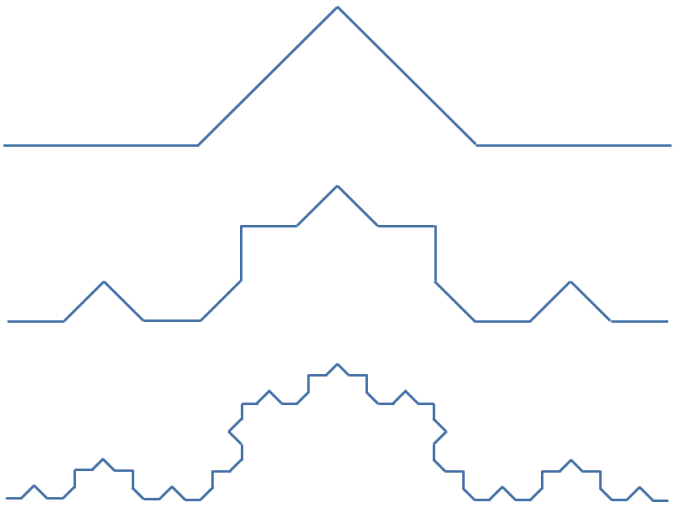

Figure 4.2 An example of a scalable fractal, the Koch curve. The curve is formed by self-replicating the original structure, resulting in a surface that looks the same no matter what the scale.[49]

In terms of applying this to real world scenarios, the concept of fractals has been applied to porous structures, although there is a limitation in transferring the concept of fractals from a mathematical perspective to reality. In a mathematically generated fractal there is a degree of self-similarity upon dilation, thus the same structures are visible at different length scales. With a real structure this degree of self-similarity in general does not exist therefore it is necessary to define two or more length scales that will allow for the concept of self-similarity. However it is possible to use the concept of a fractional dimension and apply this to determine the dimensionality of the porous structure. There are different approaches to measuring the fractional dimension of a porous structure with the most common being a box or tiling method.[54, 55]

This approach has been successfully applied to the analysis of chromatographic grade silica with a dimensional value of 2.68 obtained for the analysis of LiChrospher 300.[56] However, the concept of self-similarity upon dilation is clearly not applicable to structures which are more random than deterministic in nature, and hence the manufacture of SOS particles allows for better control of the fractional dimension as well as allowing for self-similarity. This has interesting consequences as there is an implication that the structure is self-similar, thus there is no unique point on the surface that will display significantly different mass transfer kinetics. This cannot be said for traditional fully porous media, due to the issue of non-self-similarity associated with the process by which the silica is generated. In this scenario the dispersion due to a lack of radial concentration homogeneity will be reduced, which potentially has a greater significance for larger molecules due to the lower diffusion coefficients.

The development of SOS technology has led to the possibility of generating particles with a fractal structure, with the single-layer shell morphology providing a degree of self-similarity. A truly fractal structure with both a fractional dimension and self-similarity would offer increased surface capacity without the disadvantage of increased mass transfer equilibration effects. SOS particles appear to be capable of providing this.

4.3 Experimental

The experimental work in this chapter describes the synthesis of SOS particles, surface functionalisation and subsequent packing into columns for use in HPLC. SOS particles are produced from the optimised synthesis reaction developed in chapter 2 and functionalised using the microwave irradiation method developed in chapter 3.

4.3.1 Chemicals

Ammonium hydroxide (28-30%, NH_3 basis), angiotensin II, bovine serum albumin (BSA), butylparaben (>99 %), carbonic anhydrase, chloro(dimethyl)octylsilane (C8 reagent, 97%), CTAB (≥98%), HPLC peptide standard mixture, imidazole (≥99%), insulin, leucine enkephalin (leu-enk), lysozyme, methionine enkephalin (met-enk), MPTMS (95%) myoglobin, nitric acid (ACS reagent, 70%), ovalbumin, potassium dihydrogen phosphate (≥99%), PVP (M_W = 10k), ribonuclease A, thyroglobulin, TFA (99%), TMSI (≥98%), transferrin, uracil (≥99%) and valine-tyrosine-valine (VYV) were purchased from Sigma-Aldrich. Butyl(chloro)dimethyl silane (C4 reagent, >97%) and glycine-tyrosine (GY) were purchased from Tokyo Chemical Industry. HPLC reversed phase test mixture was obtained from Thermo Scientific (Runcorn). Acetonitrile, chloroform, methanol, isopropanol and toluene (all HPLC grade) were obtained from Fisher Scientific. All chemicals were used as received. Deionised water and Milli-Q water (18 MΩ) were prepared in the laboratory.

4.3.2 Particle Synthesis

Particles were synthesised using the optimised method described in chapter 2, section 2.4.7. The large scale was required to produce sufficient amounts of particles for subsequent bonding and packing into HPLC columns. The reaction was performed at room temperature on a magnetic stirrer plate. Stirring was performed using a Teflon coated stirrer bar at a speed of 240 rpm. Brand new glassware was used for each experiment.

PVP (12.5 g) and CTAB (0.625 g) were dissolved in deionised water (250 mL). Methanol (400 mL) was added, followed by diluted ammonium hydroxide (100 mL, 1.4%). The solution was stirred for 15 minutes, before addition of MPTMS (20 mL) in 2 mL aliquots at even intervals over 10 minutes. The reaction was stirred overnight. SOS particles were

collected on a sintered glass filter and washed with distilled water (5 x 100 mL), then methanol (5 x 100 mL) before drying under vacuum at 60 °C. Example SEM images of the particles are shown in figure 4.3.

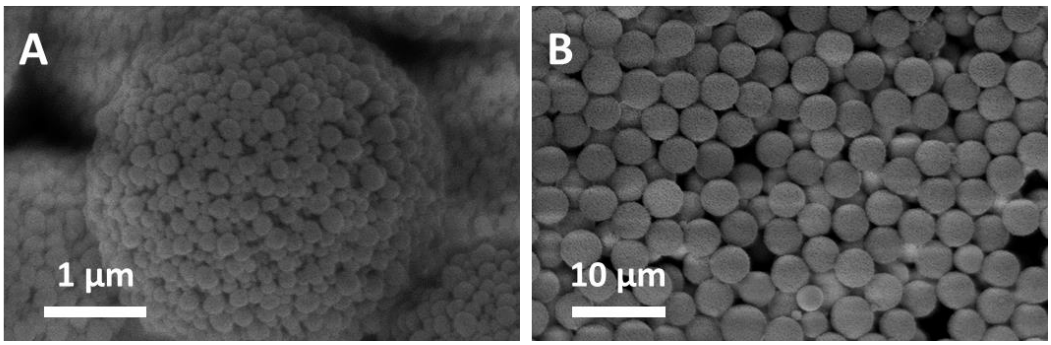

Figure 4.3 SOS particle morphology (A) and dispersity (B) shown by SEM imaging.

4.3.3 Bonding Using Microwave Irradiation

Two separate batches of particles were produced and calcined at temperatures of 550 and 1000 °C. The physical properties of the particles are shown in table 4.1, along with the data following microwave bonding. Data for a commercial core-shell material (Thermo Scientific Accucore 150-C4) is also included for comparison purposes. It should be noted that no classification was performed on any SOS materials. Particles were rehydroxylated using nitric acid as in the method described in section 3.3.3, chapter 3. All microwave reactions were performed on a CEM Explorer microwave reactor in 35 mL reaction vessels.

2 g of silica was dispersed in toluene (15 mL) with sonication in a 35 mL reaction vessel. A rare earth stirrer bar, imidazole (0.2 g) and chlorosilane reagent (0.8 g) were added and the vessel sealed. Reagent amounts were adjusted according to the mass of silica starting material, the ratio was kept constant. As in previous studies a dynamic closed vessel method was used. The reaction was run at 120 °C for 20 minutes using a high stir speed. Resultant particles were washed on a sintered glass filter with toluene (60 mL), methanol (60 mL), methanol/water (1:1 V/V, 60 mL) and methanol (60 mL). Particles were first dried in air on the filter for 1 hour, then under vacuum at 80 °C overnight. Endcapping was performed using the same method with TMSI in place of the chlorosilane and the omission of imidazole.

Table 4.1 Physical properties of bonded SOS and core-shell materials. Accucore 150-C4 data obtained from the Thermo Scientific Phase Overview brochure.

Material	Calcine temperature (°C)	Surface area (m^2/g)	Particle diameter (µm)	$d^{90}/_{10}$	% C	α (µmol/m^2)
SOS-C4-1	1000	4.3	2.90	1.36	0.13	4.20
SOS-C4-2	550	148	3.00	1.24	2.17	2.10
SOS-C8	550	155	3.00	1.24	2.99	1.68
Accucore 150-C4	-	80	2.6	1.12	2	3.57

4.3.4 Column Packing

Functionalised SOS particles were packed into 100 mm stainless steel narrow bore columns with 2.1 mm internal diameter, sealed with 0.5 µm porous titanium frits. A silica suspension was prepared by dispersing functionalised particles (0.5 g) in a solution of 72:8:20 chloroform:methanol:isopropanol (V/V/V, 30 mL). The column was packed at 600 bar using methanol (60 mL).

4.4 Results and Discussion

The SOS morphology appears to be ideal for the separation of large molecules and proteins due to the shallow shell depth. Although micropores in the silica surface are effectively inaccessible to analytes, the single layer of nanoparticles that make up the shell provide interstitial macroporosity. Additionally the shell is relatively shallow, in the region of 200 nm. This potentially reduces the mass transfer of large molecules such as proteins, as the intraparticle diffusivity depends on the ratio of diameters of solid core to the whole particle. As this ratio increases, mass transfer kinetics become faster across the particles.[57]

The performance of SOS particles has been assessed under isocratic conditions to determine efficiency, permeability, porosity and impedance. The SOS material has then

been assessed under gradient conditions for the separation of a range of peptides and proteins. Chromatographic data was obtained using a Thermo Scientific Accela UPLC system, with data analysis performed using ChromQuest 5.0 software, version 3.2.1.

As a comparison to commercially available materials, the gradient testing has been performed along with a core-shell column (Thermo Scientific Accucore 150-C4, 100 × 2.1 mm) which is optimised for the separation of proteins and larger peptides. The assessment of fractal SOS particles under isocratic and gradient conditions is also discussed and the results compared with the regular SOS material.

4.4.1 Isocratic Study

The efficiency, porosity, permeability and impedance of SOS-C4-1 particles were assessed in isocratic mode. Test compounds uracil (10 µg/mL) and butylparaben (100 µg/mL) were made up in Milli-Q water. The efficiency of the SOS-C4-1 material was first investigated by plotting reduced plate height versus reduced linear velocity for butylparaben. Uracil was used to determine t_0 values. Reduced plate height and linear velocity were used as they take into account the particle diameter and allow comparison with differently sized materials. The mobile phase was composed of 85:15 (V/V) water:acetonitrile and the flow rate varied between 25 µL/min and 1000 µL/min. The column oven was set at 30 °C to ensure constant temperature and injection volumes of 1 µL were used. Detection was set at 240 nm. The values for reduced plate height (h), linear velocity (u) and reduced linear velocity (ν) were calculated using the following equations:

$$h = \frac{H}{d_p}$$

$$u = \frac{L}{t_0}$$

$$\nu = \frac{u d_p}{D_m}$$

Where H is the theoretical plate height, d_p is the particle diameter, L is the column length, t_0 is the column dead time and D_m is the solute molecular diffusion coefficient, determined using the Wilke-Chang equation.[58] The obtained reduced plate height-reduced linear velocity plot is shown in figure 4.4.

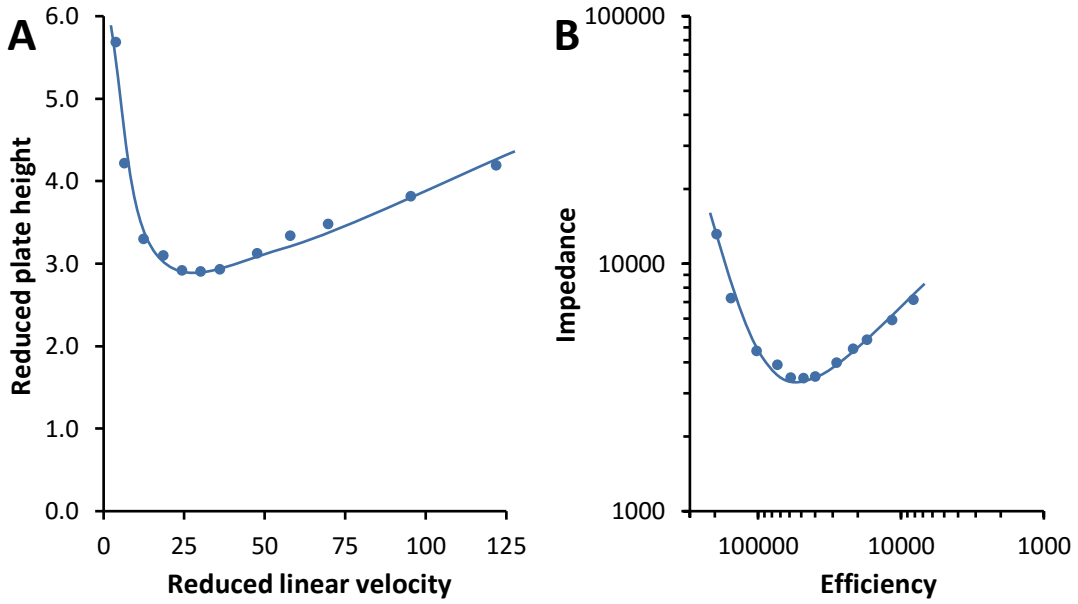

Figure 4.4 Plot of reduced plate height versus reduced linear velocity (A) and impedance plot (B) for the analysis of butylparaben on the SOS-C4-1 column.

The minimum reduced plate height (h_{min}) observed for butylparaben was 2.90. This is higher than might be expected, considering that h_{min} values of 1.2-1.8 are typically observed for core-shell materials, depending on experimental conditions and particle structure.[57, 59-61] The high h_{min} value for the SOS material may be partly caused by the short retention times observed for small analytes, due to the low surface area and non-porous silica surface. The short retention time results in a lower plate count and therefore higher reduced plate height.

It was discussed in chapter 1 that the quality of packing has a large effect on the A term, and therefore h_{min}. The packing method for SOS particles was discussed in chapter 3. Experimental work was conducted to optimise the composition of slurry solvent to keep particles in suspension during the packing process. Columns packed using this method have shown good peak shape and consistent performance, however there are still some

limitations due to the equipment used. A 50 bar drop in pressure was observed at regular intervals during the packing procedure due to the mechanism of the packing pump, which may have affected the column bed. Additionally the lack of an inline valve on the packing equipment to reduce bed expansion during the rest period could have also had an adverse effect on the column packing. With further optimisation of the packing process, improved performance should be seen.

From the data obtained from the efficiency study, it was possible to determine values for column permeability (K_V) and total column porosity (ε_T) using the following equations:[28, 62]

$$K_V = \frac{u\eta L}{\Delta P}$$

$$\varepsilon_T = \frac{4F}{d_c^2 \pi u}$$

Where u is the mobile phase linear velocity, η is the mobile phase viscosity, L is the column length, ΔP is the backpressure (after correction for system operating pressure), F is the mobile phase flow rate and d_c is the column diameter.

The total column porosity was calculated as 0.57 based on the elution time of the unretained analyte (uracil), which is slightly lower than current commercial core-shell materials due to the highly porous shell. The permeability of a packed column is defined as the proportionality factor in the relation between velocity of the solvent in the column and pressure drop. The column permeability of the SOS-C4-1 material was determined to be 2.07×10^{-10} cm^2, which is higher than observed for typical sub-3 µm core-shell materials. This is mainly facilitated by the lower back pressure of the SOS column due to the larger particle diameter. The pressure at 1000 µL/min was measured to be 354 bar after correction for the system pressure (34 bar). As a comparison, the back pressure of the Accucore 150-C4 column was 486 bar. Despite being marketed as 2.6 µm nominal diameter, particle sizing reveals the mean diameter to be 2.45 µm, accounting for the increase in pressure.

The separation impedance is a term that defines the resistance encountered by a compound as it moves down the column, relative to the performance of said column. This gives a true measure of column performance as it incorporates the plate count, analysis time and operating pressure. The lowest observed value (E_{min}) for butylparaben was 3440, calculated using the equation in section 4.2.3. This is again comparable to current HPLC columns which typically have E_{min} values between 2000 and 5000. The impedance-efficiency plot for the SOS-C4-1 material is shown in figure 4.4.

The column packed with SOS-C4-1 particles was also assessed under isocratic conditions using a reversed phase test mixture containing acetophenone (35 µg/mL), benzamide (6 µg/mL), benzophenone (7 µg/mL) and biphenyl (10 µg/mL). The mobile phase was composed of 70:30 (V/V) methanol:water at a flow rate of 250 µL/min. The column oven was set at 30 °C and an injection volume of 5 µL was used. Detection was set at 254 nm. The chromatogram is shown in figure 4.5.

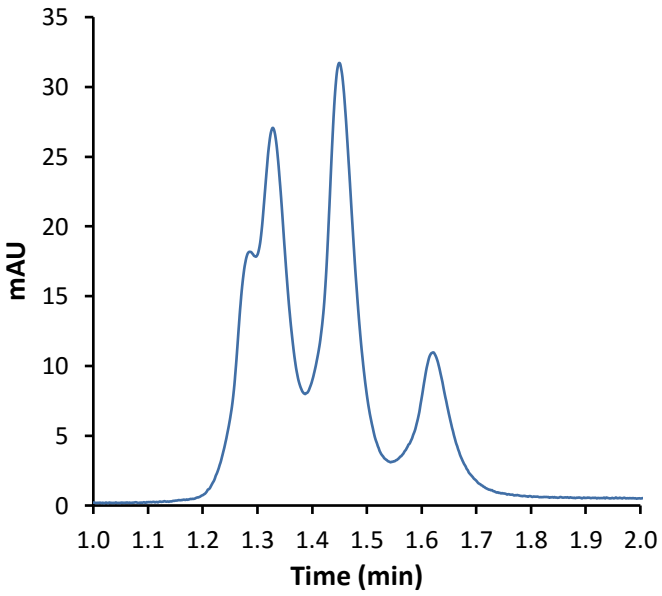

Figure 4.5 Separation of reversed phase test mixture on the SOS-C4-1 column under isocratic conditions.

Retention was determined by the polarity of the compounds. The elution order was benzamide (highly polar), acetophenone, benzophenone and biphenyl (non-polar). Short retention times were observed, resulting in coelution. This is likely to result from the low

accessible surface area and short alkyl chains providing limited retention for small molecules. However, the plate count could be measured for biphenyl, with a value of 35000 plates/metre obtained.

4.4.2 Gradient Study: Peptide Analysis

HPLC columns packed with C4 and C8 functionalised SOS particles were used to separate a peptide standard mixture containing angiotensin II, GY, leu-enk, met-enk and VYV, each in 80 µg/mL concentration. The mixture was separated using a linear gradient method. Mobile phase A: 0.02 M KH_2PO_4, pH 2.70; B: acetonitrile; gradient: 10-40% B in 4 minutes; flow rate 300 µL/min; temperature: 40 °C; detection: 220 nm; injection volume: 10 µL. Chromatograms are shown in figure 4.6.

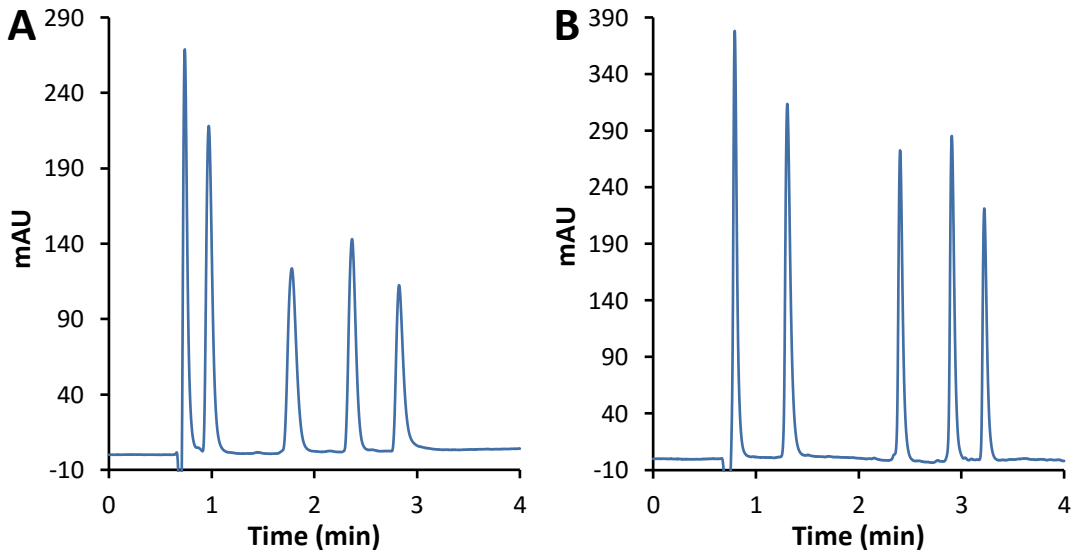

Figure 4.6 Chromatograms obtained from the separation of the peptide standard mixture on SOS-C4-1 (A) and SOS-C8 (B) columns.

The five components were fully resolved within 3 minutes on the SOS-C4-1 material and 3.5 minutes on the C8 material, with identical elution orders of GY, VYV, met-enk, leu-enk and angiotensin II. The elution order was confirmed by analysis of the individual components. Sharp, well-defined peaks were observed, particularly for the SOS-C8 column.

The average peak capacities were 52 (SOS-C4-1) and 64 (SOS-C8). The same test mixture was separated using the Accucore 150-C4 column. The retention time was increased beyond 4 minutes therefore the gradient time was increased with the steepness kept identical. A change in selectivity was observed, with the final two peaks reversed resulting in an elution order of GY, VYV, met-enk, angiotensin II and leu-enk. The average calculated peak capacity was 60. The chromatogram is shown in figure 4.7 A.

Additionally the gradient and flow rate were modified to provide full separation of the peptide mixture in under 1.5 minutes using the SOS-C4-1 column. Mobile phase A: 0.02 M KH_2PO_4, pH 2.70; B: acetonitrile; gradient: 10-14% B in 0.5 minutes, 14-60% B in 0.5 minutes, hold at 60% B for 0.5 minutes; flow rate 600 µL/min; temperature: 40 °C; detection: 220 nm; injection volume: 10 µL. The chromatogram is shown in figure 4.7 B. The peak capacity was reduced due to the short gradient time, with an average value of 37 obtained.

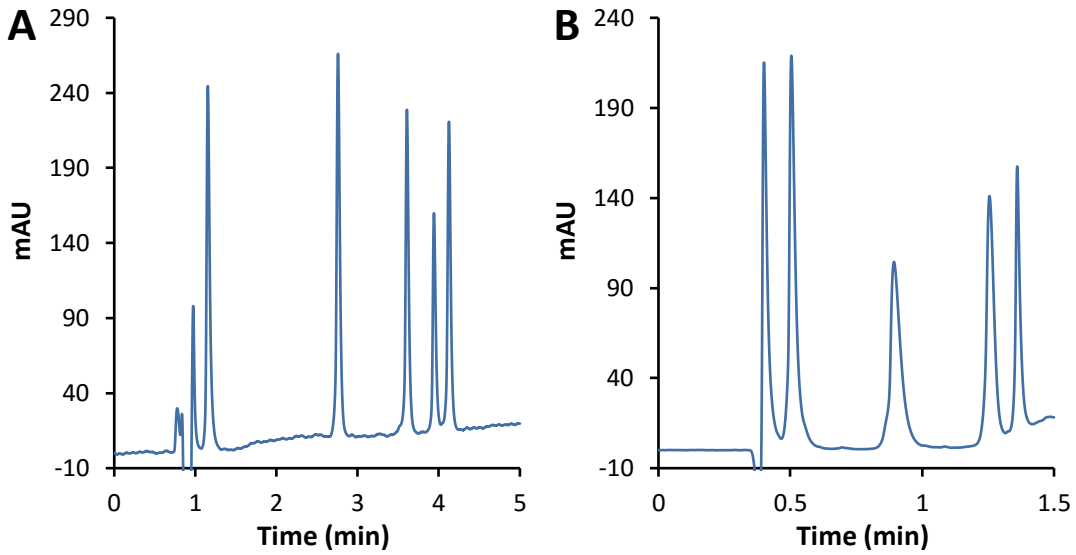

Figure 4.7 Chromatograms obtained from the separation of the peptide standard mixture on Accucore 150-C4 (A) and SOS-C4-1 (B, with modified gradient) columns.

The SOS material has shown rapid separation of the peptide mixture with excellent results for peak capacity, providing comparable performance to the commercial core-shell column. The maximum observed back pressure was also lower for the SOS columns; 120 bar (SOS-C4) and 128 bar (SOS-C8) versus 166 bar for the Accucore column.

4.4.3 Gradient Study: Protein Analysis

The SOS-C4-1 and Accucore 150-C4 columns were used to analyse a number of proteins with molecular weights in the range of 6-45 kDa. The test proteins carbonic anhydrase (30 kDa), insulin (6 kDa), lysozyme (14 kDa), myoglobin (17 kDa), ovalbumin (45 kDa) and ribonuclease A (14 kDa) were prepared in 1 mg/mL concentration in Milli-Q water. Each protein was analysed individually using a linear gradient method. Mobile phase A: water + 0.2% TFA; B: acetonitrile + 0.2% TFA; gradient: 30-66% B in 8 minutes (gradient steepness 4.5 %/min); flow rate 400 µL/min; temperature: 50 °C; detection: 220 nm; injection volume: 1 µL. Chromatograms for both columns are shown in figure 4.8.

The use of elevated temperatures is beneficial as it reduces the secondary interactions between residual silanols and charged biomolecules. High temperatures have also been shown to enhance analyte diffusion for large molecules.[12, 13] Additionally TFA was added to the mobile phase to increase the efficiency of protein separation.[63-65]

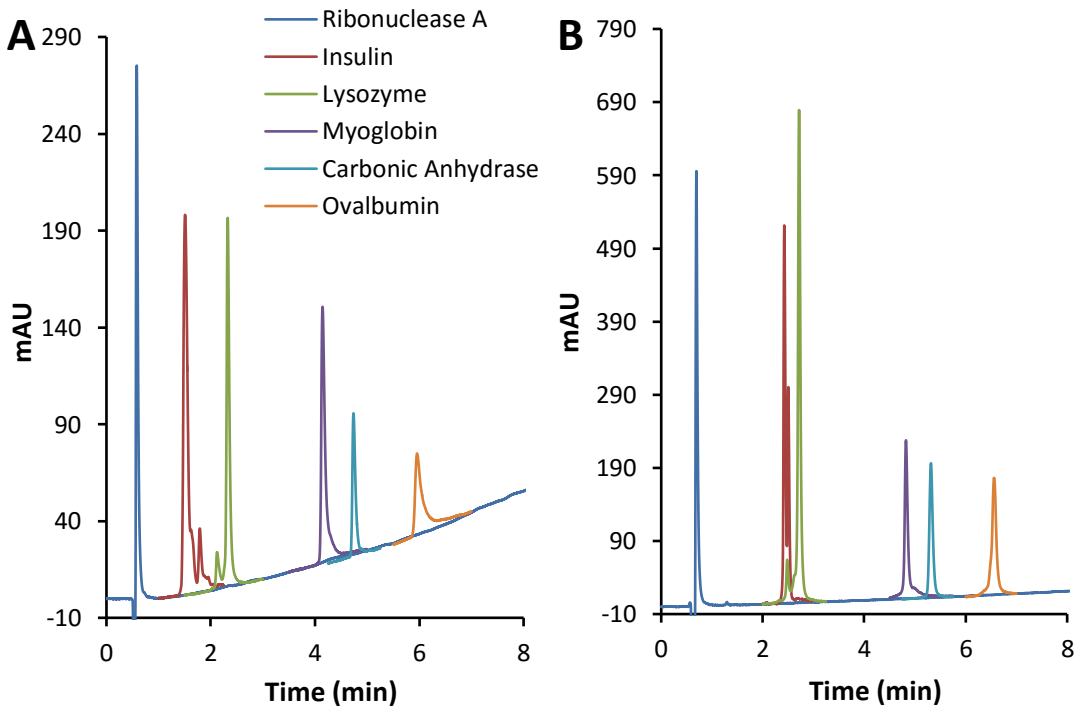

Figure 4.8 Overlaid chromatograms of individual protein separation on the SOS-C4-1 (A) and Accucore 150-C4 (B) columns. Baselines trimmed for clarity.

The two columns displayed identical selectivity and retention times of the final peak were similar. The elution order was ribonuclease A, insulin, lysozyme, myoglobin, carbonic anhydrase and ovalbumin. The peak capacities for each analyte were calculated, with an average value of 72 obtained for the SOS-C4-1 column. The Accucore column showed comparatively better performance, with an average peak capacity of 81. The major difference between the two materials was the analysis of insulin, with the SOS material providing lower performance. If the average peak capacity is calculated with the omission of insulin, the values are very similar for both materials (74 versus 77).

When comparing the analyses of the largest proteins (myoglobin, carbonic anhydrase and ovalbumin) the performance of the two columns is very similar, with the SOS material outperforming the commercial column in the case of carbonic anhydrase. This suggests that the SOS material is more suited to the analysis of larger molecules, which is expected due to the macroporosity provided by the interstitial spaces in the shell structure.

To ensure that no interactions between intact proteins within a mixture affect the chromatographic performance, a test mixture of four proteins was prepared containing carbonic anhydrase (65 µg/mL), lysozyme (65 µg/mL), myoglobin (65 µg/mL) and ovalbumin (75 µg/mL), made up in Milli-Q water. The protein test mixture was separated using a linear gradient method. Mobile phase A: water + 0.1% TFA; B: acetonitrile + 0.1% TFA; gradient: 30-65% B in 6 minutes (5.83 %/min); flow rate 400 µL/min; temperature: 50 °C; detection: 220 nm; injection volume: 20 µL.

The separation of this protein mixture has previously been discussed in the microwave bonding chapter, where the performance of SOS particles functionalised by microwave and conventional heating methods was compared alongside the Accucore 150-C4 material. The SOS column from the microwave study (SOS-C4-2) was based on a batch of silica calcined at 550 °C and thus has a microporous surface. The physical properties are included in table 4.1 for comparison purposes. This column was found to perform slightly better than the Accucore column with an average peak capacity of 58 versus 54.

Interesting results were observed when comparing the microporous and non-porous SOS materials. The very low surface area of the non-porous material leads to much lower percent carbon results, as there are simply less silanol sites to bond to. Despite the low percent values, the bonding density is double that of the microporous material. As discussed in the microwave bonding chapter, it is likely that the micropores are inaccessible

to the bonding reagents and therefore lower than expected bonding densities are observed for the microporous material.

The protein test mixture was fully resolved within 5 minutes on the SOS-C4-1 column with an average peak capacity of 52. The chromatogram of the separation is overlaid with those of the SOS-C4-2 and Accucore columns in figure 4.9. The elution order was lysozyme, myoglobin, carbonic anhydrase, ovalbumin for all three columns. The gradient steepness was modified for the Accucore column (30-68.5% B in 6 minutes, 6.42 %/min) to match the retention times of the final peak. Once again the back pressures of the SOS-C4 columns were lower than that of the commercial column, with observed values of 170 bar (SOS-C4-1), 176 bar (SOS-C4-2) and 205 bar (Accucore 150-C4).

Of the two SOS materials the retention time of the final peak was actually found to be greater on the non-porous SOS column. The greater bonding density of the non-porous material is likely to have provided this increase in retention. This observation backs up the theory that the micropores are inaccessible to analytes and that they do not have a significant effect on the retention of large molecules.

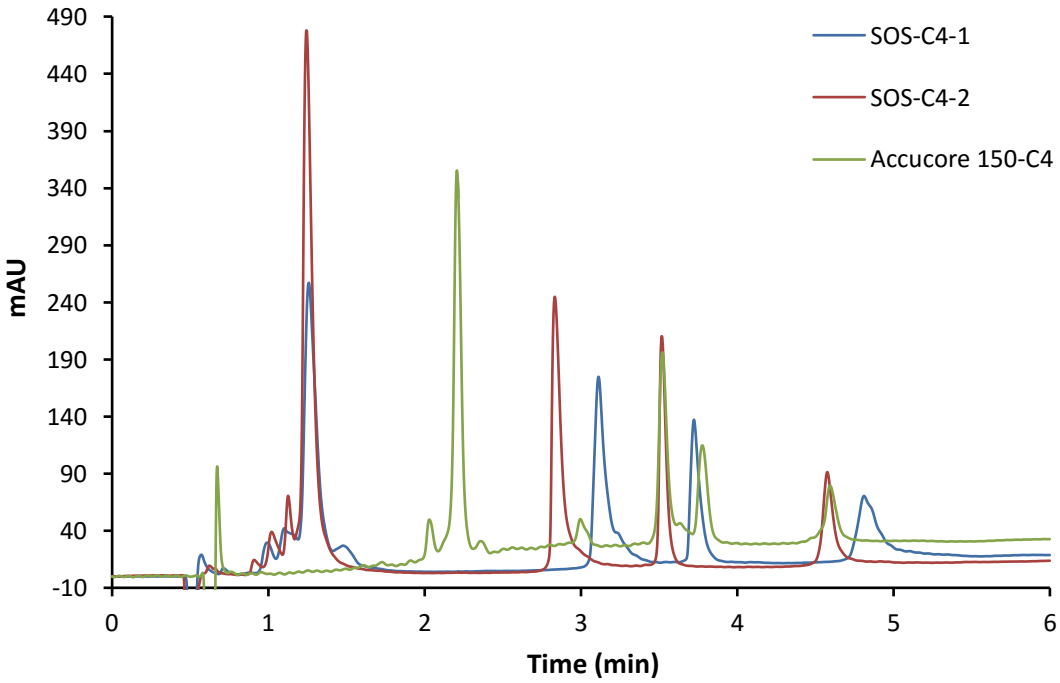

Figure 4.9 Overlaid chromatograms of protein test mixture separation on SOS-C4-1, SOS-C4-2 and Accucore 150-C4 columns.

The SOS-C4-1 and Accucore 150-C4 columns were also used to analyse two large proteins, bovine serum albumin (BSA, 66 kDa) and thyroglobulin (669 kDa). The test proteins were prepared in 1 mg/mL concentration in Milli-Q water and analysed individually using a linear gradient method. Mobile phase A: water + 0.2% TFA; B: acetonitrile + 0.2% TFA; gradient: 30-75% B in 10 minutes (4.5 %/min); flow rate 400 µL/min; temperature: 50 °C; detection: 220 nm; injection volume: 1 µL. Chromatograms are shown in figure 4.10.

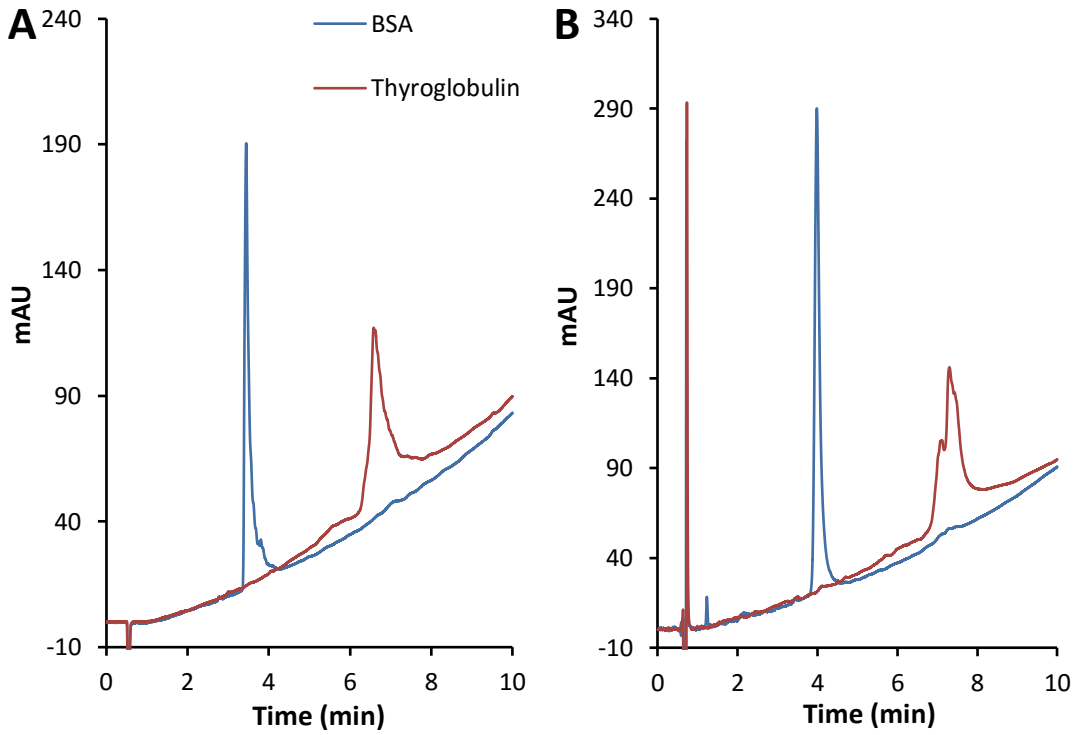

Figure 4.10 Overlaid chromatograms of large protein separation on SOS-C4-1 (A) and Accucore 150-C4 (B) columns.

Under these short gradient times, the SOS column provided faster elution and greater values for peak capacity than the Accucore column. Calculated values for peak capacity were 56 versus 48 for BSA and 25 versus 16 for thyroglobulin. These results highlight the advantages of the shallow, single layer shell which provides macroporosity and reduces mass transfer resistance, particularly for very large analytes. When considering the ratio of the solid core to the overall particle diameter (ρ), the SOS material has a ratio of 0.86 versus 0.62 for Accucore. The effects of this were discussed in chapter 1, where it

was shown that a higher value, corresponding to a thin porous layer, is advantageous when analysing large molecules and provides a large reduction in mass transfer effects.

BSA is ellipsoid in shape, approximately 7 × 2 nm in diameter. This size of analyte is able to diffuse into the pore system of the Accucore material as the average 15 nm pore size is sufficiently large to allow access. However, the large size of the protein leads to slower diffusion and hence comparatively lower value for peak capacity against the SOS column. Thyroglobulin is larger still, with a radius of approximately 9 nm. When also accounting for the space filled by the surface functionality within the pores of the packing material, it is likely that this analyte is simply too large to efficiently separate with the Accucore column due to poor diffusivity. The SOS material however has been shown by mercury intrusion to have pore size in the region of 1 µm, reducing these diffusive effects and resulting in higher performance.

4.4.4 Efficiency in Gradient Elution Mode

A study was conducted to determine the achievable peak capacity of the SOS-C4-1 column. Peak capacity values were calculated at two flow rates (250 and 400 µL/min) for three proteins: myoglobin, carbonic anhydrase and transferrin. The test proteins were prepared in 1 mg/mL concentration in Milli-Q water and analysed using a linear gradient method. Mobile phase A: water + 0.1% TFA; B: acetonitrile + 0.1% TFA. The gradient used was 20-60% B, with the time varied between 10 and 90 minutes (60 minutes for transferrin). The column temperature was 50 °C with detection at 220 nm and injection volume of 1 µL.

The peak capacity values for the SOS-C4-1 column were calculated and plotted against the gradient time. The results show how the achievable peak capacity is affected by the experimental conditions and show the column performance for different types and sizes of proteins. The peak capacity plot is shown in figure 4.11.

For the analysis of myoglobin, the peak capacity varied between 66-130 at 250 µL/min and 70-136 at 400 µL/min. For carbonic anhydrase, peak capacities of 67-114 at 250 µL/min and 73-118 at 400 µL/min were observed. The difference between values at both flow rates was calculated to be less than 5%, due the reduced intraparticle mass transfer resistance facilitated by the structure of the SOS particles. The peak capacity at 600 µL/min

was also calculated for a 90 minute gradient time with values of 141 for myoglobin and 118 for carbonic anhydrase. The small difference in peak capacity suggests that the columns are able to work over a large range of flow rates without a significant variation in performance, indicating that fast protein separation can be performed.

The analysis of the largest protein, transferrin (80 kDa), resulted in peak capacities of 49-88 at 250 µL/min and 54-88 at 400 µL/min. Again, no significant variation between flow rates was observed, even when increasing to 600 µL/min and a 60 minute gradient time, which resulted in a peak capacity of 90. This again suggests decreased mass transfer resistance and the ability to work over a large range of flow rates.

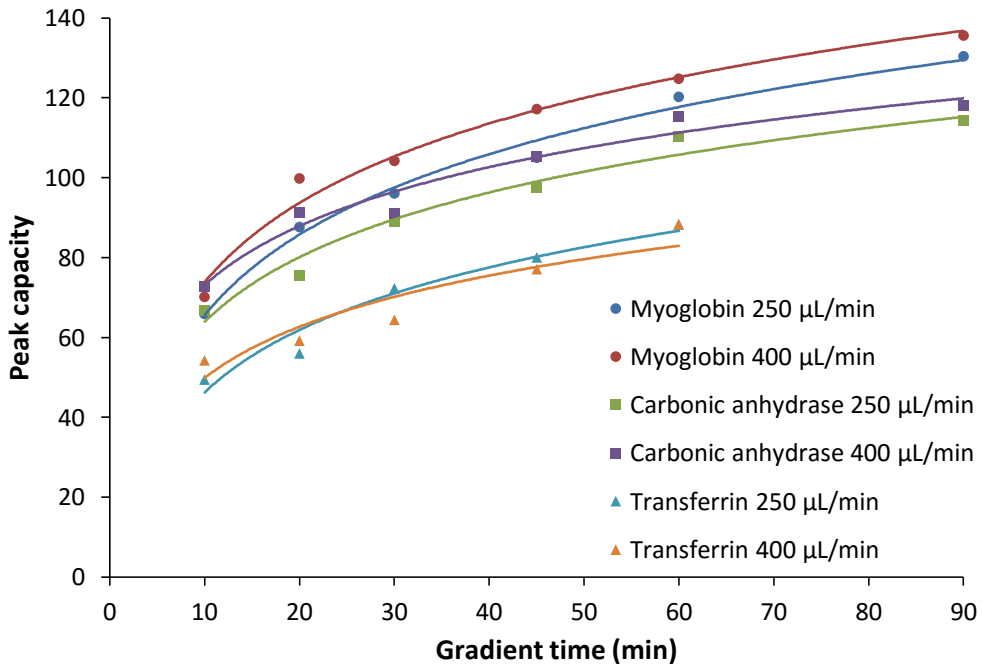

Figure 4.11 Peak capacity plot for the SOS-C4-1 column.

The achievable peak capacity of the SOS-C4-1 column was also compared to the Accucore 150-C4 column over the same gradient span. Figure 4.12 shows the overlaid peak capacity plots for the analysis of myoglobin, carbonic anhydrase and transferrin on both columns at flow rates of 250 and 400 µL/min.

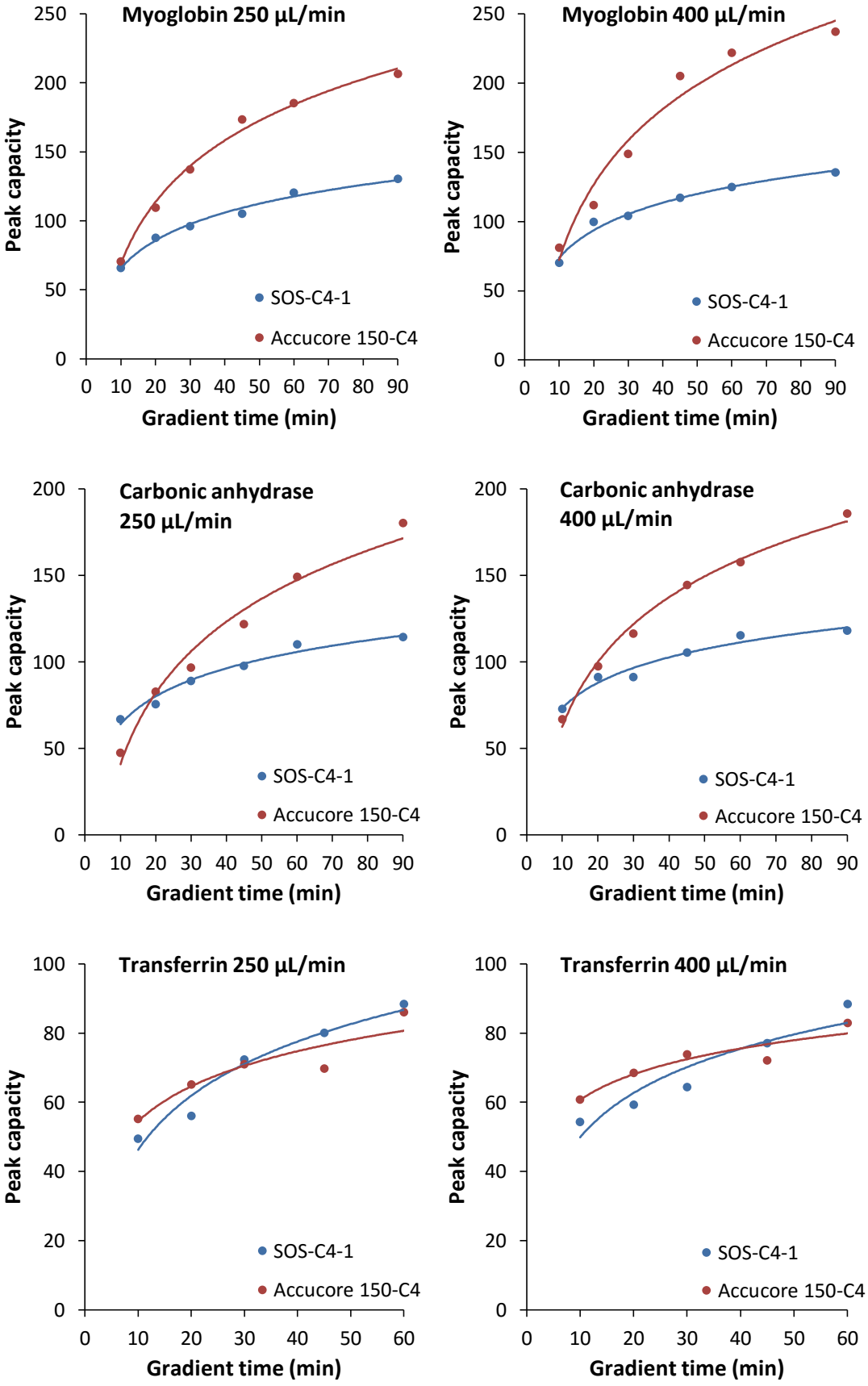

Figure 4.12 Comparison of peak capacity values obtained with myoglobin, carbonic anhydrase and transferrin on SOS and Accucore columns at 250 and 400 µL/min.

For the analysis of myoglobin the SOS column provided similar performance to the Accucore column at short gradient times for both flow rates studied. However, higher performance was observed for the Accucore column throughout the whole range of gradient times, particularly for the longest analyses. Similarly, the Accucore material provided higher performance at the longest gradient times for carbonic anhydrase, though in this case the SOS column provided comparable performance when the gradient was less than 30 minutes at a flow rate of 250 µL/min and less than 20 minutes at 400 µL/min. The SOS column provided higher peak capacity for a 10 minute gradient span at both flow rates. For the analysis of transferrin, the performance of both columns was comparable across the whole gradient span at both flow rates, with the performance of the SOS material surpassing that of the core-shell column at the longest gradient times.

These results show that the SOS column is capable of matching the performance of the commercial core-shell column when performing fast gradient separation. It has also been observed that the achievable peak capacity becomes more comparable over a longer gradient span when increasing the molecular weight of the analyte, as mass transfer effects are reduced for the SOS material. The peak capacity attained from the SOS column for proteins up to a molecular weight of 30 kDa is therefore mostly beneficial when a fast gradient (≤20 min) is applied. For the analysis of larger molecules, the SOS column is capable of efficient performance across the whole gradient span.

4.4.5 Applications

In collaborative work with the School of Pharmaceutical Sciences, University of Geneva, a 100 × 2.1 mm HPLC column packed with SOS C4 particles was supplied to assess the performance when analysing monoclonal antibody (mAb) and antibody-drug conjugate (ADC) fragments.[66] Characterisation of mAbs and other biopharmaceuticals provides useful information on purity and stability of the compound. As antibody heterogeneity is related to the conformational isoforms the reduction of the disulphide bonds, followed by reversed phase analysis of these reduced fragments is routinely used to determine if conformational variants are disulphide-related or not.

The SOS particles provided for this study had a mean diameter of 2.13 µm and $d^{90}/_{10}$ ratio of 1.44. BET surface area was measured to be 248 m^2/g by nitrogen adsorption.

C4 bonding was performed by microwave irradiation using the previously described method, with obtained carbon loading values of 4.11% and 2.46 µmol/m^2.

The intramolecular disulphide bonds of the mAb rituximab were reduced using dithiothreitol (DTT), converting the protein into the light chain (Lc) and heavy chain (Hc) fragments. The intact mAb has molecular weight of around 150 kDa, with the Lc and Hc fragments having weights of 25 and 50 kDa respectively. Analysis of both intact and reduced forms was performed using the SOS column alongside three other commercial columns designed for protein analysis: Halo Protein C4 (AMT), Acquity BEH300 C18 (Waters) and Aeris Widepore C18 (Phenomenex). The commercial columns had dimensions of 150 × 2.1 mm and therefore chromatograms have been plotted against the apparent retention factor (k_{app}) to allow direct comparison with the shorter SOS column. A linear gradient method was used with the conditions scaled for the different column lengths. Mobile phase A: water + 0.1% TFA; B: acetonitrile + 0.1% TFA; gradient: 24-37% B in 5 min (SOS), 27-40% B in 7.5 min (others); flow rate: 400 µL/min. The column temperature was 80 °C with detection at 280 nm. Overlaid chromatograms for the analysis of intact and reduced rituximab are shown in Figure 4.13.

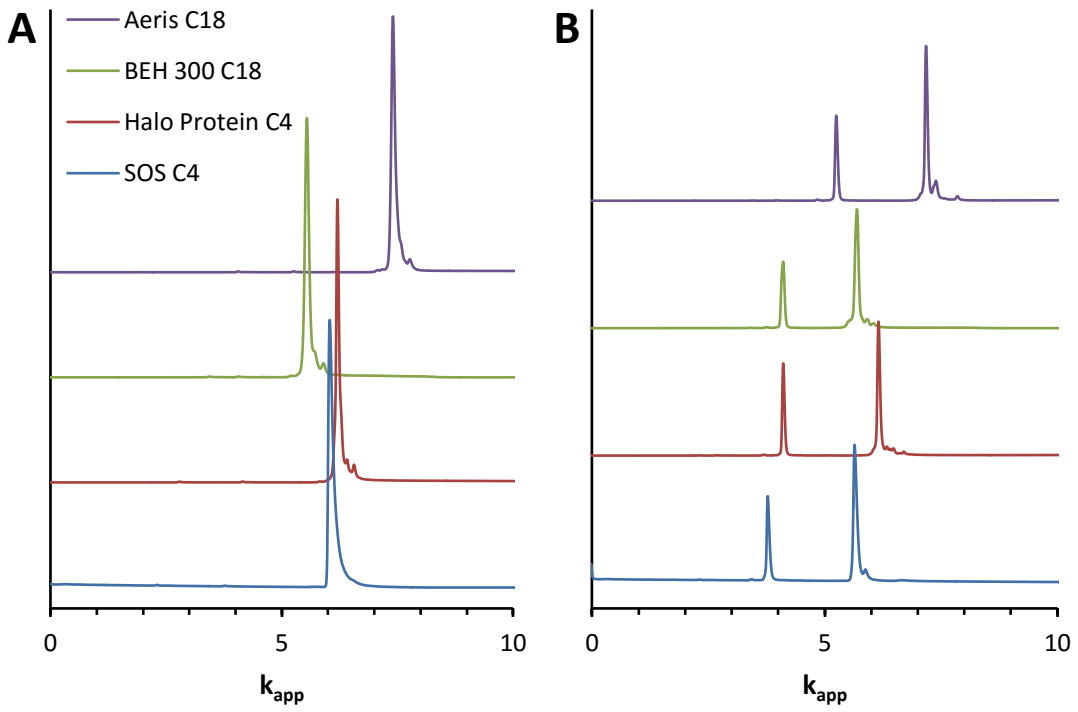

Figure 4.13 Chromatograms from the analysis of intact (A) and reduced rituximab (B) on SOS C4 and three commercial wide-pore test columns.[66]

It can be seen from the chromatograms that the heterogeneity of rituximab is related to the Hc due to the fine structure observed on the reduced protein. The quality of separation on the SOS column was found to be comparable to that of the commercial materials with peak capacities of 45 and 68 obtained for the intact and reduced mAb respectively. It can be seen however that the fine structure of closely related species is clearer for the commercial columns, particularly for the intact protein.

The same selection of columns was also used to analyse the ADC brentuximab vedotin. The protein was again reduced using DTT, converting the structure into various Lc and Hc fragments. The molecular weights of the intact and reduced analytes are similar to the previous example. An important attribute of ADCs is the average number of drugs that are conjugated, as this determines the amount of drug that can be delivered to the target cell and directly affects both safety and efficacy. Reversed phase chromatography is commonly used to measure the amount of conjugation.

Again, a linear gradient method was used with the conditions scaled for the different column lengths. Mobile phase A: water + 0.1% TFA; B: acetonitrile + 0.1% TFA; gradient: 24-42% B in 12 min (SOS), 30-45% B in 18 min (others); flow rate: 400 µL/min. The column temperature was 80 °C with detection at 280 nm. Overlaid chromatograms for the analysis of reduced brentuximab vedotin are shown in Figure 4.14.

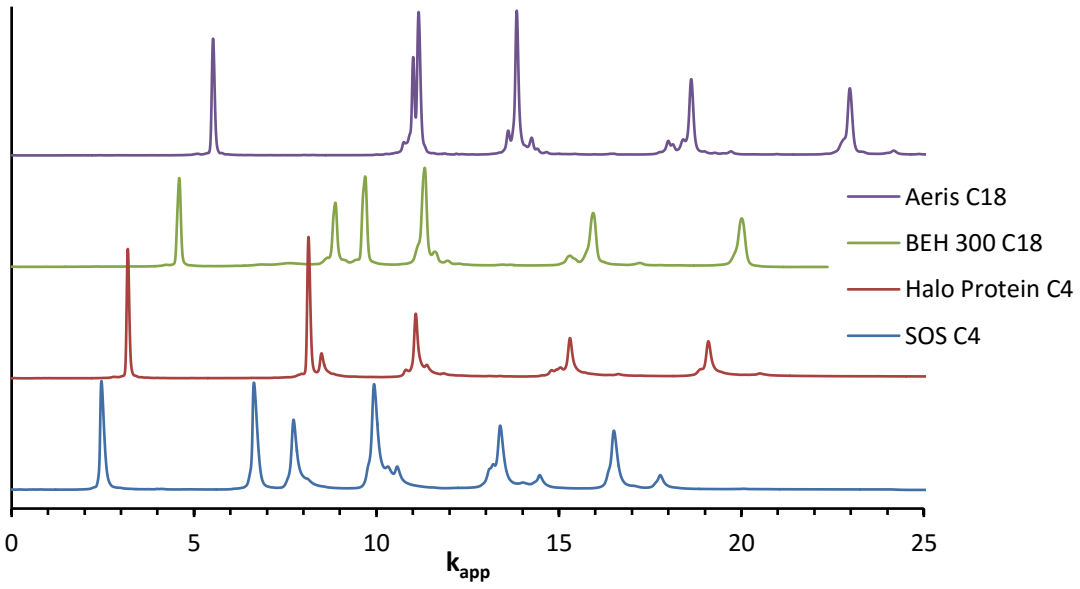

Figure 4.14 Chromatograms from the analysis of reduced brentuximab vedotin on SOS C4 and three commercial wide-pore test columns.[66]

An average peak capacity of 117 was measured for the reduced ADC when using the SOS C4 column. The peak capacity values were comparable to those obtained with the commercial wide pore columns. The chromatogram for the SOS column is comparable to what is typically observed for the analysis of IgG1 type ADCs[67] and shows excellent separation of the L0, L1, H0, H1, H2 and H3 fragments (where L and H denote Lc and Hc, and the number denotes the number of drugs attached to each chain). Additionally a number of isomers were resolved from the H1, H2 and H3 peaks.

4.4.6 Fractal Chromatography

As discussed in chapter 2, the development of the SOS synthesis method has led to the formation of discrete particles with a complete single layer of shell particles. Further modification of the method by initial addition of MPTMS precursor, immediately followed by controlled addition of precursor via syringe pump has led to the production of SOS particles displaying growth of smaller nanoparticles upon the shell surface. These particles are termed fractal SOS as they possess a structure with a higher degree of self-similarity.

Fractal SOS particles were produced from the method in section 2.4.8, chapter 2. PVP (2.5 g) and CTAB (0.125 g) were dissolved in deionised water (50 mL). Methanol (80 mL) was added, followed by diluted ammonium hydroxide (20 mL, 1.4%). The solution was stirred for 15 minutes, before addition of MPTMS (4 mL total). An initial volume of 1 mL was added, followed by a further 3 mL at 0.06 mL/min (50 minute addition). The reaction was stirred overnight. SOS particles were collected on a sintered glass filter and washed with distilled water (5 x 40 mL), then methanol (5 x 40 mL) before drying under vacuum at 60 °C. SEM images of the particles are shown in figure 4.15, showing the additional surface growth compared to SOS particles discussed in chapter 2.

Following calcination at 550 °C, the mean particle diameter was measured to be 2.06 µm with a $d^{90}/_{10}$ ratio of 1.21. The BET surface area was measured to be 179 m^2/g by nitrogen adsorption. Particles were functionalised with a C4 group and endcapped using the microwave bonding method described in the experimental section. Carbon loading was measured to be 2.42 %, equating to coverage of 1.95 µmol/m^2. Particles were packed into a 100 × 2.1 mm column.

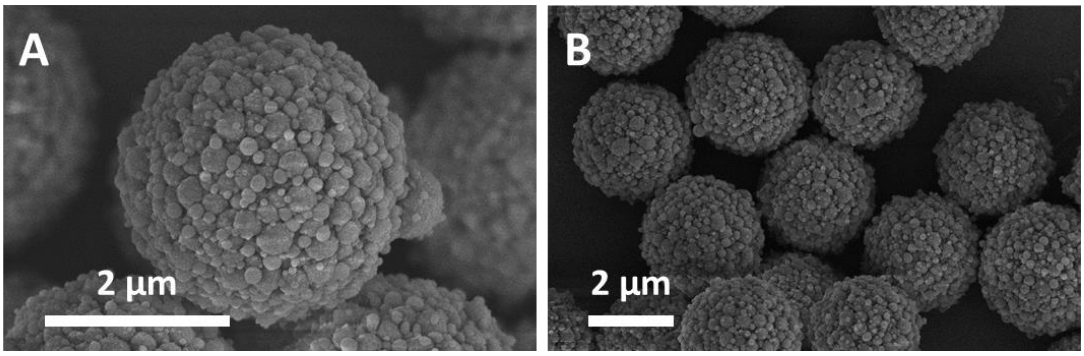

Figure 4.15 Fractal particle morphology (A) and dispersity (B) shown by SEM imaging.

As with the SOS particles, the fractal-C4 material was assessed in isocratic mode to determine efficiency, porosity, permeability and impedance. Test compounds uracil (10 µg/mL) and butylparaben (100 µg/mL) were made up in Milli-Q water. Reduced plate height versus reduced linear velocity was plotted for butylparaben, with uracil used to determine t_0 values. The mobile phase was composed of 85:15 (V/V) water:acetonitrile and the flow rate varied between 25 µL/min and 1000 µL/min. The column oven was set at 30 °C to ensure constant temperature and injection volumes of 1 µL were used. Detection was set at 240 nm. The values for reduced plate height (h), linear velocity (u) and reduced linear velocity (*v*) were calculated using the equations in section 4.4.1. The obtained reduced plate height-reduced linear velocity plot is shown in figure 4.16 A.

The value of h_{min} observed for butylparaben on the fractal-C4 column was 2.38. This shows greater efficiency compared to the SOS-C4-1 column, where h_{min} was measured to be 2.90. However this value is still higher than might be expected, particularly when compared to commercial core-shell materials. From the data obtained from the efficiency study, values for column permeability (K_V), total column porosity (ε_T) and impedance (E) were calculated.

K_V for the fractal-C4 material was determined to be 1.96×10^{-10} cm^2. ε_T was calculated as 0.55 based on the elution time of uracil. These values are very similar to those measured for the SOS-C4-1 column. The pressure at 1000 µL/min was measured to be 386 bar after correction for the system pressure (34 bar). The operating pressure is higher than for the SOS column due to the smaller particle size.

E_{min} for butylparaben on the fractal column was 2990 compared to 3440 for the SOS material. The impedance values across the whole plot were lower for the fractal

column, suggesting increased performance compared to the SOS material. The impedance-efficiency plot for the fractal-C4 column is shown in figure 4.16 B.

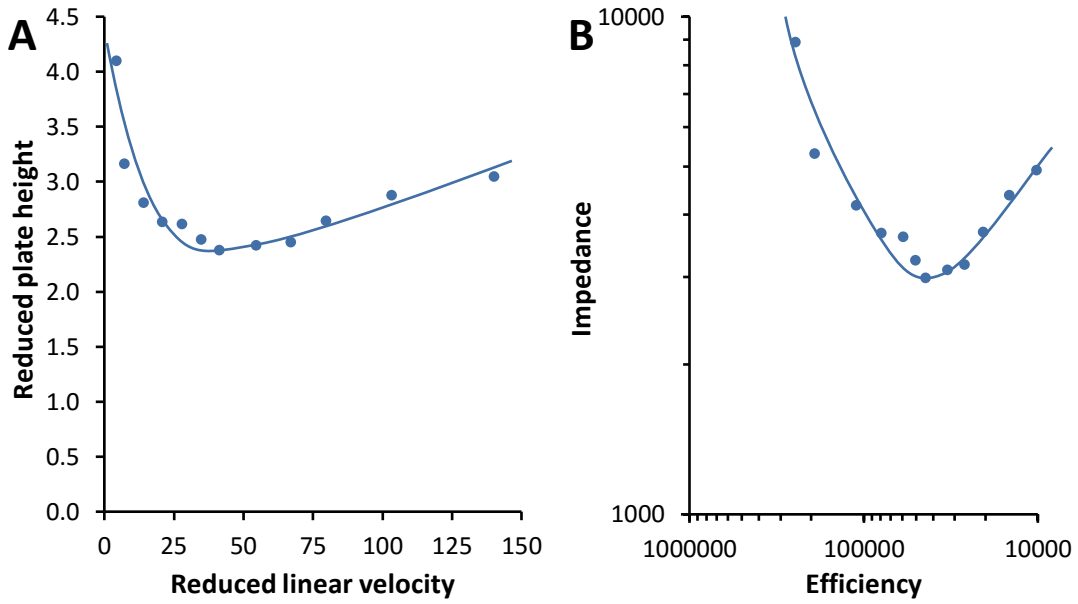

Figure 4.16 Plot of reduced plate height versus reduced linear velocity (A) and impedance plot (B) for the analysis of butylparaben on the fractal-C4 column.

Based on this data, the fractal-C4 column performs comparatively better than the SOS-C4-1 material. Although the smaller particle size of the fractal material resulted in higher operating pressure, the increased plate count led to lower h_{min}. The obtained value however is still higher than expected for this type of packing material. As previously discussed this may be due to packing effects and the short retention observed for small analytes. Values for column permeability and total porosity are both very close to those obtained for the SOS column, which is to be expected due to the similar morphologies of the two materials.

The performance of the fractal-C4 column was assessed in gradient elution mode for the analysis of individual proteins with molecular weights in the range of 6-45 kDa. As before, the test proteins carbonic anhydrase, insulin, lysozyme, myoglobin, ovalbumin and ribonuclease A were prepared in 1 mg/mL concentration in Milli-Q water. Each protein was analysed individually using a linear gradient method. Mobile phase A: water + 0.2% TFA; B:

acetonitrile + 0.2% TFA; gradient: 30-66% B in 8 minutes (4.5 %/min); flow rate 400 µL/min; temperature: 50 °C; detection: 220 nm; injection volume: 1 µL.

The large proteins BSA and thyroglobulin were also individually analysed on the fractal-C4 column. These were also prepared in 1 mg/mL concentration in Milli-Q water and analysed using the same chromatographic conditions as above, but with an increased gradient time of 30-75% B in 10 minutes. The gradient steepness was kept at 4.5 %/min. Overlaid chromatograms for the analyses are shown in figure 4.17.

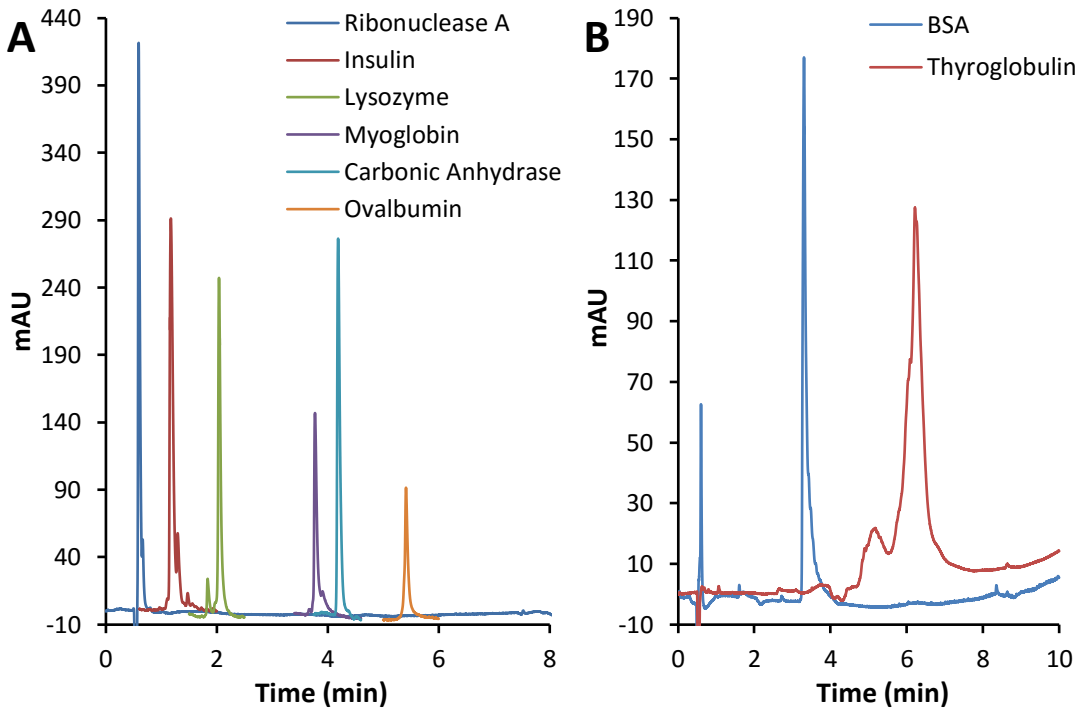

Figure 4.17 Overlaid chromatograms for separation of individual proteins (A) and large proteins (B) on the fractal-C4 column. Baselines trimmed for clarity for the protein traces.

The fractal column displayed identical selectivity to the previously analysed SOS-C4-1 and Accucore 150-C4 columns, with an elution order of ribonuclease A, insulin, lysozyme, myoglobin, carbonic anhydrase and ovalbumin for the 6-45 kDa analytes. The peak capacities for each protein were calculated, with an average value of 85 obtained. Narrow peak widths were observed, with $W_{50\%} \leq 0.05$ min for all peaks apart from insulin, and the peak capacity values for all analytes surpassed those of the Accucore column. The retention times were shorter on the fractal column than for the SOS and Accucore columns

which may be explained by the lower values of bonding density (1.95 versus 4.20 and 3.57 μmol/m^2). This does not appear to be disadvantageous however, as all peaks were well resolved and high performance was achieved.

The two large proteins were also successfully analysed on the fractal-C4 column. Calculated values for peak capacity were 64 for BSA and 18 for thyroglobulin. As in the case of the other proteins, the peak capacity for BSA is higher than for the other columns tested indicating higher performance. However, when compared against the values obtained for the other analytes, the peak capacity for thyroglobulin was lower than expected. When analysing the chromatogram, a peak associated with an aggregate of thyroglobulin is partly co-eluting before the main peak which may have caused interference with the peak width measurement. The aggregate peak is not clearly observed on the SOS or Accucore chromatograms and it is likely that the smaller particle size of the fractal material provides greater resolution as opposed to any morphology differences.

4.5 Conclusion

The chromatographic performance of SOS particles has been assessed in both isocratic and gradient elution mode. It was theorised that the SOS morphology should be ideal for the separation of large molecules, due to the shallow shell depth and interstitial macroporosity. Experimental studies have been conducted to determine this by HPLC analysis of a range of protein samples.

In isocratic mode, values for efficiency, permeability, porosity and impedance were determined for SOS particles functionalised with a C4 ligand. The minimum reduced plate height obtained using the SOS column was higher than expected when compared to commercial core-shell materials. There are two possible contributing factors. The first is that short retention times are observed for small analytes on the SOS material, as shown by the analysis of the reversed phase test mixture. The short retention time leads to a lower theoretical plate count, and therefore increased plate height. The second factor is the quality of column packing. Work was undertaken in chapter 3 to optimise the packing conditions such as the packing pressure, reservoir size and slurry solution composition. Despite this there are limitations due to the equipment used, for example a 50 bar drop in pressure was observed at regular intervals due to the packing pump mechanism which may lead to homogeneity in the packed column bed. The lack of an inline valve on the packing

equipment could have also had an effect on the column packing due to potential bed expansion during the rest period.

The calculated value for total column porosity was found to be slightly lower than for commercial core-shell materials. This is to be expected due to the shallow shell depth of the SOS particles. The permeability of the SOS material was higher than observed for core-shell materials due to the low porosity and also the larger SOS particle diameter providing lower column back pressure. Finally the SOS column also demonstrated favourable impedance values, which are comparable to current commercial columns.

A large range of compounds have been analysed under gradient conditions, from small peptides to large proteins. Fast, efficient separation of a standard peptide mixture was observed on columns packed with C4 and C8 SOS materials, with particularly high performance observed when using the SOS-C8 column. Obtained peak capacity values were comparable to the Accucore 150-C4 column. Using a modified gradient, the SOS-C4-1 column was also capable of separating the mixture in under 1.5 minutes although the peak capacity was lower due to the reduced gradient span. The observed back pressure was lower for the SOS materials, which is explained by the smaller diameter of the commercial core-shell particles. In future study it would be interesting to analyse protein digest mixtures using the SOS column and compare the results with commercial core-shell materials.

In comparison studies with the Accucore 150-C4 column over a range of gradient times and flow rates, the SOS material provided lower peak capacity across the whole gradient span for the analysis of myoglobin, although performance was comparable for a 10 minute run time. Similarly for carbonic anhydrase, performance was only comparable when the gradient span was less than 30 minutes. This indicates that the attainable peak capacity from the SOS material is mostly beneficial when performing fast gradient analysis. This has been shown to be the case when analysing individual proteins over a gradient span of 8 minutes where values for peak capacity (with the exception of one analyte) were comparable on both SOS and Accucore columns. Similarly the SOS materials provided comparable or better performance when separating a test mixture of proteins over a gradient span of 6 minutes.

From the results obtained in this study, the advantages of the SOS material are mostly observed in the separation of the largest proteins. The performance when analysing

transferrin was comparable to the Accucore column at both flow rates studied. The SOS column also provided higher performance when analysing BSA and thyroglobulin. It can be concluded from these results that the shallow shell depth does make the SOS morphology highly suitable for the analysis of large molecules, with the large ratio of core:total diameter providing a reduction in mass transfer effects. The isocratic study has also shown the particles to have low porosity and high permeability, both of which are also beneficial when reducing mass transfer effects of large molecules.

The SOS material also performed well in the analysis of mAb and ADC samples performed in collaboration with the School of Pharmaceutical Sciences at the University of Geneva. These proteins are based on IgG1 structures with intact molecular weights around 150 kDa and reduced fragments of 25 and 50 kDa. The performance of the supplied SOS C4 column was found to be comparable to current state of the art wide-pore materials designed for protein and biomolecule analysis, both in terms of peak capacity and resolution. mAbs and ADCs are currently of high interest for use as therapeutic agents and it would be interesting to conduct further analysis with SOS materials on these types of compounds.

A new type of fractal SOS morphology was also assessed in isocratic and gradient elution mode. The calculated values for permeability and total porosity are very similar to those obtained for normal SOS particles. This is to be expected due to the closely related morphology of the two materials. While a lower value for h_{min} was observed for the fractal material, it is likely that this is a result of the smaller particle diameter of the fractal material providing higher plate count. The higher efficiency also contributes to lower E_{min}, despite the higher operating pressure.

The fractal column performed well for the gradient analysis of individual proteins with peak capacity values exceeding those of the SOS-C4-1 and Accucore 150-C4 columns in most cases. The improvement in performance may again be attributed to the smaller particle diameter, and it is therefore difficult to determine whether the fractal morphology has any additional benefit over normal SOS particles. However it does appear that fractal particles share the inherent advantage of SOS particles when considering the reduction in mass transfer effects for large analytes. Additionally the synthesis method using controlled precursor addition provides a useful route to achieve an alternative particle diameter while maintaining narrow PSD, without any subsequent classification.

In future work it would be beneficial to create and assess SOS particles modified with alternative surface functionality, for example ion exchange, HILIC or diol phases which would provide alternative modes of separation for protein samples. Preliminary work towards this has been initiated through collaboration with the Centre for Gene Regulation and Expression, University of Dundee. HPLC columns packed with SOS particles bonded with diol and anion exchange phases were supplied for the analysis of proteins and other large biomolecules, although no results have yet been reported.

4.6 References

1. L. R. Snyder, J. J. Kirkland and J. W. Dolan, *Introduction To Modern Liquid Chromatography*, John Wiley & Sons, 2011.
2. M. S. Tswett, *Proceedings of the Warsaw Society of Naturalists, Biology Section*, 1905, **14**, 20-39.
3. R. Willstätter and A. Stoll, *Untersuchungen Über Chlorophyll; Methoden Und Ergebnisse*, J. Springer, Berlin, 1913.
4. A. J. P. Martin and R. L. M. Synge, *Biochemical Journal*, 1941, **35**, 1358-1368.
5. G. A. Howard and A. J. P. Martin, *Biochemical Journal*, 1950, **46**, 532-538.
6. J. C. Giddings, *Dynamics of Chromatography: Principles and Theory*, Taylor & Francis, 2002.
7. J. F. K. Huber, *Journal of Chromatographic Science*, 1969, **7**, 85-90.
8. B. L. Karger, *Journal of Chemical Education*, 1997, **74**, 45.
9. R. K. Iler, *The Chemistry of Silica: Solubility, Polymerization, Colloid and Surface Properties and Biochemistry of Silica*, Wiley, 1979.
10. G. Guiochon and F. Gritti, *Journal of Chromatography A*, 2011, **1218**, 1915-1938.
11. N. Wu and A. M. Clausen, *Journal of Separation Science*, 2007, **30**, 1167-1182.
12. P. Bristow and J. Knox, *Chromatographia*, 1977, **10**, 279-289.
13. S. Heinisch and J. L. Rocca, *Journal of Chromatography A*, 2009, **1216**, 642-658.
14. A. Tiselius and D. Claesson, *Arkiv För Kemi, Mineralogi Och Geologi*, 1942, **15B (No. 18)**.
15. E. Johnson, A. Abu-Shumays and S. R. Abbott, *Journal of Chromatography A*, 1977, **134**, 107-119.
16. J. S. Fritz and D. T. Gjerde, *Ion Chromatography*, Wiley, 2009.

17. P. Kissinger and W. R. Heineman, *Laboratory Techniques in Electroanalytical Chemistry, Second Edition, Revised and Expanded*, Taylor & Francis, 1996.
18. M. Swartz, *LCGC North America*, 2010, **28**.
19. C. G. Horvath and S. R. Lipsky, *Nature*, 1966, **211**, 748-749.
20. Y. A.-E. Hassan and S. Vince, *Photodiode-Array Detection*, Taylor & Francis, 2009.
21. R. E. Ardrey, *Liquid Chromatography - Mass Spectrometry: An Introduction*, Wiley, 2003.
22. J. B. Fenn, M. Mann, C. K. Meng, S. F. Wong and C. M. Whitehouse, *Science*, 1989, **246**, 64-71.
23. W. M. A. Niessen, *Liquid Chromatography-Mass Spectrometry, Third Edition*, CRC Press, 2006.
24. A. S. Said, *Theory and Mathematics of Chromatography*, Hüthig, 1981.
25. L. S. Ettre, *Journal of High Resolution Chromatography*, 1993, **16**, 258-261.
26. J. J. van Deemter, F. J. Zuiderweg and A. Klinkenberg, *Chemical Engineering Science*, 1956, **5**, 271-289.
27. H. Poppe, *Journal of Chromatography A*, 1997, **778**, 3-21.
28. G. Desmet, D. Clicq and P. Gzil, *Analytical Chemistry*, 2005, **77**, 4058-4070.
29. G. Desmet, D. Clicq, D. T. T. Nguyen, D. Guillarme, S. Rudaz, J.-L. Veuthey, N. Vervoort, G. Torok, D. Cabooter and P. Gzil, *Analytical Chemistry*, 2006, **78**, 2150-2162.
30. J. C. Giddings, *Analytical Chemistry*, 1967, **39**, 1027-1028.
31. J. W. Dolan, L. R. Snyder, N. M. Djordjevic, D. W. Hill and T. J. Waeghe, *Journal of Chromatography A*, 1999, **857**, 1-20.
32. S. A. C. Wren, *Journal of Pharmaceutical and Biomedical Analysis*, 2005, **38**, 337-343.
33. X. M. Lu, K. Benedek and B. L. Karger, *Journal of Chromatography A*, 1986, **359**, 19-29.
34. J. W. Eschelbach and J. W. Jorgenson, *Analytical Chemistry*, 2006, **78**, 1697-1706.
35. M. Gilar and U. D. Neue, *Journal of Chromatography A*, 2007, **1169**, 139-150.
36. L. R. Snyder, M. Stadalius and M. A. Quarry, *Analytical Chemistry*, 1983, **55**, 1412A-1430.
37. S. Yamamoto, M. Nakamura, C. Tarmann and A. Jungbauer, *Journal of Chromatography A*, 2007, **1144**, 155-160.

38. B. G. Belenkii, A. M. Podkladenko, O. I. Kurenbin, V. G. Mal'tsev, D. G. Nasledov and S. A. Trushin, *Journal of Chromatography A*, 1993, **645**, 1-15.
39. S. Terabe, H. Nishi and T. Ando, *Journal of Chromatography A*, 1981, **212**, 295-304.
40. R. Skudas, B. A. Grimes, E. Machtejevas, V. Kudirkaite, O. Kornysova, T. P. Hennessy, D. Lubda and K. K. Unger, *Journal of Chromatography A*, 2007, **1144**, 72-84.
41. J. J. DeStefano, T. J. Langlois and J. J. Kirkland, *Journal of Chromatographic Science*, 2008, **46**, 254-260.
42. U. D. Neue, T. H. Walter, B. A. Alden, Z. Jiang, R. P. Fisk, J. T. Cook, K. H. Glose, J. L. Carmody, J. M. Grassi and Y. Cheng, *American Laboratory*, 1999, **31**, 36-39.
43. Y.-F. Cheng, T. H. Walter, Z. Lu, P. Iraneta, U. D. Neue, J. M. Grassi and J. L. Carmody, *LCGC*, 2000, **11**, 1162-1172.
44. A. Ahmed, H. Ritchie, P. Myers and H. Zhang, *Advanced Materials*, 2012, **24**, 6042-6048.
45. K. Weierstrass, *Mathematische Werke*, 1895, 71-74.
46. G. Cantor, *Mathematische Annalen*, 1883, **21**, 545-591.
47. F. Klein and R. Fricke, *Leipzig: Teubner*, 1897.
48. H. Poincaré, *Acta Mathematica*, 1890, **13**, 1-270.
49. H. v. Koch, *Arkiv for Matematik*, 1904, **1**, 681-704.
50. G. Julia, *Journal de Mathématiques Pures et Appliquées*, 1918, **8**, 47-425.
51. P. Fatou, *Comptes Rendus de l'Académie des Sciences de Paris*, 1917, **164**, 806-808.
52. B. B. Mandelbrot, *Annals of the New York Academy of Sciences*, 1980, **357**, 249-259.
53. B. Mandelbrot, *Fractals, Chance and Dimension*, WH Freeman & Co., San Francisco, 1977.
54. P. Pfeifer and D. Avnir, *The Journal of Chemical Physics*, 1983, **79**, 3558-3565.
55. P. Pfeifer and D. Avnir, *The Journal of Chemical Physics*, 1984, **80**, 4573-4573.
56. A. V. Neimark and K. K. Unger, *Journal of Colloid and Interface Science*, 1993, **158**, 412-419.
57. F. Gritti and G. Guiochon, *Journal of Chromatography A*, 2011, **1218**, 907-921.
58. C. R. Wilke and P. Chang, *AIChE Journal*, 1955, **1**, 264-270.
59. S. Fekete, R. Berky, J. Fekete, J.-L. Veuthey and D. Guillarme, *Journal of Chromatography A*, 2012, **1236**, 177-188.
60. S. Fekete and D. Guillarme, *Journal of Chromatography A*, 2013, **1308**, 104-113.

61. S. A. Schuster, B. M. Wagner, B. E. Boyes and J. J. Kirkland, *Journal of Chromatography A*, 2013, **1315**, 118-126.

62. J. S. Baker, J. C. Vinci, A. D. Moore and L. A. Colón, *Journal of Separation Science*, 2010, **33**, 2547-2557.

63. R. A. Everley and T. R. Croley, *Journal of Chromatography A*, 2008, **1192**, 239-247.

64. M. Shibue, C. T. Mant and R. S. Hodges, *Journal of Chromatography A*, 2005, **1080**, 58-67.

65. M. Shibue, C. T. Mant and R. S. Hodges, *Journal of Chromatography A*, 2005, **1080**, 68-75.

66. S. Fekete, M. Rodriguez-Aller, A. Cusumano, R. Hayes, H. Zhang, T. Edge, J.-L. Veuthey and D. Guillarme, *Journal of Chromatography A*, 2016, **1431**, 94-102.

67. B. Wiggins, L. Liu-Shin, H. Yamaguchi and G. Ratnaswamy, *Journal of Pharmaceutical Sciences*, 2015, **104**, 1362-1372.

5 Alternative Morphologies

5.1 Introduction

In chapter 2 the role of each reagent within the one-pot SOS reaction was investigated to assess the effect on resultant particle morphology by changing reagent type, concentration or molecular weight. In these studies many alternative structures have been observed, for example aggregated and irregular particles, smooth spheres of various diameter, particles with rough surface and cluster-type particles.

So far, the experimental work in this thesis has been focussed on the production, optimisation and assessment of SOS-type materials, with less emphasis on the other morphologies that have been synthesised. The experimental work in this chapter will describe the formation of several interesting alternative particles structures and chromatographic applications of these, where applicable.

5.2 Experimental

5.2.1 Chemicals

Ammonium fluoride (≥98%), ammonium hydroxide (28-30%, NH_3 basis), BSA, carbonic anhydrase, CTAB (≥98%), HPLC peptide standard mixture, imidazole (≥99%), insulin, lysozyme, MPTMS (95%), myoglobin, nitric acid (ACS reagent, 70%), ovalbumin, potassium dihydrogen phosphate (≥99%), PVP (M_W = 10k, 29k, 55k), ribonuclease A, TEOS (98%), TFA (99%), thyroglobulin, TMSI (≥98%) and tridecane (>99%) were purchased from Sigma-Aldrich. Butyl(chloro)dimethyl silane (C4 reagent, >97%) was purchased from Tokyo Chemical Industry. Acetonitrile, chloroform, methanol, isopropanol and toluene (all HPLC grade) were obtained from Fisher Scientific. All chemicals were used as received. Deionised water and Milli-Q water (18 MΩ) were prepared in the laboratory.

5.2.2 Particle Synthesis

All reactions were performed at room temperature on a magnetic stirrer plate. Stirring was performed using a Teflon coated stirrer bar. Brand new glassware was used for each reaction. The specific modifications compared to the optimised reaction will be described in the results section of this chapter, however the optimised synthesis method for SOS particles is also included below for reference.

PVP (M_W = 10k, 0.25 g) and CTAB (0.0125 g) were dissolved in deionised water (5 mL). Methanol (8 mL) was added, followed by diluted ammonium hydroxide (1.4%, 2 mL). The solution was stirred for 15 minutes, before addition of MPTMS (400 µL). The reaction was stirred overnight. SOS particles were collected on a sintered glass filter and washed with distilled water (5 x 20 mL), then methanol (5 x 20 mL) before drying under vacuum at 60 °C. Particles were calcined using a Carbolite CWF1200 furnace. Conditions: heat in air at 1 °C/min, hold at set temperature for 12 hours, then allow to cool to room temperature.

5.2.3 Bonding Using Microwave Irradiation

Prior to bonding, calcined particles were rehydroxylated using nitric acid as in the method described in section 3.3.3, chapter 3. All microwave reactions were performed on a CEM Explorer microwave reactor in 35 mL reaction vessels.

For 1 g of material, the particles were dispersed in toluene (7.5 mL) with sonication in a 35 mL reaction vessel. A rare earth stirrer bar, imidazole (0.1 g) and C4 reagent (0.4 g) were added and the vessel sealed. Reagent amounts were adjusted according to the mass of silica starting material, the ratio was kept constant. As in previous studies a dynamic closed vessel method was used. The reaction was run at 120 °C for 20 minutes using a high stir speed. Resultant particles were washed on a sintered glass filter with toluene (40 mL), methanol (40 mL), methanol/water (1:1 V/V, 40 mL) and methanol (40 mL). Particles were first dried in air on the filter for 1 hour, then under vacuum at 80 °C overnight. Endcapping was performed using the same method with TMSI in place of the C4 reagent and the omission of imidazole.

5.2.4 Column Packing

Functionalised particles were packed into 50 mm stainless steel narrow bore columns with 2.1 mm internal diameter, sealed with 0.5 µm porous titanium frits. The silica suspension was prepared by dispersing functionalised particles (0.3 g) in a slurry solution. The column was packed at 600 bar using methanol (60 mL).

5.2.5 Characterisation

Particle sizing was measured using a Beckman Coulter Multisizer 3. Particle images were obtained using a Hitachi S4800 SEM. Measurement of BET surface area[1] was performed by nitrogen adsorption at 77 K, using a Micromeritics ASAP 2420 or Quantachrome NOVA 4200e adsorption analyser. Pore size distributions were calculated from BJH desorption data.[2] Samples were degassed overnight at 120 °C before analysis. Chromatographic data was obtained using a Thermo Scientific Accela UPLC system, with data analysis performed using ChromQuest 5.0 software, version 3.2.1.

5.3 Results and Discussion

5.3.1 Incorporation of TEOS

The synthesis of particles so far has discussed only a single silica precursor, MPTMS. However there are numerous examples in the literature where TEOS is commonly used to prepare silica particles using the Stöber reaction.[3-6] A set of reaction conditions was attempted where TEOS was added in a second step after the initial volume of MPTMS to assess any difference in particle morphology, specifically if any additional nanoparticle growth occurs on the surface. Each reaction was prepared using the optimised method above, followed by the secondary addition of 100 µL TEOS after 10, 20, 30 and 60 minutes. The SEM images of resultant particles are shown in figure 5.1.

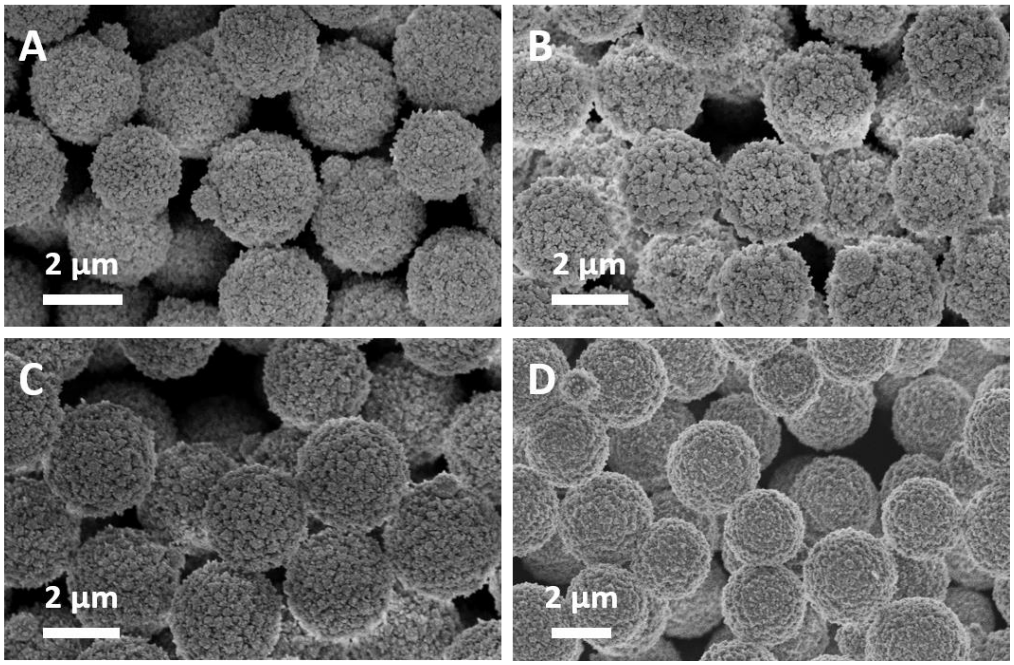

Figure 5.1 SEM images of particles produced from the optimised reaction plus secondary addition of 100 µL TEOS after 10 (A), 20 (B), 30 (C) and 60 minutes (D).

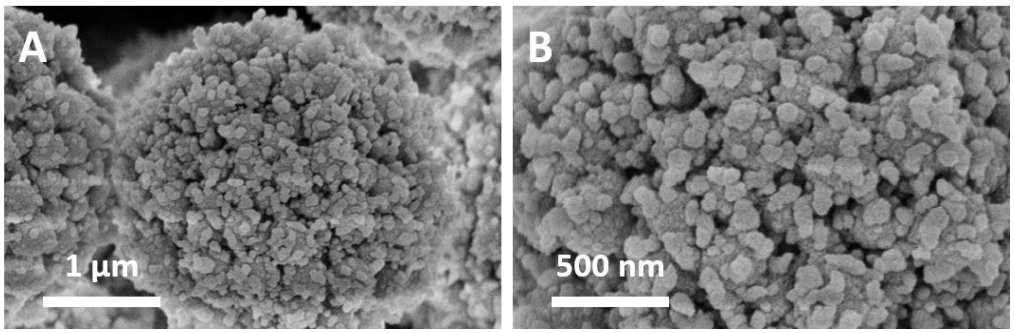

Figure 5.2 SEM images showing detail of surface morphology following secondary TEOS addition after 20 minutes.

High surface aggregation was observed for the three reactions when TEOS was added after 10, 20 and 30 minutes. The close-up SEM images in figure 5.2 show the surface morphology in detail for one reaction where TEOS is added after 20 minutes. TEOS addition after 60 minutes led to a small amount of additional growth but these particles were more alike to regular SOS particles. An observation from this study is that the nitrogen BET surface areas after calcination at 550 °C for the shortest addition times were found to be

significantly lower than for the 60 minute addition: 10 min, 27.7 m^2/g; 20 min, 32.5 m^2/g; 30 min, 24.4 m^2/g; 60 min, 233.6 m^2/g.

A second set of reactions was performed, similar to the previous study however in this case a mixture of TEOS and MPTMS (100 µL, 50:50 V/V) was added in the second step. The SEM images are shown in figure 5.3. Again, the greatest surface aggregation was observed for the shortest secondary addition times of 10 and 20 minutes. An explanation for this is that the shell growth is still proceeding at this time and further precursor addition at this point is providing more reagent to grow more shell particles.

This set of reactions was then repeated, with the volume of the secondary addition increased to 200 µL. SEM images are shown in figure 5.4. In this case a degree of particle aggregation was observed for the 10 and 20 minute reactions while the longer additions times of 30 and 60 minutes led to a number of broken and irregular particles. In the case of addition after 10 and 20 minutes this shows that further addition is detrimental to the morphology as excessive growth may cause particles to fuse together. In the case of 30 and 60 minutes it shows that excessive addition may also destabilise the reaction.

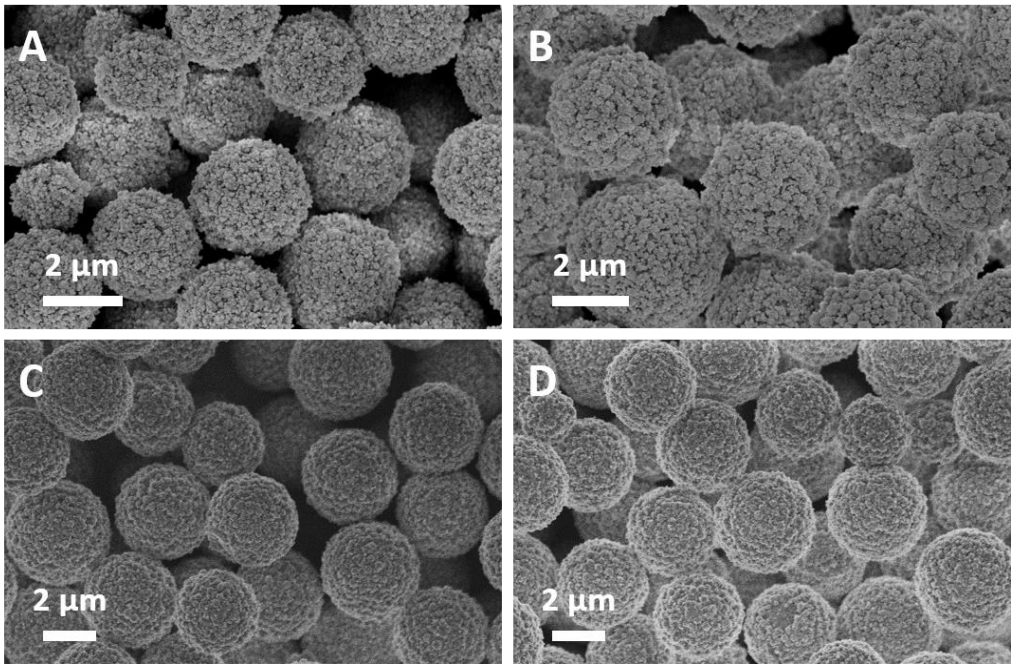

Figure 5.3 SEM images of particles produced from the optimised reaction plus secondary addition of 100 µL TEOS:MPTMS (50:50, V/V) after 10 (A), 20 (B), 30 (C) and 60 minutes (D).

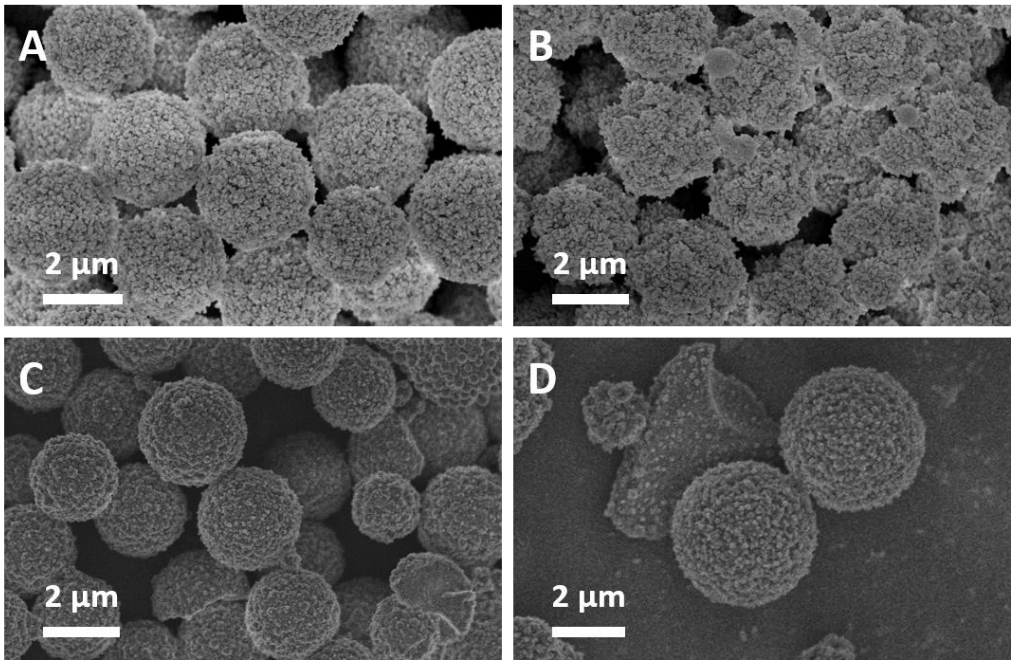

Figure 5.4 SEM images of particles produced from the optimised reaction plus secondary addition of 200 µL TEOS:MPTMS (50:50, V/V) after 10 (A), 20 (B), 30 (C) and 60 minutes (D).

The BET surface area measurements after calcination at 550 °C for these particles show the same trend as the first study where the 60 minute secondary addition time results in a much larger value. 100 µL secondary addition: 10 min, 24.5 m^2/g; 20 min, 34.1 m^2/g; 30 min, 18.4 m^2/g; 60 min, 216.3 m^2/g. 200 µL secondary addition: 10 min, 18.6 m^2/g; 20 min, 28.1 m^2/g; 30 min, 34.4 m^2/g; 60 min, 159.4 m^2/g. From these experiments alone the cause of this is unclear.

TEOS was also tested as a direct replacement for MPTMS using the optimised reaction conditions to determine whether SOS particles could be produced from this precursor alone. SOS morphology was not observed, but instead partially fused, smooth spheres were produced, shown in figure 5.5 A. A mixture of precursor was instead attempted, with ratios of 75:25, 50:50 and 25:75 TEOS:MPTMS (V/V) used, added in a single addition step. The total volume of precursor used in each reaction was 400 µL. The SEM images are shown in figure 5.5 B-D. Instead of an SOS-type morphology as seen in the previous examples, there are irregular protrusions surrounding the core microsphere. The clearest examples of this were seen when using a mixture containing 50 or 75% MPTMS. The surface morphology is shown in figure 5.6.

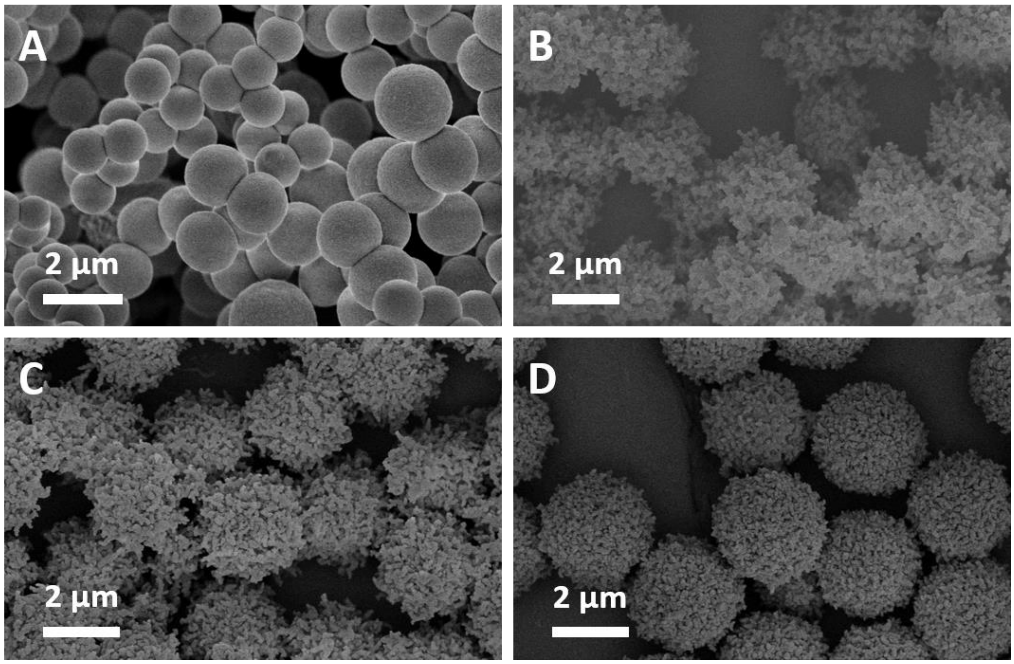

Figure 5.5 SEM images of particles produced from the optimised reaction, with varying ratio of TEOS:MPTMS (V/V). TEOS only (A), 75:25 (B), 50:50 (C) and 25:75 (D).

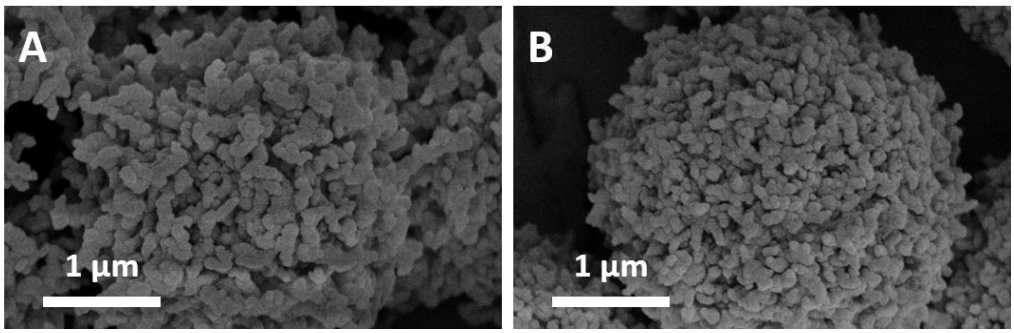

Figure 5.6 SEM images showing detail of surface morphology from addition of 50:50 TEOS:MPTMS (A) and 25:75 TEOS:MPTMS (B).

As in the previous reactions the BET surface area following calcination at 550 °C was found to be lower than expected for all samples, with values between 18 and 35 m^2/g obtained. One explanation is that TEOS may fill the largest of the pores formed during particle synthesis. A set of reactions were prepared to test this theory, where 400 uL MPTMS was initially added, followed by a varied amount of TEOS in a second step after 10 minutes. The results of the measured BET surface area after calcination at 550 °C are shown in figure 5.7, displaying a trend of decreasing surface area with increasing TEOS.

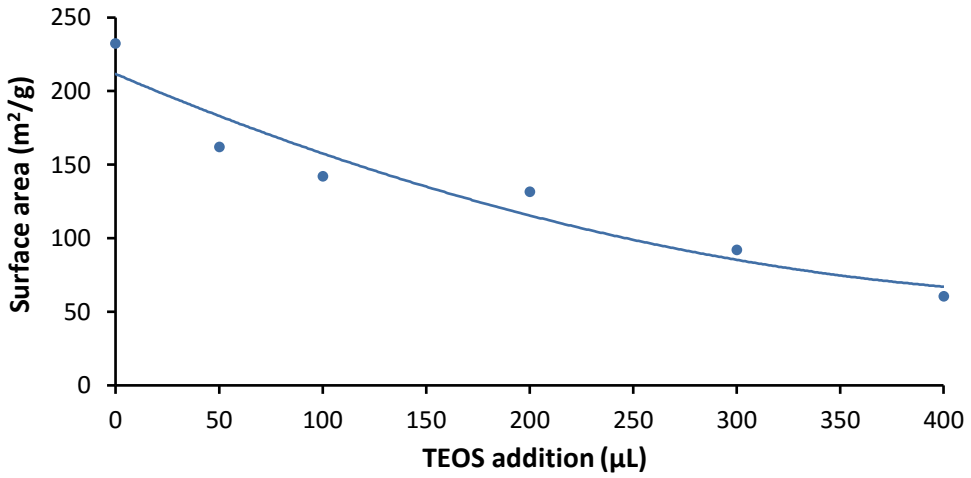

Figure 5.7 Reduction in surface area with increasing secondary addition of TEOS.

5.3.2 Cluster Particles

Interesting results were observed when changing the molecular weight of PVP in the reaction where a 50:50 mixture of TEOS and MPTMS precursor was used. A change from 10k to 29k PVP in 5% concentration led to particles with long protrusions from the surface. Additionally many of the particles were fused together due to the surface growth. Reducing the concentration of PVP (29k) to 2 and 1% led to smaller particles which were more irregular and cluster-like. The morphologies are shown in figure 5.8 A-C.

Increasing the molecular weight of PVP to 55k led to difficulties in dissolving the polymer in 5% concentration, therefore the reactions were performed using 2, 0.5 and 0.25%. The SEM images in figure 5.8 D-F again show that irregular cluster-like particles are produced, with the morphology becoming smoother and more spherical with a reduction in polymer concentration. The most interesting result from this particular study however was observed when using PVP (55k) in 1% concentration. The cluster-type particles that are produced from these conditions resemble a monolithic silica column which has been crushed into smaller pieces. The SEM images are shown in figure 5.9.

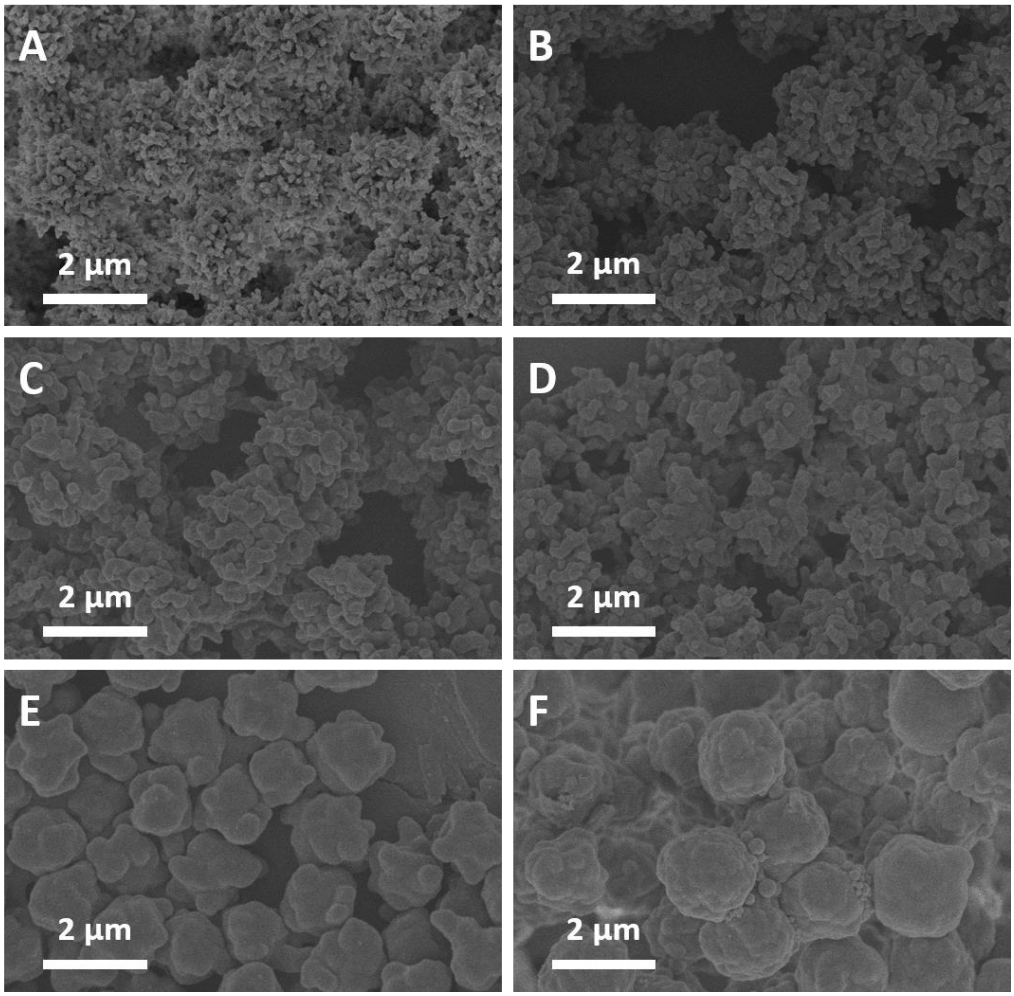

Figure 5.8 SEM images of particles produced from TEOS:MPTMS when changing molecular weight and concentration of PVP. M_W = 29k: 5% (A), 2% (B), 1% (C). M_W = 55k: 2% (D), 0.5% (E), 0.25% (F).

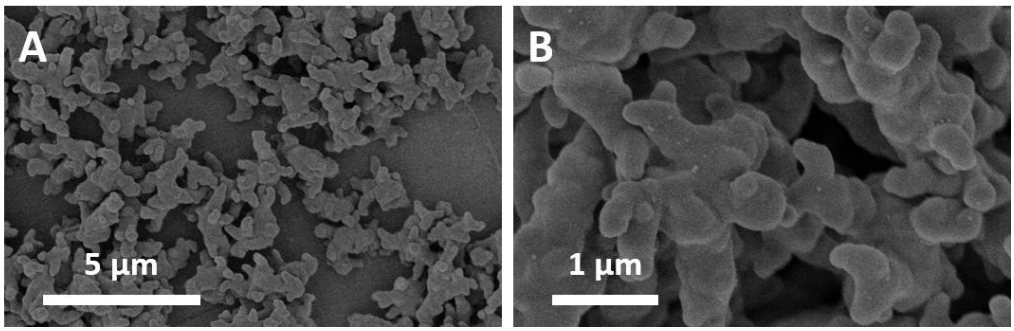

Figure 5.9 SEM images of cluster-type particles produced when using PVP (55k) in 1% concentration in the optimised synthesis reaction.

Due to the particle morphology resembling that of a broken up monolith, it was predicted that the material may form a monolithic structure when packed into a HPLC column, potentially creating a macroporous network. The reaction conditions to form the cluster particles shown in figure 5.9 were scaled up by 50 times to produce sufficient material for bonding and packing into HPLC columns. The resultant cluster particles were functionalised with a C4 ligand and endcapped using the microwave bonding method described in section 5.2.3. The BET surface area following calcination at 550 °C was measured to be 137 m^2/g. Carbon loading was 3.06%, equating to surface coverage of 3.26 $\mu mol/m^2$. Particles were packed into 50 × 2.1 mm HPLC columns using a slurry solution of 72:8:20 chloroform:methanol:isopropanol (V/V/V, 30 mL).

One column was carefully unpacked as a cylindrical rod, then cut into smaller sections to provide images of the packing structure and to confirm if the material forms a macroporous network as predicted. The SEM images are shown in figure 5.10. It can be seen in the close-up images that some large pores between particles are visible although the pore size was impossible to directly measure by mercury intrusion due to the fragile nature of the rod.

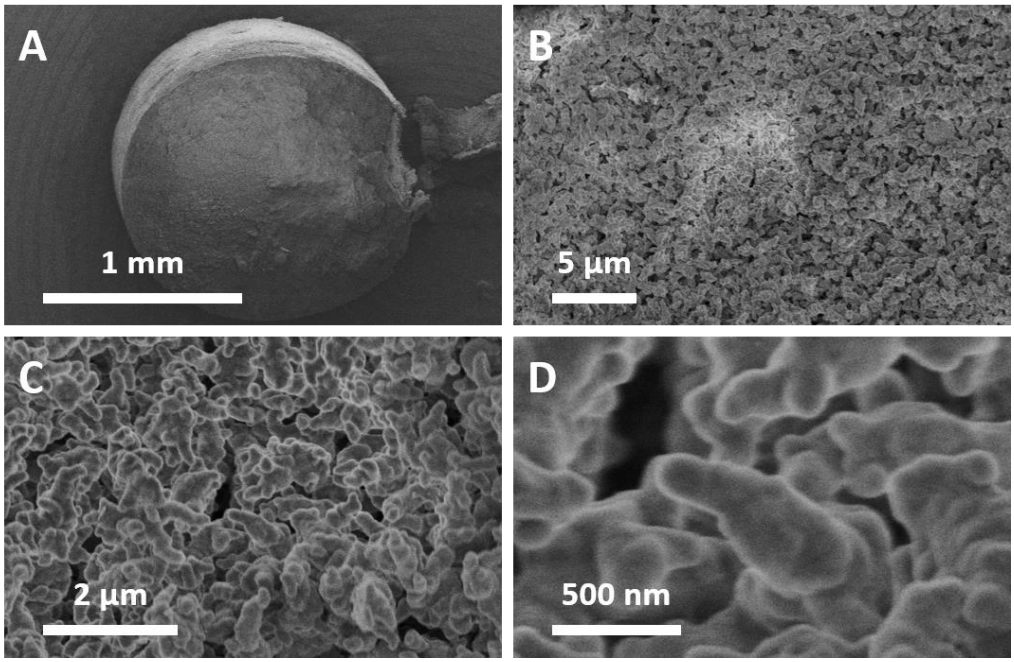

Figure 5.10 SEM images showing packing structure of clusters in the HPLC column. The packed rod is imaged at various zoom levels to show rod structure (A), overview of packing structure (B) and close-up of the pore system generated (C, D).

The HPLC column packed with Cluster-C4 particles was used to separate the peptide standard mixture using a linear gradient method. The test mixture contained angiotensin II, GY, leu-enk, met-enk and VYV, each in 80 µg/mL concentration, made up in Milli-Q water. Mobile phase A: 0.02 M KH_2PO_4, pH 2.70; B: acetonitrile; gradient: 10-40% B in 4 minutes; flow rate 300 µL/min; temperature: 40 °C; detection: 220 nm; injection volume: 10 µL. The chromatogram is shown in figure 5.11.

The mixture was separated within 2.5 minutes, however the first two peaks (GY and VYV) were found to be coeluting due to their similar retentivity and short length of the column. The elution order was GY/VYV, met-enk, leu-enk and angiotensin II.

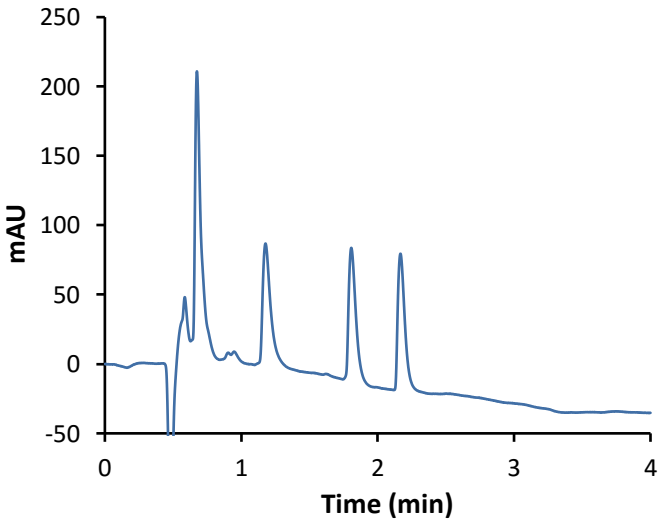

Figure 5.11 Chromatogram showing separation of the peptide standard mixture on Cluster-C4 column.

Due to the potential macroporous interstitial network between particles, it was predicted that the column could provide high performance for the separation of large analytes. The Cluster-C4 column was therefore used to analyse the same individual proteins as tested on the SOS columns, with molecular weights in the range of 6-45 kDa. The test proteins carbonic anhydrase (30 kDa), insulin (6 kDa), lysozyme (14 kDa), myoglobin (17 kDa), ovalbumin (45 kDa) and ribonuclease A (14 kDa) were prepared in 1 mg/mL concentration in Milli-Q water. Each protein was tested individually using a linear gradient method. Mobile phase A: water + 0.1% TFA; B: acetonitrile + 0.1% TFA; gradient:

30-66% B in 8 minutes (gradient steepness 4.5 %/min); flow rate 400 µL/min; temperature: 50 °C; detection: 220 nm; injection volume: 1 µL. The overlaid chromatogram is shown in figure 5.12 A. The column was also used to analyse two large proteins, BSA (66 kDa) and thyroglobulin (669 kDa). The test proteins were prepared in 1 mg/mL concentration in Milli-Q water and analysed individually using the same linear gradient method as above. The chromatogram is shown in figure 5.12 B.

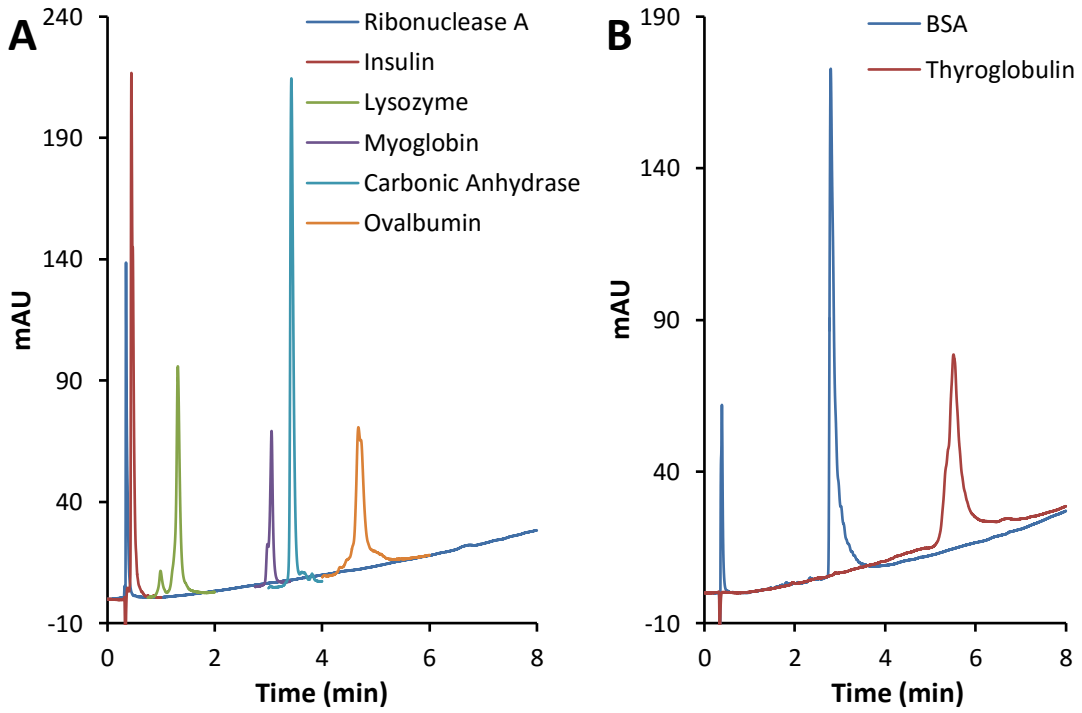

Figure 5.12 Overlaid chromatograms of individual protein separation (A, baselines trimmed for clarity) and large protein separation (B) on the Cluster-C4 column.

The elution order for the 6-45 kDa range of proteins was identical to that obtained with the SOS-C4 columns discussed in the previous chapter. The elution order was ribonuclease A, insulin, lysozyme, myoglobin, carbonic anhydrase and ovalbumin. The retention time of the final peak was shorter compared to the SOS materials, however this can be attributed to the 50 mm column length used in this study. Comparatively shorter retention was also seen for the large proteins BSA and thyroglobulin. The 50 mm column length was chosen due to the size of the particles as it was thought that the small size may result in high operating pressures. However the maximum observed pressure was 90 bar.

This may be expected to double with the column length, resulting in operating pressure similar to the previously tested SOS and core-shell columns (170 and 205 bar).

The peak capacities for the 6-45 kDa proteins were calculated, with an average value of 72 obtained. This is comparable to the SOS-C4-1 material assessed in the previous chapter (P_C = 72), however the resolution between peaks on the SOS column was better, particularly for the first two peaks. This could be improved by using a longer column length. The analysis of the two large proteins resulted in peak capacities of 48 for BSA and 22 for thyroglobulin. This is a little lower than the values obtained from the SOS-C4-1 column (P_C = 56 and 25) but comparable to the Accucore 150-C4 column (P_C = 48 and 16), indicating that there are sufficiently sized pores for large molecule separation.

5.3.3 Uniform Silica Microspheres

In the optimised SOS synthesis method described in section 5.2.2 ammonium hydroxide is used in a low concentration of 1.4% to allow sufficient time for shell formation to occur. Increasing the concentration to 14% significantly increases the reaction rate and prevents secondary nucleation from occurring. In this case, smooth microspheres are instead produced which retain the uniformity observed for SOS particles. The reaction was scaled up by 10 times to form enough material for characterisation and subsequent modification. The mean diameter was measured to be 3.19 µm with a $d^{90}/_{10}$ ratio of 1.49. The SEM images and PSD are shown in figure 5.13 A-C.

The size and dispersity of these particles are ideal for use in HPLC, however after calcination at 600 °C the BET surface area was measured to be 42 m^2/g by nitrogen adsorption, with the isotherm plot in figure 5.13 D suggesting a microporous structure.[7] For routine HPLC analysis of small molecules, the packing material should have sufficient surface area to allow high loading capacity and mesopores greater than 6 nm which allow analytes to diffuse into the pore structure. The particles produced from this reaction therefore require further modification if there are to be used for chromatographic purposes.

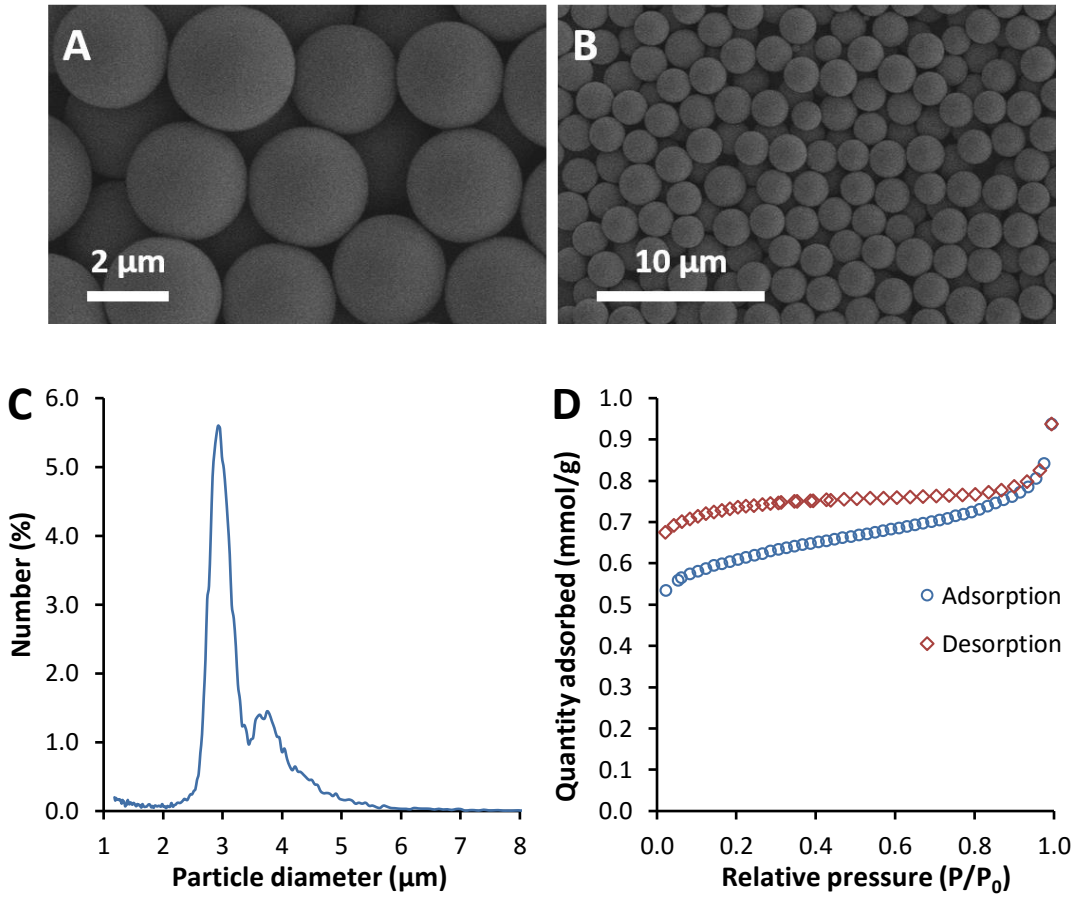

Figure 5.13 Smooth spheres produced from the reaction with increased ammonia concentration. Particle morphology (A) and dispersity (B) are shown by SEM imaging, along with the PSD (C) and nitrogen adsorption plot (D).

To increase the surface area and pore diameter of these particles, a templated dissolution procedure was applied.[8] This method was developed by Dong *et al.* to form mesoporous core-shell particles from non-porous microspheres using CTAC as a template and tridecane as a swelling agent. In this study it was found that the surface area could be increased beyond 1100 m^2/g depending on the reaction time, with typical pore diameters of around 4.5 nm achieved. The pore size did not increase significantly beyond this point regardless of the reaction time due to the size of the templating agent.[8]

The microspheres prepared in this study were treated using the templating method under the following reaction conditions. Calcined particles (1 g) were added to water (100 mL) along with CTAB (1 g) and tridecane (6 mL). The solution was sonicated for 1 hour. Ammonium hydroxide (28%, 6 mL) and ammonium fluoride (25 mg) were added and the

solution heated at 90 °C for 24 hours with stirring. Resultant particles were washed thoroughly with water, then acetone before drying under vacuum at 80 °C.

Following the pore expansion treatment the BET surface area of the modified particles was increased from 42 to 377 m^2/g. The nitrogen isotherm plot in figure 5.14 A shows a type IV curve, typically seen for mesoporous materials.[7] The plot of pore size distribution shown in figure 5.14 B confirms the presence of mesopores, with an indicated pore size of 4 nm.

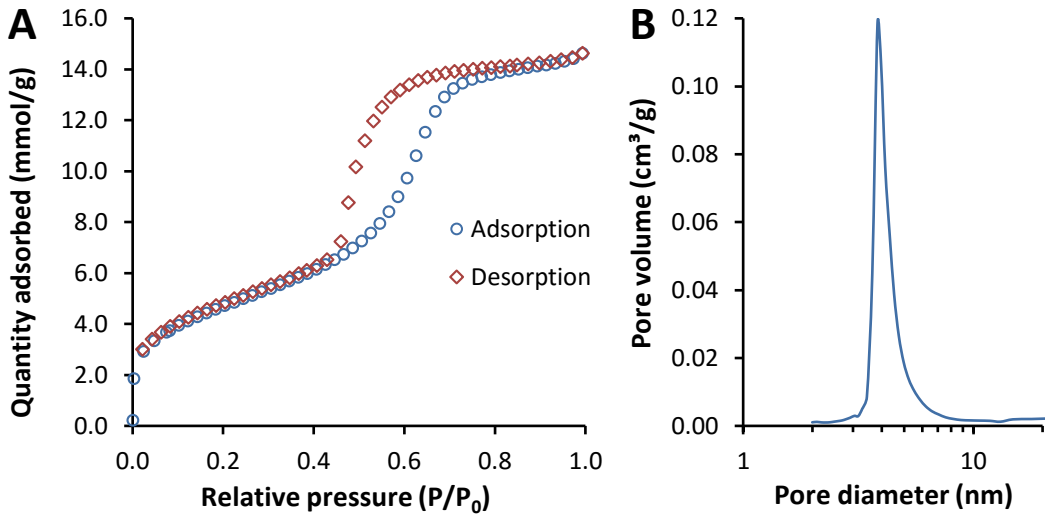

Figure 5.14 Nitrogen isotherm (A) and pore size distribution (B) of silica particles following pore expansion treatment.

The synthesis and subsequent modification to these particles has potential to provide a fast, simple alternative to the current methods of producing mesoporous silica suitable for chromatographic use. Acceptable PSD ($d^{90}/_{10}$ <1.5) is achieved in a one-pot reaction which removes the need for time-consuming and wasteful classification steps, while the particle diameter of around 3 µm is ideal for use in HPLC. Although the pore size of 4 nm is possibly too small for routine HPLC analysis, the templating method was successful in introducing porosity into the particles. Modification to the method, for example with larger templates, may allow formation of larger mesopores in future study.

5.4 Conclusion

While the use of TEOS as a direct replacement for MPTMS in the SOS synthesis method leads to the formation of smooth spheres only, its inclusion in a secondary addition step or as a mixture with MPTMS has led to a number of alternative morphologies. When TEOS is introduced in a secondary addition step, fractal-type particles with high amounts of surface growth were obtained up to a secondary addition time of 30 minutes. Likewise the secondary addition of 100 µL TEOS:MPTMS also formed fractal particles. In both cases less surface growth was observed with increasing time between initial and secondary addition.

When increasing the amount of secondary addition to 200 µL, the resultant particles displayed a similar amount of surface growth for intervals of 10 and 20 minutes. However several particles were fused together, particularly for the 20 minute reaction indicating that the increased volume of additional precursor is detrimental to the morphology, causing fusing rather than growth onto discreet particles. Increasing the time for secondary addition to 30 and 60 minutes led to the formation of broken and irregular particles suggesting that excessive addition may also have a destabilising effect on the reaction.

An observation from these reactions is that the surface area after calcination at 550 °C is quite low (18-35 m^2/g) for all reactions where the secondary addition is performed within 30 minutes. For the 60 minute reactions the surface area is significantly higher (159-234 m^2/g). A further set of reactions was performed with increasing secondary TEOS addition after 10 minutes which showed a trend of decreasing surface area as the amount of TEOS was increased. An explanation is that TEOS blocks some of the pore structure during early stages of particle synthesis, but is not able to do so after 60 minutes. This is perhaps due to the stage of particle formation. It would be beneficial in future study to isolate samples of the particles at intervals during the reaction for SEM imaging and assess any morphology difference between 30 and 60 minutes to explain this further.

Mixtures of TEOS and MPTMS were also used in place of MPTMS in the optimised SOS reaction conditions, added in a single step. Formation of a core microsphere is still observed, but unlike SOS particles the shell structure is made up of irregular clustered structures rather than nanospheres. This is interesting as there may be additional porosity created by these surface growths. Further modification to this reaction using alternative molecular weights of PVP at different concentrations led to the formation of various types

of cluster particles. The most interesting of these was obtained when using 1% PVP (M_W = 55k) and a 50:50 mixture of TEOS:MPTMS. In this case small irregular clusters were formed which were further assessed for functionalisation and packing into HPLC columns.

From the SEM images it appears that the structure of the packed cluster particles leads to the formation of large through-pores within the column, alike to a monolithic material. When functionalised with a C4 group the column provided fast analysis of a variety of proteins, with comparable peak capacity values to the previously tested SOS materials. The material is interesting as an alternative to monolithic columns as cluster particles are easily generated from a one-pot reaction as opposed to formation of a monolith within the column itself. This removes the issue of shrinkage and detachment from the column wall and also the need to clad the monolithic rod. Instead, a slurry packing method can be employed which ensures there are no significant voids between the packed material and column wall. The synthesis method provides a degree of control over the particle morphology and with further development could potentially lead to reproducible packed monolith columns.

A method of producing uniform smooth microspheres has also been described. By increasing the concentration of ammonia in the optimised SOS synthesis, the reaction rate is increased and shell growth is prevented, leading to the formation of smooth particles only. The size and dispersity of these particles is ideal for use in HPLC and the scale up of this reaction should be assessed as this method has the potential to produce uniform silica microspheres from a one-pot reaction. In the commercial manufacture of porous silica particles, reaction sizes may be as large as 50 litres in volume, producing kilogram scale batches of unclassified particles. However, following subsequent washing, treatment and classification, the yield is significantly reduced. This highlights the advantage of a one-pot method which does not require classification, which may lead to a faster production process with reduced waste.

The particles produced from this method have been shown to be microporous. However treatment with templating and swelling agents has been shown to increase the pore size into the mesoporous range. The obtained pore size in this study was limited to around 4 nm by the template and swelling agent which may be too small for use for HPLC applications. In future study, larger templates and alternative swelling agents could therefore be assessed in this method. For example dihexadecyldimethylammonium bromide (DiCTAB) has successfully been used as a templating agent with 1,3,5-

trimethylbenzene and N,N-dimethyldecylamine as swelling agents in previous studies,[6] leading to pore diameters up to 6.5 nm. Similarly, pore sizes of up to 9.6 nm could be obtained using high molecular weight Jeffamine type surfactants.[9]

5.5 References

1. S. Brunauer, P. H. Emmett and E. Teller, *Journal of the American Chemical Society*, 1938, **60**, 309-319.
2. E. P. Barrett, L. G. Joyner and P. P. Halenda, *Journal of the American Chemical Society*, 1951, **73**, 373-380.
3. W. Stöber, A. Fink and E. Bohn, *Journal of Colloid and Interface Science*, 1968, **26**, 62-69.
4. G. H. Bogush and C. F. Zukoski, *Journal of Colloid and Interface Science*, 1991, **142**, 1-18.
5. A. van Blaaderen and A. Vrij, *Journal of Colloid and Interface Science*, 1993, **156**, 1-18.
6. A. Ahmed, R. Clowes, E. Willneff, H. Ritchie, P. Myers and H. Zhang, *Industrial & Engineering Chemistry Research*, 2009, **49**, 602-608.
7. P. B. Balbuena and K. E. Gubbins, *Langmuir*, 1993, **9**, 1801-1814.
8. H. Dong and J. D. Brennan, *Journal of Materials Chemistry*, 2012, **22**, 13197-13203.
9. K. Skinley, PhD thesis, University of Liverpool, 2012.

6 Conclusion

In recent years there has been renewed interest in particle technology for HPLC, mainly due to the introduction of modern core-shell particles in 2007. Prior to this there was little development in the morphology of silica particles beyond reducing the particle diameter from 10 µm and 5 µm through the 1970s and 3 µm in the 1980s to sub-2 µm materials in the 2000s. As such there has been no significant evolution in the basic structure of particles, only modification of properties such as the pore size, surface area and bonded phases. Even when examining core-shell particles, the pore structure is found to be very similar to that of totally porous materials, the only difference being that the total porosity is much lower due to the solid core.

Many of the advances in chromatographic performance have been reliant on reducing the particle size with the expectation that LC instrumentation should also evolve to be able to utilise such materials. The modern generation of core-shell particles broke this trend with the introduction of 2.7 µm particles, released to the fanfare of sub-2 µm performance with the operating pressure of 3 µm materials, allowing their use on regular HPLC instruments. However the latest advancements in core-shell technology appear to be following the same evolution path as for totally porous particles, with the recent introduction of sub-2 um core-shell materials. There is clearly a limit on how far this can be taken: either how far the particle size can be reduced, or the ability and cost-effectiveness of developing instrumentation capable of handling the operating pressures associated with smaller particles.

It is clear that the development of entirely new materials is required in order to create the next generation of particles for LC. Whether these materials are based on silica, polymer, MOF, or a combination of these remains to be seen. The discovery of SOS particles is interesting as it represents a move away from the typical porous structure found in core-shell and totally porous silica. Instead the unique morphology provides an alternative type of interstitial porosity despite the silica surface itself being effectively non-porous to analytes.

The experimental work in chapter 2 has investigated the basic production of SOS materials, observing the various effects on morphology from changing the reaction conditions. It became apparent that the resultant morphology is extremely sensitive to concentration and type of reagent used. Polymer (PVA or PVP) and surfactant (CTAB) were

both found to be essential in the reaction to produce SOS particles, however when used in a concentration outside of an optimal range the SOS morphology was either significantly reduced or lost completely. Likewise, changing the type of reagent also led to a loss of SOS structure. Only two polymers (PVA and PVP) were found to form SOS particles, while the choice of molecular weight was also found to be important, with the best results obtained when using molecular weights of around 9-10k (PVA) and 10k (PVP). The only surfactants that were found to form SOS particles were cetyltrimethylammonium derivatives, with the use of CTAB powder preferred due to the ease of handling.

A key observation is that the PSD showed improvement as the concentration of CTAB was reduced although this also caused a loss of SOS morphology, with smooth spheres formed when CTAB was omitted from the reaction. Likewise the omission of polymer from the reaction also led to small smooth particles, many of which were aggregated. One theory is that the reduction in concentration of these two chemicals results in a reaction solution which is more alike to a Stöber type synthesis, which typically results in the formation of smooth, uniform microspheres. This theory was confirmed with the study of the SOS reaction when omitting both polymer and surfactant, leaving just the four required components of a Stöber reaction: water, alcohol, base and silica precursor. In this case smooth, uniform spheres around 1.5 µm in diameter were produced.

The concentration of ammonium hydroxide was found to have a large effect on the reaction rate, with higher concentration resulting in faster particle formation. The density of the nanoparticle shell was also found to be directly related to the rate of reaction, with increasing shell coverage observed as the concentration of ammonia was reduced. With high ammonia concentration and therefore a fast reaction rate, particle growth proceeds quickly and there is less opportunity for nanoparticle growth upon the core microspheres. Reducing the concentration reduces the reaction rate and provides much more time for surface nucleation to occur, resulting in a denser shell structure.

Through a combination of the effects of changing reagent type and concentration, reaction conditions were determined that allowed the formation of SOS particles around 3 µm in diameter, with a complete single layer shell of nanoparticles around 200 nm in size. Additionally a narrow PSD was obtained with a $d^{90}/_{10}$ ratio of 1.31, well within the target value of <1.5. Scale up of the reaction by 50 times led to formation of particles with near identical surface morphology, mean diameter and equally narrow PSD, highlighting the potential to increase reaction size further and produce SOS materials on a commercial

scale. One key advantage of this optimised method is that there is no need to improve the size distribution with time-consuming classification steps, leading to faster production and improved product yield.

Another observation of the particles produced by this optimised method is the highly spherical nature, aside from the rough surface due to the nanoparticle shell. This can clearly be seen when directly comparing SOS to core-shell particles produced by the LbL method. For core-shell particles produced by numerous layers of nanoparticles being added in multiple steps, it is inevitable that some areas of uneven coverage will occur and result in a non-spherical product. By contrast, the one-pot process for SOS particles results in a uniform shell over the entire core, providing high sphericity.

The optimised synthesis could be further investigated in future work to scale up the reaction to a manufacturing scale to assess the feasibility of a large-scale reaction and observe any morphology changes that may occur. The largest reaction described in this work had a total volume of 770 mL, resulting in a yield of 7.2 g following calcination. Importantly, particles did not show any significant difference in size or morphology from the smaller sized reaction. Final batch sizes for core-shell silica may exceed 500 g, although this may be composed of a blend of different batches. The equipment required for large-scale synthesis of SOS particles would be relatively simple to set up, and a 50 L reaction vessel would allow production of a batch of SOS particles around 450 g in size, although it would be uneconomical to use new glassware each time and a thorough cleaning procedure would need to be developed and applied.

A controlled method of MPTMS addition was attempted using a syringe pump which also led to the formation of highly uniform SOS particles. It was thought that with constant controlled addition the reaction volume would be kept in a homogenous state, resulting in more reproducible particles. In scaled-up reactions pooling of the precursor at the bottom of the vessel had previously been observed for several seconds due to large addition steps via pipette, which may have had an effect on the resultant particle size. While the pipette addition method provided uniform particles, the syringe pump addition was found to improve the PSD further with the lowest observed $d^{90}/_{10}$ ratio of 1.21.

For the controlled addition reactions it was found that to obtain the clearest SOS morphology an initial addition of MPTMS was required to begin particle formation, immediately followed by constant addition using the syringe pump. The best results were

obtained when using an initial volume of 1 mL followed by further addition of 3 mL at 0.065 mL/min. In this case a new type of SOS structure, described as fractal SOS particles, are produced with increased amounts of surface aggregation. Fractal particles are interesting as they possess a degree of self-similarity, creating the possibility of having a surface topography which is essentially homogeneous to solute molecules and potentially increasing the accessible surface area for analytes when bonded and packed into HPLC columns.

The use of TEOS in the synthesis reaction led to further interesting morphologies, discussed in chapter 5. While the use of TEOS alone as a direct replacement led to the formation of smooth spheres, alternative SOS structures were produced with its inclusion as a secondary addition step or as a mixture with MPTMS. For example, fractal SOS particles with high amounts of surface growth could be produced with either TEOS or a mixture of TEOS:MPTMS added in a secondary addition step within 30 minutes of the initial MPTMS addition.

Not all of the products from modification to the reaction possess SOS morphology, and many fascinating alternative structures have been observed. One notable example was the formation of cluster-type particles, created when changing molecular weight and concentration of PVP, and using a mixture of TEOS and MPTMS in a single addition step. The resultant cluster morphology resembled a monolith that had been broken into smaller pieces. It was thought that when packed into a HPLC column the resultant bed structure would form a network of pores, much like a monolith. This was confirmed by SEM imaging of a carefully unpacked rod from the column, which showed a number of large pores between particles. The packing procedure for monoliths is generally quite difficult due to shrinkage and detachment from the column wall, resulting in the requirement to clad the monolithic rod. This type of particle may provide an interesting alternative to monolithic materials, as they can be easily formed from a one-pot reaction and slurry packed into the column ensuring there are no voids between the stationary phase and column wall.

Another interesting outcome from modification to the reaction is the possibility of forming uniform smooth spheres with a mean diameter of 3.19 µm. Large particles are typically difficult to achieve via Stöber synthesis methods, with a maximum particle size of around 800 nm reported. Although the particles are initially microporous, modification using a templating method with CTAB has been shown to increase the pore size into the mesoporous range, with a mean diameter of 4 nm. This synthesis method represents a

potential route to producing totally porous silica particles with narrow PSD without the need for a time-consuming and wasteful classification process. Particles straight out of the reaction have comparable PSD to totally porous particles that have undergone extensive classification, with a $d^{90}/_{10}$ ratio of 1.49. Further investigation into the templating method is required to increase the pore diameter, as pores larger than 6 nm are typically required for routine HPLC analysis of small analytes. This should be possible by using larger templates and swelling agents.

In chapter 3 the suitability of microwave irradiation was assessed as an alternative heating method for the production of silica bonded phases. This has led to a bonding method which facilitates fast, reproducible functionalisation of SOS particles, providing a considerable reduction in reaction time compared to commonly used reflux methods. A reaction time of 20 minutes was found to be optimal for toluene-based reactions, with no increase in carbon loading observed until the reaction time was increased beyond 2 hours. Additionally it was possible to use a technique known as superheating for the microwave reactions, where the reaction can be performed at a temperature above the boiling point of the solvent due to the use of a sealed reaction vessel. It was found that superheating in toluene at 120 °C provides an increase in carbon loading and bonding density compared to reactions at 110 °C.

The C4 bonded SOS particles produced from a 20 minute microwave method were found to have slightly lower bonding densities than those from a 16 hour reflux. However, the variability between repeat reactions was greater for the reflux method. Despite the differences in bonding density, the SOS-C4 materials produced from both microwave and reflux methods provided almost identical performance in the HPLC separation of a protein test mixture. This highlights the vast reduction in reaction time, with a 20 minute reaction representing a 98% reduction in heating time alone. This does not consider the time required to heat the vessel to temperature. The microwave reactor is capable of extremely rapid heating, as high as 125 °C/min was observed for DMF based reactions, which again provides a further time advantage.

As the heating time is significantly reduced, the microwave reactor also provides a massive reduction in power consumption. Although the maximum power output is 300 W, the reactor only requires this amount of power for initial heating. As little as 6 W is required to maintain constant temperature. By comparison, a 600 W hot plate running for 16 hours requires a great deal more power.

The microwave bonding method has been shown to be highly reproducible, both in terms of individual reactions on the same batch of silica and when comparing bonding density between batches. The highest measured RSD for bonding density within each batch was 3.54%, while the RSD between all samples was 4.56%. The reproducibility of these particles when packed into columns was also assessed with HPLC, using a protein test mixture. In total nine columns from three different batches were used. Some variation was observed in the retention times, particularly between batches, however all fell within ±5% of the average for each peak. Differences in the particle morphology were likely to have caused this, as the materials used were produced from the standard reaction rather than the optimised synthesis method that was developed later.

One observation is that lower bonding densities were obtained for SOS-C4 particles compared to commercially available C4 materials. This was noted for both heating methods applied to the SOS material. An explanation is that after calcination at 550 °C micropores are present within the SOS surface, many of which may be inaccessible to bonding reagents. Therefore silanisation only occurs upon the accessible surface area and lower than expected values for carbon loading are seen. This theory can be confirmed by analysing the results from the investigation into alternative bonding solvents. In this case SOS particles were calcined at 600 °C, closing up much of the microporous structure. The accessible surface area did not appear to be reduced as higher bonding densities were achieved, which were directly comparable to commercial materials. For example the highest value obtained for SOS-C4 was 3.48 µmol/m^2, compared to 3.57 µmol/m^2 for the Accucore 150-C4 material.

The experimental results in chapter 3 suggest that microwave bonding is a suitable replacement for conventional reflux heating, with the added benefits of significantly reduced reaction time, associated reduction in energy consumption and improved reproducibility of carbon loading and bonding density values. It has also been shown that depending on the properties and pre-treatment of the SOS silica to be bonded, comparable bonding densities to commercial materials can be achieved. Microwave reactors large enough to accommodate 5 litre vessels are available, and therefore further investigation should be undertaken to increase the reaction size to commercial scale as the method would be highly advantageous in a manufacturing capacity.

The use of SOS particles in HPLC was discussed in chapter 4, where functionalised particles were assessed under isocratic and gradient conditions. In isocratic mode, values

for efficiency, permeability, porosity and impedance were determined for SOS-C4 particles packed into 100 × 2.1 mm HPLC columns. The minimum plate height of 2.90 for butylparaben was higher than expected, especially when compared to commercial core-shell materials which typically have h_{min} of 1.2-1.8. There are two reasons that this may occur. Firstly the retention time for small analytes was found to be very short on the SOS material due to the lack of porosity, demonstrated by the separation of a reversed phase test mixture, leading to a low theoretical plate count. Secondly the quality of column packing could be improved due to limitations of the equipment used.

Total column porosity of the SOS material was found to be slightly lower than for commercial core-shell materials, while the permeability of the packed column was higher. These observations can be attributed to the shallow shell depth, low porosity and the larger particle diameter which results in lower operating pressure than sub-3 µm core-shell materials. The minimum value for impedance was 3440, which is comparable to both commercial core-shell and totally porous materials which typically have values of 2000-5000. The values all suggest that SOS particles are capable of efficient separation. The combination of low porosity and high permeability is beneficial in terms of reducing mass transfer effects of large molecules, which has been shown in the gradient analysis of proteins. The HPLC column packed with fractal-C4 particles was also assessed in isocratic mode, with calculated values for total porosity and permeability that were close to those obtained for normal SOS particles. This is not surprising, given the similarity of the morphology of the two materials. However, lower values for h_{min} and E_{min} were obtained on the fractal column. This is likely to be a result of the smaller particle diameter which provides higher plate count.

The separation of a range of peptides and proteins using gradient conditions was performed using columns packed with SOS particles. In particular the SOS-C8 column provided fast separation of the peptide standard test mixture with sharp, narrow peaks and comparable peak capacity values to the commercial Accucore 150-C4 column. With a modified gradient it was also possible to reduce the analysis time to less than 1.5 minutes on the SOS-C4-1 column, while still maintaining resolution between all peaks.

Comparison studies of SOS-C4-1 and Accucore 150-C4 columns were performed for three test proteins over a range of gradient times between 10 and 90 minutes, and at two flow rates of 250 and 400 µL/min. It was found that the SOS material provided lower peak capacities for myoglobin over the whole gradient span, with most comparable performance

achieved at the shortest gradient time of 10 minutes at both flow rates. Similar results were achieved for carbonic anhydrase, although the SOS material provided similar performance up to a gradient time of 20 minutes. However when testing the largest protein, transferrin, the SOS column was shown to provide peak capacity values that were comparable across the whole gradient span at both flow rates. In a separate study the SOS column was also found to provide higher peak capacity values for other large proteins, BSA and thyroglobulin. It appears that the large ratio of core:total particle diameter due to the shallow shell depth provides a reduction in mass transfer effects for the largest molecules.

The results have shown that the advantages of the SOS materials are mainly observed for the study of the largest proteins, or when fast gradient times are applied. The analysis of individual proteins and a protein test mixture at short gradient times of up to 10 minutes confirm this, with peak capacity values of the SOS material close to those obtained using the Accucore column. The observed back pressure was lower for the SOS column, which is explained by the larger particle diameter compared to the commercial core-shell material. The column packed with fractal-C4 particles also provided high performance in the analysis of individual proteins under short gradient conditions, with peak capacity values exceeding those of the SOS-C4-1 and Accucore 150-C4 columns in most cases. It is difficult to determine if the fractal morphology has any additional benefit over normal SOS particles, as the improvement in performance may be attributed to the smaller particle diameter, however it can be concluded that the fractal material shares the advantage of SOS particles in terms of reducing mass transfer effects, particularly for large molecules.

A column packed with SOS-C4 particles was supplied to the School of Pharmaceutical Sciences at the University of Geneva. The material was used to analyse mAb and ADC samples alongside several state of the art wide-pore materials designed for protein analysis. The SOS column performed well, in some cases providing performance equal to or greater than some of these materials. mAbs and ADCs are of high interest for use as therapeutic agents, with many drugs already marketed. SOS materials have been shown to be effective for the analysis and characterisation of these types of compounds and future work should be undertaken into this type of application.

The experimental work detailed in this thesis has outlined the development of SOS silica particles. This has included the optimisation of the reaction conditions to provide particles with the desired physical properties for HPLC, development of a microwave bonding method to functionalise the surface, and the HPLC assessment of these particles

for a range of compounds, particularly for the analysis of large molecules. However, there are still a number of areas where further study could be undertaken, for example the increase of the reaction volume to a manufacturing scale would be beneficial to assess if there are any changes to the morphology.

The range of bonded phases should be expanded in future work. The method of bonding via microwave irradiation can be easily applied to functional groups other than alkyl chains and initial work into the bonding of SOS particles with ion exchange and diol phases has been attempted, although the results are not reported here. The use of these phases can provide alternative retentive mechanisms to the reversed phase materials described in this thesis which may result in different selectivity or improve the analysis of proteins and other large molecules, however no HPLC analysis has yet been performed with columns packed with these materials.

Further experimentation into fractal SOS particles should also be undertaken. The materials formed when including TEOS along with MPTMS as the precursor show greater amounts of surface growth than when using MPTMS alone. This may provide additional surface area and porosity, and therefore increased retention for analytes. Short HPLC gradient analysis has been conducted, with excellent results obtained for the analysis of individual proteins. This work should be continued with the separation of protein mixtures and also study into the use of longer gradient spans, as was conducted on the SOS-C4 material, to determine the achievable peak capacity. This work could also be performed on the cluster-type particles to provide comparison between all materials produced from this work.